Production of Functionally Gradient Materials Using Model Thermosetting Systems Cured in a Thermal Gradient

David S. Porter

Dissertation Submitted to the Faculty of the
Virginia Polytechnic Institute and State University
in partial fulfillment of the requirements for the degree of

Doctor of Philosophy
in
Chemistry

Thomas C. Ward, Chair

John J. Lesko
Herve Marand
James E. McGrath
James P. Wightman

April, 2005
Blacksburg, Virginia

Keywords: Polymers, Gradient Materials, Thermoset, Toughening, Polycyanurates, Phase Separation, Relaxation, Dynamic Mechanical Analysis, Mixing Thermodynamics, Polymer Solutions

Production of Functionally Gradient Materials Using Model Thermosetting Systems Cured in a Thermal Gradient

David S. Porter

ABSTRACT

Thermosetting polymers can cure at a gradient of cure temperatures due to a variety of factors, including heat transfer in the thermoset during heating and the exotherm due to the chemical reaction occurring during the cure. A new method for assessing the effect of cure conditions on mechanical behavior of toughened thermosets has been developed. Modeling of the phase separation process of a model thermoset system provided detailed understanding of the mechanism of property variation with cure temperature for this material. Subsequent characterization of gradient temperature cured samples has shown important variations, illustrating not only the importance of cure conditions, but the possibility of producing materials with new and useful properties.

A special mold was developed to cure samples in a controlled gradient of temperature. Example systems known to show pronounced variations in microstructure cured in this gradient mold showed large variations of microstructure as a function of position within the sample, corresponding to the cure temperature at that point.

A model toughened thermoset system was developed to demonstrate gradients of properties following cure in the gradient temperature mold. Cyanate ester materials were modified with hydroxyl-terminated butadiene-acrylonitrile copolymers as well as low T_g amorphous polyesters. The polyesters showed very desirable properties for a toughener, including relatively good thermo-oxidative stability in comparison with the butadiene-

acrylonitrile toughener. However, the variation of properties of the cured materials with temperature was small, and to better understand the property variation possible using a gradient cure temperature technique, the butadiene-acrylonitrile toughened cyanate ester system was chosen for further study. This system showed a significant variation of glass transition temperature of the cyanate-rich phase as a function of cure temperature.

Modeling of the phase separation process of this material was varied out employing a modeling procedure developed for epoxy materials. Various characteristics of the system were determined in order to apply the model to the chosen toughened thermoset. These included viscosity, surface, and thermodynamic parameters in addition to a careful characterization of the morphological parameters developed during cure at the chosen temperatures. Results show excellent predictive capability of the model for microstructure. Prediction of phase composition as a function of cure temperature is also possible, again with good agreement with experiment results. Higher cure temperatures result in a non-equilibrium phase composition, depressing the glass transition temperature of the continuous cyanate ester rich phase. This provides a mechanism by which properties of the system change as a function of position within a gradient temperature cured sample.

Dynamic mechanical analysis was employed to characterize the relaxation properties of gradient and isothermally cured samples. The Havriliak Negami equation was chosen to describe the relaxation behavior of these samples. Comparison of the fitting of isotherms over the small, experimentally accessible range of frequencies showed that the use of time-temperature superpositioning could more reliably discern relatively small differences. The breadth of the relaxation corresponding to the glass

transition of the polycyanurate phase was increased with a gradient cure temperature relative to isothermally cured samples. This increased broadness was expressed in an alternative way through the use of an autocorrelation function, which allows direct comparison of the time-dependent transition from a fully unrelaxed condition to a fully relaxed one.

DEDICATION

This work is dedicated to my my wife, Shelley; my parents, Doris and Andrew Porter; and my late grandfather, Emil Michalek.

ACKNOWLEDGEMENTS

It is only fitting to begin these acknowledgements by recognizing the unlimited inspiration, encouragement, guidance, patience and assistance provided by Professor Thomas C. Ward. In addition, my parents (Doris and Andrew Porter) have always supported me, provided for me, and raised me that I might be able to do accomplish any of the things that I've done, and succeed at anything that I might try. To you, all the thanks I can give here will ever be inadequate.

Special thanks are due my committee (Professors Ward, Lesko, Marand, McGrath, and Wightman) for guidance and patience. The other faculty members and other members of the Virginia Tech community have been vital to my educational experience; there are too many to mention throughout my graduate and undergraduate studies. And though all of my instructors at Virginia Tech have been memorable, two stand out as true mentors and role models: Professors John Dillard and Jim Wightman. These are two of the finest educators, scholars, researchers, gentlemen and friends anyone could hope to associate with. They are a credit to their profession and community.

The students of Professor Ward's PolyPkem research group were indispensable resources and friends. The academic and social exchanges were wonderful experiences I'll cherish forever, whether it was a cookout or other get together; Macado's; a long lunch; a Thursday afternoon after a short course; tailgating and football games; ASC, ACS and Adhesion Society meetings; late nights working in the lab (maybe preparing for a Christmas short course appearance by Santa); or afternoons downtown - all of these made life good. Those people are (in no particular order): Mark Muggli, Kermit Kwan, Ojin Kwon, Mark Vrana, Dan Hahn, Saikat Joardar, Tony Williams, Jianli Wang, Emmett O'Brien, Amy Eichstadt, Taigyoo Park, Sandra Case, Rob Jensen, Jennifer Robertson, Sean Christian and Chitra Subramanian. Thank you for your friendship, fellowship and for your help in the lab. I know that somewhere and somehow we'll all be together again getting a presentation ready (at the last minute, of course), or at least celebrating its completion.

There are a great many needs both large and small to successfully carry out research, and many have helped shoulder that burden. Financial support is obviously an important consideration for a student, and The Center for Adhesive and Sealant Science at Virginia Tech and the Adhesive and Sealant Council have been more than generous in their continued support of me throughout my studies, both undergraduate and graduate. In the technical area Ojin Kwon and Taigyoo Park were of tremendous assistance in the modeling work and in characterizing the relaxation behavior of the materials. Steve McCartney was always willing to help with microscopy, and is a great and knowledgeable resource; Qing Ji and Limin Dong provided GPC characterization; the Physics machine shop and Fred, John, Melvin, and Scott were ever helpful and always ready with a joke, and the electronics shop was always available and willing with their time and resources. Susmita Bhattacharjee helped tremendously with the hydrogenation work, and Drs. Ming Chen and Allan Schultz were always available for technical

discussion and an expert opinion. The late Franz van Damme was also both a help and a friend. Administrative support was provided by the friendly and helpful Kim Mills, Katy Hatfield, Tammy Jo Hiner, and Linda Haney in the CASS office and Joyce Moser, Millie Ryan and Esther Brann in the NSF office. And many thanks to Mary, who helped keep the lab looking great.

And it is only fitting to end this acknowledgement by recognizing my patient and long-suffering wife, Shelley. Her love, encouragement, prayers and support have meant more to me than anything; I'm not sure how I'd make it without her helping to bear my pains and celebrate my joy. She has shared with me the good graces of God that have helped us through life and sustain us still. Thank you, wife – no words or gesture could ever be sufficient.

To all I have listed above and to all who I've missed, please accept my eternal gratitude.

TABLE OF CONTENTS

LIST OF FIGURES AND TABLES

Chapter 1: Introduction

The usefulness of thermosetting polymers depends upon their unique properties: processibility, high temperature capabilities, good adhesive properties and low creep. However, thermosetting materials often suffer from unacceptable brittleness arising from high crosslink densities. To offset this tendency, toughening agents have been employed to enhance their fracture properties. However, the introduction of toughners is not without disadvantage. Toughners, especially lower molecular weight materials with low glass transition temperatures, can lower high temperature performance significantly while imparting significantly improved toughness. (1)

This brittleness may be aggravated by details of the polymer cure schedule. It is difficult to overstate the importance of cure schedule on toughened thermoset properties. Cure conversion, morphology, glass transition temperature, toughness, and tensile strength, among other important properties, depend on not only the extent of cure, but the particular processing pathway taken to obtain a given degree of cure. (2) Because toughners typically function through the formation of a two-phase morphology, the particular composition of both thermoset-rich phase and toughener-rich phase is affected by the cure cycle.

Cure conditions within a single sample may vary considerably from those intended. (3) The exothermic nature of the crosslinking reaction produces gradients of cure temperature within the resin/thermosetting system, which may be attributed to poor thermal conductivity of the resin/thermoset. Additionally, the low thermal conductivity

causes a significant lag in the heating of the core of the thermoset system compared to the outer regions, which can also result in cure temperature gradients. (Figure 1-1)

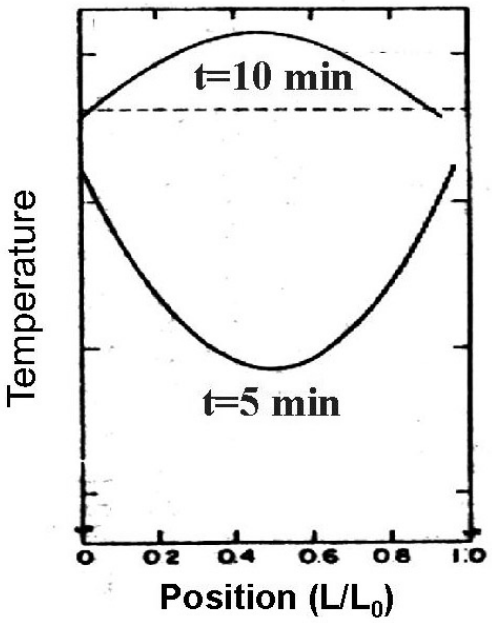

Figure 1-1. Depiction of natural thermal gradient a in curing thermoset composite system, after 5 and 10 minutes of cure. After Loos et al., Journal of Composite Materials, 17, (1983), p. 158.

The properties developed by variations in cure temperature in realistic cure situations are typically variant across one or more dimensions within the sample, producing a continuous gradient material. This effect has not be considered in the performance of these materials. This principle may also be applied to produce intentional temperature gradients within a single sample to both model the actual cure behavior of toughened thermosets and to intentionally produce materials having intentionally variant properties to address specific materials challenges.

Recent research on advanced composite materials has suggested new materials with property gradients might solve unique problems posed by performance requirements. For example, specific materials problems in a Japanese spaceplane project

suggested development of a new type of material, the functionally gradient material, or FGM. (4) These gradient materials have controlled properties, or functions, that vary as a function of position within the sample. (Figure 1-2)

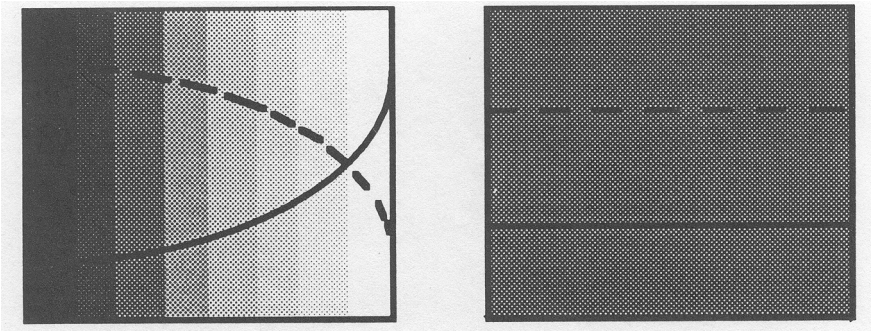

Figure 1-2. Depiction of a functionally gradient material, relative to homogeneous material, showing elastic modulus (solid line) and thermal conductivity (dashed line). After Cherradi et al., Composites Engineering, 4, (1994), p. 884.

By combining properties and varying them continually, FGMs can offer properties such as hardness and toughness that could not be provided by a homogeneous material. (5) A common example of this is a natural composite such as bamboo, where the constituents change in composition continuously from the surface to the interior of the structure. (6) Gradient materials may be designed to have specific advantages over non-gradient materials. Most development of FGMs has been accomplished using ceramic/metal composites. Polymeric gradient materials have received less attention. Most of this research centers upon non-equilibrium swelling of network polymers with a second monomer and its subsequent polymerization to produce gradients of composition. The intentional production of gradient properties within a polymeric material using a thermal gradient processing technique could offer advantages over other types of FGM polymers.

This present study seeks to characterize specific cure condition effects on mechanical behavior for novel toughened thermosetting systems, as well as properties imparted by gradient cure temperatures. It will be shown that the incidental and intentional variation of cure temperature within a single sample can have unexpected and significant effects on physical properties. These gradient physical property effects have yet to be considered, and the production and testing of these materials was undertaken using a unique methodology.

1.1 Approach

The system used to model temperature gradient cure behavior was based on a toughened thermoset. The thermoset resin examined was bisphenol-A dicyanate (BADCy), a commercially produced material with several outstanding properties, such as high glass transition temperature, low monomer viscosity and low dielectric loss. Like many high performance thermosets, this material has a high crosslink density when cured that may result in unacceptable brittleness for some applications. Enhancement of the fracture toughness may be accomplished through the introduction of ductile inclusions. This has been achieved in many commercial thermoset systems by dissolution of a preformed polymer that phase separates during cure of the thermoset, forming particles that improve the fracture properties. The microstructure of the toughener-rich phase has been shown to have a strong effect on the final properties. (7) Significantly, the introduction of such a toughener may have deleterious effects on other properties. This may include the lowering of the glass transition temperature of the thermoset-rich phase, which results from incomplete phase separation of the typically low-T_g toughener. High

T_g tougheners may be employed; however, the toughness-enhancing effect of these materials is typically smaller than that of the elastomeric additives.

The cure temperature of a thermoset resin has many effects on the final properties. The degree of cure obtained may be affected by the relation of cure temperature to the T_g of the fully cured resin ($T_{g\infty}$). At cure temperatures lower than $T_{g\infty}$, the increasing glass transition temperature of the curing resin will eventually equal the cure temperature, at which point the physical state of the curing resin will change from liquid (or rubber for those systems beyond gelation) to a glass (vitrification). Beyond vitrification, there is insufficient molecular mobility remaining for reaction to continue to any significant degree due to the restrictions on unreacted species coming into contact with other unreacted species. Therefore, cure temperature, first of all, may have an effect on the ultimate degree of conversion of the thermoset. In addition, curing at temperatures above $T_{g\infty}$, especially with high performance thermosets, may result in degradation of the material through a number of mechanisms. This degradation can have an impact on physical properties.

Cure temperature also has an effect on the phase microstructure of the cured system. For the phase separation process of nucleation and growth, the influence of cure temperature on the microstructure is a function of the difference in the activation energies for the reaction and for the viscosity of the system. Where this is a large difference (i.e. the activation energy for the reaction is significantly greater than the activation energy for viscosity) increasing the cure temperature decreases the concentration of disperse phase particles, forms a maximum in the particle radius with increasing temperature, and decreases the volume fraction of these particles. (8) For the case of phase separation

occuring by the spinodal decomposition mechanism, no specific model for particle size has been developed, but particle size has been shown to vary considerably with cure temperature. (9)

In addition, cure temperature affects the composition of the phases in these toughened polymers. The mechanism controlling the composition depends on the type of phase separation taking place. In the case of a nucleation and growth-type phase separation mechanism, phase composition may deviate significantly from equilibrium values. This is due to the speed at which the phase separation occurs. While spinodal decomposition occurs rapidly, nucleation and growth is a time consuming process. The ongoing polymerization may reach the gel point quickly, depending on cure temperature. At the gel point, transport of toughener molecules across the concentration gradient (which contributes to the growth process) effectively ceases due to the infinite viscosity of the system. This can "lock" the system in a state which significantly departs from thermodynamic equilibrium. The presence of this dissolved low-T_g toughener molecularly mixed in the thermoset-rich phase depresses the latter's glass transition temperature.

In the present study, only variations in particle size and phase composition will be considered to control properties. Cure has been equalized in all instances and decomposition was not a variable. Experiments have been conducted to obtain information about the mixing thermodynamics. Modeling of the particle size development as well as predictions of phase composition have been performed using additional experimental data such as interfacial energy, reaction kinetics, rheology and particle size distribution. This predicted phase composition was compared to the

experimentally determined phase composition as measured from glass transition temperatures. Two different systems have been examined in this respect. In one system the composition was found to be close to that predicted by equilibrium thermodynamics, while another case necessitated a careful consideration of the mechanism of phase separation in order to predict the phase composition as it varied from equilibrium values. In this case, the particle size distribution predicted was found to reasonably match the measured particle size distribution.

Functionally gradient samples were prepared from systems described above. This was accomplished using a thermal gradient mold designed for this study. Morphological variations within the gradients were examined using electron microscopy. The variation in fracture toughness due to the variation in cure temperature was measured for single-temperature cured samples, and did not vary beyond statistical significance, and therefore would not produce detectable variations in fracture in the functionally gradient polymer. The gradient mechanical property used to characterize these new materials was their distributions of relaxation times. The gradient of glass transition temperatures produced in a single specimen by the gradient temperature cure indicated differences in relaxation time of each discrete region within the gradient. Acting together, these macroscopic variations in composition produce an effective broadening of the relaxation time distribution, an effect usually considered to arise from molecular-level phenomena. The quantitation of these changes in relaxation time distribution together with comparison to a non-gradient-composition relaxation distribution was used to demonstrate the physical property effects of the gradient temperature cure.

1.2 References

(1) S. A. Srinivasan, Ph. D. Dissertation, VPI&SU, (1994).

(2) S. Montarnal, J. P. Pascault, and H. Sautereau. In Rubber-Toughened Plastics, C. Keith Riew, Editor, Advances in Chemistry Series 222, ACS, Washington, D. C., (1989), p. 204.

(3) Loos, A. C., Journal of Composite Materials, 17, (March 1983), p. 158.

(4) M. Koizumi, "The Concept of FGM", Functionally Gradient Materials, J. B. Holt, M. Koizumi, T. Hirai, and Z. A. Munir, eds., Ceramic Transactions, 34, (1993), p. 3.

(5) Ibid., p. 4.

(6) S. Amada, T. Munekata, Y. Nagase, Y. Ichikawa, A. Kirigai, and Y. Zhifei. Journal of Composite Materials, 30, (1996), p. 800.

(7) A. J. Kinloch. In *Rubber-Toughened Plastics*, C. Keith Riew, Editor, Advances in Chemistry Series 222, ACS, Washington, D. C., 1989, p. 79.

(8) S. M. Moschiar, C. C. Riccardi, R. J. J. Williams, D. Verchere, H. Sautereau, and J. P. Pascault, Journal of Applied Polymer Science, 42, (1991), p. 733.

(9) D. S. Porter and T. C. Ward, Proceedings of the 19th Annual Meeting of the Adhesion Society, (1996), p. 40.

Chapter 2: Functionally Gradient Materials from Toughened Thermoset Resins

2.1 Introduction

Material systems are constantly being developed which have improved properties for specific applications. The trend in research on advanced polymer-based materials systems is to reliably produce homogeneous materials, with no spatial variations in properties. (1) In other materials fields, there are large demands for inhomogenous materials, in particular for percussive rock-drilling tools. To satisfy these requirements, the unique problems posed by a given situation may dictate a novel material system that simultaneously possesses two otherwise mutually exclusive properties. Where this is the case, conventional materials may somehow combined, joined by some fastening technique, such as a bolt, weld or adhesive. In some situations however, this may not be an adequate, or even possible, solution.

In addition to the need for new materials which meet multiple conflicting parallel demands, there is a need to more thoroughly understand the characteristics of existing materials to better define their applications and limitations. This will lead to a better fit between design parameters and material response, enhancing both durability and performance. Toughened thermosetting polymeric materials fall into this category, and have been increasingly employed in both high performance as well as conventional-use environments. The performance and properties of this class of materials has been shown to have a large dependence upon cure conditions. (2) Unfortunately, it has been determined that the intended cure temperature is seldom the system's actual cure temperature. (3) This anomalous effect is mainly due to the relatively low thermal

conductivity of the resin system and the resulting heat transfer into the initially cooler resin, followed by heat transfer of the cure exotherm out of the reacting mass. The unintended result of this heat inhomogeneity is a gradient in final properties.

In this chapter, a survey of the gradient material literature will be presented, including both polymeric and nonpolymeric examples. While most gradient materials have been produced using gradient composition formation or non-equilibrium swelling, the experimental portions of this chapter detail the formation of gradient materials using a thermal gradient technique. This approach demonstrates a rapid and simple method for producing gradient materials. Additionally, this thermal technique produces samples that allow for systematic investigation of a thermal gradient cure various samples, as opposed to the unintentionally generated thermal gradients that have been shown to exist in cured samples. Examination of these controlled gradient samples will assist in understanding the implications of this phenomenon on final properties. In the following, the ideas used to design a thermal gradient mold, together with the subsequent characterization of the thermal gradient cured samples, will be detailed.

2.1.1 Literature Review

2.1.1.1 Gradient Materials

The various properties desired for specific material applications are often mutually exclusive, e.g. high modulus and toughness. This problem confronted the Japanese space program in the mid-1980s. (4) The divergent properties required in this case were high thermal resistance for a nose cones, where frictional and other heating required thermally resistant materials, along with enhanced toughness. These requirements could not be met by then-current technology, so a new approach was

pursued. The so-called Functionally Gradient Material (FGM) system was developed and studied, where the new materials possessed a change in properties, or function, with position within the sample. These materials can have properties varying in one or more dimensions, depending on how they are produced. These materials are inhomogeneous and may have gradients of composition, phase distribution, porosity, texture, particle grain size or fiber reinforcement. (5) The resulting FGMs are characterized by compositional and other types of gradients; in addition, they also have complex mechanical and thermal behavior in comparison with conventional homogeneous materials. (6)

Gradient materials have also been generated previously through ceramic production methods that varied the composition through the part thickness. In these cases a more thermally resistant material was formed on the outer surface, and the inner surface was a tougher material, with the composition varying continuously as a function of the position within the sample's thickness. Gradient materials can provide a better match of properties such as coefficient of thermal expansion, modulating this dimensional change with position as well as temperature. This could minimize mismatch of CTEs in joining dissimilar materials, distributing stresses over a larger area to inhibit fracture. These materials may also vary the relaxation time distribution, with mean relaxation times within a given cross-section of the sample differing significantly from that of neighboring sections. The mechanical loss maximum frequency at a given temperature may then vary depending on the composition and location within the gradient sample. Therefore, damping over a larger range of frequencies is possible in FGMs. Currently, use is made of gradient materials to produce optical elements with a graded refractive index. (7) This

allows the focusing of light with a cylindrical element. Biomedical and agricultural applications are feasible using a gradient in diffusion properties available with FGMs, allowing distributed release of substances such as drugs and fertilizer.

While the concept of man-made gradient materials is relatively new, naturally occurring FGMs abound. Teeth are a good example of gradient materials; the outer surface is rich in inorganic material, which provides hardness, and the inorganic concentration decreases continuously to the center, which is tougher and more resilient. Bamboo is another example where nature has produced a superior material with gradient properties. (8) **(**Figure 2-1 and Figure 2-2**)** The structure of bamboo shows an increase in bundle sheaths (the discrete dots) towards the outside of the composite. This microscopic gradient structure distributes strength in a radial direction, improving adaptation to the bending stress due to wind loads. There is additionally larger scale, macroscopic gradient of structure in bamboo. The lengthwise sections of bamboo are separated by nodes within the hollow culm, whose separation varies as a function of height from the ground. This structure provides constant surface stress at any height.

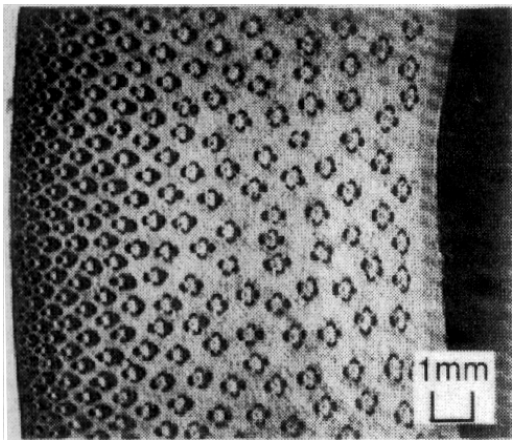

Figure 2-1. Microscopic gradient of structure in bamboo. (After S. Amada et al., Journal of Composite Materials, 30(7), (1996), p. 800.)

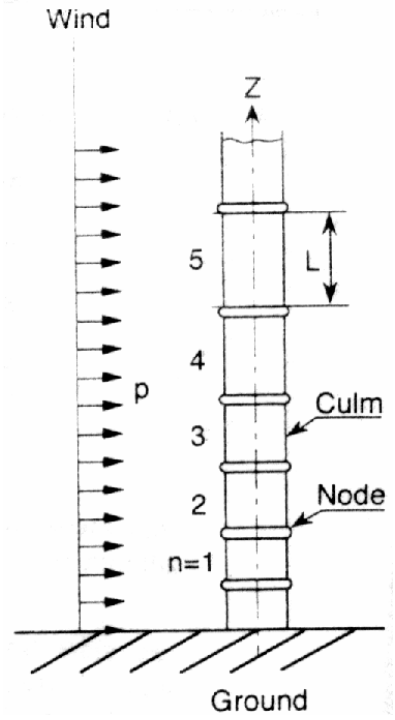

Figure 2-2. Macroscopic gradient of structure in bamboo. (After S. Amada et al., Journal of Composite Materials, 30(7), (1996), p. 800.)

Gradient materials based on ceramics and metals are often produced by varying the composition of the materials as they are formed. Examples of this are vapor deposition (both chemical and physical), spray forming, and powder metallurgy. (9) The resulting materials are all created with a variation in the composition of the composite-

forming components, which otherwise would be a complex, expensive and time-consuming process.

2.1.1.2 Test Methods for Gradient Materials

Testing methods for gradient structures are not generally well developed. Investigations into of the performance of these systems includes various microscopic and microspectroscopic experiments and other conventional tests usually designed for homogeneous materials. These experiments involve sectioning the materials into thin films to be tested individually as homogeneous elements. These methods need to be modified to fully examine behavior as affected by the special property gradients. An example of this is the change in fracture of metal/ceramic FGMs from brittle to ductile over a response continuum. Because of these described limitations, especially in global properties, research evaluations for FGMs are needed urgently - there have been few developments reported. (10)

2.1.1.3 Polymeric Functionally Gradient Systems

A number of gradient property polymer systems have been generated, and some effort has been made to characterize these materials. (11) Since first discussed by Shen and Bever (12), the unique behavior of gradient polymer materials has been investigated mainly in the form of diffusion-type interpenetrating network structures. However, there is some discussion of other types of systems. Gradients of crosslink density, molecular weight, orientation (direction and degree), percent crystallinity (controlled via cooling rate, tacticity, or copolymerization), orientation and size of spherulites, composition of blends, composition of copolymers, particle volume fraction, size, and shape of

heterophase systems, and concentration gradient of filler materials have been proposed and/or investigated.

The usefulness of gradient structures is a product of the unique spatial and global properties that are generated or combined. Generally, it has been suggested that chemical response may be varied within a material via gradient structure, such as hydrophobicity, oxidative resistance, thermal degradation, weather resistance, irradiation, and chemical attack. Mechanical property gradients would appear in the form of variations in strength, fracture stress, impact resistance, modulus, hardness, and viscoelastic damping. Gradients in biocompatibility could provide materials with the rigidity of a glassy or semicrystalline polymer while possessing the excellent biocompatibility of silicone, a liquid or rubbery material. Transport properties, such as thermal and electrical conductivity could be applied to produce materials such as a semiconductor with insulating backing layer. Gradient diffusivity could provide selective permeability where permeability is both undesirable and where it may be desirable, such as in dialysis applications. Thermal shock in cryogenic rocket fuel tanks can cause delamination in the layered structure, which could possibly be prevented by the use of a gradient material - a porous section providing insulating properties graded to a nonporous structure to provide mechanical strength and impermeability. The interest in gradient materials has been driven by a desire to combine two useful properties that may have heretofore been mutually exclusive in nongradient samples. While many suggestions have been made with respect to what gradient properties may be produced, few specific examples have been offered to demonstrate which systems might be used to achieve these gradients. (13)

Diffusion-process interpenetrating networks are formed via swelling of a pre-formed network with a different monomer, and subsequent polymerization of that monomer in-situ. The gradient of composition is formed by crosslinking in a non-equilibrium swollen state, that is, where the rate of diffusion is such that the concentration on the outer surface of the network is richer in monomer than the inside portion. Attempts at a variation of this technique have been made (14) where the network is swollen to equilibrium followed by a non-equilibrium swelling of the crosslinking agent. Here, the example was a polyurethane system swollen with acrylamide in ethanol solution. This did not, however, result in a significant gradient of composition. Methods used in the example to investigate the gradient of composition included FTIR and electron microscopy, which were used to investigate both composition and domain size of phase separated poly(acrylamide) regions.

A gradient polymer system consisting of polystyrene (PS) with a gradient composition of polyacrylonitrile (PAN), as well as a poly(methylmethacrylate) sample with a gradient composition of poly(methylacrylate) were prepared by Akovali et al. (15) using the non-equilibrium diffusion scheme. The resultant PS/AN systems showed gradients of composition that were characterized using analysis of combustion products for nitrogen, yielding acrylonitrile composition distribution. The PS/PAN networks were compared to those expected from Fickian diffusion calculations, from which composition gradients were mapped and diffusion constants were calculated.

Diffusion rates were further treated by Dror et al. (16) in a study of poly(ether urethane) gradient polyacyrlamide (PAM) systems. Increasing concentration of crosslinker and of the swelling acrylamide monomer resulted in a higher concentration of

PAM until a concentration of 0.09M was reached, when increasing concentration no longer had any effect. Increasing time of swelling increased the concentration of PAM in the network.

One gradient IPN system has been evaluated for thermodynamic compatibility of the components. This material is based on a butyl methacrylate-triethylene glycol dimethacrylate copolymer combined with a polyurethane (BMA-TrEGDMA). (17) This system phase-separates and, due to the gradient swollen structure, each layer into the gradient will vary in phase separation conditions. A sequence of layers through the gradient sample was examined for variation in composition, glass transition temperature and specific volume as a function of temperature. The gradients in composition were resolved by an elemental analysis of each section, where the nitrogen content revealed the amount of polyurethane. The polyurethane mass fraction increased as successive sections toward the center of the sample were examined. Because the glass transition temperatures of the component polymer are quite different, the glass transitions of the IPNs changed due to partial phase mixing, producing two phases of variable composition. In the region of the glass transition, the specific volume showed transitions that shifted as a function of composition, and therefore position, within the IPN. This allowed calculation of the composition of that section. This data agreed well with the elemental analysis.

The solvent uptake properties of the BMA-TrEGDMA system were also explored. Using benzene uptake measurements, average free energy of mixing of the individual components was obtained, and from this the free energy of mixing of the polyurethane and copolymer was calculated. The free energy of mixing of the polymer system

components was positive - confirming the incompatibility necessary for phase separation to occur. This free energy varied depending on position within the sample, which was an effect of the varying conditions of polymerization from gradient swollen composition. The polymerization then "froze" the composition and structure at a non-equilibrium state rather than allowing for complete phase separation. These non-equilibrium states varied as a function of position within the sample.

Lipatov et al. (18) investigated the mechanical properties of gradient polymer systems. These systems were compared to normal IPN systems of the same average composition, allowing comparison of properties. The temperature dependence of the dynamic mechanical Young's modulus and tan delta were compared. For the nongradient samples, the tan delta values indicated two transitions which shifted as a function of concentration. These transitions were assigned to the multiphase nature of the systems; the peaks narrowed and shifted away from one another in temperature due to increasingly complete phase separation. In the study of the gradient material, two types of samples were taken. One type of sample was taken perpendicular to the gradient, while another was taken along the gradient. Results for tan delta as a function of temperature for the sections perpendicular to the gradient show differences in broadness as well as position of the maximum. Along the gradient the loss peak was quite broad, and this was attributed to the superposition of multiple maxima which resulted from the glass transitions of layers of different composition. This was visualized as being a practical material for broadband noise and vibration dampening applications.

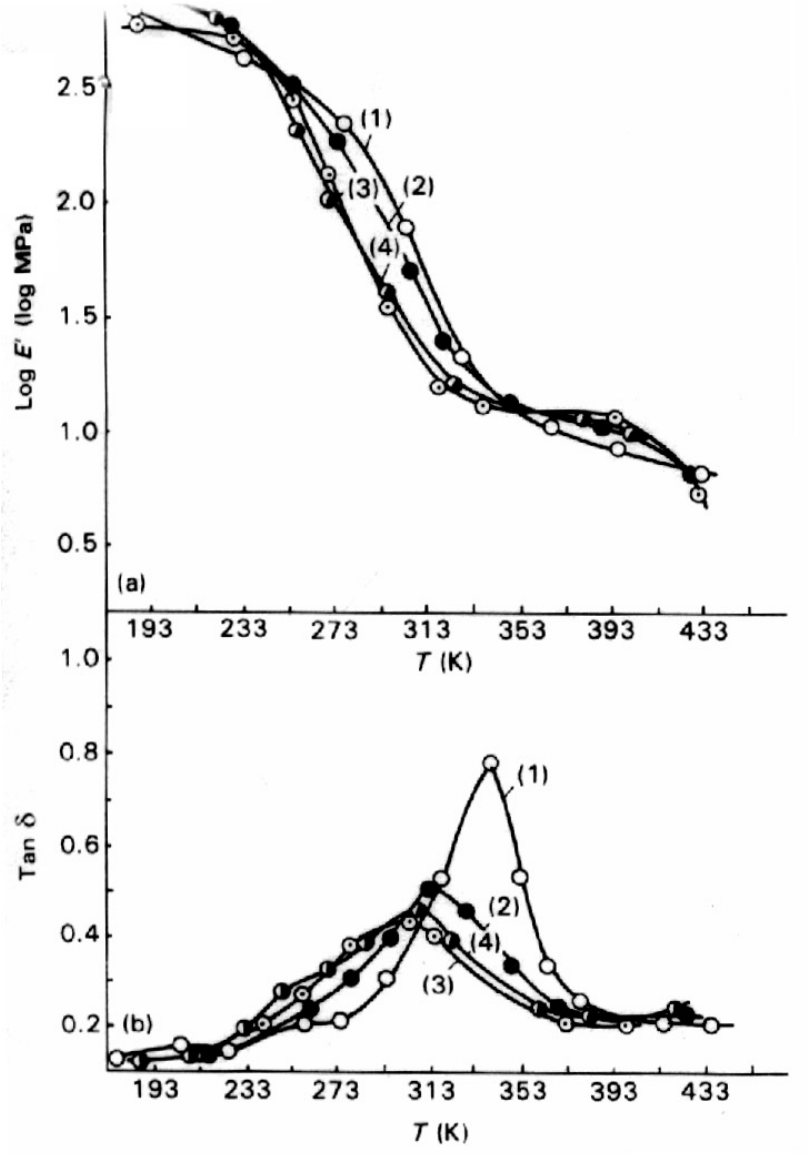

Figure 2-3. Temperature dependence of both modulus and tan delta in sections perpendicular to the gradient of a BMA/TrEGDMA in polyurethane gradient interpenetrating network. Section numbers move from surface (1) (rich in BMA/TrEGDMA) to the core (4) (rich in polyurethane). After Lipatov et al., Polymer International, 28(2), (1992), p. 99.

Within this same system of Lipatov, the ultimate tensile strength was demonstrated to be substantially higher than in a nongradient sample. The area beneath the stress-strain curve was greater for the gradient sample as well. The Young's modulus

for the gradient IPN was also observed to be greater than for a nongradient IPN of the same average composition.

Similar gradient IPN experiments are reported for a system based on butylmethacrylate (BMA) and dimethacrylate triethyleneglycol (DMTEG) copolymerized in a matrix of polyurethane (PU). (19) Swelling of the PU with the mixture of DMTEG and BMA resulted in a system that could be photopolymerized before equilibrium distribution was obtained. Again, results for tan delta versus temperature for the sections perpendicular to the gradient showed differences in broadness as well as position of the maximum. Along the gradient the dynamic mechanical loss peak was again broad in comparison to nongradient samples.

Gradients of polymethylmethacrylate/methyl acrylate (PMMA/MA) were studied in detail by Akovali et al. (20) and compared to nongradient materials. Pure PMMA fails at a tensile strain of about 2%. In a gradient system, the failure of a material containing 10.3% methyl acrylate (MA) failed at a strain greater than 10%. At a concentration of MA of 19%, the strain at break became about 80% for the gradient system. In comparing nongradient systems to gradient materials of the same average composition, the gradients had the largest failure stress and largest area under the stress-strain curve. Additionally, it was determined that the impact strength of gradient IPNs was higher than the nongradient sample.

Mechanical modeling of relaxation properties of gradient samples has been undertaken. (21) No relationships had previously existed for prediction of glass transition temperature of a sample consisting of an infinite number of layers of varying glass transition. Using a model with a number of layers between 2 and 11, it was found

that additional layers beyond 10 did not produce a significant effect on the predicted viscoelastic properties. Using this idea, a model was produced using 11 layers, each layer having a difference in glass transition temperature of 2, 5 or 7 K.

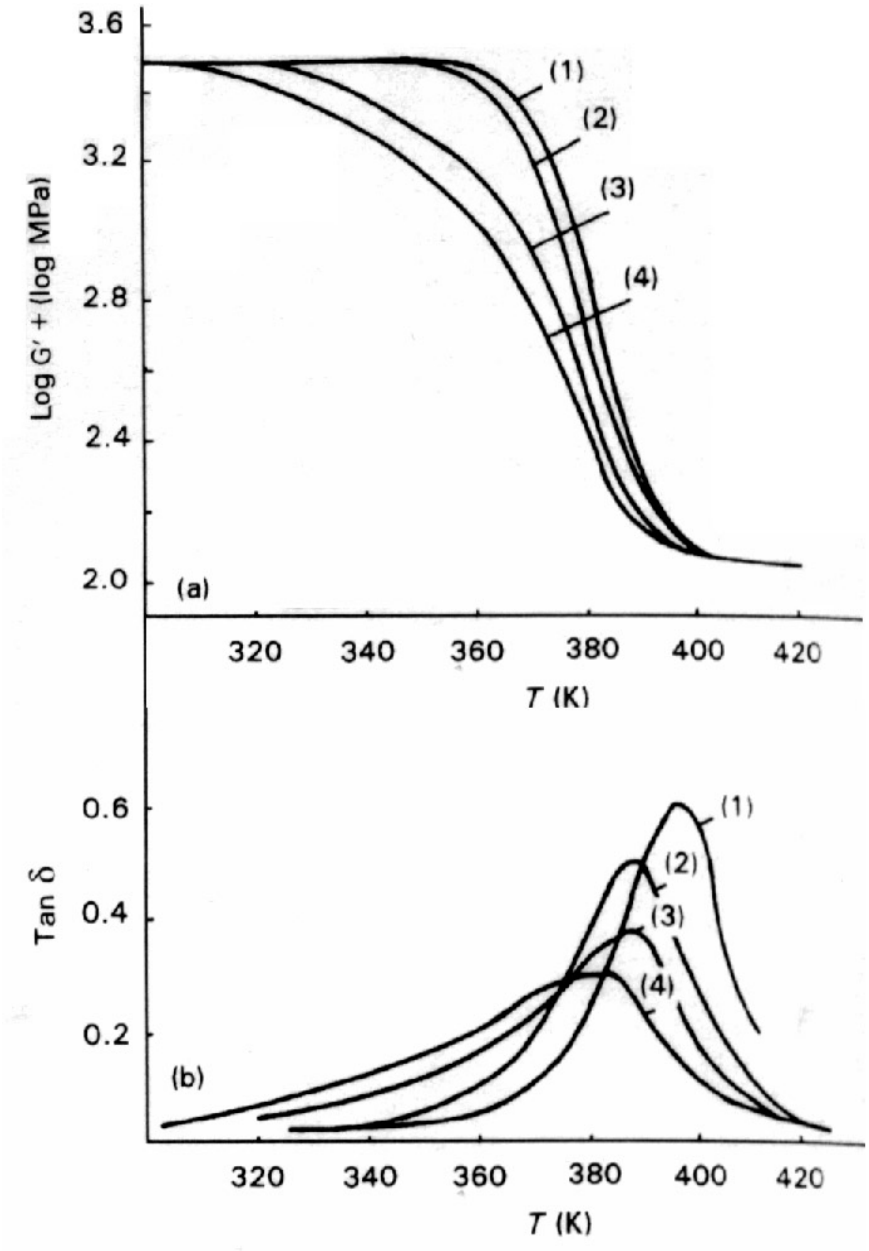

Figure 2-4. Calculated mechanical response of shear modulus and tan delta in a gradient sample. Curve (1) represents the component with the highest glass transition temperature followed by a gradient geometry with 11 layers, with each layer differing in T_g by (2) 2 K, (3) 5 K, (4) 7 K. After Lipatov et al., Mekh. Kompoz. Mater., 4, (1986), p. 585.

This model predicted a much broader decrease in the modulus/temperature curve, as well as a flatter and much broader tan delta transition as the difference in glass transition temperature increases (Figure 2-4). These calculations were based on the assumption that the sample is deformed perpendicular to the direction of the gradient. Interestingly, the calculations demonstrated that the maxima for the tan delta of the model gradient material shifts significantly toward the glass transition temperature of the lowest T_g material in the case of the sample taken along the gradient, but does not change appreciably in magnitude. The gradient of glass transition temperatures in a material's makeup therefore should change the apparent temperature range of the glass transition temperature of the composite.

In a study of gradient polymeric materials, Martin et al. (22) examined gradients of both PMMA in poly(2-chloroethyl acrylate) (PClEA) and PClEA in PMMA produced by swelling a preformed network structure in monomer and crosslinking via photopolymerization. The chemical composition gradient was determined by chemical analysis of chlorine content as a function of depth. The composition of the ClEA swollen PMMA was much richer in the swelling component towards the surface than for the case of MMA swollen PClEA. Examination of viscoelastic properties showed two glass transition temperatures for the material with the PMMA matrix gradient, indicating the presence of two phases. For the PClEA matrix gradient, only one dynamic mechanical loss modulus peak could be resolved. This peak fell between the glass transitions of the individual components and was shifted downward in temperature with increasing concentration of PClEA. It has been proposed by Lipatov (23) that the single transition

could be the result of the superposition of layers differing in composition and glass transition temperature producing a composite loss modulus peak.

Fracture testing of the PMMA/PClEA gradient systems demonstrated higher fracture energy than nongradient materials. The strain at break for the PMMA matrix/gradient PClEA was higher by an order of magnitude than for unmodified PMMA. For a PClEA matrix and 50% inclusion of PMMA, the tensile strength was higher than neat PClEA by more than 1000%. (24)

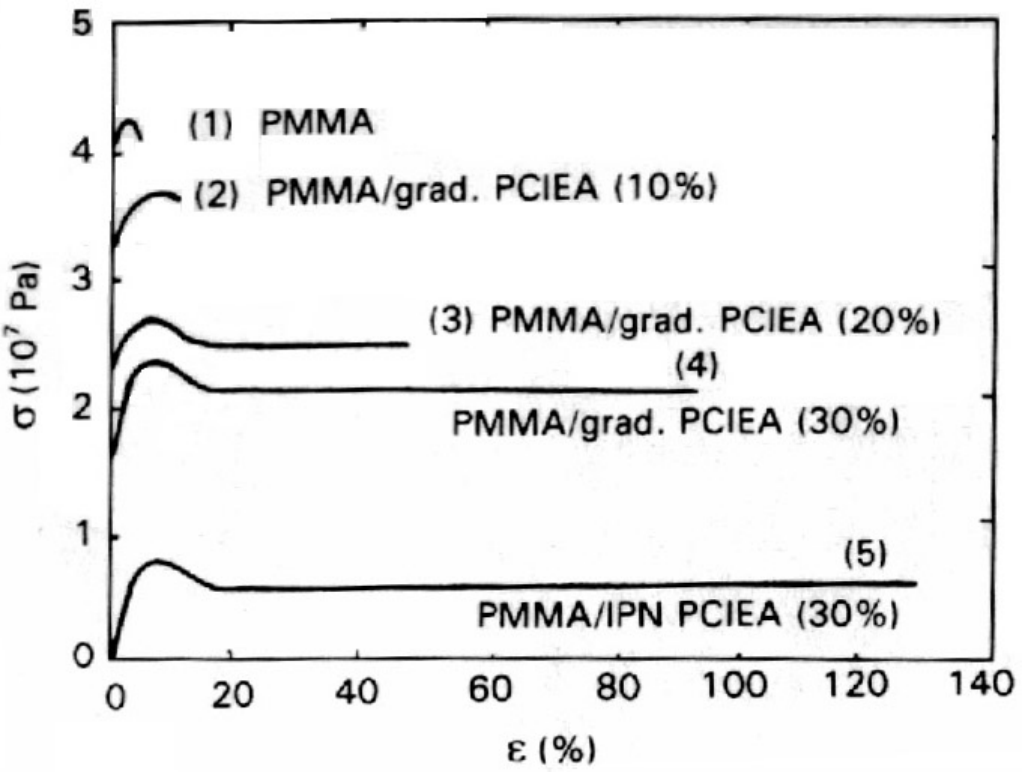

Figure 2-5. Variation in stress-strain characteristics of various gradient and homogeneous materials. After Lipatov et al., Journal of Materials Science, 30, (1993), p. 2481.

The increased strength of this type of gradient system has been considered by both Akovali et al. (25) and Martin. (26) Gradient materials may be considered to be stacked layers of material with varying composition and, in specific cases, modulus. On

deformation, each deforms to an equivalent degree, and the corresponding stress within each layer is a function of its modulus. This increases plastic deformation, limiting brittle fracture and increasing strain at break and fracture energy. The increase in fracture strength of gradient materials might also be attributed to the case of a gradient with a higher concentration of elastomeric component in the surface, which would prevent crack initiation. Examination of the surface layers of fractured specimens of gradient IPNs with surface composition richer in elastomer content show greater smoothness, indicating the retardation of crack extension within them. On the other hand, inner layers show features typical of crack propagation, where imperfections initiated the cracks.

The strength advantages attributed to the type of gradients discussed apply only to those systems possessing a gradient of a glassy component in a matrix which is above its glass transition temperature (or vice versa) at the use temperature. These advantages do not appear in systems in which both components are below their glass transition temperatures. PMMA with a gradient of PAN as well as PMMA with a gradient of PS were explored by Akovali and Labban. (27) However, these IPN systems demonstrated a higher dynamic modulus while other properties remained the same as the equivalent non-gradient sample.

Gradient materials were described by Kim et al. (28) in systems comprised of the methacrylic acid derivative of diglycidyl ether of bisphenol-A (bis-GMA) in acrylonitrile-butadiene rubbers (NR). The initial crosslinking of the NR was accomplished using electron beam (EB) radiation. After the monomer was absorbed, it was polymerized using further EB radiation. In this case, the gradient samples are referred to as "asymmetric materials" and were compared to materials with a

homogeneous distribution of swelling agent (bis-GMA). The concentration of swelling agent in the NR was determined using an FTIR microscope and the position dependency of characteristic peaks was investigated. The resulting material's microstructures were characterized using scanning electron microscopy (SEM). Micrographs of the gradient structure demonstrate a spatial gradient of particles of phase-separated bis-GMA. Using dynamic mechanical analysis (DMA), the loss tangent was probed for both the gradient and non-gradient samples. In comparison to the non-gradient sample, the gradient sample had a significantly broadened DMA tan delta peak which was shifted to lower temperatures. The presence of the gradient structure was demonstrated using birefringence techniques. NR shows birefringence when stretched, but upon release this disappears. Bis-GMA will retain birefringence when deformed due to its glassy nature. When stretched, the bis-GMA/NR samples will show greater birefringence in the areas that contain the most bis-GMA. The gradient samples demonstrated a gradient of birefringence.

Another study was conducted on gradients produced by EB reactions of poly(vinylchloride) (PVC) immersed in styrene and n-butyl methacrylate. While EB radiation did not polymerize the styrene to any significant degree, the n-butyl methacrylate was polymerized within the PVC, which sorbed the n-butyl methacrylate quickly. High-density polyethylene (HDPE) was also immersed in the two monomers and subsequently irradiated. Characterization of the gradient composition was performed by a unique IR depth profiling technique developed by the authors. The HDPE was not deeply penetrated by either monomer, and typically contained only 23-43% at a depth of 17-24 microns. The PVC samples were examined for tensile strength, and it was found

that as the monomer soak time (and subsequent depth and concentration of gradient polymer) were increased, tensile strength decreased, with strain at break increasing.

A very different type of gradient system was described by Kaerger, composed of gradients of fibers within composites. (29) In a sample of poly(phenylene sulfide), a gradient of carbon fiber content was produced. The process involved aqueous powder prepregging, in which layers are assembled unidirectionally. This arrangement was characterized using image analysis of micrographs of sections perpendicular to the gradient. The gradient was suggested to yield higher resistance to warping with reduction of thermal and internal stresses.

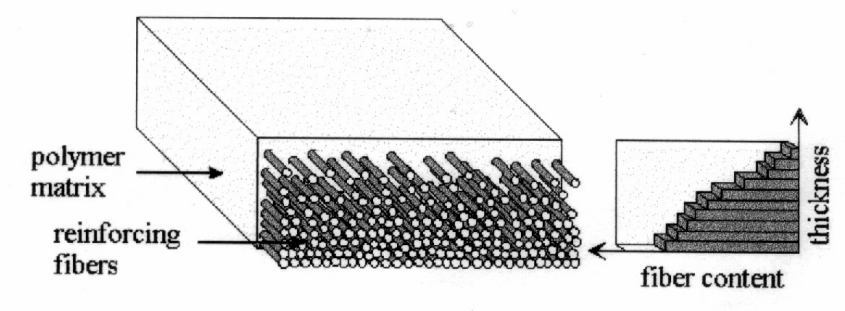

Figure 2-6. Gradient of fiber composition. After Kaerger, http://dynamik.fb10.tu-berlin.de/~hinrichs/kaerger/kaerger.html

In addition to gradients of fiber content in composites, gradient fiber materials have been produced for application in composites. Polyamide fibers have been produced with gradients of phenolformaldehyde polymer which modified the surfaces for better wetting and better thermal stability. (30) Such composites prepared from the gradient fibers proved about 50% stronger than those prepared from non-gradient fibers.

Gradients in refractive index, called gradans, have been prepared and are currently employed in multiple applications, including medical engineering and optoelectronics. (31) These materials consist of styrene-ethylene glycol copolymers or

dialyl isopthalate with a gradient of methyl methacrylate. These are produced by forming a cylinder of a high refractive index monomer which is then polymerized to an extent required to maintain the cylindrical shape. The cylinder is submerged in a low refractive index monomer. There, some of the monomer still within the cylinder diffuses out and is replaced by guest monomer, producing a parabolic profile. This entire mass is subsequently polymerized. The monomers are selected so as to ensure compatibility, and a transparent cylindrical element capable of focusing light is produced.

2.1.1.4 Heat Flow

An effective analogy for heat flow through a conductor is electrical conductivity. Given adequate time and depending upon boundary conditions, a heat source applied at one point of a thermal conductor will create a stable temperature profile throughout the conductor. The rate at which the heat flows through the conductor is a function of the differences in temperature at various locations. The quantity of heat Q flowing through an infinite slab of cross-sectional area A in time t is

$$Q = k\frac{A}{\partial x}(T_1 - T_2)\partial t \quad \textbf{(2-1)}$$

between temperatures T_1 and T_2, with x being the distance between planes in the conductor. The thermal conductivity of the substance through which the heat is flowing is k. The rate of conduction q, or heat flux, in the above condition is

$$q = \frac{1}{A}\frac{dQ}{dT} = -k\frac{\partial T}{\partial n} \quad \textbf{(2-2)}$$

with the temperature gradient being $\partial T / \partial n$. (32)

Where a system's spatial distribution of temperature is invariant with time, the heat flow model is known as steady conduction. Heat flow through a plane in which only

temperature varies in one dimension is called one dimensional (1-D). In this 1-D condition, the form of the potential equation for heat flow is

$$\frac{d^2T}{dx^2} = 0 \qquad \textbf{(2-3)}$$

which upon integration becomes

$$T = Bx + C \qquad \textbf{(2-4)}$$

with boundary conditions $T=T_1$ at $x=x_1$ and $T=T_2$ at $x=x_2$. B is defined as:

$$B = \frac{T_2 - T_1}{x_2 - x_1} \qquad \textbf{(2-5)}$$

Considering the heat flow q, we arrive at

$$q = -k\frac{dT}{dx} = -kB \qquad \textbf{(2-6)}$$

2.1.1.5 Phase Separation

The practice of toughening glassy thermosetting resins through inclusion of a separate ductile phase is well known. A very large number of investigations of the resulting material properties have been reported in the literature. While alternative strategies for improving material toughness have been proposed, such as inclusion of preformed particles (33), the bulk of the literature reports on polymer toughening (as well as current industrial practice) involve creating an initial solution of the polymeric toughener in the thermoset resin. As the resin polymerizes, the increase in its molecular weight causes a decrease in the total configurational entropy of the system. This can produce an overall shift in the free energy of mixing of the system and thus lead to phase separation.

It is this process of phase separation that produces a second phase rich in the toughening component. This second phase is responsible for the improvements in toughness. The nature of the second phase, including geometry as well other factors, has been theorized as well as demonstrated to affect the final properties of the system. Therefore, it is very important to understand not only the thermodynamics of the phase separation process, but also the mechanism of particle formation and the effect of the particle microstructure on the system in order to optimize the final physical properties.

2.1.1.5.1 Thermodynamics of Phase Separation

All solutions have miscibilities that are governed by the Gibbs free energy of mixing, described by

$$\Delta G_{mix} = \Delta H_{mix} - T\Delta S_{mix} \qquad \textbf{(2-7)}$$

where ΔG_{mix} is the Gibbs free energy of mixing, ΔH_{mix} is the enthalpy of mixing, T is the absolute temperature and ΔS_{mix} is the entropy of mixing. This equation works well with low molecular weight substances. But to better describe the thermodynamic behavior of solutions of high molecular weight compounds, a lattice-based model was developed independently by Flory and Huggins (34, 35) and is described in detail because it is critical to the modeling process described later in this thesis.

This model accounts for the decrease in available conformations of the polymer chains in solution relative to the same number of low molecular weight units. Sites on the lattice occupied by polymer must be connected, decreasing their entropy. This is a consequence of the long chain/repeating unit nature of polymeric substances. The Flory-Huggins equation for a solution of two monodisperse molecular weight polymers is

$$\Delta G_{mix} = \frac{RT}{V_1}\left(\phi_1 \ln\phi_1 + \frac{\phi_2}{z}\ln\phi_2 + \chi\phi_1\phi_2\right) \quad \textbf{(2-8)}$$

where χ is the interaction parameter, which accounts for enthalpic interactions between polymer solvent and solute, and ϕ_1 and ϕ_2 are volume fractions of the solvent and solute respectively. χ is related to the enthalpy of mixing through the relation

$$\Delta H_{mix} = \chi_{12}\phi_1\phi_2 RT \quad \textbf{(2-9)}$$

and the remaining terms in equation (2-8) arise due to entropic considerations as follows

$$\Delta S_{mix} = -R\left[\frac{\phi_1}{x_2}\ln\phi_1 + \frac{\phi_2}{x_2}\ln\phi_2\right] \quad \textbf{(2-10)}$$

ΔS_{mix} is always positive, and so contributes negatively to ΔG_{mix}. ΔH_{mix} can, of course, be positive or negative, and may lead to a positive or negative value of ΔG_{mix}. Demixing may occur when certain thermodynamic driving conditions exist. In a binary system of components 1 and 2, the temperature, pressure and chemical potential of 1 and 2 in each of two potential phases which demixing must result from become equal at certain compositions. However, kinetic limitations may still prevent the phase separation. It is the enthalpy interaction which dominates miscibility of polymers, and it must be highly favorable for a single phase to result, due to the long chain construction of polymers, producing small entropic driving forces. This long chain architecture produces very modest gains in entropy upon mixing in comparison to a low molecular weight solution. The molecular mixing of two high molecular weight polymers is therefore difficult and only occurs under conditions of strong specific interactions such that the enthalpy term is of a large magnitude.

Where mixing occurs spontaneously, we may consider the chemical potentials of the two components

$$\Delta G_{mix} = \phi_1 \Delta\mu_1 + \phi_2 \Delta\mu_2 \qquad \textbf{(2-11)}$$

where the change in chemical potential of component 1 is $\Delta\mu_1$ (μ_1-μ_1^0) and component 2 is ($\Delta\mu_2$)μ_2-μ_2^0. The chemical potential of each component is decreased as a result of mixing. With the use of the Flory-Huggins equation, the existence of the critical solution temperature may be determined, where the inflection points on the free energy curves merge. This is defined as the point where the first, second and third derivatives of the free energy with composition are zero:

$$\frac{\partial \Delta G_{mix}}{\partial x_2} = \frac{\partial^2 \Delta G_{mix}}{\partial {x_2}^2} = \frac{\partial^3 \Delta G_{mix}}{\partial {x_2}^3} = 0 \quad \textbf{(2-12)}$$

This may be put into terms of partial molar free energies and this gives the condition for phase separation:

$$\frac{\partial \mu_1}{\partial \phi_2} = \frac{\partial^2 \mu_1}{\partial {\phi_2}^2} = \frac{\partial^3 \mu}{\partial {\phi_2}^3} \quad \textbf{(2-13)}$$

knowing that ΔG_1=(μ_1-μ_1^0), and examining the Flory-Huggins equation in terms of the chemical potential of the pure solvent (μ_1^0) and that of the solvent in solution

$$\frac{\partial \Delta G_{mix}}{\partial N_1} = (\mu_1 - {\mu_1}^0) = RT\left[\ln(1-\phi_2) + \left[1 - \frac{1}{z}\right]\phi_2 + \chi_1 {\phi_2}^2\right] \quad \textbf{(2-14)}$$

where N_1 is the number of solvent molecules. The first derivative of this equation is then

$$(1-\phi_{2c})^{-1} - \left(1 - \frac{1}{x_n}\right) - 2\phi_{2c}\chi_{1c} = 0 \quad \textbf{(2-15)}$$

and the second derivative is

$$(1-\phi_{2c})^{-2} - 2\chi_{1c} = 0 \quad \textbf{(2-16)}$$

These relations all denote critical conditions with the subscript *c*. The composition at which phase separation is first detected (critical composition) is

$$\phi_{2c} = \frac{1}{1 + x_n^{1/2}} \qquad \textbf{(2-17)}$$

A graphical representation of the free energy of the solution with changes in temperature is shown in Figure 2-7. This illustrates the relation of the phase diagram to the free energy curves, and how the phase diagram is thereby obtained as well as the critical point.

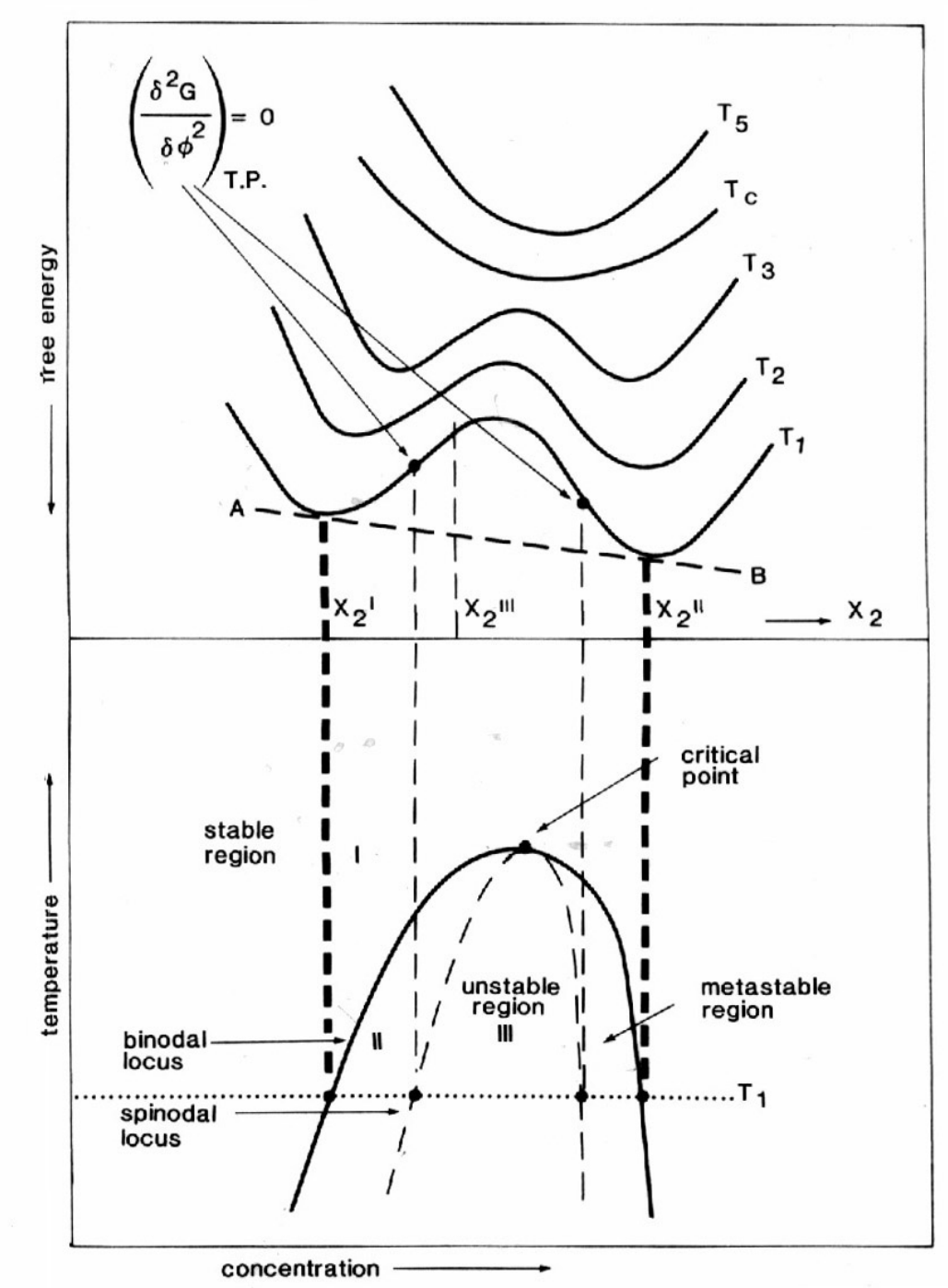

Figure 2-7. Relation of free energy with temperature and resultant phase diagram. After J. M. G. Cowie, Polymers: Chemistry and Physics of Modern Materials, 2nd edition, Blackie Academic and Professional, Glasgow, (1991), p. 162.

Rewriting the Flory-Huggins equation in terms of ϕ_2, we obtain

$$\Delta G_{mix} = \frac{RT}{\overline{V_1}}\left[(1-\phi_2)\ln(1-\phi_2) - \frac{\phi_2}{z}\ln\phi_2 + \chi\phi_2(1-\phi_2)\right] \quad \textbf{(2-18)}$$

where V_1 is the average molar volume of the solvent and z is the ratio of the molar volume of solute to solvent. This allos description of the demixing phenomenon in terms of the second component, which, in the case of a toughened thermoset, is the preformed toughening polymer.

While it was initially assumed that the chi parameter was independent of molecular weight, temperature and concentration, it has been demonstrated subsequently that there are contributions to chi from all of these factors. χ is also recognized to not only represent enthalpic interactions in the model, but works better when considered to be a free energy expression containing entropic as well as enthalpic contributions. There have been many shortcomings pointed out in the Flory-Huggins approach; however, it can yield good predictions, and it allows for useful interpretation of phase separation phenomena. Flory-Huggins theory will be covered in greater depth in Chapter 4. Additionally, it should be emphasized that typical thermodynamic descriptions deal with equilibrium phenomena and, as will be described later, phase separation in toughened thermosets often deviates significantly from equilibrium due to kinetic processes.

2.1.1.5.2 Kinetics of Phase Separation

2.1.1.5.2.1 Nucleation and Growth

In the region between the spinodal and binodal lines of the phase diagram Figure 2-7, a metastable state is formed in which the global system thermodynamics favor phase separation, but only one phase persists because of “local” free energy minima in concentration. Iin the absence of local fluctuation in composition or external stimuli, no

change would occur. Such fluctuations occur continually and eventually cause phase separation but kinetic considerations are now involved. This process is considered kinetically slow. (36) The expression for the rate of nucleation N is

$$N = N_0 e^{-\frac{E_a}{RT}} e^{-\frac{\Delta G^*_n}{RT}} \qquad \textbf{(2-19)}$$

and the rate of growth G is expressed as

$$G = G_0 e^{-\frac{E_a}{RT}} e^{-\frac{\Delta F^*}{RT}} \qquad \textbf{(2-20)}$$

where E_a is the activation energy required for the diffusion of a mixed component to the new phase. The ΔG^* and ΔF^* terms represent the contributions of surface energy per unit area and the free energy of phase separation per unit volume. Nucleation requires energy to create the initial unstable nucleus which is sometimes referred to as the embryo. This nucleus is the consequence of fluctuations in composition and density within the mixture and is discernible from its surroundings in that the surface free energy (or surface tension) of this region is relatively high, leading to the aggregation of a new phase. If the fluctuations are the result of an impurity (another species creates a surface that nucleates the new phase), the nucleation is referred to as heterogeneous. For the case of fluctuations where there is no impurity the nucleation is known as homogenous. The nucleation density is affected by the type of nucleation, whether heterogeneous or homogeneous.

Growth of the phases in this process is driven by the difference between the instantaneous composition and the equilibrium composition. This change in composition lowers the overall free energy of the system by a local diffusion against the concentration

gradient; this is movement from areas of lower concentration to areas of higher concentration. This mechanism will be described in greater detail in Chapter 4.

2.1.1.5.2.2 Spinodal Decomposition

The spinodal decomposition mechanism may also generate a second phase of differing composition from the original mixture. This spinodal process results from phase separation occurring not at a nucleus, but from periodic fluctuations in the local concentration in the mixture. This growth is continuous and fast relative to phase decomposition in the metastable region. The spinodal region occurs beyond the spinodal line in the phase diagram (Figure 2-7); here, thermodynamics dictates that the decomposition occur spontaneously. The kinetics of this mechanism determine the length scale of the domains of each phase that will be produced by the process. The new phase, compositionally rich in one of the components, arises from concentration fluctuations that produce clusterings of molecules. This clustering produces further increases in fluctuation amplitude which increases the diffusion of molecules to the two phases being formed and brings the system closer to thermodynamic equilibrium. This process is depicted in Figure 2-8, which also illustrates the development of microstructure in this phase separation mechanism. Though the developing phases are modeled as a wave with a single frequency, a more realistic portrayal is that of waves of many amplitudes randomly arranged in space. The frequency of these fluctuations remains fixed, though the amplitude increases towards the equilibrium composition.

The intermediate stage of this process is a random and interconnected particle structure, which then begins to change due to interfacial tension. These final changes produce a more spherical microstructure, which minimizes the interfacial energy. This

process (as well as the nucleation and growth mechanism) may be impeded, arrested or prevented in polymerizing thermoset systems due to a concomitant increase of viscosity and gelation. In low viscosity systems, the coalescence of these particles could occur to further minimize the interfacial energy - these could then separate, based on density, to produce a two-layer macroscopically phase separated system.

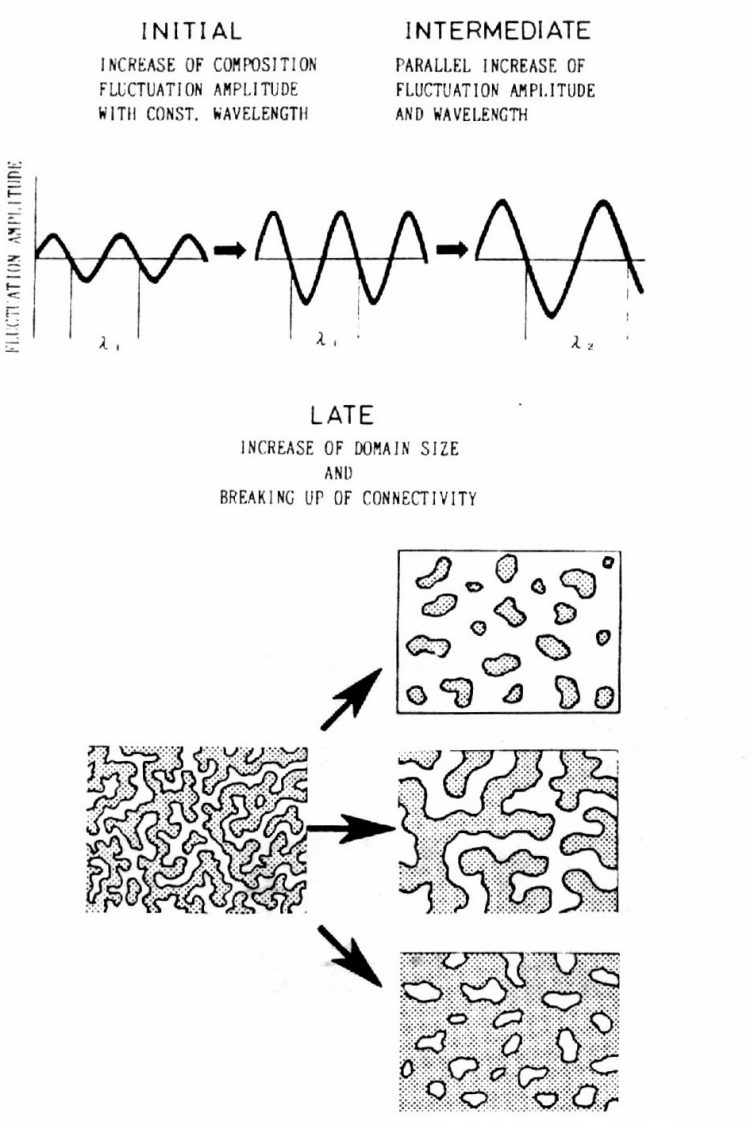

Figure 2-8. Depiction of fluctuations in the spinodal phase separation process, together with evolution of microstructure. After Nakanishi and Soga, Journal of Non-Crystalline Solids, 139, (1992), p. 1.

The spinodal decomposition mechanism may be treated as a diffusion problem. (37) The difference in chemical potential as a result of the concentration fluctuations in a homogeneous binary system is

$$\mu_1 - \mu_2 = \frac{\Delta G}{\partial \psi_1} \qquad \textbf{(2-21)}$$

where the segment fraction of component 1 is ψ_1. If the systems is in the first stages of becoming heterogeneous, there is a concentration gradient and a gradient term may be added to (2-21). It accounts for the difference in chemical potential between the phases, and basically reflects the difference between the areas of nonhomogeneity. This may be represented as

$$\mu_1 - \mu_2 = \left(\frac{\partial G}{\partial \psi_1} \right) - 2K\nabla^2 \psi_1 \qquad \textbf{(2-22)}$$

with K being a constant. This is termed the gradient energy coefficient, which shows the effect of the difference in composition on free energy. This creates a driving force for diffusion, which is

$$\Omega \nabla(\mu_1 - \mu_2) = -j = \Omega \left[\frac{\partial^2 G}{\partial {\psi_1}^2} \nabla \psi_1 - 2K\nabla^3 \psi_1 \right] \qquad \textbf{(2-23)}$$

in which the flux is j and Ω is an Onsager-type coeffieicent. This may be envisaged as a proportionality between the flux and the gradient in chemical potential. The well-known Cahn-Hilliard equation is obtained by substituting a continuity relationship:

$$\frac{\partial \psi_1}{\partial t} = \nabla \cdot \Omega \nabla(\mu_1 - \mu_2) = -\nabla \cdot j = \Omega \left[\frac{\partial^2 G}{\partial {\psi_1}^2} \nabla^2 \psi_1 - 2K\nabla^4 \psi_1 \right] \qquad \textbf{(2-24)}$$

This predicts negative diffusion constants in the phase separation process.

$$\frac{\partial \phi}{\partial t} = M \frac{\partial^2 G}{\partial \phi^2} \nabla^2 \phi - 2k \nabla^4 \phi \quad \textbf{(2-25)}$$

This is Cahn's diffusion equation, with M being a mobility coefficient and k and energy gradient coefficient. This equation is typically solved as follows

$$\psi_1 - \psi_{1,0} = \sum_{\text{all } \beta} \left[\exp[R(\beta)t] \right] \left[A(\beta) \cos(\beta \cdot X) + B(\beta) \sin(\beta \cdot X) \right] \quad \textbf{(2-26)}$$

In this equation, β (wavenumber) is related to the wavelength of the fluctuations by $\beta = 2\pi/\lambda_i$, with λ_i being the wavelength of the fluctuation. The growth rate R(β) is expressed by

$$R(\beta) = -\Omega \beta^2 \left[\frac{\partial^2 G}{\partial \psi_1^2} + 2K\beta^2 \right] \quad \textbf{(2-27)}$$

Here, $\partial^2 G / \partial \psi_1^2$ controls the value of the growth rate, and its sign. Where this term is small and negative, the longer wavelength fluctuations which may grow. The shorter wavelengths only grow as the value becomes a larger negative value. The scale of the phase separation is therefore determined to be

$$\lambda_m = \frac{2\pi}{\beta_m} = 2\sqrt{2} \left[-\left(\frac{1}{2K} \right) \frac{\partial^2 G'}{\partial \phi_1^2} \right]^{-\frac{1}{2}} \quad \textbf{(2-28)}$$

Discerning the mechanism of a system's phase separation mechanism is not straightforward. Though a mutually interconnected phase structure is often considered to be indicative of a spinodal mechanism, it may also result from a nucleation and growth mechanism. The particle interconnectedness (percolation) may originate from interaction of large particles which are formed via a nucleation and growth mechanism that subsequently coalesce.

2.1.1.5.3 Phase Separation in Polymerizing Thermoset Systems

Where a binary system possesses one component of preformed polymer within a "second component" polymerizing matrix, a non-equilibrium phase behavior may be observed. The phase behavior of these systems is important due to the control of morphology which becomes possible depending upon reaction rate, kinetics of phase separation and the interaction thermodynamics of the pair. This may lead to novel structures as will be seen later in this thesis.

Because of the formation of polymer bonds in a crosslinking system, the increase in molecular weight in the system produces changes in the mixing thermodynamics. (38) The so-called equivalent temperature is decreased as crosslinking proceeds. This produces the equivalent of a physical cooling in the system as the reaction proceeds. Therefore, in a phase diagram, the temperature coordinate may be replaced with a conversion coordinate, with higher conversions being equivalent to cooler temperatures. This has been referred to as a "chemical quench". (39) This procedure is utilized in the investigations described below.

As a thermosetting system approaches the gel point, its physical state becomes more elastic than viscous due to the formation of the network. Physically, the retardation of relaxation times runs parallel to changes that a cooling or approaching glass transition might produce. The presence of the polymeric toughener, component 1, may or may not affect the polymerization rate; and, therefore, the rate of this physical transformation accompanying the chemical reaction progress. The phase behavior of a given mixture also may reflect a lower critical solution temperature (LCST) or upper critical solution temperature (UCST) behavior, or some combination of these on heating and cooling.

Considering the effect of chemical reaction as producting an equivalent temperature change, one concludes that as the reaction proceeds there may be an LCST shift to a lower temperature, or a UCST shift to a higher temperature strictly as a result of the chemical process. Where the binary polymerizing system becomes (phase) metastable (passes through the binodal line), the temperature equivalence, in conversion units, is therefore the binodal temperature of the system. If the system obeys UCST type behavior, the polymerization takes the system beyond the binodal line at the cure temperature, and the system may phase separate.

Note that metastable phase separation is a transport process, and hence viscosity dependent. Equilibrium thermodyamics does not consider the physical state (viscosity) of the system, and so the final phase microstructure and/or composition is determined by other factors as well. This produces three possibilities for outcomes of phase separation. The first is high degrees of phase separation due to the binodal conversion being lower than the gel conversion where the time required for phase separation is less than the time to gel. The second is moderate phase separation where the conversion at gelation is close or identical to the binodal conversion where the time to gel is equivalent to the time required for phase separation. Lastly, phase separation may only occur to a very limited extent in which case the conversion at gel is lower than the binodal conversion (time to gel is shorter than the time required to phase separate). These three scenarios are illustrated in Figure 2-9.

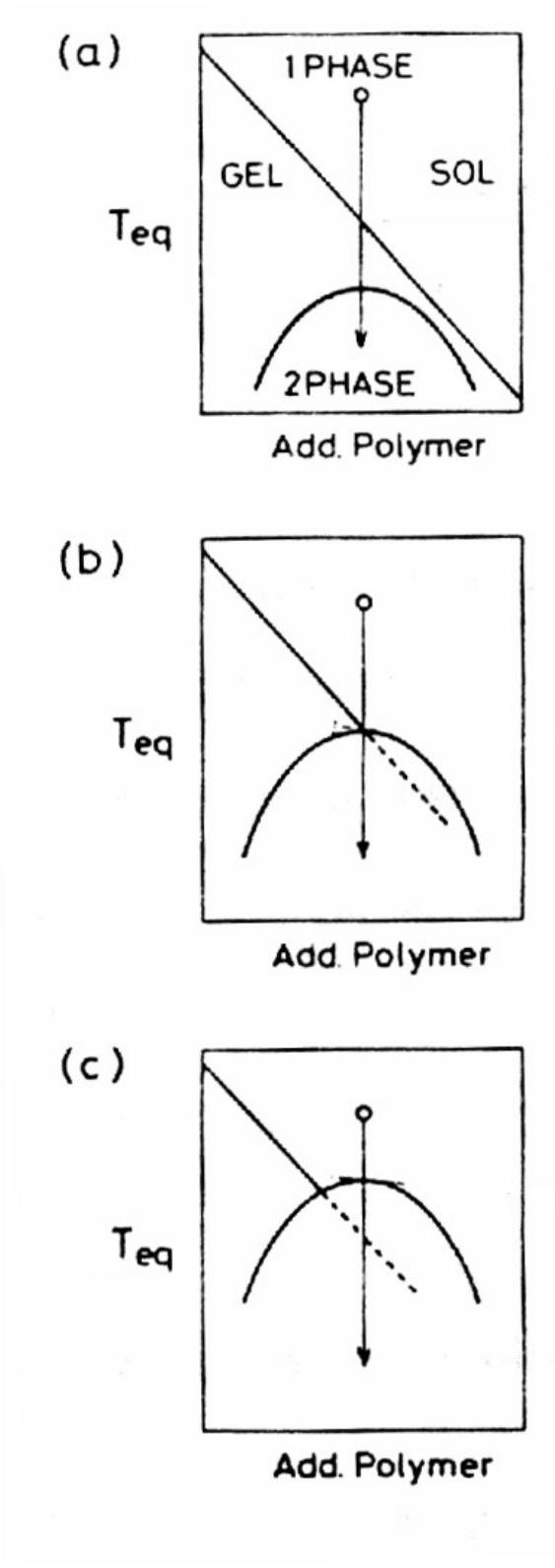

Figure 2-9. Depiction of the various possibilities of phase separation depending on the physical state of the system. In (a), phase separation is impeded by gelation, in

(b), gelation is occurring simulataneously with phase separation, and in (c) phase separation may occur unhindered, prior to gelation. After K. Nakanishi et al., Journal of Non-Crystalline Solids, 139, (1992), p. 1.

In the case of a high degree of phase separation on curing the binary mixture, phase separation has a chance to take place long before gelation. Because of a lower viscosity as phases start to develop, the nucleation and growth mechanism may take place. But, depending on conditions, spinodal decomposition is also a possible mechanism. The dominant path is dependent upon the particular system's stability in the binodal region of the phase diagram. If it becomes unstable, it will phase separate via nucleation and growth; if it stays stable, it encounters the spinodal conditions and phase separation takes place spontaneously. Spinodal phase separation is particularly likely where the initial overall composition is close to that of the critical point.

Where phase separation is more moderately achieved, gelation takes place simultaneously with phase separation. Due to viscosity increases, growth of nucleated particles takes significant time, which allows the cure path to progress through the binodal line and continue through the metastable state to the spinodal condition where phase separation occurs spontaneously. These phase separated domains may coarsen in structure depending on time and the length scale of the network formed. The thermoset rich phase continues to increase in viscosity while the toughener rich material separates to a phase of lower viscosity, depending on its molecular weight, which can affect polymerization kinetics.

Poor phase separation results from gelation occurring while the toughener and thermoset are still in a single phase solution. The equivalent conversion at the binodal line may be reached, but phase separation cannot take place, because high viscosity

prevents the nucleation and growth mechanism from occurring. After gelation, spinodal decomposition may occur even though the network formation is complete. This occurs even though the viscosity prevents growth of dispersed phase particles larger than the decreasing "mesh size" of the network. The result will be an extremely fine dispersion of the toughener within the network.

2.2 Experimental

2.2.1 Producing Gradient Temperature Molds

A controlled thermal gradient cure may be obtained by using the principles of heat transfer by conduction according to Fourier's Law to generate a proper mold design. (40) If a heat source and heat sink maintained at temperatures T_2 and T_1 are connected via a solid bar of area A, the quantity of heat Q flowing in time t maintains a thermal gradient described by

$$q = \frac{1}{A}\frac{dQ}{dt} = -k\frac{\partial T}{dn} \qquad \textbf{(2-29)}$$

where k is the material's constant of thermal conductivity and $\partial T / \partial n$ is the thermal gradient. In practice, these concepts may be applied by placing a special mold between two temperature-controlled press platens, allowing time for equilibration, and calibrating the resulting temperature gradient.

2.2.1.1 Mold Design

Design of an apparatus to provide a linear thermal gradient has been accomplished by targeting for certain desirable assumptions including that the source and sink applied to the mold are of infinite capacity. Additionally, it was desired that the temperature of the curing monomer becomes the temperature of the nearest point on the mold wall; and, further, that the heat released from the material's cure exotherm is

quickly carried away by the mold so that its contribution to the cure temperature is negligible. The exothermic heat rise in curing cyanate ester materials may be considerable (41), especially at high cure temperatures and their accompanying high rates of reaction. Using aluminum for the mold's construction allowed for the high thermal conductivity necessary to carry away the heat of reaction. Finally, the thickness of the sample was kept to a minimum and sample mass was small in comparison to the mold.

Details of the mold construction are shown in Figure 2-10. This mold was designed in three sections so that the cured sample might be easily removed. The front section contains the inlet port (1/4" NPT), together with runners on the reverse side to direct the resin flow into the cavity formed by the center section. The front also contains the outlet port and runners to vent air and excess monomer. There are 1/16" holes drilled regularly down the front of the mold, corresponding to the bottom of the cavity and spaced equally ½" from the top of the mold cavity. The center section was fashioned of 1/8" aluminum, with a cavity 1/4" wide by 2 1/2" high machined in the center. The back section was drilled and tapped to accept bolts to hold the sections together and complete the cavity. Shallow slots were machined down one side on both front and back sections to facilitate prying the mold apart and subsequent removal of the sample.

2.2.1.2 Mold Use

The mold was assembled in two ways: either with the monomer held within or with a valve and syringe fitting in place. The valves used were standard brass air stopcocks (McMaster-Carr), cleaned by disassembling and wiping twice with acetone on all surfaces to remove grease and other contaminants. The valve pieces as well as mold surfaces were sprayed with mold release agent (Miller-Stephenson MS-122N), allowed to dry, and reassembled. The valve was fitted with a ¼" NPT-Luer lock adapter fitting

(syringe adapter) (Popper Company 6333) using thread sealing tape on all threaded joints. Temperature was monitored with an Extech handheld two-channel digital thermometer and an Omega 1/16" K-type thermocouple placed into the monitoring holes on the mold.

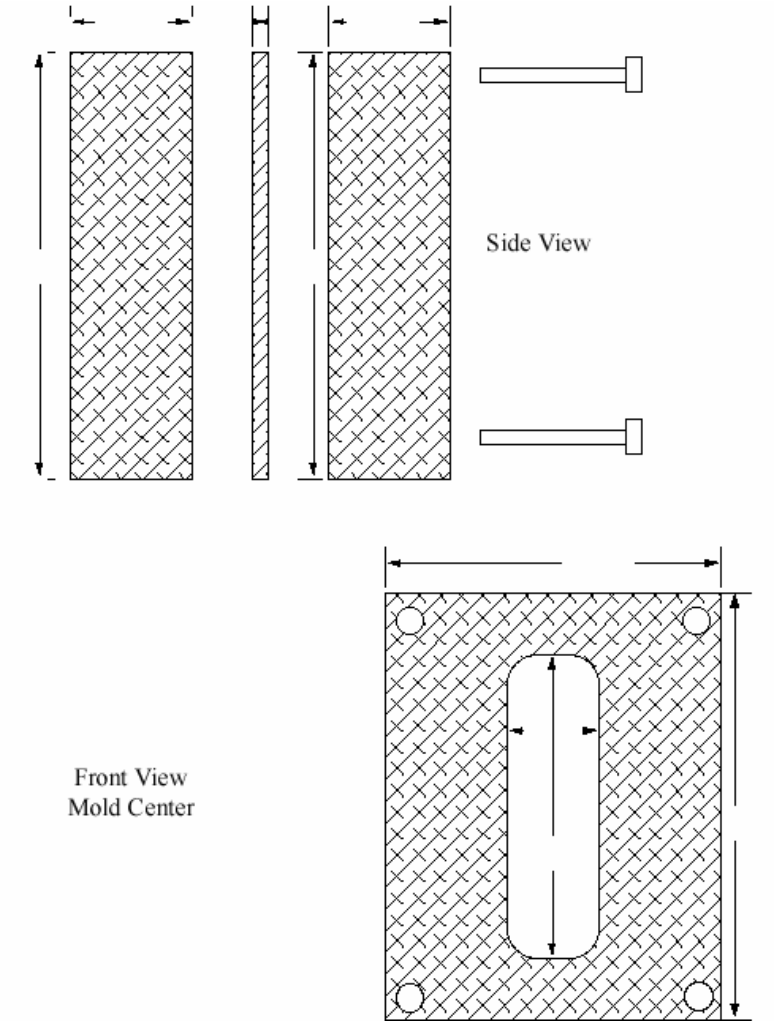

Figure 2-10. Exploded side view depicting mold assembly and front view of mold center section.

Unfortunately, the high thermal conductivity of the aluminum mold requires a large capacity heat source and sink to establish the gradient. The proper quantity of heat for the desired linear temperature gradient depends on the length and cross sectional area of the mold. A suitable heat source was found to be a platen press (PHI model P-210-C)

with 800 watts of heating capacity in each platen. This amount of heat is not sufficient to establish the thermal gradient at the requisite temperature range with the required cross-sectional area, so provisions had to be made to limit the heat flow through the mold. A thin insulating layer of copy paper was placed between the heat sink and the mold to limit the amount of heat flowing through the system. Establishing a stable thermal gradient using this apparatus is subject to variations in the supplied electrical power, the amount of heat dissipated by the heaters in the press platens, the air and water temperature and pressure, and the pressure used to hold the mold between the platens and the resulting intimacy of contact. Therefore, as a practical matter, establishment of the temperature gradient involved a great deal of tweaking of the various parameters. However, with care a suitable temperature gradient could be repeatably formed.

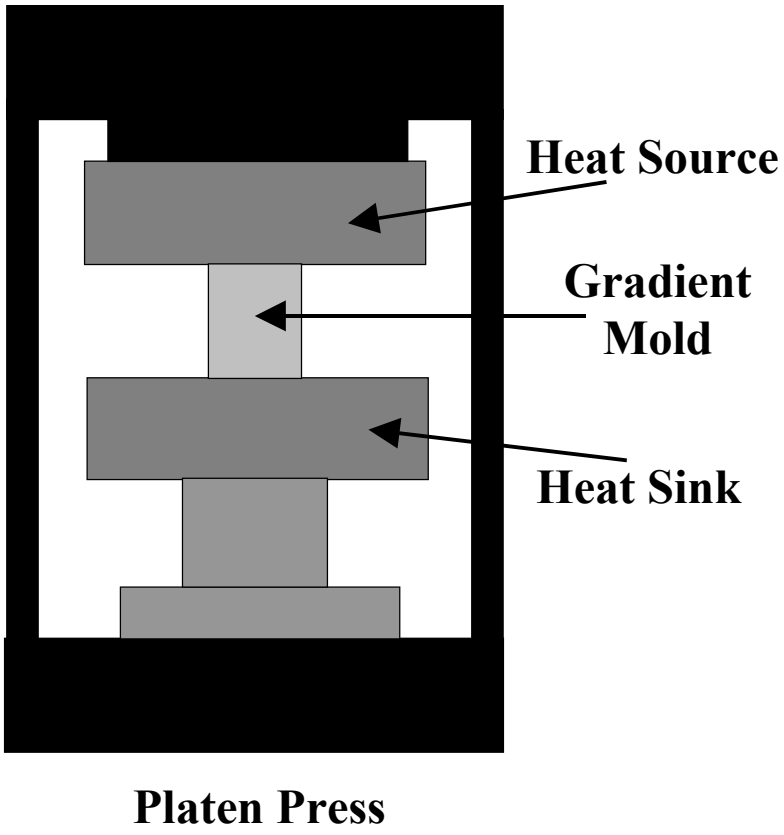

Figure 2-11. Platen press used to provide heat source and sink to gradient mold

Experimental results using thermocouple temperature measurement of the mold close to the interior surface of the cavity indicate that the temperature gradient is both highly stable and highly uniform. (42) (Figure 2-12) Initial gradient samples were prepared in the mold without provisions to introduce the resin system after establishing the gradient - the mold was assembled with monomer in place. However, the stabilization of the temperature gradient required a considerable amount of time relative to the cure process, especially at higher temperatures, and so a method was found to first bring the mold to temperature and then quickly (<10 seconds) introduce the monomer. The mold was therefore modified to accept the valve and syringe fitting. With these modifications, the resin could be introduced into the mold cavity by injection via syringe

after sufficient time to establish and stabilize the temperature gradient had elapsed. The resin system was injected into the preheated mold using a preheated glass syringe with the resin system at 90 °C. The valve was then closed and the cure cycle began.

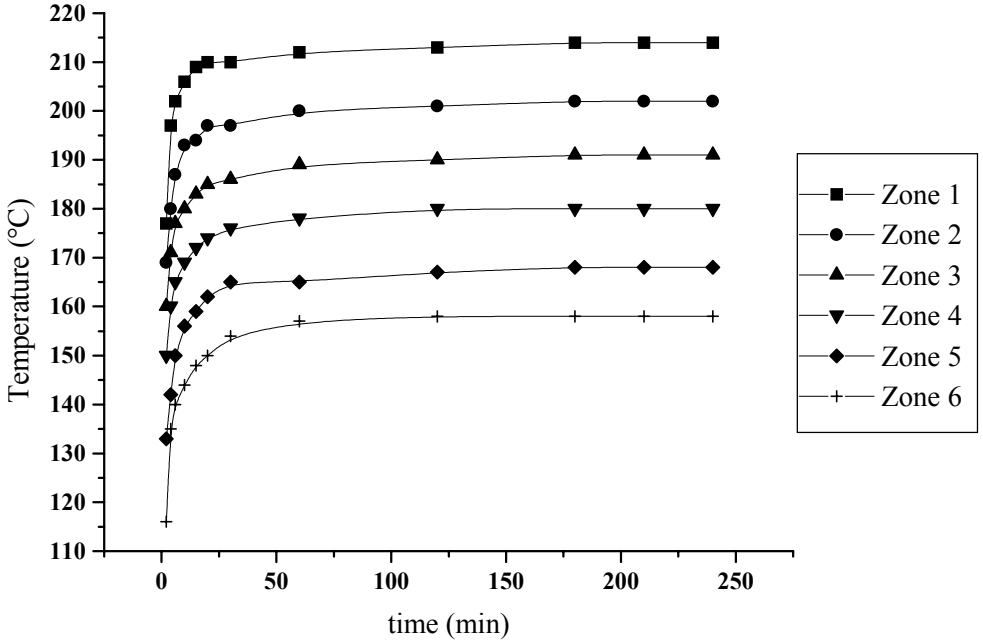

Figure 2-12. Equilibration of gradient mold temperatures.

Cured thermal gradient bars were examined to establish the extent of variation as a result of the gradient processing. Samples were sectioned every ½ inch, corresponding to the location of temperature monitoring holes on the exterior of the mold. The resultant specimens were carefully labelled and microtomed for examination using scanning transmission electron microscopy (STEM). The microtome used was a Reichert-Jung Ultracut and samples were stained using osmium tetroxide. The microscope used was a Philips 420T electron microscope in STEM mode.

2.2.2 Materials

The resin system used in this experiment was based on bisphenol-A dicyanate (BADCy). This material was toughened using a phenolpthalein-based polysulfone ($<M_n>$=15000 g mol^{-1}) having hydroxyl termination. This thermoplastic has been developed and optimized for toughening the polycyanurate. (43, 44) This material system has been shown to produce a large change in microstructure with cure temperature. The cyanate ester monomer was purchased from Ciba (281 Fields Lane, Brewster, NY) and used as received. This polysulfone was synthesized at Virginia Tech, using a procedure outlined previously. (45) Alternatively, a hydroxyl-terminated butadiene-acrylonitrile copolymer (HTBN) ($<M_n>$=3850 g mol^{-1}) was also used to toughen the polycyanurate. This material was supplied by Echo Resins and Laboratory (Rt. 3, Box 359, Versailles, Missouri) and had a specified acrylonitrile content of 9.5% by weight. Catalysis of the cyanate ester polymerization was by aluminum acetylacetonate (Al(acac)) predissolved in nonylphenol. This solution was added to the resin to provide 2 phr nonylphenol and 250 ppm Al(acac). The cure schedule chosen varied; however, in all cases it was followed with a "postcure" step at 250 °C for two hours to bring all systems to an equivalent final degree of cure. For this catalyst system, the chosen cure cycles have been shown to bring the cyanate to high conversions, with confirmed cures for this system greater than 99% (FTIR). (46) The structure of the BADCy is shown in Figure 2-13, and the structure of the polysulfone used is shown in Figure 2-14.

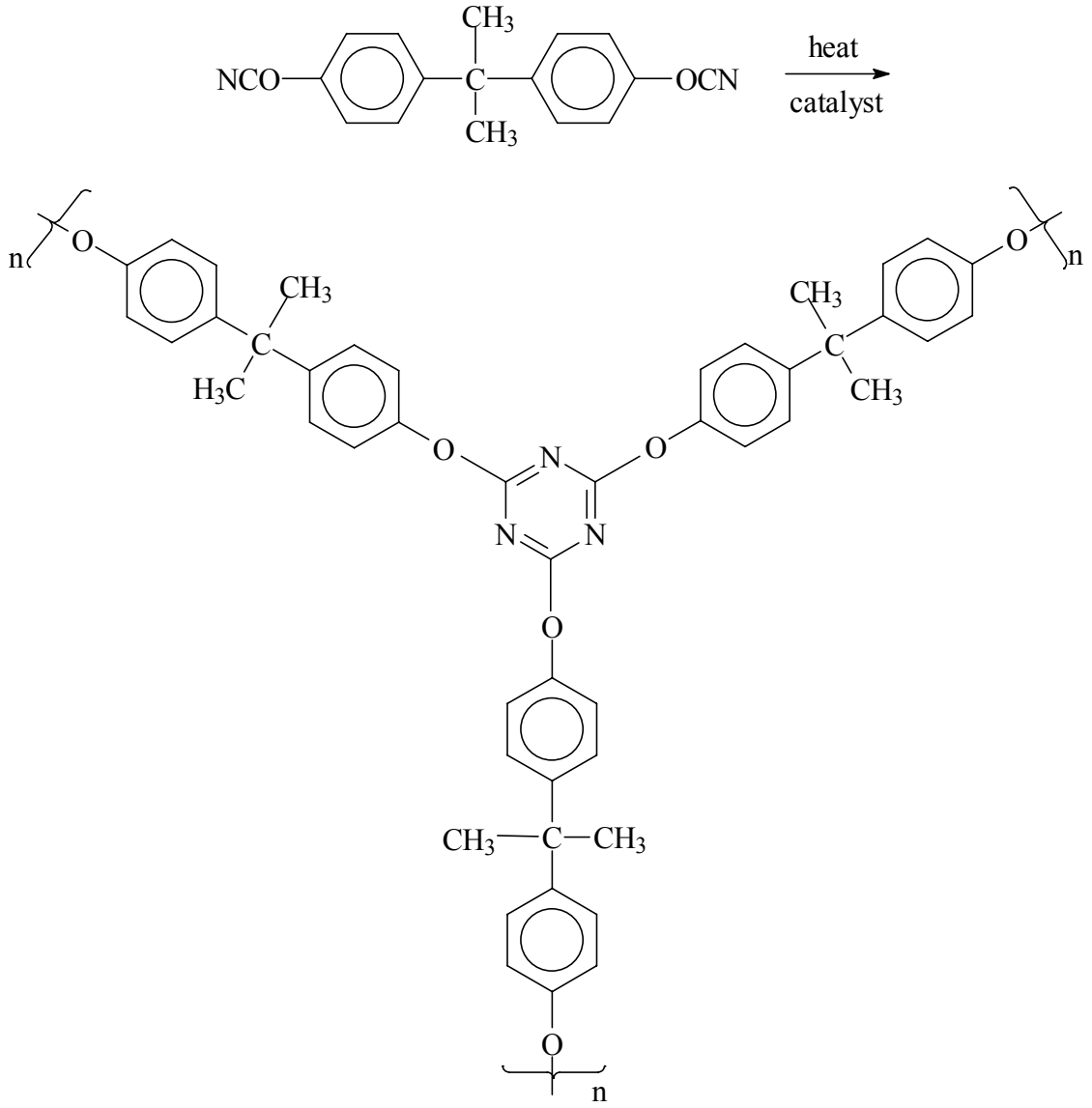

Figure 2-13. Chemical structure of BADCy and resultant polycyanurate.

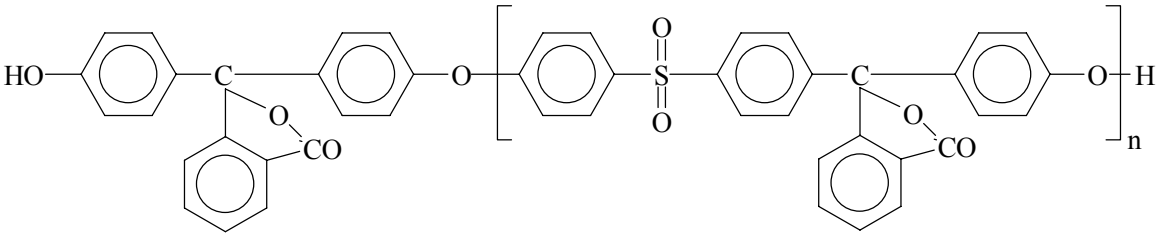

Figure 2-14. Chemical structure of polysulfone utilized.

2.3 Results

2.3.1 Scanning Transmission Electron Microscopy

Microscopy results for the initial two gradient polycyanurate samples toughened with the polysulfone are shown in Figure 2-15 and Figure 2-16. These specimens were cured in the thermal gradient; however, the exact cure temperatures were not isotherms as a result of the time required to establish the gradient. Note that at the initial temperature range chosen, the observable changes in microstructure were small. The process of development of microstructure is tied to reaction rate, and the reaction rates at the lower temperatures are expected to be much smaller than in the higher cure temperature case (47) (this will be explored in greater depth in Chapter 4). Here, the monomer mixture was placed in the mold at room temperature, secured in the gradient apparatus, and heated until the temperature gradient was established. This produces an undesirably large variation in cure temperature at a given spatial location in the gradient and, subsequent to these experiments, the new method of injecting the sample (described earlier in this chapter) into the preheated mold was developed.

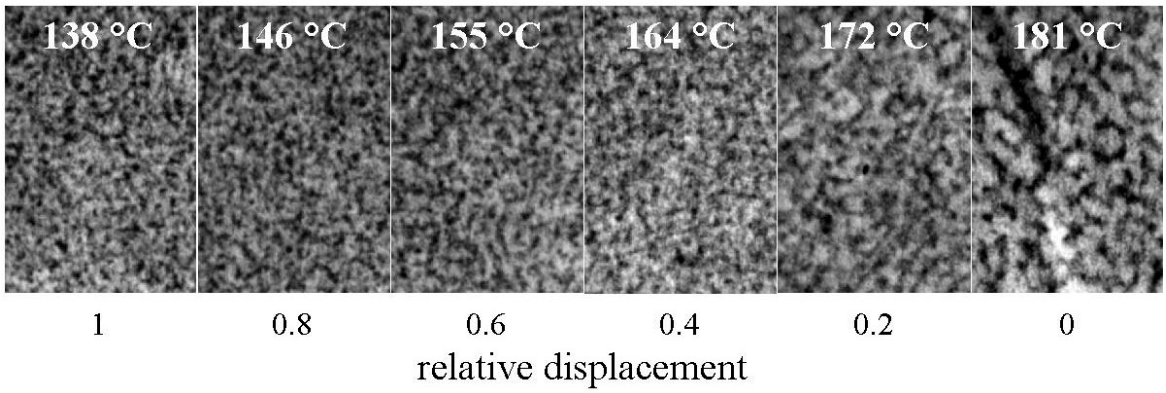

Figure 2-15. Gradient microstructure, 25 weight% polysulfone in polycyanurate, relative displacement over 2.5 inches from hottest end, 181 °C to 138 °C gradient. (12500X)

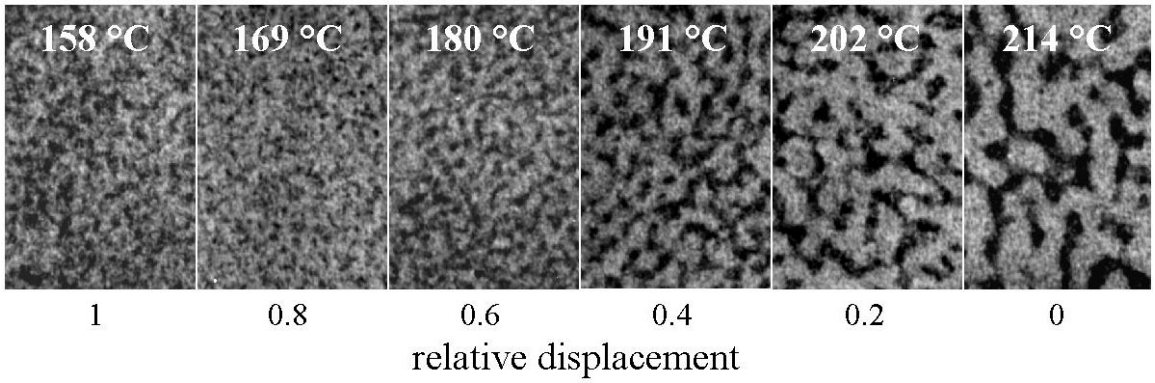

Figure 2-16. Gradient microstructure, 25 weight% polysulfone in polycyanurate, relative displacement over 2.5 inches from hottest end, 214 °C to 158 °C gradient. (12500X)

Gradient temperature cured samples were prepared using the injection technique described previously. Two temperature ranges were explored, 158 °C to 222 °C and 191 to 247 °C. These injected samples were cured using the same mold-method as with the previous samples, and their microstructures are shown in Figure 2-17 and Figure 2-18. It is clear from these figures that a dramatic change in polymer morphology exists from end-to-end over both temperature gradients. Coarse-grain structures are seen at higher cure temperatures versus fine-grained structures at the lower cure temperatures.

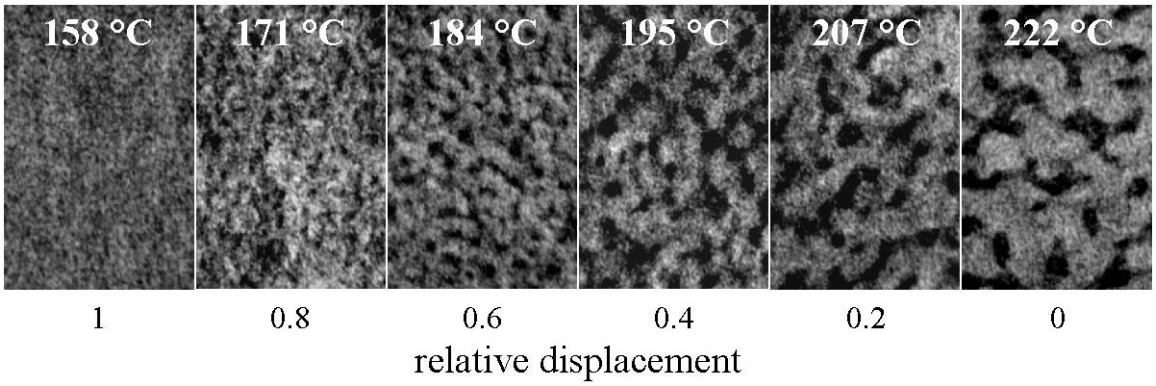

Figure 2-17. Gradient microstructure, 25 weight% polysulfone in polycyanurate, relative displacement over 2.5 inches from hottest end, 222 °C to 158 °C gradient. (12500X)

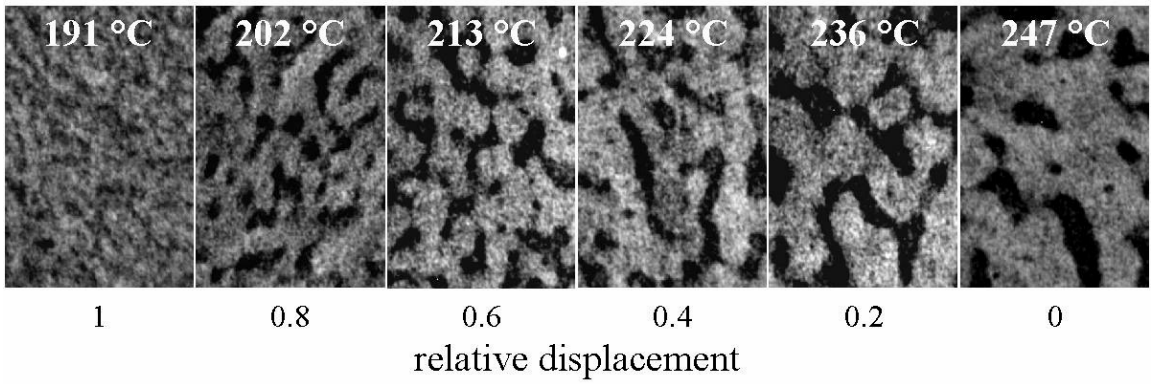

Figure 2-18. Gradient microstructure, 25 weight% polysulfone in polycyanurate, displacement from hottest end, 247 °C to 191 °C. (12500X)

The various characteristic microstructures observed in Figures 2-16 through 2-18 formed depending upon the specific conditions and competitions taking place in the phase separation mechanisms. Some workers have attempted to identify the exact mechanism of phase separation based upon the appearance of the resultant microstructure. This approach has been shown to be inaccurate due to the microstructural changes that may occur after phase separation has occurred. (48) If the matrix material remains of a sufficiently low viscosity, then either Ostwald ripening (in the case of

dispersed structures) or a coarsening due to interfacial tension will occur (in the case of interconnected structures). (49) These may mask the original structure produced by the initial phase separation process.

This present system in this research has been theorized to phase separate via a spinodal mechanism. (50) This proposal is reinforced by the relatively high molecular weight of the toughener, the typical level of the initial toughener concentration, and the usually observed resultant microstructure. Photomicrographs taken during the phase separation process support this conclusion. (51) The change in particle size scale with cure temperature is pronounced as noted above. The present results agree with what has been previously found for this system. (52)

A second type of toughener, having a much lower glass transition, was of interest for contrasting the phase separation process. The hydroxyl-terminated butadiene-acrylonitrile (HTBN) described above was chosen. The gradient sample toughened with 5% by weight of HTBN also demonstrates a pronounced particle size dependence on cure temperature. (Figure 2-19) The particle size trend is reversed from that found for the polysulfone-toughened samples, however. The particle geometry now appears spherical, while in the preceding case the particles were of random shape. Though spherical particles alone cannot conclusively determine the phase separation mechanism, the small initial concentration of this HTBN toughener initially used, along with its relatively low molecular weight, suggest that a nucleation and growth mechanism is likely in this case. These assumptions will be examined in greater depth in Chapter 3 and Chapter 4.

The HTBN particle size decreases with increasing cure temperature, and the number of particles per unit area is much larger. This fine versus coarse grained structure is opposite of that for the polysulfone toughener. Typically, it has been suggested for the case of rubber toughened epoxies (with a rubber toughener very similar to the current HTBN-modified cyanate ester system) that the decrease in particle size was attributable to a smaller volume fraction of phase-separated toughener. Also, a higher cure temperature impedes the phase separation process as described previously. However, in some cases, it has been shown using DMA (53) or particle size analysis that the actual volume fraction of toughener is quite similar at various cure temperature extremes.

The particle size and distribution are important to physical properties of these thoughened high T_g polymers. If the volume fractions of phase separated toughener are similar for all cure temperatures, it is necessary to examine the other possible contributions to particle size variation. Williams et al. have developed a model for phase separation in toughened thermoset resins that considers many factors affecting microstructural development. These include reaction kinetics, diffusion, nucleation and surface energy, and rheology. (54) This sophisticated model predicts several possible effects of cure temperature on particle size development, depending on the system parameters. It is clear, however, that cure temperature can increase the particle nucleation density and therefore produce smaller particles in larger number. On initial inspection this distribution of particles can appear to represent a smaller volume fraction of toughener-rich phase. This type of system could serve to demonstrate the variability of fracture toughness with particle size (as opposed to volume fraction). While some toughener studies have indicated the dependence of fracture toughness on particle size

(55), others indicate that the volume fraction may be a more important factor. (56) The Williams model for phase separation is illuminating in this regard and its application will be covered in greater depth in Chapter 4.

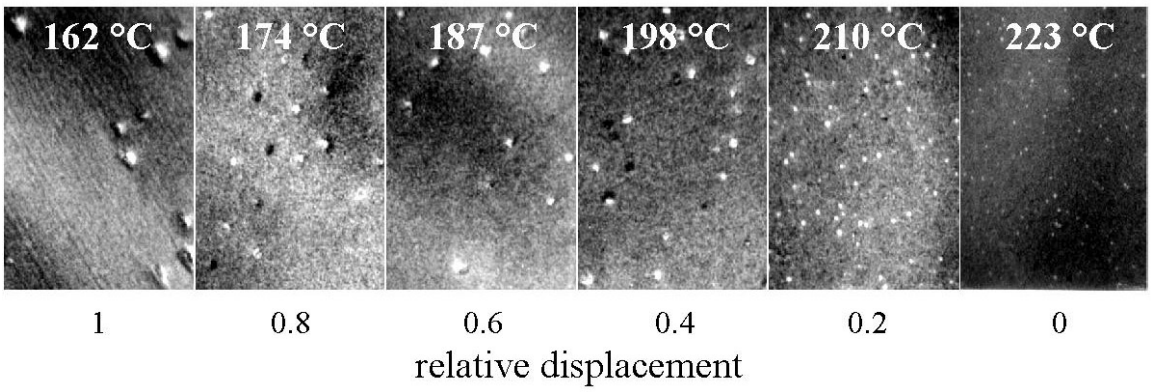

Figure 2-19. Particle size variation in gradient temperature cured polycyanurate with 5% HTBN. (STEM, 6400X)

2.3.2 Fracture Toughness

Changes in cure cycle and temperature of toughened thermosetting resins have been reported to produce large changes in the properties of high performance polymers. (57) Because this thesis deals with temperature gradient cures this background is relevant. Thus, it is important to understand how cure temperature affects each of the characteristic polymer properties specifically; however, for the current discussion, the effects of cure temperature on the particle size will be the focus. The effect of particle size on toughness in thermoset resins has long been the subject of debate and the results of the various studies are often contradictory. (58, 59, 60, 61, 62, 63, 64). It is reasonable to conclude that particle size distribution may have a significant effect on toughness of the system.

2.3.2.1 Fracture Toughness Testing

Fracture toughness testing was accomplished using a three point bending apparatus on an Instron 5500R universal testing machine. Specimens were prepared by casting in a preheated aluminum mold at the cure temperature to obtain a sample with a homogeneous (non-gradient) cure temperature. Fracture specimens and test details conformed to ASTM D5045-96. Specimens were cracked using a liquid nitrogen cooled razor blade. Additional details of the fracture toughness experiments, together with literature survey on this topic, are provided in Chapter 3.

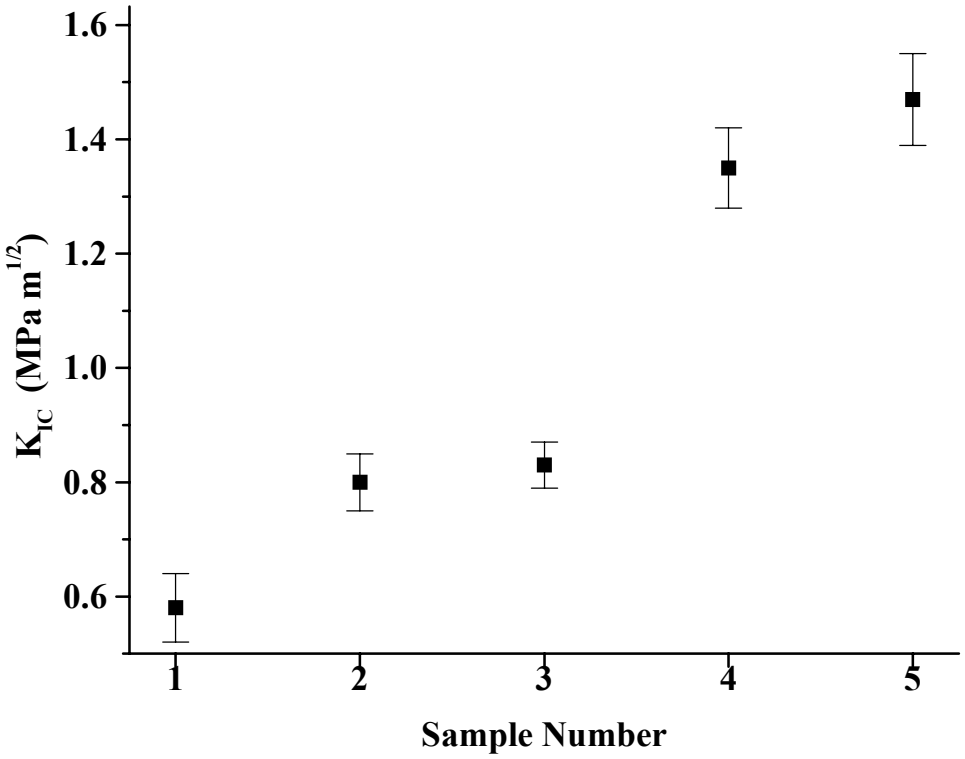

Figure 2-20. Variation of fracture toughness with cure cycle. Sample (1) is neat polycyanurate, (2) is 5% HTBN cured at 150 °C, (3) is 5% HTBN cured at 210 °C, sample (4) is 25% polysulfone cured at 150 °C, and sample (5) is 25% polysulfone cured at 210 °C.

The fracture toughness results are shown in Figure 2-20. The untoughened reference sample is sample 1, showing reasonable toughness for a high T_g thermoset resin. The next samples, 2 and 3, are those modified with 5% HTBN and cured at 150 °C and 210 °C, respectively. There is an approximately 30% improvement in fracture toughness produced by the toughener due to the due to the resulting small volume fraction of toughener-rich phase. The fracture toughness difference brought about by varying the cure temperature is small, especially when viewed in light of the large difference in microstructure that should be produced by these cure cycles as discussed previously. The extent of phase separation could result in a smaller volume fraction of particles for the higher cure temperature, but the fracture toughness result in this case is actually slightly higher, though it is within statistical significance. This suggests that the smaller particle size is at least as effective as a toughener as are the large particles, at least within the range of consideration here. The higher cure temperatures should produce a smaller particle size due to the onset of gelation "freezing" the process while phase separation is occurring. The observed results suggest that gelation occurs well after phase separation which allows the phase separation mechanism time to approach thermodynamic equilibrium.

Samples 4 and 5 in Figure 2-20 are the 150 °C and 210 °C cured 25% polysulfone toughened materials. Here, good improvements in fracture toughness (great than 100%) were obtained, in agreement with previous results. However, the large variation in particle size that should result from the two cure cycle differences for these samples does not produce significant differences in measured fracture toughness. Because the phase separation mechanism is thought to be spinodal, the volume fractions of phase separated

toughener should be very similar for each cure temperature. This again suggests that volume fraction of toughener is a more important factor for performance in this case than particle size.

2.4 Conclusions

Functionally gradient samples of toughened thermoset have been prepared using a thermal gradient mold which produces a well-defined gradient cure temperature along a single 2.5 inch long specimen. The thermal gradient mold produces linear, stable thermal gradients which, when combined with an injection technique, provides excellent control of cure conditions within the sample.

The toughened thermoset properties examined, particle size and fracture toughness, show widely varying effects as a result of the gradient cure temperature. Particle size in both the polysulfone and HTBN-toughened samples shows strong cure temperature dependence. While this has been theorized to produce significant changes in fracture toughness, no difference in this property is evident from the present data within statistical significance. Because many properties in toughened thermosets are affected by cure temperature, additional work is necessary to elucidate these changes. Thus, additional systems must be developed and investigated.

2.5 References

(1) N. Cherradi, A. Kawasaki, and M. Gasik, Composites Engineering, 4, (1994), p. 883.

(2) S. Montarnal, J. P. Pascault, and H. Sautereau. In *Rubber-Toughened Plastics*, C. Keith Riew, Editor, Advances in Chemistry Series 222, ACS, Washington, D. C., (1989), p. 204.

(3) A. C. Loos, Journal of Composite Materials, 17, (1983), p. 158.

(4) M. Koizumi, "The Concept of FGM", Functionally Gradient Materials, J. B. Holt, M. Koizumi, T. Hirai, and Z. A. Munir, eds., Ceramic Transactions, 34, (1993), p. 3.

(5) B. Ilscher, Proc. First International Symposium on FGMs, Sendai, Japan,

M. Yamanouchi, et. al., eds., (1990), p. 101.
(6) N. Cherradi, A. Kawasaki, and M. Gasik, Composites Engineering, 4, no. 8, p. 885.
(7) M. Shen and M. B. Bever, Journal of Materials Science, 7, (1972), p. 741.
(8) S. Amada, T. Munekata, Y. Nagase, Y. Ichikawa, A. Kirigai, and Y. Zhifei, Journal of Composite Engineering, 30(7), (1996), p. 800.
(9) N. Cherradi, A. Kawasaki, and M. Gasik, Composites Engineering, 4, no. 8, p. 886.
(10) M. Takahasi, Y. Itoh and H. Kashiwaya, Proceedings of the First International Symposium on FGMs, M. Yamanouchi et. al, eds., (1990), p. 129.
(11) Yu. S. Lipatov, L. V. Karabonova, Journal of Materials Science, 30, (1993), p. 2475.
(12) M. Shen and M. B. Bever, Journal of Materials Science, 7, (1972), p. 741.
(13) Ibid., p. 744.
(14) M. Z. Elsabee, M. Dror, and G. C. Berry, Journal of Applied Polymer Science, 28, (1983), p. 2151.
(15) G. Akovali, K. Biliyar, and M. Shen, Journal of Applied Polymer Science, 20, (1976), p. 2419.
(16) M. Dror, M. L. Elsabee, and G. C. Berry, Journal of Applied Polymer Science, 26, (1981), p. 1741.
(17) Yu. S. Lipatov, L. V. Karabanova, L. A. Gorbach, E. D. Lutsyk and L. M. Sergeeva, Polymer International, 28(2), (1992), p. 99.
(18) Yu. S. Lipatov, Journal of Materials Science, 30, (1993), p. 2475.
(19) Yu. S. Lipatov, L. M. Sergeeva, L. V. Karabanova, V. F. Rosovitskii, L. A. Gorbach, and N. V. Babinka, Mekhanika Kompozitnykh Materialov, no. 6, (Nov.-Dec. 1988), p. 1033.
(20) G. Akovali, K. Biliyar, and M. Shen, Journal of Applied Polymer Science, 20, (1976), p. 2419.
(21) Yu. S. Lipatov, L. N. Perepelitsina and V. F. Babich, Mekh. Kompoz. Mater., 4, (1986), p. 585.
(22) G. C. Martin, E. Enssani and M. Shen, Journal of Applied Polymer Science, 26, (1981), p. 1465.
(23) Yu. S. Lipatov and L. V. Karabanov, Journal of Materials Science, 30, (1993), p. 2481.
(24) G. C. Martin, E. Enssani and M. Shen, Journal of Applied Polymer Science, 26, (1981), p. 1465.
(25) G. Akovali, K. Biliyar, and M. Shen, Journal of Applied Polymer Science, 20, (1976), p. 2419.
(26) G. C. Martin, E. Enssani and M. Shen, Journal of Applied Polymer Science, 26, (1981), p. 1465.
(27) G. Akovali and A. Labban, in IUPAC macro Florence, 1980, International Symposium on Macromolecules Preprint, Pisa, 3, (1980), p. 264.
(28) H. C. Kim, A. M. El-Naggar, and G. L. Wilkes, Journal of Applied Polymer Science, 42, p. 1107.
(29) J. C. Kaerger, http://dynamik.fb10.tu-berlin.de/~hinrichs/kaerger/kaerger.html.
(30) Yu. S. Lipatov, L. M. Sergeeva, O. A. Novikova and M. I. Glukhovskaja, Khim.

Volokna, 4, (1983), p. 14.
(31) Y. Ohtsuka, Applied Physics, 23, (1973), p. 247.
(32) F. J. Bayley, J. M. Owen, and A. B. Turner. Heat Transfer. Barnes and Noble, Publishers, (1972), p. 15.
(33) H. J. Sue, E. I. Garcia-Meitin, D. M. Pickelman, and P. C. Yang. In *Toughened Plastics I: Science and Engineering*, C. Keith Riew,and A. J. Kinloch, Editors, Advances in Chemistry Series 233, ACS, Washington, D. C., 1993, p. 256.
(34) M. L Huggins, J. Phys. Chem, 36, (1942), p. 151.
(35) P. J. Flory, J. Chem. Phys., 10, (1942), p. 51.
(36) O. Olabisi, L. M. Robeson and M.T. Shaw, Eds., Polymer-Polymer Miscibility, Acadamic Press Inc., (1979), p. 19.
(37) J. W. Cahn and J. E. Hilliard. Chemical Physics, 28, (1958), p. 258.
(38) P. G. deGennes, Scaling Concepts in Polymer Physics, Cornell University Press, Ithaca, New York, (1979), chapter 5.
(39) J. P. Pascault, J. Galy and F. Méchin, Additives and Modifiers for Cyanate Ester Resins, in Chemistry and Technology of Cyanate Ester Resins, Ian Hamerton, Ed., Blackie Academic and Professional, London, 1994, p. 137.
(40) F. J. Bayley, J. M. Owen, and A. B. Turner. Heat Transfer. Barnes and Noble, Publishers, (1972), p. 15.
(41) Rhone-Poulenc Technical Document, Specialty Resins-Formulating AroCy Cyanate Esters for Resin Transfer Molding Applications, (1992), p. 3.
(42) D. S. Porter, L. T. James, and T. C. Ward. Proceedings of the 20th Annual Meeting of the Adhesion Society, (1997), p. 40.
(43) S. A. Srinivasan and J. E. McGrath. Journal of Applied Polymer Science, 64, (1997), p. 167.
(44) S. A. Srinivasan and J. E. McGrath. Polymer, 39, (1998), p. 2415.
(45) S. A. Srinivasan, Ph. D. Dissertation, Virginia Polytechnic Institute and State University, (1994), p. 138.
(46) Ibid, p. 153.
(47) Ibid, p. 319.
(48) K. Yamanaka and T. Inoue, Polymer, 30, (1989), p. 662.
(49) L. P. McMaster, ACS Advances in Chemistry Series, 142, (1975), p. 43.
(50) Dr. S. A. Srinivasan, personal communication.
(51) S. A. Srinivasan, Ph. D. Dissertation, Virginia Polytechnic Institute and State University, (1994), p. 280.
(52) S. A. Srinivasan, Ph. D. Dissertation, Virginia Polytechnic Institute and State University, (1994), p. 275.
(53) A. J. Kinloch and D. L. Hunston. Journal of Materials Science Letters, 6, (1987), p. 137.
(54) R. J. J. Williams, J. Borrajo, H. E. Adabbo, A. J. Rojas, In *Rubber-Modified Thermoset Resins*; C. K. Riew and J. K Gillham, Eds. Advances in Chemistry 208, ACS, Washington D.C., (1984), p. 195.
(55) A. J. Kinloch. In *Rubber-Toughened Plastics*, C. Keith Riew, Editor, Advances in Chemistry Series 222, ACS, Washington, D. C., 1989, p. 79.
(56) S. C. Kunz, J. A. Sayre, and R. A. Assink. Polymer, 12, (1982), p. 1897.
(57) S. Montarnal, J. P. Pascault, and H. Sautereau. In *Rubber-Toughened Plastics*,

C. Keith Riew,Editor, Advances in Chemistry Series 222, ACS, Washington, D. C., 1989, p. 204
(58) F. A. Yee and R. A. Pearson. Journal of Materials Science, 21, (1986), p. 2462.
(59) L. C. Chan, J. K. Gillham, A. J. Kinloch, S. J. Shaw. In *Rubber-Modified Thermoset Resins*, C. K. Riew and J. K. Gillham, Eds., Advances in Chemistry 208, ACS, Washington, D.C., (1984), p.261.
(60) A. J. Kinloch and D. L. Hunston. Journal of Materials Science Letters, 6, (1987), p. 13.
(61) C. B. Bucknall and T. Yoshii. British Polymer Journal, 10, (1987), p. 53.
(62) S. C. Kunz, J. A. Sayre, R. A. Assink. Polymer, 12, (1982), p. 1897.
(63) J. N. Sultan and F. J. McGarry. Journal of Polymer Engineering and Science, 13, (1973), p. 29.
(64) W. D. Bascom, R. Y. Ting, R. J. Moulton, C. K. Riew, A. R. Seibert. Journal of Materials Science, 16, (1981), p. 2657.

Chapter 3. Development of Model Toughened Thermoset Systems

3.1 Introduction

The usefulness of high performance thermosetting polymers depends upon their unique properties: good processibility, high temperature capabilities, good adhesive properties and low creep. However, these thermosetting materials often suffer from excessive brittleness arising from the high crosslink density that is responsible for many of the desirable properties. To offset this tendency, toughening agents have been employed to enhance the fracture properties. Unfortunately, the introduction of tougheners is not without disadvantage. Tougheners, especially lower molecular weight materials with low glass transition temperatures, can lower high temperature performance, e.g. modulus, while simultaneous significantly improving toughness. (1)

Negative contributions to properties as a result of toughener incorporation may be aggravated by details of the cure schedule. It is difficult to overstate the importance of cure schedule on toughened thermoset responses. Cure conversion, morphology, glass transition temperature, toughness, and tensile strength, among other important properties, depend on not only the extent of cure, but the particular processing pathway taken to obtain that given degree of cure. (2) This effect is due to the multiple nature of the mechanisms of formation of the toughened systems. Typically, a second phase rich in the toughener component is formed during a cure which begins from an initially homogeneous solution. It is the presence of this second toughener-rich phase that improves the fracture toughness, a situation demonstrated in Chapter 2. The exact composition of both thermoset-rich phase and toughener rich phase is affected by the cure temperature since both components of the binary system are dissolved in both phases.

Selection of the toughener thus presents many contradictory requirements. Examples are as initial solubility, degree of phase separation upon cure, control of morphological features, and overall thermal stability of each phase. Additionally, the greatest improvement in toughness is usually found with elastomeric inclusions (3), and better adhesion of the resultant particles to the continuous phase is produced by toughener chain terminations which chemically react with the resin. The above properties can often be mutually exclusive, complicating selection of a material.

In this thesis, systematic study has been made of two commercial materials as tougheners for polycyanurates. Investigation of thermal stability, oxidative stability, phase separation, microstructure and toughening efficacy is presented in this chapter to determine the suitability of these materials in view of several cure and use conditions. Two extremes of cure cycle were used to determine the variability of final properties on processing. Comparison was made of the effects of these two cure conditions and also relative to the other toughener. This research leads to materials which allow a more detailed study of gradient cure process and of cure temperature/property variations in general.

3.1.1 Literature Review

3.1.1.1 Thermosetting Polymers

Thermosetting materials are those polymeric species which form three dimensional interconnected molecular networks which will not dissolve or flow on heating unless chemically degraded. This is accomplished through covalent bonding which incorporates branch points sufficient to produce an "infinite" molecule, or gel. This overall reaction is known as the curing process and it develops the properties we usually associate with thermoset polymeric materials such as strength and rigidity even while having the convenience of easily soluble and fluid

starting materials. It is the time-temperature profile of this cure with respect to final structure that is to be explored in this chapter.

Advancing the cure reaction of a thermoset produces an increase in the crosslink density and average molecular weights in a sequence which determines the properties of the cured polymer. A higher value of crosslink density typically yields an increase in modulus, glass transition temperature and, to some degree, tensile strength. After a point, the increase in crosslink density produces a highly crosslinked structure which requires long times for molecular relaxation associated with the covalent links with neighboring chemical units, combined with the rising glass transition. Such long relaxation times lead to brittle characteristics as well as low elongation to failure. Crosslinked species that form thermosets can be produced from chemical reactions which join molecules so long as the average functionality of the reacting species and the conversion are sufficient. In Figure 3-1 is a representation of the polymerization stages as a network is generated from various monomer units. The most important quantity characterizing the network is the crosslink density, in moles per unit volume, which is easily converted to an inversely related average molecular weight between crosslinks via the density and Avogadro's number.

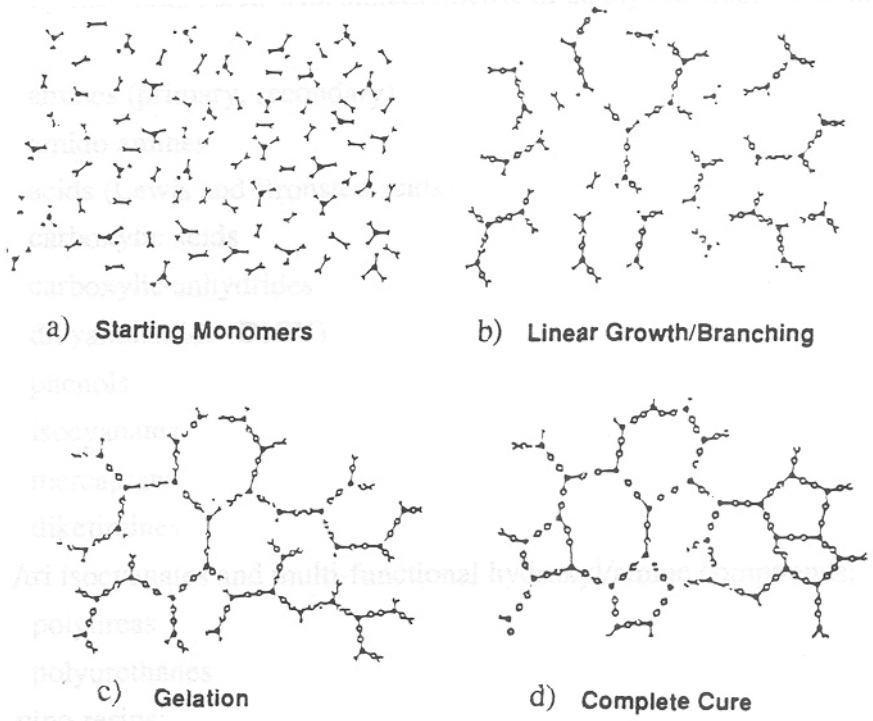

Figure 3-1. Schematic of thermoset polymerization. After Turi, Thermal Characterization of Polymeric Materials, Academic Press, Inc., 3rd edition, (1991).

The resultant crosslinked species in panel d) of Figure 3-1 shows a model of an insoluble, infusible network created in three dimensional space. The equivalent of salvation of linear polymers is swelling with a solvent to form a gel for the network. As mentioned above, a characteristic of networks is the absence of any viscous flow (assuming no chemical changes take place), and an essentially constant modulus above the glass transition temperature where rubbery elastic behavior is observed. The point where the weight average molecular weight of the polymerizing reaction mixture increases to infinity is termed the gel point. The gel point is not necessarily the point of ultimate reaction; actually, the reaction may proceed past the gel point to further increase the crosslink density at the expense of the soluble fraction of reactive species, which is the quantity per volume of crosslinks. This portion of the sample which is not covalently linked into the three dimensional network is called the sol fraction and typically is

determined by extractions and weighing. The residual insoluble portion is the gel fraction, and the conversion, *p*, at first gel formation is the gel point.

3.1.1.2 Statistical Prediction of Molecular Weights and Gelation Point

The gel point of many possible crosslinking reactions have been explored and may be classified in one of several ways. The Carothers equation (4) defines a gel point where the number average degree of conversion approaches infinity for a step-growth polymerization as $p_{gel}=(2/f_{avg})$ where f_{avg} is the average functionality of the reactants and p_{gel} is the extent of reaction at the gel point. This equation does not hold for the case where the reactants are not of equivalent functionality. Typically, it also usually calculates an excessively high gel point.

A statistical approach to gel point prediction was taken independently by Flory (5) and Stockmayer for step growth chemistries. (6) These theories predict a gel point beginning with the relationship

$$M_{w(p)} = \frac{M_{w(0)}(1+p)}{(1-p)(f-1)} \qquad \textbf{(3-1)}$$

where $M_{w(0)}$ is the weight average molecular weight before reaction, $M_{w(p)}$ is the weight average molecular weight at a given time, and f is the weight average functionality of the reacting species. As $M_{w(p)}$ goes to infinite molecular weight, the gel point becomes

$$p_{gel} = \frac{1}{f-1} \qquad \textbf{(3-2)}$$

This expression does not consider such non-ideal conditions such as reactants of unequal functionality, reactivity changes during polymerization diffusion limitations of reactivity, and polydispersity of reactants. For systems of two species of differing functionality, the gel point is given by

$$(p_{gel})^2 = \frac{1}{r(f_A - 1)(f_B - 1)} \quad \textbf{(3-3)}$$

where f_A and f_B are the weight average functionalities of the species, N_A and N_B are the numbers of each type of molecule, and $r=N_A/N_B$. This equation holds if species A and B are present in stoichiometrically balanced quantities, only one type of functional group is present on each molecule, and the reaction between A and B is the exclusive reaction.

A different case is chain reaction polymerization, where fully grown polymer chains exist in the reacting mixture and the sol portion of the mixture consists exclusively of monomer. For this type of reaction, the gel point is predicted by

$$p_{gel} = \frac{1}{(DP_w - 1)f} \quad \textbf{(3-4)}$$

where DP_W is the weight average degree of polymerization and f is the fraction of unsaturated bonds in a multi-vinyl monomer. This formula (3-4) is correct when all reactive groups have an equal reactivity (not usually the case) and where the monomer is low in concentration of groups with different functionalities.

The Carothers and the statistical predictions of gel point in step-growth cures differ in the result they predict. The Flory approximation overcomes the limitation of the Carothers approach in that the gel point prediction is based on the molecular weight distribution, and the point where the averages of this approaches infinite size considered the gel point. This latter statistical approach is more often employed in predictions of gel point.

The Flory-Stockmayer predictions assume that each crosslink point is randomly generated with no cyclic species being produced. Further, it does not consider excluded volume or steric effects, so any change in reactivity due to size considerations is not taken into account. The controlling variables are the functionality f and the probability that a functional group has

reacted, p. These approximations are together taken as being part of a "mean field theory" approach to the statistics of the calculation.

Modifications of the mean field approach have been proposed (7) which consider the possibility of loop formation instead of an exclusively random lattice. Instead of the classical lattice (Bethe lattice), the "random percolation" theory (8) considers that a bond between neighboring lattice sites also is formed randomly, and with a probability p, but allows ring formation. Monte Carlo computer simulations have also been used to predict gel points.

An additional statistical treatment of network polymerization has been made by Macosko and Miller. (9) This calculates the probability of a certain molecular weight being produced at a given conversion. This approach does not yield a distribution of molecular weights at the given conversion, as does the Flory-Stockmayer approach. The Macosko derivation provides a straightforward scheme for gelation that is more general due to its ability to handle homopolymerization. It also allows for consideration of reaction byproducts. This theory begins by considering the weight W_A^{out} of any species obtained by moving out from the parent molecule to a functionality A'. W_A^{in} is the weight of groups attached to A moving toward the parent molecule. W_A^{out} is varied according to its reactivity, so W_A^{out} is zero when unreacted. If this molecule reacts with a molecule having reacting site B, W_B^{in} equals W_A^{out}.

According to Macosko and Miller, the probability of observing a weight attached to A, $E(W_A^{out})$ is

$$E(W_A^{out}) = E(W_A^{out} \mid A_r)P(A_r) + E(W_A^{out} \mid A_u)P(A_u) \quad \textbf{(3-5)}$$

where ($W_A^{out}|A_u$) is the unreacted condition and ($W_A^{out}|A_r$) is the reacted condition. P(x) is the probability of x occurring. The extent of reaction p may be obtained by considering the fraction of A_r remaining after a certain conversion, $A_{ft,}$ divided by the total amount of A, A_{f0}:

$$p = p_A = \frac{A_{f0} - A_f t}{A_{f0}} \quad \textbf{(3-6)}$$

Consider that P(A_r) is p and P(A_u)=1-p. Additionally, if it is assumed that there is no reaction between A and A, only between A and B, then p_A and p_B are given by

$$p_B = \frac{fA_f}{gB_g} p_A = rp \qquad \textbf{(3-7)}$$

where $r=fA_f/gB_g$ and f is the functionality of that reacting species. This, together with the probability expression above, gives

$$E(W_A^{out}) = pE(W_B^{in}) \quad \textbf{(3-8)}$$

with a similar expression for component B. The molecular weight of a molecule attached to a group will be the sum of weights moving toward that group and the weights moving away from that group. So, the average molecular weight is

$$E(W_{Af}) = E(W_A^{in}) + E(W_A^{out}) \qquad \textbf{(3-9)}$$

with a similar expression for component B. The expected weight attached to A moving toward the parent E(W_A^{in}) is the molecular weight of A_f together with the total weight of attachments to the A groups with the (f-1)A groups, which is

$$(f-1)E(W_A^{out}) \qquad \textbf{(3-10)}$$

which produces the relation for the expectation value of the weight moving inward

$$E(W_A^{in}) = M_{Af} + (f-1)E(W_f^{out}) \quad \textbf{(3-11)}$$

again, with a similar expression for $E(W_B^{in})$. Together with previous equations, they arrive at the expressions

$$E(W_A^{in}) = \frac{M_{Af} + p(f-1)M_{Bg}}{1 - rp^2(f-1)(g-1)} \quad \textbf{(3-12)}$$

and

$$E(W_{Af}) = M_{Af} + pf\frac{rp(g-1)M_{Af} + M_{Bg}}{1 - rp^2(f-1)(g-1)} \quad \textbf{(3-13)}$$

The weight average molecular weight may be obtained from this equation

$$\overline{M}_w = \omega_{Af}E(W_{Af}) + (1-\omega_{Af})E(W_{Bg}) \quad \textbf{(3-14)}$$

where ω_{Af} is the weight fraction of the monomer A_f, which is

$$\omega_{Af} = \frac{M_{Af}A_f}{M_{Af}A_f + M_{Bg}B_g} \quad \textbf{(3-15)}$$

So, with a monomer A of functionality f and a B monomer with a g functionality polymerizing, the weight average molecular weight at conversion p is

$$Mw = \frac{\frac{rg}{f}(1 + (g-1)rp^2M^2_{Af} + (1 + (f-1)rp^2)M^2_{Bg} + 2rpgM_{Af}M_{Bg}}{\left(\frac{rg}{f}M_{Af} + M_{Bg}\right)(1 - (f-1)(g-1)rp^2)} \quad \textbf{(3-16)}$$

The number average molecular weight is then calculated. This is the total mass divided by the number of molecules. Knowing that the number of monomers active until a conversion p is fA_f and the number of molecules before reaction is A_f+B_g, the number average molecular weight at some conversion is

$$\overline{M}_n = \frac{M_{Af}A_f + M_{Bg}B_g}{A_f + B_g - pfA_f} = \frac{\frac{rg}{f}M_{Af} + M_{Bg}}{1 + \frac{rg}{f} - rpg} \quad \textbf{(3-17)}$$

3.1.1.3 Time Temperature Transformation Diagrams

The physical states and mechanical responses of a thermosetting system change as cure progresses. A useful diagram to portray the evolution of the changes in physical state for such a system is the time-temperature-transformation (tTT) diagram (10). The events depicted in a tTT diagram include vitrification, devitrification, degradation, gelation, and, for two-phase systems, the point of phase separation. The main regions found on the diagram are the liquid, sol glass, gel glass, gel rubber, and the char. Critical temperatures depicted on the diagram include the T_g of the fully converted system, T_g at the gel point, and T_g of the unreacted material. A representative tTT diagram is shown in Figure 3-2.

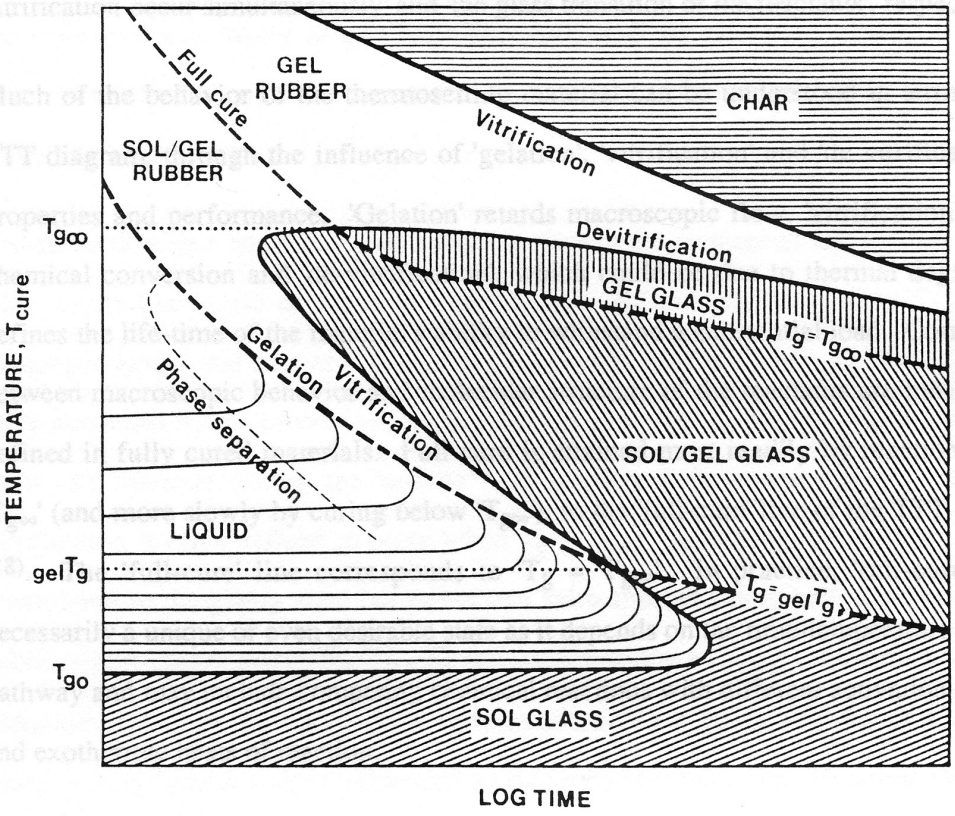

Figure 3-2. Representative tTT diagram. After Ellis, Chemistry and Technology of Epoxy Resins, Blackie Academic and Professional, (1993), p. 205.

The major physical states of the material can be interpreted using the phase boundaries on the tTT diagram which correspond to gelation, vitrification, and devitrification. Gelation corresponds to the cessation of viscous flow, while vitrification occurs as the material acquires a glass transition temperature equaling that of the cure temperature, beyond which the material behaves like a glass. The devitrification line indicates conditions beyond which the material suffers degradation sufficient to depress the glass transition temperature below the sample temperature. Achieving the highest degree of cure only is found beyond $T_{g\infty}$ which is not necessarily the degree of cure obtained in industrial application, or even the most desirable degree of conversion. Gelation corresponds to a specific degree of conversion as described in the models above, and further cure beyond gelation increases the gel portion while decreasing

the sol portion. This further cure increases the glass transition temperature of the material. The viscosity of the mixture is important and necessitates curing above the glass transition temperature at gelation. At the gel point the zero shear rate viscosity of the mixture becomes infinite. This phenomenon yields a useful additional method of determining cure kinetics since isothermal cures within a viscometer may then yield the gel points found on the tTT diagram.

The vitrification process occurs when the glass transition temperature of the reacting mixture rises to equal the cure temperature. At reasonable times, prolonged isothermal cure will result in a glass transition temperature nearly equivalent to the cure temperature. Practically, the cure process results in a glass transition temperature that is somewhat higher than the cure temperature. This is a consequence of the T_g actually being a range over which vitrification takes place rather than a sharply defined temperature. (11) Because there is limited mobility across this range, some cure may proceed. Reaction may continue in the glassy state depending on the reaction mechanism, but the extent of this additional cure is highly limited. In common systems such as polyimides and epoxies, the T_g of the sample is commonly greater than the temperature of cure by about 30-50 $^{\circ}$C, reflecting the effects of a large exothermic reaction enthalpy. (12) This raises the actual cure temperature beyond that which is intended.

Producing the tTT diagram requires isothermal cures while some probe (usually mechanical) is made of the physical state of the material. This may be achieved using dynamic mechanical methods such as the TBA, or torsion braid analyzer, a torque rheometer, dielectric techniques and also with DMA. Data from TBA measurement of a curing thermoset is shown as an example in Figure 3-2. Rheological methods involve determination of gel point extrapolated to zero shear rate viscosity; however, many instruments cannot resolve sufficiently high viscosities in the region of the gel point. In this case, the dependence of the reciprocal of

viscosity on time is examined, and an extrapolation is made to the inaccessible region. Dynamic mechanical methods use the mechanical loss peak (tan δ), which is the ratio of loss modulus to storage modulus, and the quantity related to it by π, the log decrement, Λ. This peak goes through a maximum when the sample goes through a physical transition. The gel point has been shown to produce such a peak. (13) Dielectric methods depend on the dipolar nature of the reactants in a thermosetting mixture. In an AC electric field, the dipole's motions as temperature and frequency are changed lead to energy absorption under certain conditions. The dielectric tan delta is monitored in a manner analogous to the mechanical equivalent and has a similar interpretation. It must be recognized that the apparent T_g shifts with the frequency of the probe in both DMA and dielectric experiments.

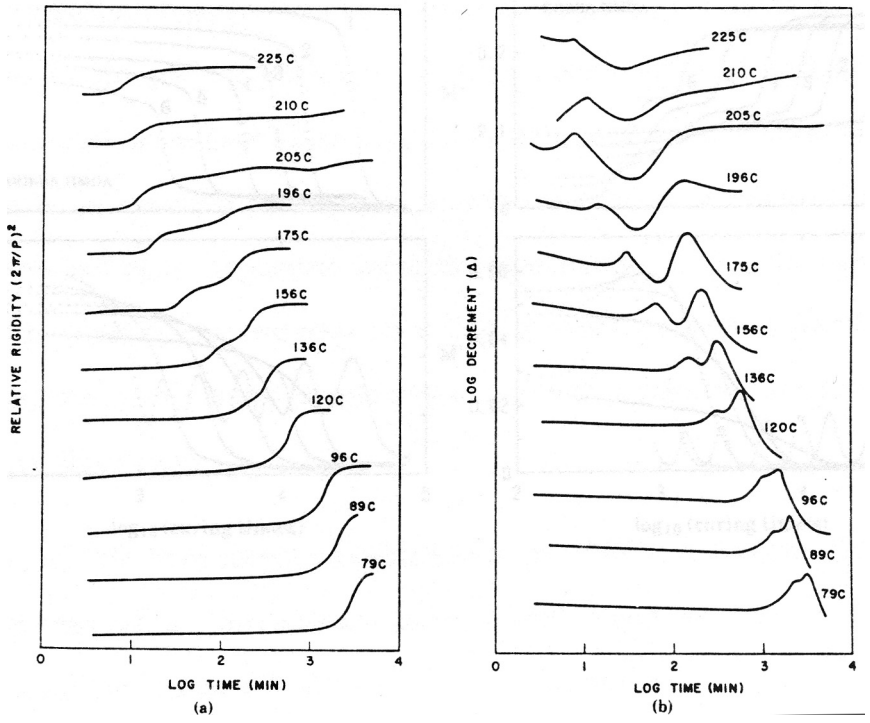

Figure 3-3. Torsion braid analysis of a curing thermoset system, showing gelation and vitrification points. After Enns and Gilham, Journal of Applied Polymer Science, 28, (1983), p. 2831.

It has been frequently noted above that practical thermosetting systems are often multiphase to overcome inherent brittleness of the unmodified thermoset. The tTT diagram may also describe the separation of a second phase from the initially homogeneous solution. The final morphologies of the cured thermoset are highly dependent on cure conditions. The tTT diagram's inclusion of the phase separation phenomenon provides information that should be of use in controlling and interpreting the final size of the morphological features. Often for these materials, control of the morphology is produced by curing to gelation at one temperature and postcuring at another temperature. Phase separation may be characterized by the variation of light scattering with cure time. The spatial fixation of the phase separated morphology is defined as the point where the scattering peak angle levels off. Therefore, this point may be assigned to the tTT diagram on the phase separation line corresponding to the appropriate time-temperature coordinate.

A variation on the tTT diagram is the cure-temperature-property diagram, in which the glassy polymer's properties are related to the extent of conversion. This process can be a complex one due to the non-linearity of T_g change with cure conversion. (14) For example, the relationship of an elastic property P in the glassy state to the cure conversion is

$$P = f(T, C) \quad \textbf{(3-18)}$$

where T is the temperature of the measurement and C is the cure parameter. The choice of relating the magnitude of C to some measurable quantity is a difficult one. One choice would be to use the measured T_g to calculate the cure parameter C (15), and this represents the changes on a T_gTP diagram. One proposed modification to this scheme is to replace T_g with C and a normalizing expression for extent of conversion, where C varies from 0 to 1 as the cure proceeds to full conversion. A representative cure-temperature-property diagram is shown in Figure 3-4.

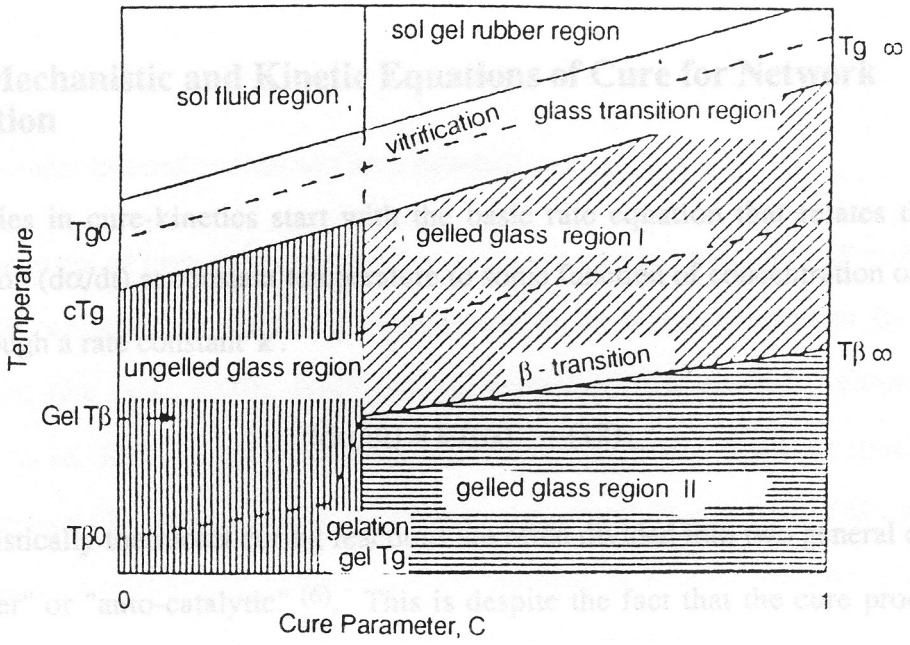

Figure 3-4. Representative cure-temperature-property diagram. After Ellis, Chemistry and Technology of Epoxy Resins, Blackie Academic and Professional, (1993), p. 72.

3.1.1.4 Cyanate Esters

The cyanate ester class of compounds were first synthesized by Grigat and Putter (16) who developed a simple synthesis of a phenolic cyanate ester. This chemistry depends upon the reaction of a cyanogen halide with an aryl hydroxide, where the aryl component prevents rearrangement to a isocyanate and produces good yields. The cyanate esters may undergo further reactions (17), probably the most significant for polymer applications being a direct ring closure to form triazine structures. This generates a three-dimensional network structure.

Cyanate ester monomers are typically aryl derivatives terminated with the cyanate (OCN) functionality. These compounds are the esters of phenolic compounds and cyanic acid, and the phenolic compounds used are typically bisphenol or polyphenolic. Upon thermal activation, the cyanate esters cyclotrimerize to form the three dimensional network structure via addition and thereby produce oxygen-linked triazines with no volatile by-products. (18) These resins became

commercial products initially under the name "Triazine A", produced by Bayer/Mobay in 1976, which was a dicyanate pre-polymer. Problems with performance led to the discontinuance of these materials in 1978. Mitsubishi Gas Chemical then used the Bayer/Mobay process to produce blends of bismaleimide resins with cyanate esters, marketed under the name "BT Resin". The patent rights were licensed from Bayer-AG to Rhone-Poulenc in 1984 - a manufacturer that began the production of a variety of phenolic precursor-based cyanate esters in high purity, including fluorinated, sulfur-linked, and asymmetrically linked materials as the AroCy line of cyanate resins. In addition, Dow Chemical has produced an experimental cyanate ester resin which includes a cyclo-aliphatic precursor bisphenol (19). The cyanate business unit of Rhone-Poulenc was sold to Ciba-Geigy.

Another class of phenolic triazines was patented by AlliedSignal Corporation in 1989 (20) with structure similar to the epoxy novolacs, where the reactive cyanate groups are placed along the molecule off the phenyl rings. By varying the number of cyanate-containing phenyl links in the center of the molecule, the amount of hydrogen bonding was changed. This altered the physical form of the resin anywhere between a crystalline solid and a low viscosity liquid. These materials can possess glass transition temperatures of 300 ºC or higher, and degradation in air begins beyond 440 ºC.

Bisphenol cyanate ester monomers have been synthesized by Abed and McGrath (21) containing various linkages between phenyl substituents. These monomers include SO_2, CO, C(Ph)(CF_3), O-pAr-SO_2-pAr-O, PO(Ar), and O-pAr-PO(Ar)-pAr-O (where the cyanate group is in both the meta and para position from the bisphenol linkage). These monomers may be used to demonstrate the effect on reactivity of the cyanate group with the addition of electron-withdrawing groups. The phosphine oxide-containing monomers demonstrated good thermal-

oxidative stability and excellent char yields on thermal decomposition, often translating into good flame retardancy.

The mechanism of cyanate polymerization has been investigated with NMR in solution and in the solid state (22). The main reaction as determined by NMR and MS is triazine formation, which was characterized using X-ray diffraction on a crystalline compound using mono-substituted cyanates. In the presence of water in a solvent, side products were observed. No observation was made of dimers before the triazine ring is formed. In the solid state, only the trimerization was detected. Others (23) have examined the catalysts used for practical reaction rates on the bisphenol-A dicyanate system. The catalysts examined were zinc and manganese octoate and napthenate and cobalt acetylacetonate, using up to 750 parts per million of metal, with a cocatalyst of nonylphenol in concentrations up to 8 parts per hundred. In general the thermal stability of the cyanate system was decreased by increasing zinc catalyst concentration, but manganese had no such effect, and did not harm high temperature stability in increasing concentration. The final T_g of the cured system was significantly affected by the choice of catalyst package used. It was observed that the cyanate cure with a catalyst is described by second order kinetics, and with no catalyst, the reaction proceeded autocatalytically.

While cyanates require only thermal activation to cyclotrimerize, the conversion proceeds at commercially attractive rates only when catalyzed. (24). Catalysts suggested by the manufacturer include a cocatalyst mixture of an active hydrogen compound such as nonylphenol which supplies nonvolatile active hydrogen and predissolves the transition metal complexes used for catalysis. The soluble organic coordination metal compounds speed the conversion process significantly. The commonly used metals are zinc, copper, manganese, and cobalt, in organic complexes such as octoates, napthenates and acetylacetonates. Antimony, tin, titanium and iron

also catalyze the reaction, but can lead to hydrolysis of the cyanate ester linkage. The acetylacetonates are preferred for catalysis because they provide a large heat latent catalysis effect. This acceleration effect is much greater at higher temperatures.

Cyanate trimerization rate has been investigated by Gupta. (25) Using a kinetic solution approach to the Flory-Stockmayer statistical theory, and assuming that trimerization is the only reaction, he derived the equation for weight average degree of polymerization as

$$< DP_w >= \frac{1+2\alpha}{1-2\alpha} \quad \textbf{(3-19)}$$

which predicts the gel point at 50% conversion. This degree of conversion at gel point ws confirmed experimentally by the data of Bauer et al. (26), but is at odds with the experimental data of Barton et al. (27), Gupta and Macosko (28), Simon and Gillham (29), and Shimp et al. (30), who report gel conversions of between 60 and 65% for the various dicyanate monomers examined.

The discrepancy between the theoretical prediction and experimentally determined gel point is considerable, and may stem from several causes. The trimerization might not be the exclusive reaction in the cure of these materials, but the data suggest that this is not the case. Upon examination of the mean field theory's assumptions, the reaction mechanism should be "reaction controlled", which was determined to not be the case (31) because the reaction takes place in very localized areas characteristic of a diffusion controlled polymerization. Diffusion limitations yield relatively smaller network chain molecular weights for a particular cure conversion and this could retard gelation. One possible description of this diffusion dominated network uses the growth of isolated clusters which originates from the limited accessibility of reacting species. This reaction is therefore best described as diffusion controlled. It is a function of steric hinderance which limits the local area that reacting species can interact in. In other

words, certain terrain of the reaction landscape potential is blocked. The introduction of a steric consideration factor into the kinetic model can account for the increase in cluster size and the corresponding change in diffusion characteristics. (32) This factor considers the reactivity change as the difference in reactivity between a free cyanate group and one in a cluster.

The cyanate monomers have also been employed as co-monomers for epoxy curing reactions (33). In this application, the economy of the epoxy chemistry with the high temperature performance of the cyanates are combined. The cyanate triazine rings catalyze the epoxy, with the steps of the curing process being trimerization, the epoxide insertion into the cyanurate, isomerization to isocyanurate and further epoxide reaction to form chain extending oxazolidinone ring linkages (34).

3.1.2 Toughening Thermoset Resins

3.1.2.1 Deformation of Polymers

Discussion of the mechanical deformation of polymers should correlate their individual structures with corresponding properties. Polymers can exhibit both plastic deformation as well as elastic behavior. Such viscoelastic behavior shows pronounced changes depending upon the specific test conditions, especially the test rate and temperature in stress-strain experiments. Typical polymeric materials may demonstrate Hookean elastic behavior only at small strains. Certain combinations of strain, strain rate and temperature lead to distinct nonlinearities, plastic flow, hysteresis and yielding. In the process of enhancing the fracture toughness of these materials, two key mechanisms of dissipating fracture energy must be considered: crazing and shear yielding.

3.1.2.1.1 Crazing

Glassy polymers undergo crazing as a mechanism of energy dissipation and therefore toughening by the formation of microcracks. These microcracks have fibrils that bridge the

structure and have a stabilizing effect on the crack. These microcracks are nucleated at imperfections where there is a hydrostatic component of the stress. These crazes may form ahead of a propagating crack, preceding its advance and producing a toughening effect. Crazing is accompanied by an increase in the specimen volume.

3.1.2.1.2 Shear Yielding

Plastic deformation in a polymeric material may result from an applied shear stress field due to translational movement of the polymer chains without scission. This phenomenon occurs in highly localized shear bands as well as in larger areas of shear deformation. Conditions of relatively higher temperature or lower strain rate lead to this yielding mechanism. While this suggests ductile failure, the overall failure process for the sample may appear as linear elastic (brittle) fracture except that large amounts of strain energy are absorbed. Shear yielding has been indentified as one of the most significant contributions in failure of toughened thermosets. (35)

3.1.2.2 Fracture Toughness

In order that a material's fracture properties may be better understood, an accurate definition of toughness must be established. Toughness is the amount of energy required to fracture a given volume of that material. However, many factors influence the observed toughness beyond the bulk material properties, such as test rate, temperature, presence of flaws and other inhomogeneities. A common approach to measuring toughness is the tensile test, where the area under the resultant stress-strain curve is integrated to obtain energy per volume required for fracture. This method depends upon the adventitious formation of a crack in the material at a stress concentration along with the propagation of that crack. This type of experiment does not separate the contributions from before the formation of the crack and the resistance of the material to the crack once it is formed. The resistance of the material to

propagation of a preformed sharp crack is also known to as the fracture toughness. Two definitions follow from this type of measurement: 1) the critical stress intensity factor (K_c) and 2) the strain energy release rate (G_c). G_c is the threshold energy per area above which the crack is driven forward, and K_c is the threshold stress (associated with the crack size parameters) above which the crack is propagated.

3.1.2.2.1 Failure Mode

There are three fundamental geometries associated with the crack. (Figure 3-5) The solution for finding the fracture toughness is dependent upon knowledge of the failure mode, which is often controlled experimentally to provide a single mode of failure. The nomenclature of fracture toughness usually includes the mode which was used to test the fracture toughness. Thus, K_{Ic} would indicate the critical stress intensity factor in mode I.

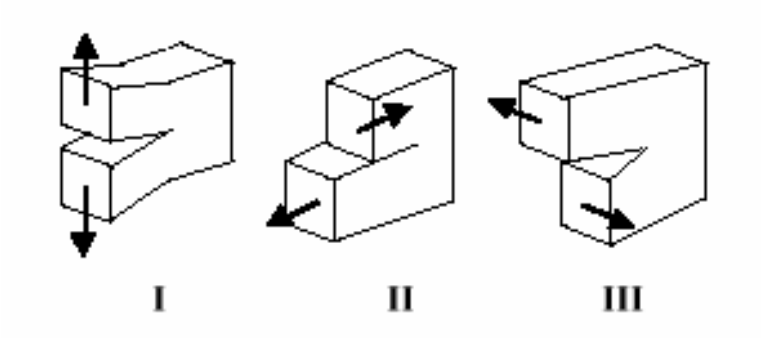

Figure 3-5. Various modes of fracture. Mode I: tensile opening. Mode II: in plane shear. Mode III: out of plane shear.

3.1.2.2.2 Critical Stress Intensity Factor

K_c is defined by the stress field formed around a sharp crack. For infinitely thin, isotropic and linear elastic samples, an infinitely sharp crack tip of length *a* is deformed uniaxially by an applied stress σ_0. This produces the following components of the stress tensor in a volume of radius r and angle θ from the crack tip (36, 37)

$$\sigma_x = \sigma_0 \frac{\sqrt{\pi a}}{\sqrt{2\pi r}} \cos\frac{\theta}{2}\left(1 - \sin\frac{\theta}{2}\sin\frac{3\theta}{2}\right) \qquad \textbf{(3-20)}$$

$$\sigma_x = \sigma_0 \frac{\sqrt{\pi a}}{\sqrt{2\pi r}} \cos\frac{\theta}{2}\left(1 + \sin\frac{\theta}{2}\sin\frac{3\theta}{2}\right) \qquad \textbf{(3-21)}$$

$$\tau_{xy} = \sigma_0 \frac{\sqrt{\pi a}}{\sqrt{2\pi r}} \sin\frac{\theta}{2}\cos\frac{\theta}{2}\cos\frac{3\theta}{2} \qquad \textbf{(3-22)}$$

where τ is the tensile stress and σ is the shear stress. An interesting consequence of these relations is that they predict an infinite stress at the crack tip. This is, of course, impossible, because no material can resist an infinite stress. Therefore, to produce a reasonable representation of the mode I fracture criteria, the stress intensity factor has been given as (38)

$$K_I = \sigma_0 \sqrt{\pi a Q} \qquad \textbf{(3-23)}$$

where Q is a geometry factor. Q varies with specimen shape and size and is specified by standards (39) or handbooks. (40, 41, 42) This factor allows reconciliation of real sample thickness with the theoretical assumption of infinitely small thickness. The critical stress intensity then follows as

$$K_{IC} = \sigma_c \sqrt{\pi a Q} \qquad \textbf{(3-24)}$$

Here, crack propagation occurs where the stress intensity factor is greater than the critical stress intensity factor.

3.1.2.2.3 Strain Energy Release Rate

It has been proposed that the critical energy required for fracture arises from interfacial phenomena, i.e., because failure creates two new surfaces, the interfacial energy of the new surfaces created defines the energy necessary to propagate the crack. Therefore, the amount of energy input into the system must exceed increase in the internal energy of the system, which includes the interfacial energy. For an increase in crack length ∂a

$$\frac{\partial(F-U)}{\partial a} \geq \frac{\partial 2A\gamma}{\partial a} = 2b\gamma \qquad \textbf{(3-25)}$$

where F is the energy put into the system, U is the system's internal energy, A is the surface area of the crack, and b is sample thickness.

It is clear from available data that the energy required for fracture is many times the sample's interfacial energy alone. Some of the additional energy required is dissipated because of the energy required to break both secondary bonds as well as chemical bonds in the material. For polymeric materials, there are further considerations needed to explain the large energy dissipation. The additional energy required to fracture polymeric materials is due to viscoelastic dissipation can occur either globally or locally in these systems. Viscoelastic energy loss mechanisms may occur regardless of whether the material appears to exhibit overall brittle fracture. The approach often taken in fracture models (44) is to sum the various contributions arriving at a total energy dissipation. Using this approach, we replace the interfacial energy term in equation (3-25) with the critical energy to obtain

$$\frac{1}{b}\frac{\partial(F-U)}{\partial a} \geq G_c \qquad \textbf{(3-26)}$$

3.1.2.3 Thermoset Toughening

Thermosetting materials are useful and popular in many applications in part due to their low viscosity before cure and good high temperature performance after cure. The disadvantage of thermosets originates from high crosslink density, in many cases, contributing to the brittleness in these materials. Successful attempts to improve the toughness of these materials have allowed their widespread use and make available the advantages of the unique properties of the cured polymers.

Early efforts to refine thermoset properties focused on the incorporation of a low T_g

modifier to act like a plasticizer. This improved toughness but had deleterious effects on the high temperature performance of the thermoset. As a result of significant solubility within the thermoset rich phase, the plasticizer substantially lowers the final glass transition temperature. Improvements were made using low T_g tougheners which phase separate, producing a two-phase system with small (0.1-1 μ) rubbery particles that effectively toughen; but, due to the phase separation, the T_g depression is lessened.

These phase separating tougheners are materials such as terminated copolymers of acrylonitrile and butadiene. These also may depress the T_g of the thermoset somewhat. The toughness of these types of systems is a function of the chemical nature of the thermoset resin and its final crosslink density, the interfacial adhesion between the resulting continuous phase and disperse phase, and the size and volume fraction of the dispersed particles. (45) Unfortunately, the chemical unsaturation in these types of tougheners provides advantageous points for oxidative degradation to occur. One class of tougheners that can provide advantages in oxidative and thermal degradation as well as moisture and weather resistance is the functionally terminated polysiloxanes. (46) Inorganic particulate fillers also have been employed (47), both alone and in combination with elastomeric tougheners, displaying less efficacy as tougheners than the low T_g elastomers.

The marketplace need for polymers that can withstand high temperatures has fuelled an optimization of high performance behavior. In the case of toughened thermosets, the tougheners themselves had become the limiting factors and improvements are required for them to be able to withstand higher temperatures. The incorporation of thermoplastic tougheners in thermosets was an effort to toughen with more thermally stable substances and has resulted in materials with somewhat higher temperature capabilities. Previously, commercial thermoplastics have been

employed (48); however, poor adhesion between continuous phase and the discrete toughener phase has proven problematic from the standpoint of toughening efficiency as well as solvent resistance. The modification of such thermoplastics with terminal reactive terminal groups has been found to be much more desirable, improving the critical properties such as toughness as well as preserving their high modulus and high temperature capabilities. Such examples are available in the in epoxies and polyimides (49, 50, 51) as well as cyanate esters. (52)

3.1.2.4 Toughening Mechanisms

Many attempts have been made to elucidate the origin of the improvements in toughness of brittle thermosets which are gained through the inclusion of a second phase. Some of the possible mechanisms that were studied are shear yielding in the matrix adjacent to particles, crazing, crack bridging, crack blunting, tearing and cavitation of particles, crazing and crack pinning. (53) Some of these mechanisms are depicted in Figure 3-6.

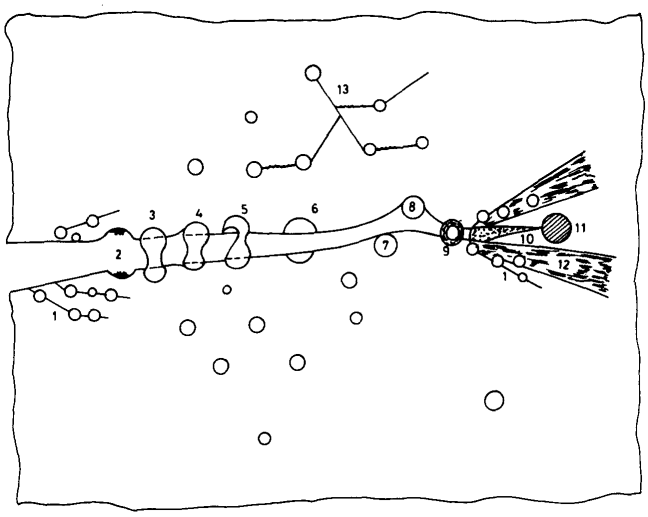

Figure 3-6. Depiction of possible toughening mechanisms. After A. C. Garg, Y. W. Mai, Composite Science and Technology 31, (1988), p. 179.

In investigations on rubber-toughened epoxies (54), the mechanism of energy absorption was first suggested to involve increased crazing in the vicinity of the rubber particles due to

stress whitening, which is a dilatational process leading to lower density regions that scatter light. This was disputed by Yee and Pearson (55, 56) who suggested voiding about the rubber particles produced the increases in toughness as well as the stress whitening process. The authors further asserted that volume dilation could be produced by particle voiding (separation from the matrix), disputing the assertions of Bucknall (57) that increased volume during tensile creep was due to crazing. Other proposed mechanisms include the rubber stretching and tearing mechanism (58), which was refuted by Yee and Pearson (59, 60) who claimed that this could not account for the observed toughness increases. This model also ignores stress whitening, cavitation of the rubber rich domains, and shear yielding of the matrix. (61) Further, Kinloch suggested that failure of toughened, glassy materials involves plastic shear yielding in the matrix as well as cavitation in the particle or in the particle/matrix interface. This requires dilatation near the tip of the growing crack which Kinloch includes. The type of shear yielding in the matrix was not discussed by Kinloch, though it is proposed as the largest contributor to the increased toughness. The shear yielding could be shear banding, or inhomogeneous, or diffuse, or a combination of the two. The cavitation and shear yielding are also suggested to be complemented significantly by stretching and tearing of the rubber particles. (62)

In thermosets filled with inorganic particles, the toughness enhancement is suggested to be due to the effects of increased surface area that must be produced to surround the particles as the crack grows. This process is called “crack pinning” (63) as well as “plastic deformation”. This is a product of shear band formation which produce localized yielding of the matrix around the dispersed particles thus blunting the crack tip. The mechanisms of crack blunting and crack pinning considered to be the major contributors to the higher toughness seen in these types of composites.

Encouraged by the possible superior features of thermoplastic-toughened thermosetting resins, substantial investigations have has been made of these systems. A review of the various proposed toughening mechanisms has been made by Yee and Pearson (64, 65) in the 1980s. Later, McGrath et al. researched DGEBA-type epoxies that had been modified with a bisphenol-A based polysulfone. (66) There, analysis of SEM micrographs of the fracture surfaces suggested a particle bridging mechanism, which arose from ductile tearing of the particle in the crack. Thermoplastic particle as well epoxy matrix plastic deformation accounted for the majority of the energy absorption. Small rings were observed around the dispersed particles which suggested plastic deformation, drawing and crack pinning mechanisms of toughening. As a result of stress concentrations arising from modulus differences between toughener and matrix resin, the local plastic deformation of the matrix could produce these rings. Dilatation of the thermoplastic-rich particles was not suggested to be a possibility due to the similar thermal expansion coefficients of the matrix resin and toughener in these investigations.

Resorcinol based epoxies have been toughened with thermoplastics as well. (67) This work suggested particle bridging in addition to yielding within individual particles that was caused by stress concentration in the interface between particle and matrix. This was suggested to increase shear banding within the matrix. In other work, poly(etherimides) were introduced into tetrafunctional epoxy to generate much improved toughness. (68) This publication suggested particle bridging as the mechanism of improved toughness. Zengli and Yishi suggested plastic deformation of the matrix as well as the particles as toughening sources. (69) Crack pinning is suggested to be the dominant mechanism for improved toughness, arising from interactions between crack front and dispersed particles, which produced so-called "river markings" on the fracture surface perpendicular to the crack direction.

In further research, modification of epoxies with poly(phenylene oxide) demonstrated that bifurcation (microcracking) was the dominant toughening mechanism. This work excluded crack bridging as the major source of enhanced toughness. (70, 71) Analysis of SEM micrographs of fracture surfaces showed the markings resulting from particle tearing, a clue to a particle-bridging mechanism. However, subsurface microcracking indicated initiation from a single point, arising from bifurcation of the main crack. No shear banding was observed at the crack tip. In view of the small enhancements of toughness, the conclusion was made that because the crack tip is not planar, particle bridging was not the operative mechanism. The authors do suggest that particle bridging could stabilize the resultant microcracks.

3.1.2.5 Toughening Cyanate Esters

Given the progress described in the above section, it may be concluded that significant inroads have been made that point to an understanding of toughening of cyanate ester systems. Cyanate composites have been toughened using particulate additives, namely, nylon 6 particles of about 20 microns diameter. (72) Fracture mode-sensitive improvements in toughness were demonstrated. The Dow Corporation cyanate ester experimental polymer has been toughened through incorporation of core-shell pre-formed rubber particles which provided large toughness enhancements (73). The enhancements were presumably due to an increase in shear yielding in the cyanate ester matrix. The introduction of siloxane modifiers into the cyanates has also been reported to improve toughness, oxygen plasma resistance and microcrack resistance. (74)

Many of the toughening approaches for the cyanates have involved thermoplastic modifiers. A fluorine-containing cyanate monomer has been described which uses a compatible engineering thermoplastic, and the resulting morphologies were investigated using scanning force microscopy. (75) Shimp et al. have reporter toughness improvements stemming from

incorporation of various thermoplastics into cyanate systems. (76) Control of the resulting morphologies (and therefore, properties) has been reported by Pascault for both rubber modified (acrylonitrile-butadiene copolymer) and thermoplastic (polyethersulfone) toughened cyanates. (77)

A comprehensive study of cyanate toughening was made by Srinivasan et al. (78) using the bisphenol-A based cyanate monomer. A variety of thermoplastic tougheners were explored, including bisphenol-based poly(arylene ether sulfone), poly(arylene ether ketone), poly(arylene ether phosphine oxide), phenolpthalein-based poly(arylene ether), poly(arylene ether sulfone), a copolymer of bisphenol/phenolpthalein based poly(arylene ether sulfone), bis-aniline-P/oxydiphthalic anhydride based polyimide, as well hydroxyl-terminated materials of the preceding classes. Conclusions were drawn about the utility of solubility parameter for selecting tougheners for the cyanate materials (79). It was observed that as the solubility parameter of the toughener became closer to that of the cyanate, the degree of phase separation changed from gross macrophase separation, with undesirable properties, to better defined microphase separation, which resulted in favorable properties and enhanced toughness. In that work, phase separation behavior of the tougheners was observed by both fracture surface SEM and TEM of thin sections, as well as DMA. A closer match of the solubility parameters resulted in either controlled microphase separation in a homogeneous mixture. The effect of chain termination was explored by these authors. They noted that while reactive chain termination may result in good interfacial properties between cyanate-rich phase and toughener-rich phase, the solubility may be enhanced as well, producing a considerable degree of phase mixing. This phase mixing may be enhanced to the degree where there is no discernible dispersed phase. The absence of a second phase may lead to no improvement in toughness of the matrix as well as causing the high

temperature performance of the matrix to be degraded and only a single T_g. The desirability of phase separating as much toughener as possible arises from the objective of maintaining high temperature performance of the resin. The solubility parameter of the polycyanurate was determined to be 9.3-9.5 $(cals/cc)^{1/2}$. (79)

Srinivasan also explored use of the functionally-terminated (hydroxyl or cyanate) bisphenol-A based poly(arylene ether sulfones) which did not toughen the cyanate ester well due to poor phase separation and the formation of only very small domains. By blending in proportions of non-functionally terminated polysulfones, control of phase size was achieved, and overall properties improved. Functionally terminated bisphenol-A based poly(arylene ether ketones) toughened the system well but were found to degrade the high temperature performance of the system. It was noted that the non-terminated polymeric toughenes resulted in much less improvement in fracture toughness properties. This was attributed to improved interfacial adhesion which also improves solvent resistance and solvent stress cracking properties. Toughening of the cyanate esters by inclusion of hydroxyl-terminated poly(arylene ether sulfone) derived from phenolphthalein resulted in good mechanical properties with little degradation of high temperature performance due to the high glass transition temperature of the toughener (about 250 °C). The modulus of the system was also maintained. The microstructure of the toughened cyanate demonstrated marked variability with cure schedule. Though the particle size varied significantly, the fracture toughness response was not found to change within the error of the test.

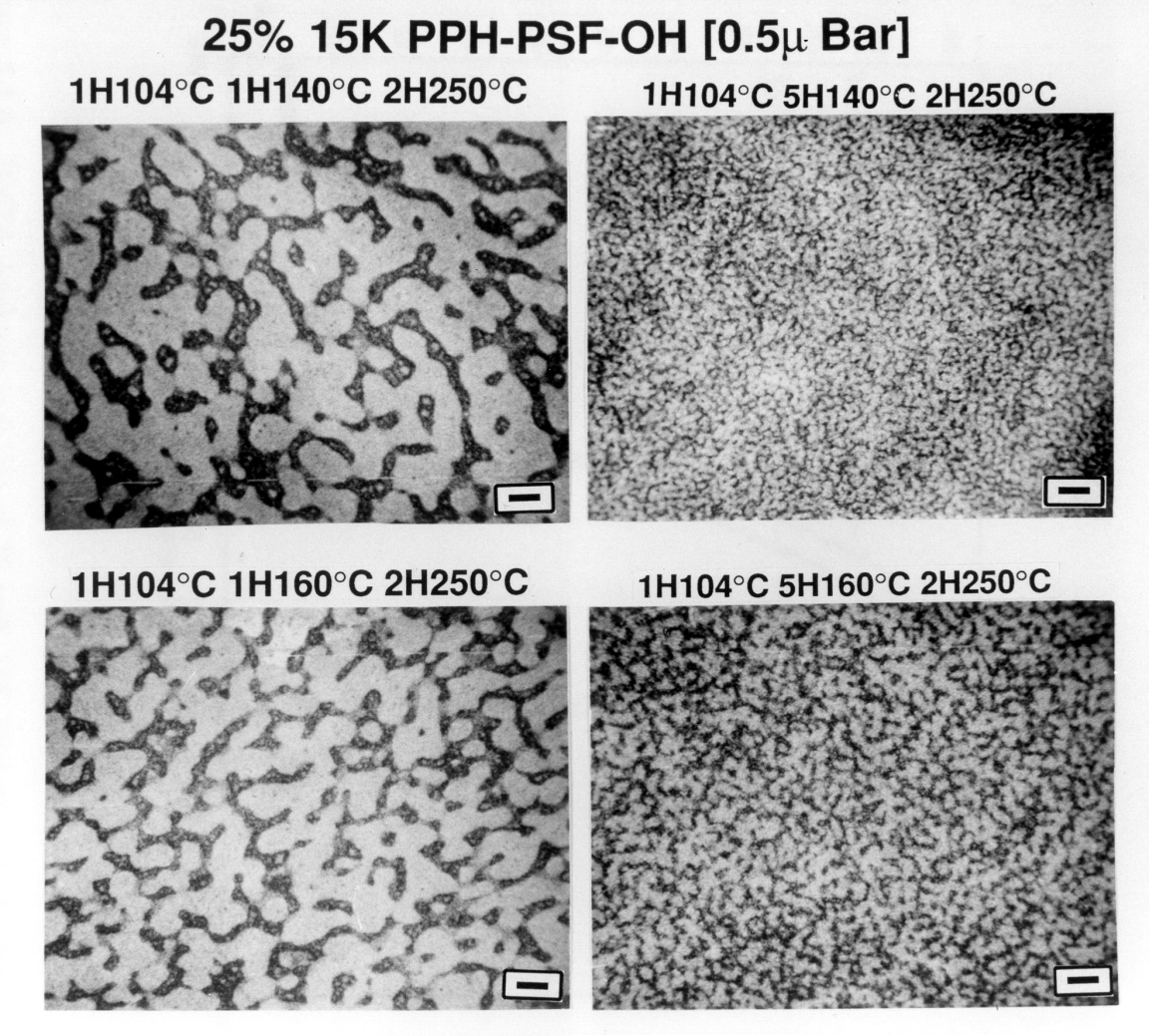

Figure 3-7. Variation in microstructure of phenopthalein-based polysulfone-toughened cyanate ester networks. After Srinivasan, Ph. D. dissertation, Virginia Polytechnic Institute and State University, Blacksburg, Virginia, (1994), p. 277. (Bar is 0.5 μ)

The results of Srinivasan's very detailed study indicate the complexity of the toughening mechanisms in thermosetting systems. The molecular weight, backbone structure, and termination of the chain all play a role in the nature of the phase separation as well as the final properties. Phase separation characteristics are also a strong function of the cure conditions as they affect the kinetics of the network formation as well as the viscosity of the curing system.

The amount of toughening produced is also affected by the particle volume fraction, and this is varied by the amount of their addition to the system. (80)

Significant progress has been made in the area of cyanate ester resin toughening by work done in association with the manufacturer. (81) Various tougheners were employed, including a polyetherimide (Ultem 1000), polysulfone (Udel p1700), polyarylates (Ardel D100 and Durel 400), as well as a low T_g copolyester resin (Vitel PE307) added to the bisphenol-A based dicyanate as well as a methyl-shielded functional group dicyanate and a sulfur-linked dicyanate. The inclusion of such additives to the cyanate material yielded toughnesses up to four times the homopolymer value. The actual improvement varied widely with the nature of the thermoplastic and was a non-linear function of the amount added.

The morphologies of the toughened materials in the Shimp study (81) varied widely. The copolyester toughener produced a sample with no discernible phase separation in the case of the bisphenol-A resin, while the methyl-shielded resin produced spherical domains of diameter 0.2 to 0.6 μ. The sulfur-linked material produced small (0.1 to 0.2 μ) particles rich in toughener as well as a cocontinuous, nodular structure reflecting good phase separation. This range was attributed to changes in solubility parameters - the bisphenol-A based resin having a smaller value of solubility parameter than the methyl-shielded resin, which in turn has a smaller value than the sulfur-linked material. These solubility parameters were obtained using measurement of solvent uptake with solvents of known solubility parameter.

The resulting toughness values reported by Shimp (81) were shown to increase with the larger particles sizes and better phase separation. Increasing the content of toughener was also shown to increase toughness, which was thought to result from increased average particle size. The temperature at which the resin was cured also was shown to affect the material's morphology

and therefore its toughness. Lower cure temperatures were shown to increase G_{IC} and strain at break for each case. It was concluded that development of certain morphological features in the cured matrix was essential for optimization of mechanical properties including heat distortion temperature and fracture toughness.

3.2 Experimental

3.2.1 Materials

The materials chosen in this investigation are a commercial cyanate ester material, bisphenol-A dicyanate (BADCy) (figure 1) together with two commercially available polymers which were used as the toughening agents. The basic resin is the same material employed in the previous chapter.

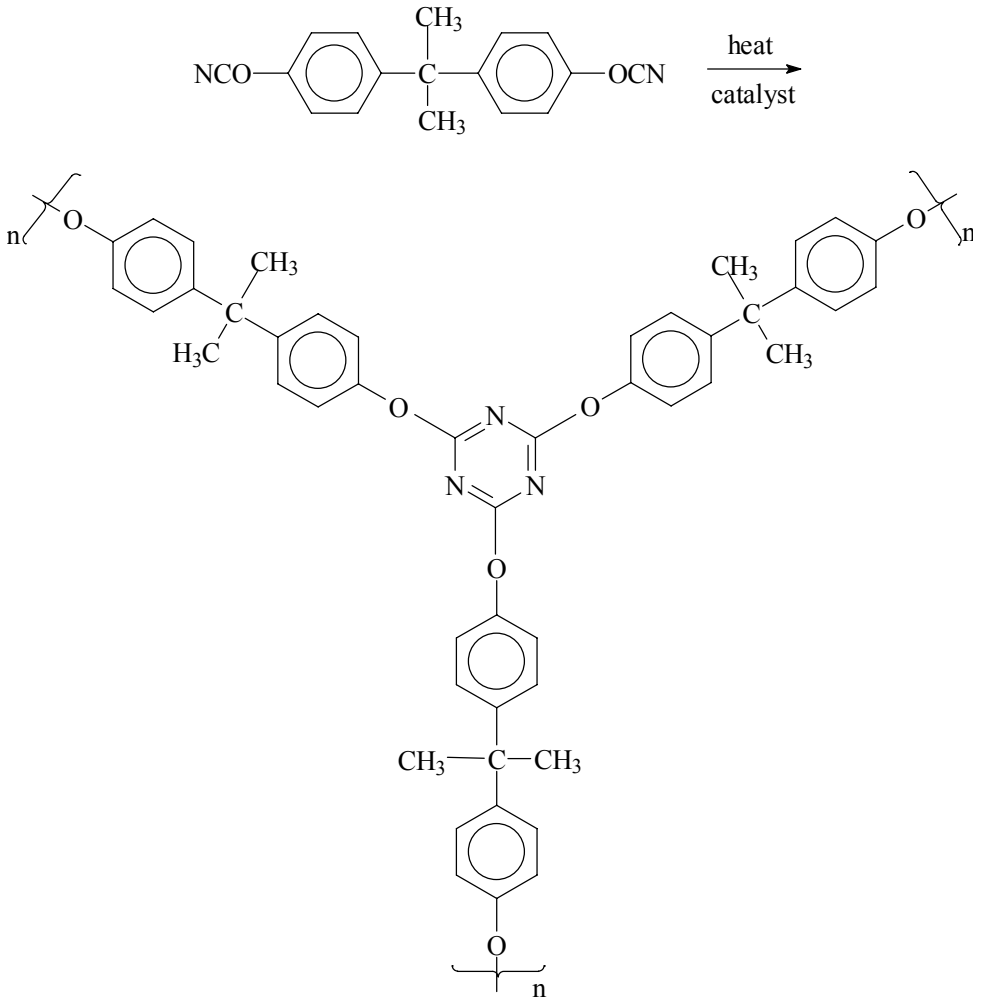

Figure 3-8. Chemical structure of bisphenol-A dicyanate and resultant polycyanurate.

The toughening used are a hydroxyl-terminated butadiene-acrylonitrile copolymer (HTBN) or series of amorphous, low-T_g copolyesters. The HTBN was used as received from Echo Resins and Laboratory (Rt. 3, Box 359, Versailles, Missouri) at a specified acrylonitrile content of 9.5% by weight. The molecular weight of this material was determined from gel

permeation chromatography (GPC, Waters 150C with absolute molecular weight viscosity detector) that yielded a number average molecular weight of 3850 g mol^{-1}. The glass transition temperature of this material was found to be –62.3 °C (TA Instruments 2920 DSC, 10 °C min^{-1}).

The four copolyesters used were supplied by Bostik Inc. (211 Boston Street, Middleton, Massachusetts) as Vitel 3200, 3300, 3500 and 3550. These materials are the product of a condensation polymerization of mixtures of glycols and dibasic acids. They are hydroxyl terminated and have number average molecular weights of 33,600, 36,300, 23,200 and 21,900 g $mole^{-1}$, respectively (GPC). The glass transition temperatures of these polymers are 16.1 °C, -10.3 °C, -10.0 °C, and -9.1 °C (DSC, 10 °C min^{-1}), respectively.

The HTBN-toughened samples were prepared by dissolution of the modifier in the molten monomer at 90 °C using mechanical stirring. The resulting solution was held under vacuum to remove dissolved gas and any volatiles. Catalyst was added as a predissolved mixture of aluminum acetylacetonate in nonylphenol to deliver 250 ppm of aluminum acetylacetonate and 2 phr of nonylphenol using mechanical stirring followed by a final hold under vacuum. The resulting solution was cast in preheated aluminum molds. Vitel-toughened samples were prepared by first dissolving the toughener in a small amount of methylene chloride. Then the resultant solution was added to the molten monomer under mechanical stirring. This mixture was held under vacuum to remove all solvent, allowed to crystallize at room temperature and subsequently remelted under vacuum. The resulting mixture was catalyzed and cast as above for the HTBN-toughened samples.

The viscosity of the BADCy monomer melt is quite low, about 30 cP at the melt point. (82) Addition of the relatively low molecular weight HTBN modifier, even at the higher concentrations, appeared to produce only small changes in this viscosity. Upon addition of

higher concentrations of the higher molecular weight Vitel 3200, the viscosity increased significantly and clearly diminishes this favorable property of the BADCy material.

Samples were cured isothermally at the prescribed cure temperature for sufficient time to polymerize the BADCy to conversions beyond the gelation points. Following this cure step, all samples were postcured at 250 °C for two hours to bring the degree of conversion to near completion and to equalize the degree of cure in all cases regardless of initial cure temperature.

An initial series of experiments using 10% modifier concentration demonstrated phase separation of the Vitel 3200 and HTBN-toughened samples and enhanced fracture toughness of those samples. Therefore, additional experiments were conducted which shifted the concentration of the toughener in the matrix between 5, 10, 15, 20 and 25 weight percent modifier. In this second set of experiments, the cure temperature was varied between two extremes: 150 °C for four hours, or 210 °C for one hour. These cure temperatures actually are practical limits for the cure of the catalyzed BADCy, with cure conversions of 60% (gelation point) (83, 84, 85, 86) achieved in approximately six minutes for the 210 °C cure profile, and 120 minutes for the case of the 150 °C isothermal cure. (87)

3.2.2 Results

3.1.1.5 Thermal Stability

The evaluation of toughening agents in high performance thermoset adhesive materials requires consideration of the stability of the toughening agent at the cure, postcure and use temperatures of the material. Therefore, assessment of thermal stability is an important part of testing of tougheners for a system. Thermal stability measurements are often made using thermogravimetric analysis (TGA) which provides information about decomposition based upon the loss of sample mass as a function of increasing temperature or time. However, oxidative

degradation processes may be present that do not result in the simple mass loss of sample, and which consequently are not resolvable by this technique. An alternative technique is outlined below after presentation of the more traditional TGA approach.

Thermogravimetric analysis was performed on all tougheners using a TA Instruments ® 2950 TGA. Samples were weighed to 10 ± 1mg and placed in the instrument which was programmed to ramp up in temperature at 10 ºC per minute in air with a flow rate of 25 mL min^{-1}. The resultant scans are shown in Figure 3-9. Comparison of the samples shows that significant weight loss occurs above 300 ºC in all cases. This is above the glass transition temperature of the unmodified cyanate ester matrix material but little difference is seen in mass at lower temperatures. Significantly, this thermoset can suffer thermo-oxidative stability problems above about 220 °C, especially at long times (more than two hours) and with certain metal catalysts. (88) One concludes that it is the thermo-oxidative stability of the tougheners at temperatures below 220 °C that needs to be examined by some other technique.

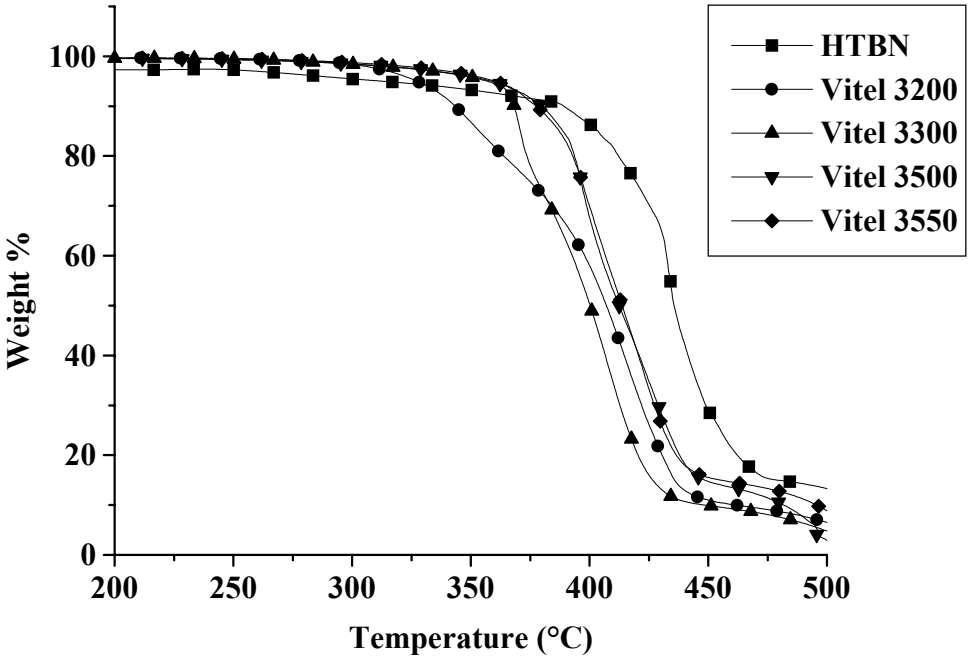

Figure 3-9. Comparison of TGA results in air for tougheners.

It is well known that butadiene-acrylonitrile copolymers suffer thermal instability at elevated temperatures, in part due to the double bond present in the polymer's backbone. This unsaturation can be the subject of thermal degradation and oxidative attack. (89) These degradative mechanisms take place well below the observed significant change in weight for this material as observed by TGA presented above. The calculated onset of the initial weight loss was determined to be 428.9 °C for HTBN, 376.5 °C for Vitel 3200, 368.2 °C for Vitel 3300, 372.7 °C for Vitel 3500 and 379.0 °C for Vitel 3550. (Figure 3-9) However, it is obvious that these samples are subject to chemical change at temperatures of 250 °C in air because heating to these temperatures produces obvious color changes. For optimal performance, the ideal toughener will provide reasonable thermal and oxidative stability at the cure and use temperatures of the thermoset in addition its other critical properties.

3.2.2.1.1 Differential Scanning Calorimetry (DSC) Oxidation

An informative comparison of the oxidative stability of the tougheners was accomplished using a DuPont Instruments 912 Dual Sample DSC. Samples were weighed to 10 ± 1mg and placed in open aluminum pans. The pans were placed in the DSC and purged with nitrogen at 40 mL/minute for at least 15 minutes. The DSC was heated at maximum rate to the experimental temperature then held isothermally under nitrogen purge for 10 minutes. The purge gas was subsequently switched from nitrogen to air at 40 mL/minute and the sample was held isothermally. Results from these evaluation at 250 °C are shown in Figure 3-10.

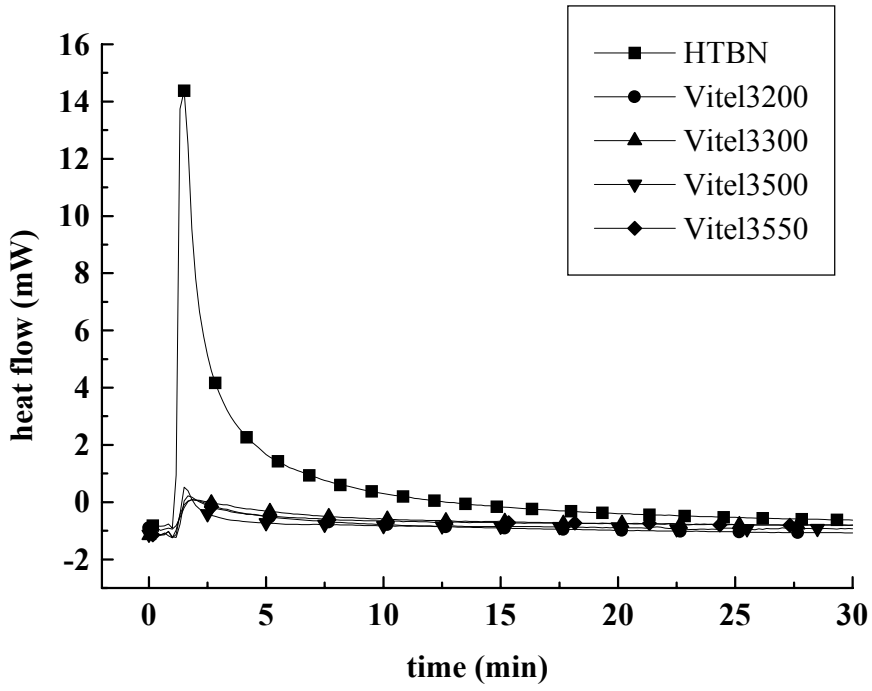

Figure 3-10. 250 °C DSC Oxidation of Tougheners

The admission of an oxidizing environment (air) to the DSC cell at elevated temperatures allows the oxidation reaction to be monitored as it takes place by the exotherm produced by the

reaction. For the case of HTBN, increasing test temperatures lead to a larger exothermic peak area and peak height, plus faster attainment of a maximum in the exotherm. In addition, there was a shorter time for completion for the oxidation process (Figure 3-11) for all temperatures up to 225°C. There is comparatively little difference between the 225°C and 250 °C tests. The same trends are apparent for the Vitel copolyesters but to a much smaller extent. There was little apparent difference within this series of materials. At the lower temperatures, no exotherm due to the oxidation reaction is detectable, with the first signs of reaction appearing at 200 °C.

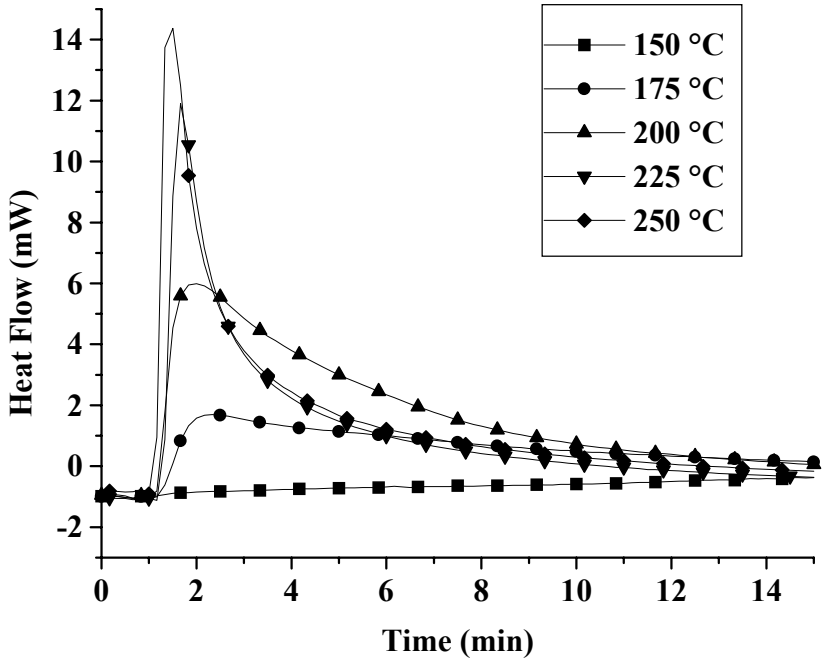

Figure 3-11. DSC Oxidation of HTBN

Integration of the peak areas should provide a measure of the degree of reaction occuring. Unfortunately, large baseline shifts in all of thermograms make their use in quantitative calculations difficult. This appears to be due to a change in both the heat capacity and area of sample contact with the pan bottom upon both heating and oxidation. Whereas a trend of

increasing exotherm area due to an increase in temperature is obvious, the exact differences in integrated areas are uncertain. It is apparent that the thermo-oxidative stability of the Vitel series of materials is much better than HTBN from the much smaller resultant exothermic peak areas. Approximately an order of magnitude less reaction occurs under oxygen at 250 °C.

3.2.2.2 Dynamic Mechanical Analysis

Dynamic Mechanical Analysis (DMA) was used to investigate the phase separation of the toughened samples. Prepared samples were evaluated using a TA Instruments 2980 DMA in single cantilever bending mode, using a heating rate of 1 °C per minute, and a frequency of one Hertz. The low temperature portion of the mechanical spectrum is represented by the loss factor, tan δ, in Figure 3-12. Later figures will illustrate the high temperature region where alpha relaxations are noted.

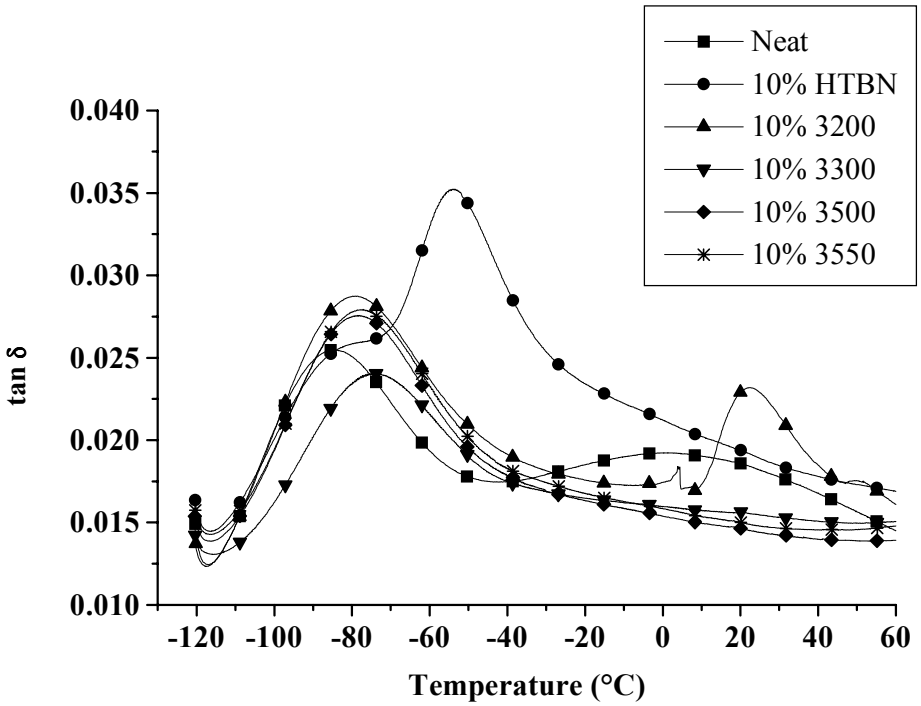

Figure 3-12. Low Temperature DMA, 10% Modification

In Figure 3-12 the loss peaks appear as a function of temperature for the neat polycyanurate material, as well as this material modified with 10 weight percent of HTBN and Vitel materials 3200, 3300, 3500, and 3550. These materials were all cured at 150 °C for four hours, and followed by postcure. Evidence of beta and gamma relaxation processes of significant magnitude was visible for the untoughened material as reported previously. (90) In comparison, the most obvious feature of the modified materials at these temperatures is the presence of a distinct loss peak at the glass transition temperature of the toughener only in the two cases of the HTBN and Vitel 3200 additions. This indicates the presence of separated domains sufficiently rich in toughener, and of sufficient size, to relax independently of the matrix. For the samples containing Vitel 3300, 3500 and 3550, there were no such relaxations. Significantly, the beta transition appears suppressed with addition of Vitels 3300, 3500 and 3550; however, the gamma transition is still apparent in each example, with only small differences in magnitude and position. To maintain miscibility at higher conversions, specific interactions between the modifier chains and the BADCY/polycyanurate must be present to promote exothermic processes to overcome the large decrease in configurational entropy associated with molecular weight increase. The molecular segments associated with the motions responsible for the polycyanurate beta transition are affected by this interaction. Therefore, molecularly mixed toughener (as opposed to the material included in the disperse phase) increases the thermal energy required for the motion responsible for the beta transition due to having to overcome this interaction, and the beta transition is shifted to a higher temperature.

In Figure 3-13, the high temperature region of the mechanical spectrum is shown for these same samples.

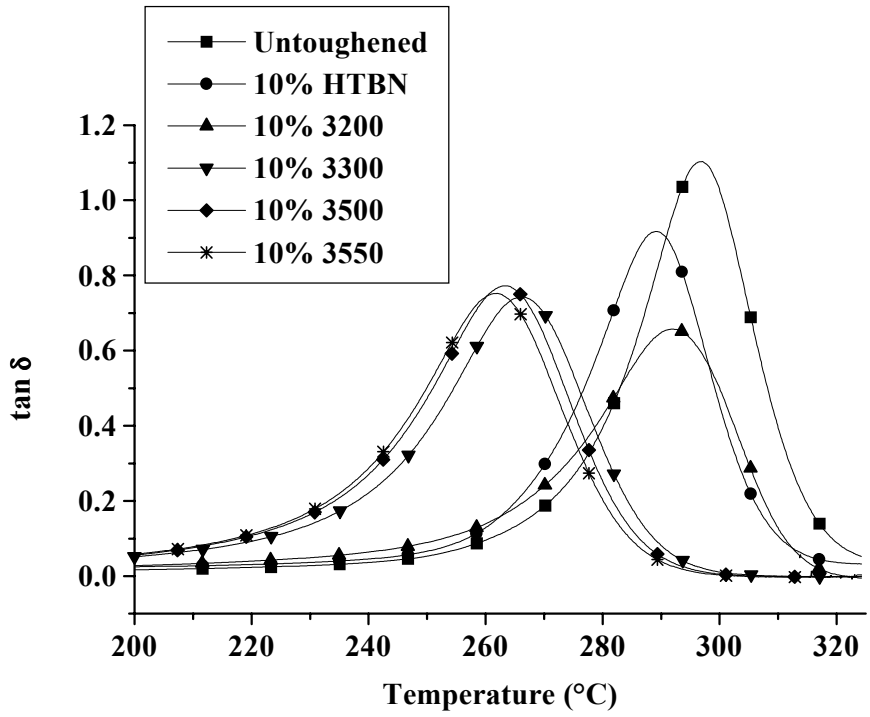

Figure 3-13. High Temperature DMA, 10% Modification

The high glass transition temperature of the unmodified matrix is readily apparent from the loss maximum, and the glass transition temperatures of the Vitel 3200 and HTBN-modified samples are only slightly diminished as a result of the addition. The glass transition peaks corresponding to the Vitel 3300, 3500, and 3550 modified samples are significantly shifted to lower temperatures. This is indicative of the absence of phase separation on any large scale which would demix the initial solution of toughener in BADCy. Because the glass transition temperature of the toughener is much lower than the polycyanurate, the molecularly mixed resin/toughener system displays a glass transition temperature that is depressed as a function of the composition of the sample and the glass transition temperatures of the component polymers.

The amount of dissolved toughener may be calculated from standard equations such as that of Fox.

3.2.2.3 Atomic Force Microscopy

Atomic Force Microscopy (AFM) was used to establish the topological characteristics of the microstructure of all samples. A Digital Instruments Dimension 3000 AFM was used in Tapping Mode™, which provides contrast based on the phase angle between the signal applied to the AFM tip and the actual oscillation of that tip, with a resultant image using this difference as contrast. Micrographs were taken of samples microtomed to produce flat surfaces. AFM micrographs of samples cured with no toughener as well as 10% inclusion of HTBN, Vitel 3200, 3300, 3500 and 3550 at 150 °C are shown in Figure 3-14 through Figure 3-19.

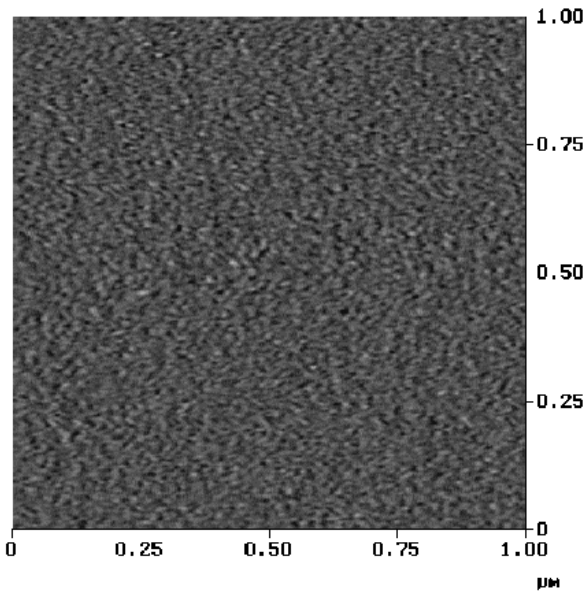

Figure 3-14. AFM image of unmodified polycyanurate

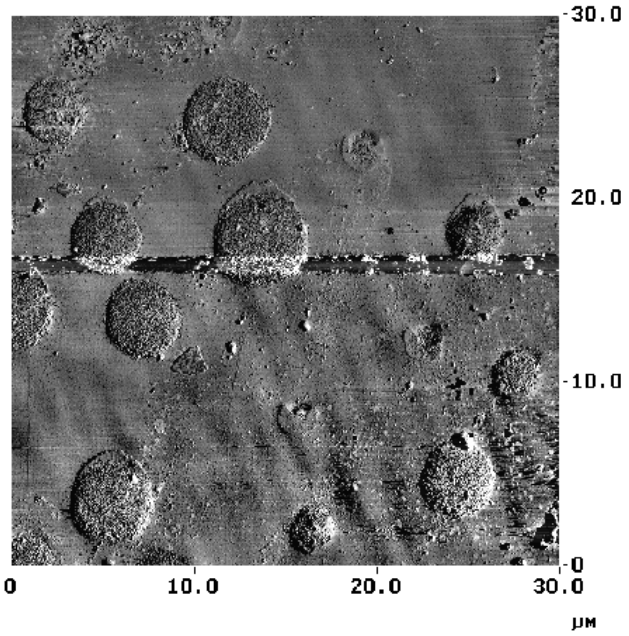

Figure 3-15. AFM image of 10% HTBN in polycyanurate

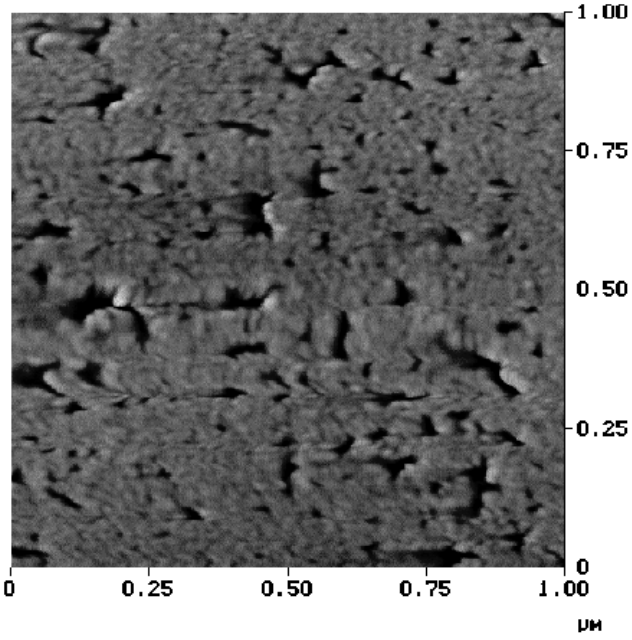

Figure 3-16. AFM image of 10% Vitel 3200 modified polycyanurate

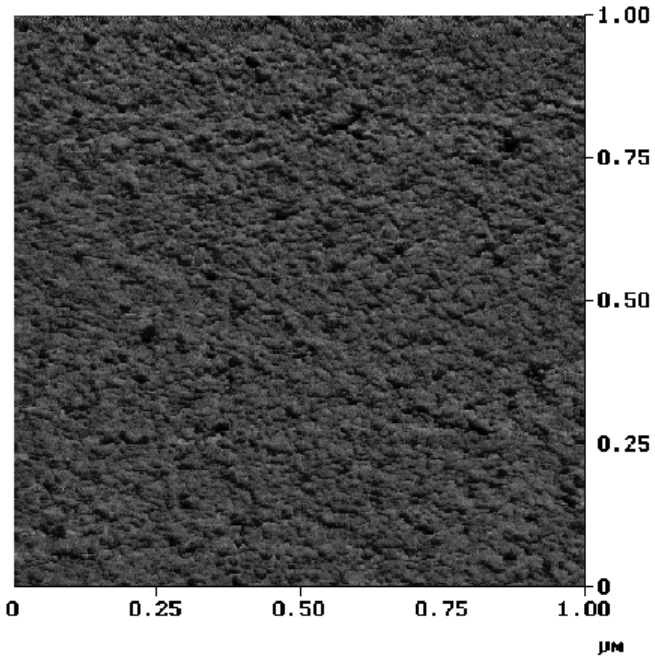

Figure 3-17. AFM image of 10% Vitel 3300 modified polycyanurate

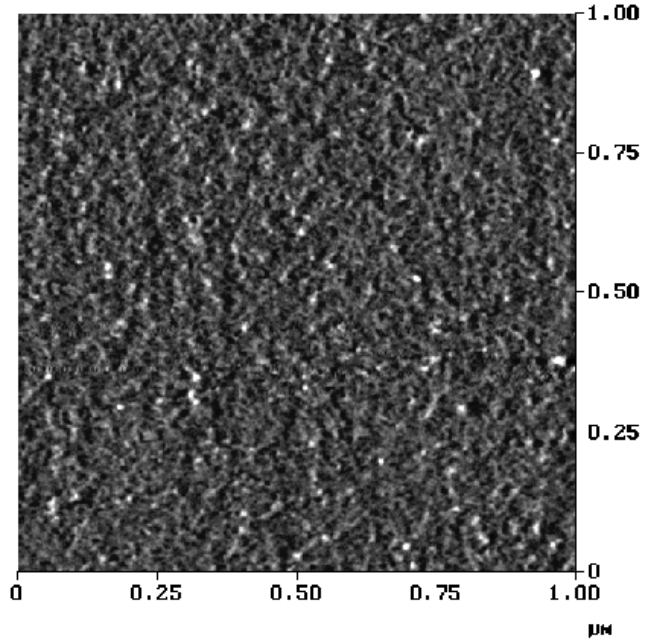

Figure 3-18. AFM image of 10% Vitel 3500 modified polycyanurate

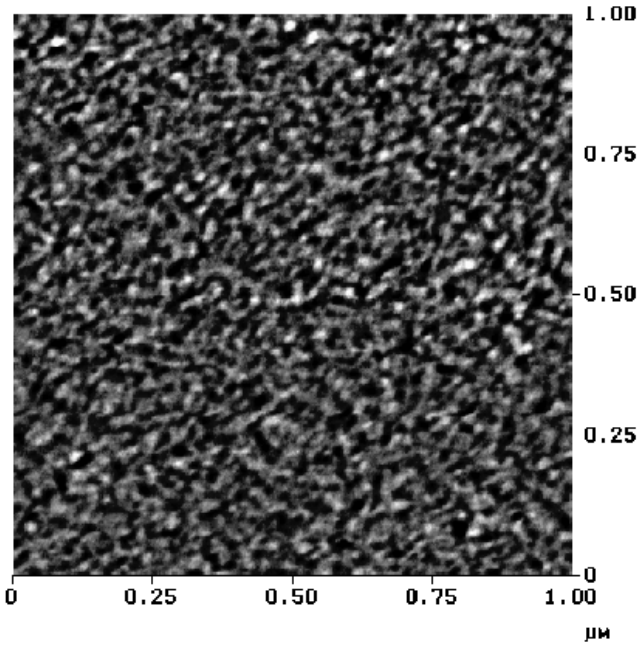

Figure 3-19. AFM image of 10% Vitel 3550 modified polycyanurate

Clear evidence of phase separation is visible in the HTBN toughened sample (Figure 3-15), in comparison to the relatively featureless image of the unmodified polycyanurate (Figure 3-14). Spherical particles of the toughener-rich phase about 5 microns in diameter are apparent, confirming the presence of second phase which was detected using DMA. This type and size of particle are typical for butadiene-acrylonitrile toughened epoxy systems which are well known to exhibit excellent improvements in toughness with the addition of the modifier. The Vitel 3200-modified material is shown in Figure 3-16. This micrograph region represents 1 square micron. Toughener-rich particles are present, but are much smaller (about a quarter of a micron in the largest dimension). They are much more irregular and angular in shape and possibly somewhat interconnected in comparison with the sample containing HTBN. The presence of toughener-rich domains suggests that there should be a corresponding increase in fracture toughness, though the very small size of the particles relative to those commonly found in toughened thermosets suggests the possibility of low toughening effectiveness. (91) Although irregular

particle shape may arise from either a binodal or spinodal mechanism of phase decomposition (92), it is most often associated with of spinodal phase separation.

No areas of obvious toughener-rich particles are visible for the samples modified with Vitel 3300, 3500, or 3550 (Figure 3-17, Figure 3-18, and Figure 3-19, respectively), which agrees with the results found using DMA. The absence of toughener-rich particles detectable either with microscopy or DMA suggests there will be very little or no improvement in the fracture toughness as a result of the addition of the second component. This has an additional undesirable result which is the depression of the glass transition temperature as a result of the apparent large miscibility of the toughener in the cured polycyanurate.

3.2.2.4 Fracture Toughness

Improvements in fracture toughness are advantageous in bulk, composite, and adhesive bond applications. For the materials in this study, the critical stress intensity factor in mode I ($K_{IC,}$ discussed in Chapter 2) was measured using a three-point bending apparatus in the single edge notch geometry following ASTM guidelines. (93) Samples were machined from castings to correct dimension and a saw notch inserted, followed by cracking on insertion of a liquid-nitrogen-cooled razor blade. This sharp crack was propagated to produce a precrack length-to-width ratio of 0.45 to 0.55. The test was conducted at 24 °C, and the tensile tester crosshead speed used was 1 mm min^{-1}. As the sample was strained, the load required to propagate the crack was recorded, and the K_{IC} value calculated.

The addition of HTBN to the polycyanurate produced good improvements in fracture toughness. For the untoughened polycyanurate, the K_{IC} value was measured at 0.58 MPa m^{-2}. Addition of 10% HTBN with cure at 150 °C produced a fracture toughness value of 1.05 MPa m^{-}

^{2}. This is a considerable improvement and a reasonably good value for a material with such a high glass transition temperature and crosslink density.

Fracture toughness results for the Vitel 3200 modified material also showed a significant improvement in fracture toughness, obtaining a value of 0.94 MPa m^{-2}. As expected from the lack of a second toughener-rich phase, the samples modified with Vitel 3300, 3500 and 3550 produced a statistically insignificant improvement in fracture toughness. A comparison of K_{IC} values is shown in Figure 3-20.

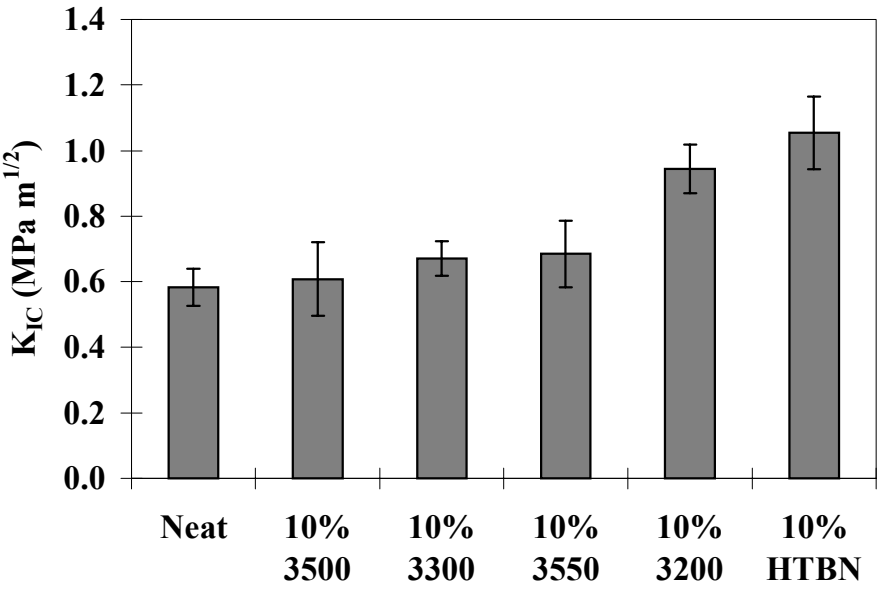

Figure 3-20. Comparison of fracture toughness values

It is interesting to note the improvement in fracture toughness for the Vitel 3200 containing material almost reaches the level of the HTBN sample in view of the size of its toughener-rich particles. Unfortunately, due to the irregular shape of these particles, quantitative study of their size and size distribution is extremely difficult. However, the volume fraction of this toughener-rich phase is related to the peak area of the DMA tan delta curve. The high-

temperature end of the spectrum shows a tan delta peak area somewhat smaller than that of the HTBN-toughened material, indicating a smaller volume fraction of the polycyanurate-rich phase and a larger volume fraction of the toughener-rich phase. A larger volume fraction of toughener-rich particles has been shown to increase toughness. (94, 95) However, some studies have indicated (96, 97) that larger particles are more efficient at toughening. If this were true, the Vitel 3200 should produce only small improvements in fracture toughness for this material, contrary to the experimental facts. Consideration of the mechanism of the improved toughness for toughened thermosets may give an indication of the origin of the improvement that were noted.

Unfortunately, a single, definite mechanism for the improvement of fracture toughness as a result of ductile inclusions is not generally accepted, and may not exist. (98) Many different mechanisms have been proposed (99, 100, 101, 102, 103, 104, 105) and it appears that multiple mechanisms may be simultaneously and jointly responsible for the observed improvement in fracture toughness. In addition, it is difficult to change only particle size without changing other such important characteristics, e.g. initial composition, volume fraction, and particle plus continuous phase composition. This makes determination of the particle size and size distribution relationship to toughness through a specific mechanism difficult. However, analysis of selected mechanisms yields their dependence on particle size; and, in the current case of a system with an extremely small particle size, may provide some insight into the predominant mechanism(s) of toughness enhancement observed.

The crack-bridging mechanism as proposed by Kunz-Douglas et al. (106) predicts a fracture toughness improvement ΔG_{IC}, derived from rubber elasticity theory:

$$\Delta G_{IC} = 4\gamma V_f \left(1 - \frac{6}{\lambda^2 + \lambda + 4}\right) \qquad \textbf{(3-27)}$$

where λ is the extension ratio, γ is the energy per unit interfacial area required to debond or tear the particle, and V_f is the volume fraction of toughener-rich phase. This yields a decrease in the extension ratio of particles at the crack tip with an increase in the particle size if the number density is uniform. This may be reduced to the effect of number density and particle size through the relation $V_f \propto N_V r^3$, where N_V is the number density of particles per unit volume. This produces a linear increase in fracture toughness with number density, but a cubic increase with particle radius. In effect, a much more significant dependence on particle size than on the number of particles per unit volume is the conclusion.

In the case of a crack deflection mechanism, fracture toughness is increased due to the addition energy required to form the resultant larger surface area created by crack deflection. The dependence on particle size is

$$\Delta G_{IC} = \pi r^2 N_A \gamma_m \qquad \textbf{(3-28)}$$

where N_A is the number of particles per unit area and γ_m is the energy per unit area of the matrix material. In this case, there is also a prediction of greater improvement in fracture toughness with larger particles. Consideration of the analysis of the crack pinning mechanism, however, shows an inverse dependence on the interparticle distance, d_p:

$$G_{IC} = G_{IC}(matrix) + 2\frac{T_L}{d_p} \qquad \textbf{(3-29)}$$

where T_L is the energy per unit length of the crack front. The good improvements in fracture toughness seen in the present example of Vitel 3200 tends to discount those mechanisms of excellent toughening derived from large particle sizes.

Test temperature can have a large effect on the observed fracture toughness. Because polymeric materials are viscoelastic there are dependencies on test rate as well. The results may

be correlated with test temperature through well-known time-temperature relationships. The presence of a second phase in a polymer which is rich in a second component causes additional thermorheological complications. Because the glass transition temperature of Vitel 3200 (16.1 °C) is quite close to the test temperature, the measured toughness may be increased, although this effect is small for rubber-toughened epoxies. (107) At temperatures either higher or lower than the glass transition temperature of the toughener-rich phase, the system would not display as great an energy dissipation at standard test speeds, and the observed improvement of toughness may be diminished.

3.2.2.5 Effect of Variation of Initial Composition and Cure Temperature

Prior experiments with rubber-epoxy formulations have attempted to optimize fracture toughness through increasing the volume fraction of the second phase by increasing the precure rubber concentration. In addition, it has been demonstrated that cure temperature can have a marked effect on the microstructure of toughened thermosets. (108) The ability of HTBN and Vitel 3200 to produce enhanced toughness in polycyanurate discussed previously suggests benefit might be gained by optimization through variation of composition and processing conditions for these two modifiers. The effect of two extremes of cure temperature on phase separation was examined as well as the variation of initial composition from 5 to 25 weigh percent of the toughener component.

Samples were prepared as discussed previously. The cure cycles chosen were at the extremes possible with this catalyst system. At a cure temperature of 210 °C, only small amounts of resin may be cured and only in molds with good thermal conductivity to carry away the significant and quickly generated cure exotherm of energy. (109) Cure at 150 °C brings the

sample to the gel point in about 2 hours. This was taken to be a practical low-end cure temperature limit. Samples are postcured as discussed previously.

3.2.2.5.1 Dynamic Mechanical Analysis

Examination of these new compositions using DMA reveals the effects of a larger amount of toughener used for the case of both HTBN (Figure 3-21 and Figure 3-22) and Vitel 3200 (Figure 3-23 and Figure 3-24) incorporation. For the example of HTBN incorporation, the loss peaks associated with the toughener-rich phase increase in with increasing amount of rubber (Figure 3-21).

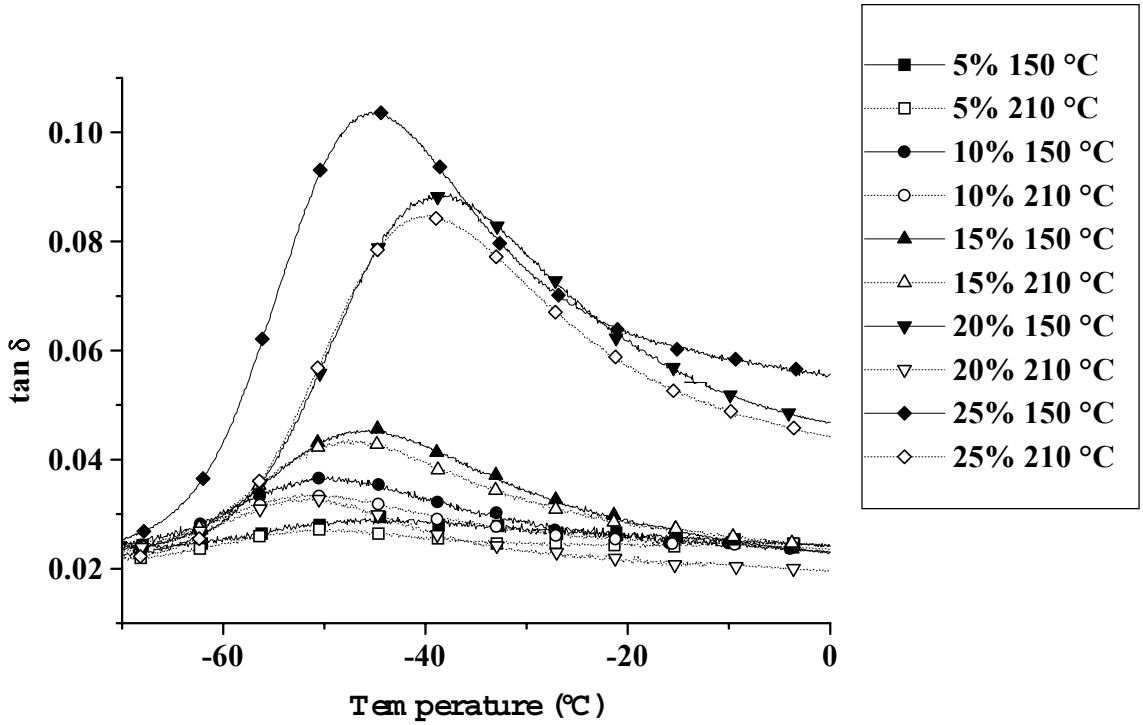

Figure 3-21. HTBN-modified low temperature DMA

In each of these experiments, a slightly larger loss peak was found for the 150 °C cure which is indicative of more complete phase separation and a correspondingly larger volume

fraction of toughener in the system. This is the result of the kinetic control of formation of the second phase by the nucleation and growth mechanism. At higher temperatures, this relatively sluggish process causes the system to reach the gel point before phase separation is complete thereby creating modest differences in the volume fraction of toughener-rich phase. However, in the case of 20% by weight inclusion of HTBN, there are two radically different loss peaks depending on cure temperature. At the higher cure temperature a rather small peak is apparent while at the low cure temperature an extremely large peak is apparent. Consider a representative phase diagram in terms of temperature (as discussed in Chapter 2) versus volume fraction of the toughener component. It has been noted that an increase in the degree of conversion can be viewed as equivalent to a decrease in temperature, and in fact the increasing conversion of a thermoset has been called a "chemical quench". (110) For the case of an upper critical solution temperature (UCST) phase diagram at higher initial toughener compositions phase separation occurs earlier in the polymerization. At low cure temperatures, significant time elapses between the start of phase separation and gelation where the phase separation stops. This time allows coalescence to take place, along with separation based on density, and phase separation may take place with little influence over phase size or dispersion. This produces a much larger DMA relaxation peak associated with the very complete phase separation into macroscopic domains under less constraint. This behavior is further illustrated by a large decrease in modulus at temperatures above the T_g of HTBN which does not occur in the samples without the bilayered, large-scale structure.

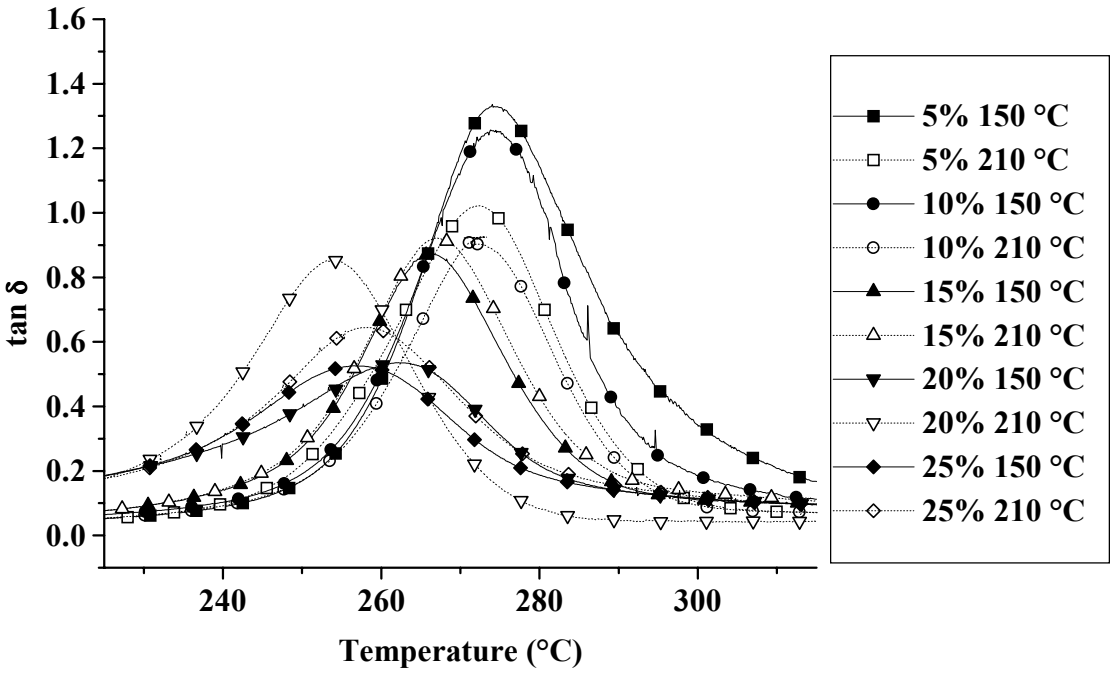

Figure 3-22. HTBN-modified high temperature DMA

At the high temperature end of the spectrum of the composition series samples, the glass transition temperature depression of the polycyanurate-rich phase increases with increasing initial toughener concentration (Figure 3-22). For the inclusion of 5% and 10% HTBN, the lower cure temperature produces more complete phase separation and less T_g depression. At 15% HTBN levels, there is less difference between samples. With 20% HTBN, there is a large difference in the size and position of the polycyanurate-rich phase peak, reflecting the differences discussed previously about the dependence of the toughener-rich phase behavior on cure temperature. The differences in the 25% initial composition samples are also rather small and probably begin to reflect equilibrium values due to the relatively long time between the onset of phase separation and gelation.

Examination of the low temperature region of the DMA spectra for the Vitel 3200 toughened material (Figure 3-23) indicates that the effect of increasing initial toughener composition appears as an increase in the volume fraction of toughener-rich second phase.

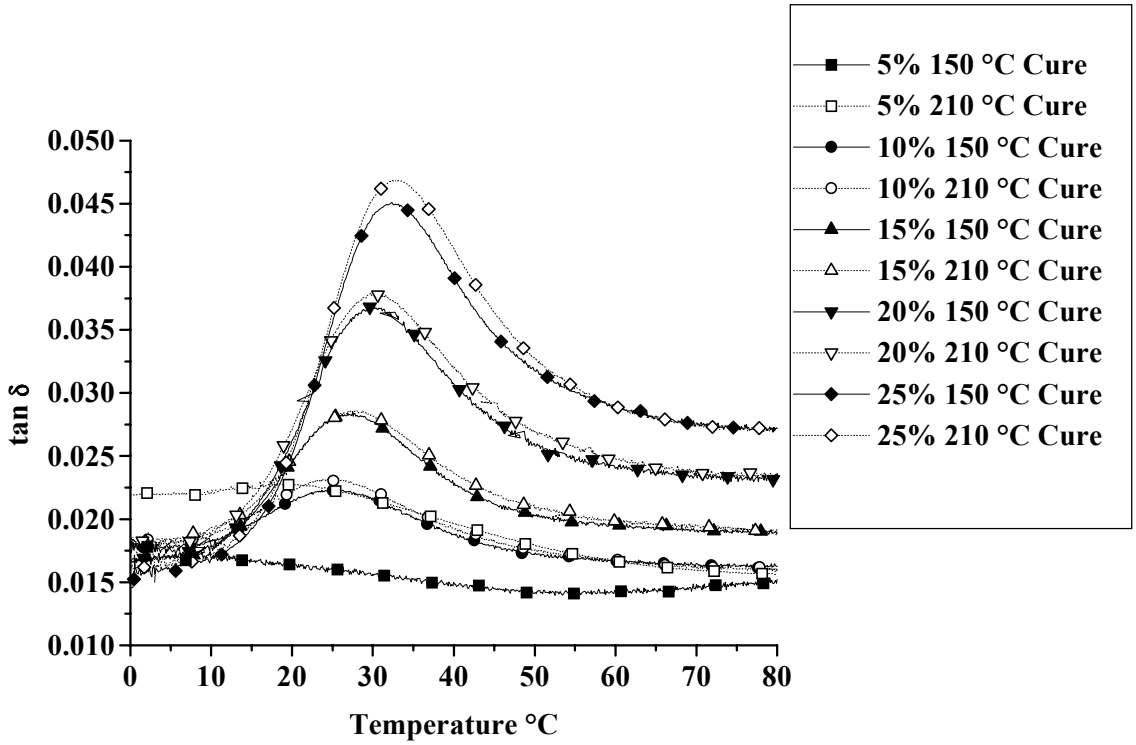

Figure 3-23. Vitel 3200-modified low temperature DMA

The tan delta peak areas increase in Figure 3-23 for each sample with increasing initial composition. Additionally, higher cure temperatures produce slightly larger peak areas than the cooler cure temperature for that composition level, indicating a greater volume fraction of separated toughener. This is due to the effect of temperature and is interpretable on the phase diagram. Higher temperatures shift location on the phase diagram to higher conversions, and this in turn shifts the equilibrium phase compositions of the coexisting phases towards one another at the gel point. The net effect creates a toughener-rich phase with a larger amount of

polycyanurate and a larger overall volume fraction at higher cure temperatures. The DMA peak positions of the toughener-rich phases also indicate a slightly higher glass transition temperature of that phase, supporting the conclusion that there is more polycyanurate in the toughener-rich phase. At the 5% concentration level, the tan delta response for the lower cure temperature does not follow this trend. The phase diagram indicates that at low initial concentrations, it is much easier for the system to remain in the metastable state. This increases the likelihood that phase separation will be supressed and less phase separation will occur.

At the high temperature end of the mechanical spectrum of this Vitel 3200 composition series, the loss peak positions fall on approximately the same temperature with the exception of the 150 °C cured 5% sample suggesting that these systems are relatively close to thermodynamic equilibrium (Figure 3-24).

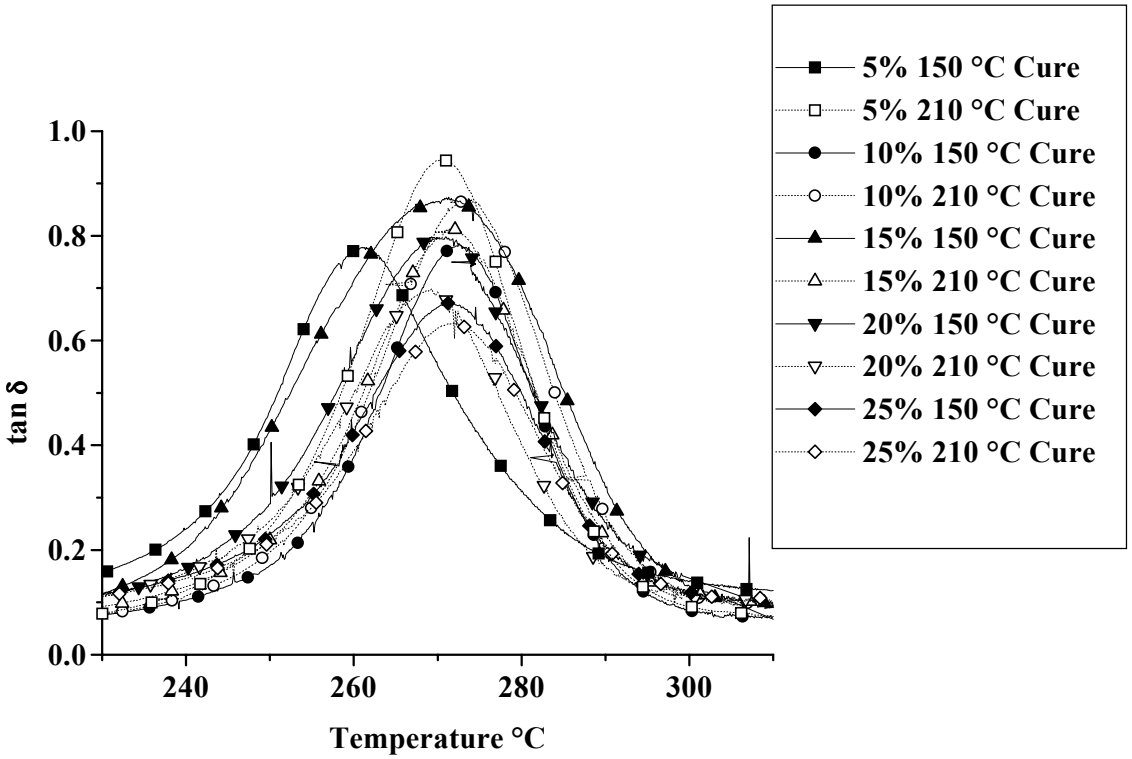

Figure 3-24. Vitel 3200-modified high temperature DMA

Vitel 3200 is found to exhibit relatively small changes in the phase composition with cure temperature leading to only small changes in the final matrix glass transition temperature. This suggests a spinodal mechanism of phase separation, with its fewer kinetic effects, which is supported by both the phase diagram for higher molecular weight modifiers and the irregular particle shape seen using AFM. There is also a general trend to smaller observed particle areas with increasing toughener concentration indicating a smaller volume fraction of the polycyanurate-rich phase. For the case of the 150 °C cured, 5% modifier sample, the suppression of phase separation in the metastable state produces the depressed glass transition temperature of the polycyanurate-rich phase.

3.2.2.5.1 Atomic Force Microscopy

AFM was used to examine the particle size and particle size variation with initial composition and cure temperature in these composition investigations. Micrographs from the Vitel 3200-modified samples are shown in Figure 3-25. Here, the effect of increasing the initial concentration of toughener is readily apparent. The average size of the particles appears to increase somewhat with increasing concentration of toughener, along with a significant increase in particle density. Together, these produce an increasing volume fraction of that phase. This is consistent with the increase in DMA loss peak area found for this phase, and should produce corresponding improvements in the fracture toughness. It is significant that no large differences are seen for the two extremes of cure temperature. This serves to minimize the effects on fracture toughness resulting from variations in cure cycle which presents obvious practical advantages. Again in this Vitel example, determination of volume fraction of the second phase quantitatively using microscopy is complicated by the irregular shape of the particles.

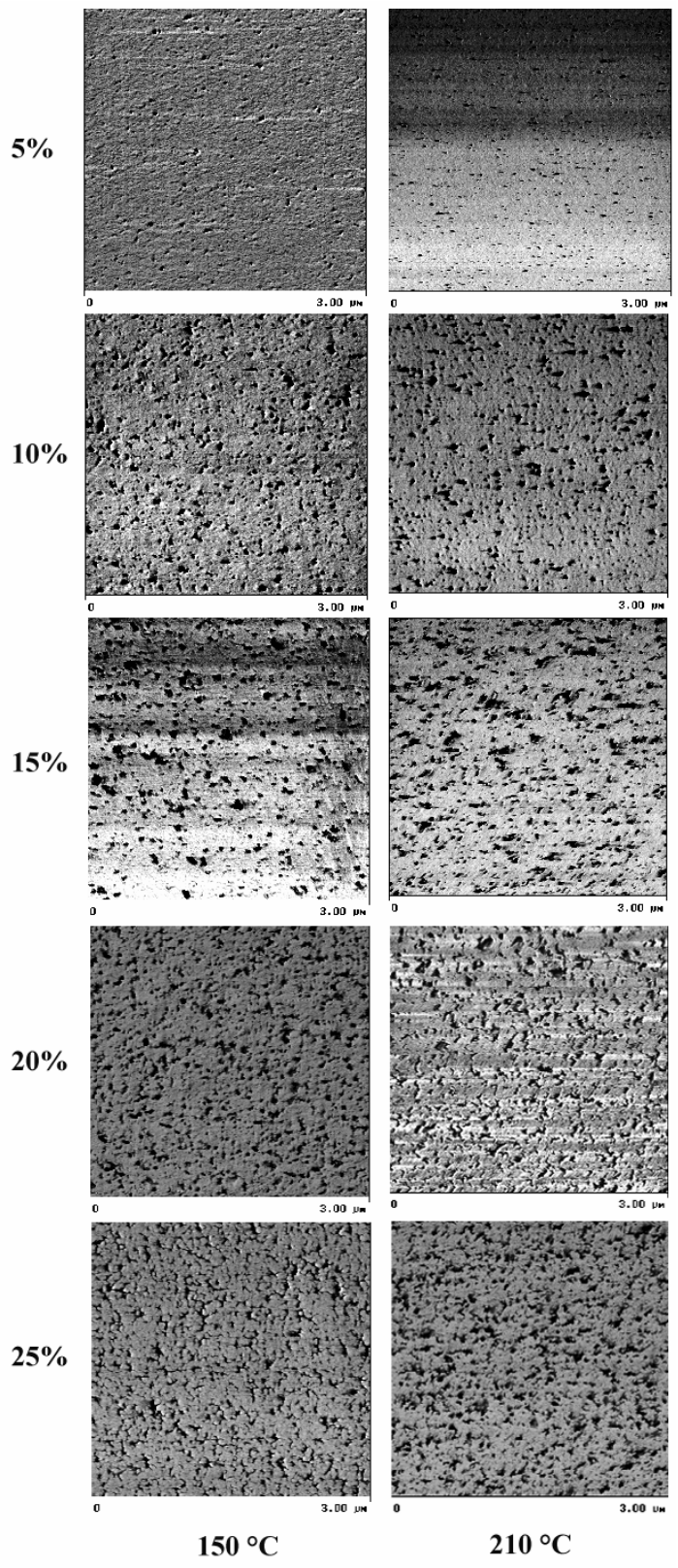

Figure 3-25 AFM images of Vitel 3200-toughened polycyanurate

In contrast, examination of the microstructure of the HTBN-modified samples shows the spherical toughener-rich particles typical of the nucleation and growth phase separation mechanism (Figure 3-26). The particle size and density show marked differences between cure temperature extremes. This variation in particle size results from a relatively large discrepancy between the activation energy for the polymerization reaction and the activation energy for viscosity, which affects diffusion, controlling the phase separation as temperature is changed. (111) The nucleation density of the higher cure temperatures is obviously greater, resulting in a larger number of particles per unit volume. At equivalent phase separations, mass balances dictate that the average particle size is also smaller, and at the lower cure temperature the lower nucleation density results in a larger particle size. Volume fractions of the second phase as determined by DMA show only moderate differences due to cure temperature, though the apparent volume fraction by visual inspection changes significantly due to the large particle size variation. The difference in particle size is readily apparent for the 5% and 10% HTBN samples, but is less pronounced in the 15% case. Significant differences in fracture toughness between the two cure temperatures would therefore be the result of the variation of particle size and number density rather than a change in volume fraction of second phase.

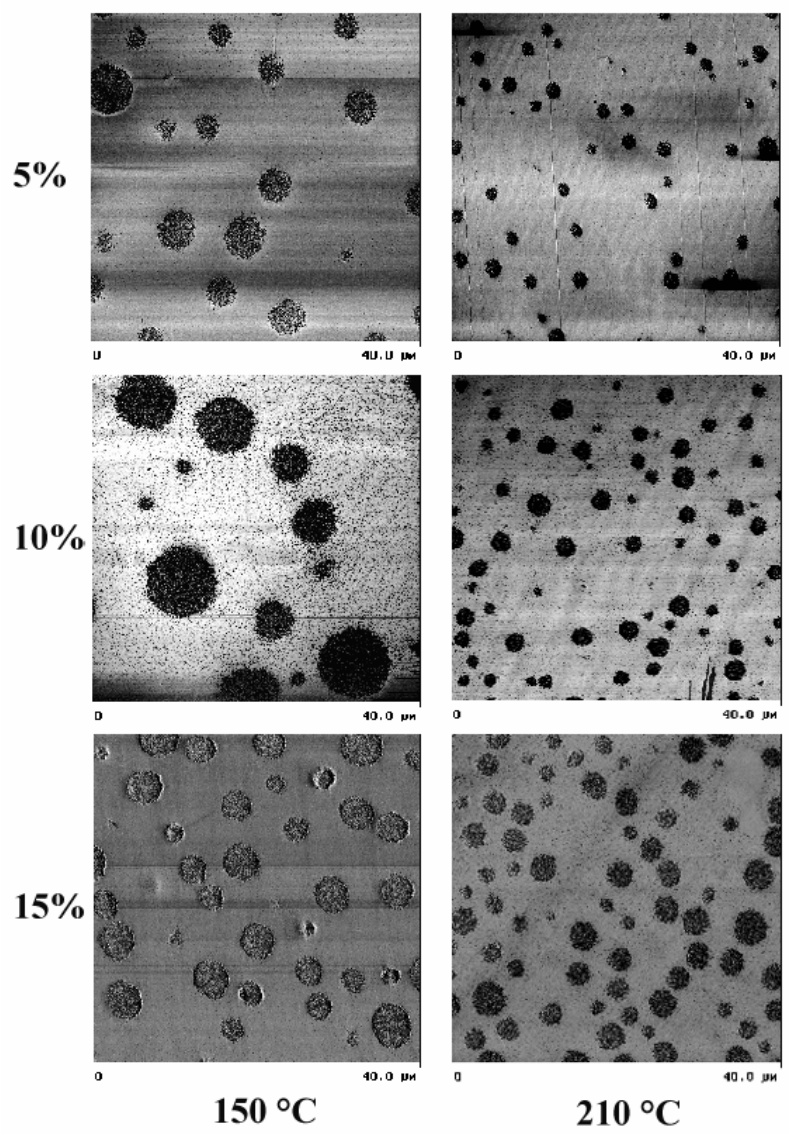

Figure 3-26. AFM images of HTBN-toughened polycyanurate

3.2.2.5.3 Scanning Electron Microscopy

Scanning Electron Micrscopy (SEM) was obtained using an ISI SX-40 Scanning Electron Microscope. Examinations of fracture surfaces were made. For the Vitel 3200-toughened systems, the particle size was insufficient to provide good resolution of the details of the fracture surface. It appeared that the toughener-rich domains remained well adhered to the matrix. The

inclusion of this toughener produces a highly roughened surface (Figure 3-27) in comparison to the untoughened polycyanurate fracture surface shown in Figure 3-28.

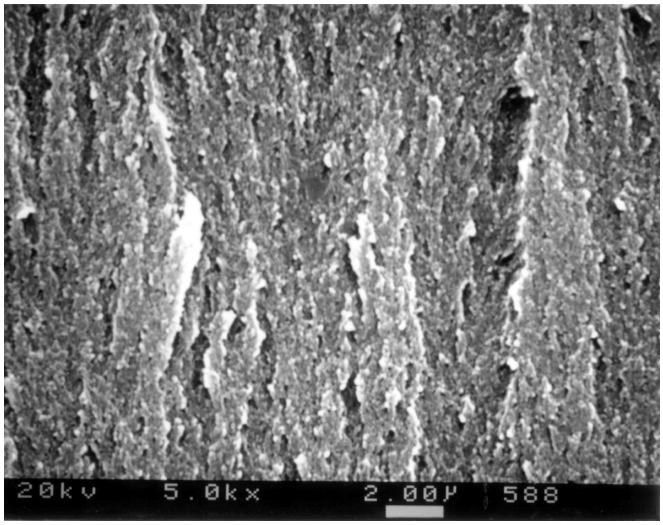

Figure 3-27. SEM image of Vitel 3200 toughened polycyanurate (25%, 150 °C) fracture surface, 5000X

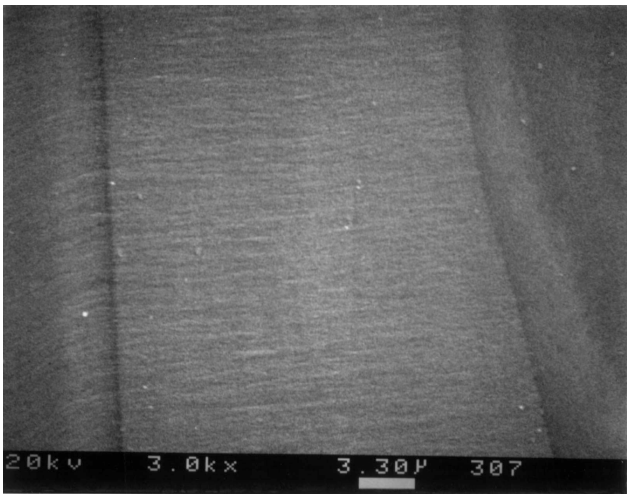

Figure 3-28. SEM image of untoughened polycyanurate fracture surface, 3000X

In the case of the HTBN-modified samples of 5%, 10% and 15% addition, fracture tore the toughener-rich particles, which remained attached to the matrix. A typical result for these samples is shown in Figure 3-29.

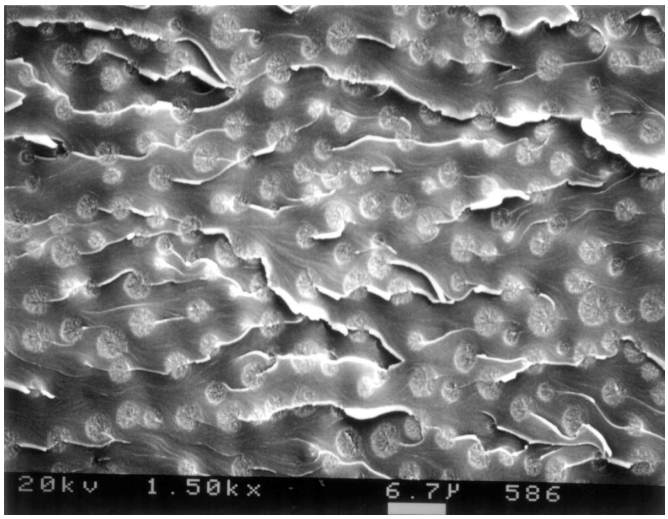

Figure 3-29. SEM image of HTBN-toughened fracture surface (10%, 150 °C), 1500X

Good adhesion of the toughener-rich particles to the matrix has been shown to be important to the efficacy of the toughener. (112) In the case of both toughenners examined, the hydroxyl termination allows the formation of covalent bonds between matrix and toughener-rich phases (113) providing good adhesion between phases. The "rivulet" topography typical of a toughened epoxy system is also apparent for the present HTBN-modified samples. It is interesting to note the path of the fracture features shown in Figure 3-29. Ridges clearly originate from some of the particles which continue and typically connect to several other particles. The fracture surface between particles appears quite smooth in the SEM, with no furrows indicative of plastic shear bands. No evidence of large-scale cavitation of the rubber particles may be seen; the fracture surface of the toughener-rich particles is flush with the fracture surface, and no holes are detected.

There is a large difference in the roughness of the fracture surface of the Vitel 3200 and HTBN-modified samples. Because one mechanism of energy dissipation in fracture is the creation of two new surfaces in a broken sample, the polymers with the greatest fracture roughness, or texture, necessarily will absorb more energy on fracture. However, this

mechanism cannot explain all of the observed improvement in fracture toughness. Given the comparable values of fracture toughness measured between tougheners for equivalent concentrations, different mechanisms of toughening probably predominate for each toughener examined.

At higher initial concentrations of HTBN (20% and 25%), the DMA tan delta peak at the glass transition of the toughener-rich phase suggested a difference in phase separation. A bilayered structure was visible to the unaided eye at the fracture surface. SEM images reveal the presence of unusually large and poorly controlled toughener-rich phase particles for both cure temperatures in the case of 25% inclusion of HTBN. (Figure 3-30)

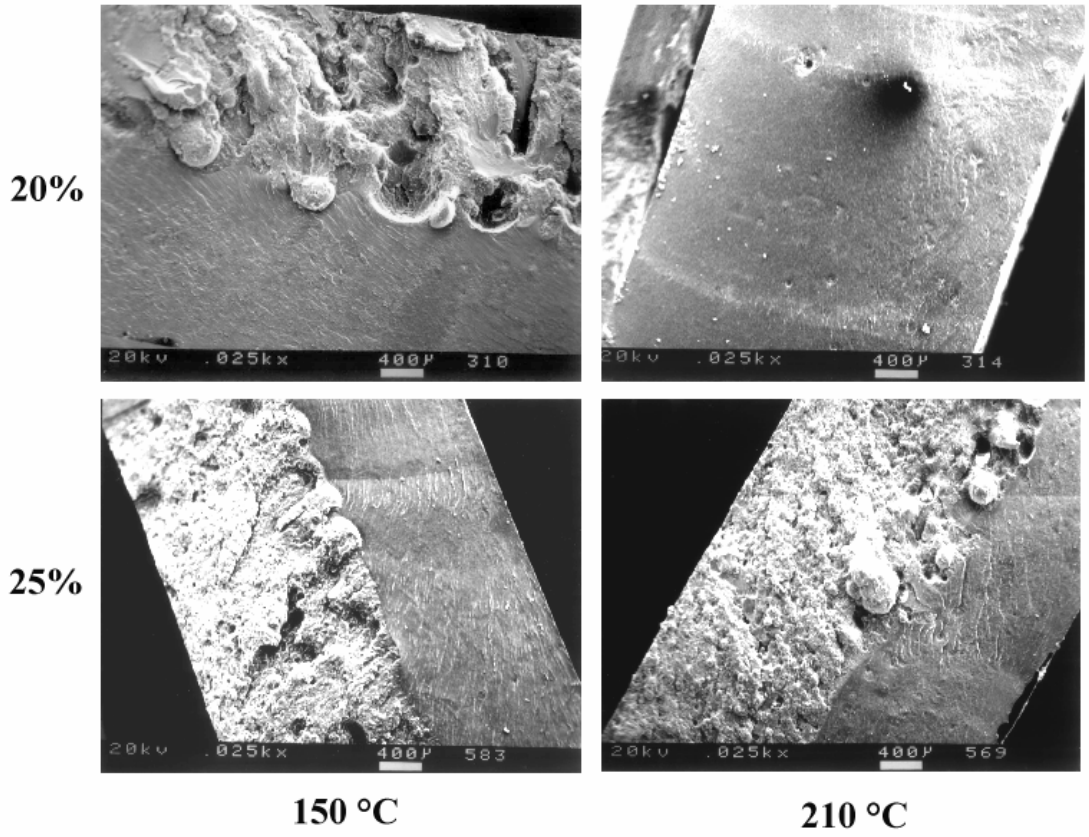

Figure 3-30. SEM images of fracture surface of high HTBN concentration polycyanurate (25X)

The sample is divided into an upper region that was obviously rich in the rubber toughener, due to its compliance. The other region (formed toward the bottom of the mold) is rich in the stiffer, denser polycyanurate. HTBN's density was 0.941 g cm^{-3} (Micromeritics AccuPyc 1330 pycnometer), whereas the density of the polycyanurate is 1.240g cm^{-3} (114), both at 25 °C. These layers are formed and originate due to coalescence of the particles generated which minimizes interfacial energy. In the case of 20% modification, the sample cured at the higher temperature does not display the bilayered structure, whereas the lower temperature cured sample does. This is due to the length of time the sample was maintained between the onset of phase separation and the end of the phase separation at the gel point, as discussed previously. Additionally, the higher cure temperature shifts the phase diagram to higher conversions which also reduces the time between the onset of phase separation and gelation. In summary, the higher cure temperature did not provide sufficient time for kinetically controlled processes and there was a much more controlled distribution of toughener-rich particles. At an initial concentration of 25%, the time between the beginning of phase separation and gelation was greater for both cure temperatures, and was sufficient in both cases to create the bilayered structure.

3.2.2.5.4 Fracture Toughness

A summary of the fracture toughness results for the Vitel 3200 and HTBN modified samples is presented in Figure 3-31 which illustrates the dependence of toughness on both composition and cure temperature.

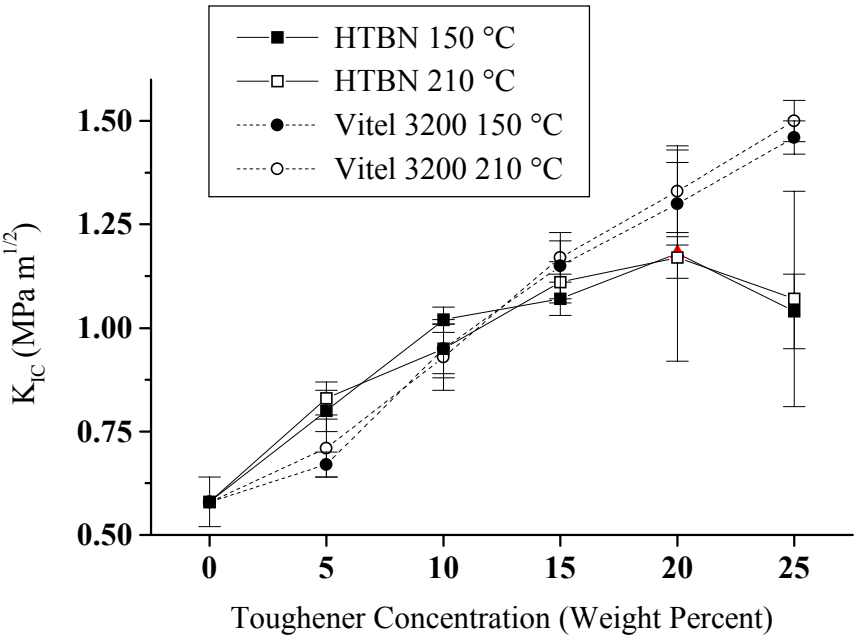

Figure 3-31. Fracture toughness variation with initial composition and cure temperature

A first conclusion drawn from Figure 3-31 deals with the HTBN material. Due to the poor control of microstructure at the higher compositions of HTBN, the efficacy of this modifier diminishes at higher concentrations beyond about 20%. Interestingly, although the higher cure temperature in the 20% concentration of HTBN case controls microstructure better than the lower cure temperature, the average fracture toughness is quite similar in both cases. However, the standard deviation of the 150 °C cured samples is almost twice that of the higher temperature cured sample, which is probably an effect of the large difference in microstructure. The 25% HTBN sample shows very poor values of fracture toughness (in addition to a significantly depressed glass transition temperature) at both cure temperatures.

The second set of conclusions from Figure 3-31 concerns the polyester toughener. The fracture toughness values for the Vitel 3200 toughened samples show continuing improvements with increasing concentrations of toughener. The samples containing 5% show only modest

improvements in comparison to the untoughened samples, barely beyond statistical certainty, and with a larger discrepancy between the two cure temperatures. For the 150 °C cure, 5% modified sample, DMA results showed less phase separation and a smaller volume fraction of the toughener-rich phase. There was also a larger difference between cure temperatures than any other initial composition. This corresponds with the larger difference in fracture toughness improvement at that initial composition than at any other.

For the higher concentrations of Vitel 3200, the improvements in fracture toughness are excellent and continue upward almost linearly with concentration. Fracture energy correlates well with the volume fraction of toughener-rich phase. These fracture toughness values are especially notable considering the high glass transition temperature of the system and its good thermo-oxidative stability. There is no statistically significant difference in toughness between the two cure temperatures at these high concentrations, though the average value is greater for the higher cure temperature at compositions greater than 10%. Because of the small difference in both toughness and microstructure, processing temperatures for this Vitel-based material become less important to final properties. While the use of HTBN also shows only small differences in fracture toughness with cure temperature variation, the large differences in particle size produced by cure conditions emphasize the differences that may be produced by even incidental cure profile variations.

3.3 Conclusions

The toughening of a polycyanurate thermosetting resin was investigated using two commercial, low T_g materials. The thermo-oxidative stability of the copolyester Vitel materials was shown to be greater than the butadiene-acrylonitrile copolymer. Phase separation produced domains rich in toughener for formulations including HTBN and Vitel 3200 as shown by DMA,

and confirmed through use of AFM. When combined with the cyanate ester based matrix polymer, both tougheners produced marked improvements in fracture toughness. Examination of the fracture surface of these systems using SEM revealed good particle-matrix adhesion for the HTBN-containing samples and a highly roughened surface for the Vitel 3200-containing samples with no obvious particle debonding.

Increases in the initial composition of both modifiers produced good toughness improvements up to 15% inclusion in the case of HTBN and continued improvement up to 25% addition of Vitel 3200. Only small differences in fracture toughness resulted from a 60 °C variation of the cure temperature in either case even though the HTBN-containing samples showed large variations in particle size.

The effect of particle size difference on fracture toughness appeared small, while increasing the volume fraction of toughener-rich particles through higher initial compositions had significant effects. The small resultant particle size of the Vitel 3200 modified samples was though to result in large fracture toughness improvements. This suggests that in this case, toughening mechanism dependent upon a positive correlation of toughness with particle size are less significant. Because of significant differences in surface roughness and particle size, it is probable that contributions from several different mechanisms important in these experiments.

DMA data suggested profound microstructural differences in the case of the 150 °C cured 20% HTBN specimens and both 25% HTBN containing samples. This was confirmed through the use of SEM. The mechanism of phase separation was determined to be nucleation and growth for the HTBN-containing samples and spinodal decomposition for the Vitel 3200-containing samples. This was determined with consideration of the molecular weights of the tougheners, the cure temperature dependence of the glass transition temperature of the

polycyanurate-rich phase, and the resultant microstructure. The Vitel 3200 copolyester produced better improvements in fracture toughness at every initial concentration above 5%, better thermo-oxidative stability, and smaller microstructural variation with differences in cure temperature.

3.4 References

(1) S. A. Srinivasan, Ph. D. Dissertation, VPI&SU, (1994).
(2) S. Montarnal, J. P. Pascault, and H. Sautereau. In Rubber-Toughened Plastics, C. Keith Riew, Editor, Advances in Chemistry Series 222, ACS, Washington, D. C., (1989), p. 204.
(3) Y. Huang, D. L. Hunston, A. J. Kinloch, and C. K. Riew, In Toughened Plastics I, C. K. Riew and A. J. Kinloch, eds., Advances in Chemistry 233, American Chemical Society: Washington, D. C., 1993, p. 1.
(4) W. H. Carothers, Transactions of the Faraday Society, 32, (1936), p. 39.
(5) P. J. Flory, Journal of the American Chemical Society, 63, (1941), p. 3083.
(6) W. H. Stockmayer, Journal of Polymer Science, 9, (1953), p. 69.
(7) P. Irvine and M. Gordon, Macromolecules, 13, (1980), p. 761.
(8) S. R. Broadbent and J. M. Hammersley, Proceedings of the Cambridge Philosophical Society, 53, (1957), p. 629.
(9) C. W. Macosko and D. R. Miller, Macromolecules, 9(2), (1976), p. 199.
(10) J. K. Gillham in Developments in Polymer Characterization, J. V. Dawkins, Ed., Vol. 3, Chaper 5, Applied Science Publishers, Ltd., London, (1982), p. 159-227.
(11) J. B. Enns and J. K. Gillham, Advances in Chemistry Series, 203, (1983), p. 27.
(12) L. C. Chan, H. N. Nae and J. K. Gillham, Journal of Applied Polymer Science, 29, (1984), p. 3307.
(13) J. K. Gillham, Polymer Engineering Science, 19, (1979), p. 676.
(14) G. Wisanrakkit and J. K. Gillham, Journal of Applied Polymer Science, 41, (1990), p. 2885.
(15) X. Wang and J. K. Gillham, Journal of Coatings Technology, 64, (1992), p.37.
(16) E. Grigat and R. Putter, Chem. Ber., 97, (1964), p. 3012.
(17) E. Grigat and R. Putter, Agnew. Chem. internat. ed., 6, no. 3, (1967), p. 206.
(18) D. A. Shimp, J. R. Christenson and S. J. Ising, 'AroCy Cyanate Ester Resins: Chemistry and Properties', Rhone-Poulenc, Inc., publication, (1989).
(19) G. W. Bogan, SAMPE Journal, 24(6), (Nov/Dec 1988).
(20) S. Das and D. C. Prevorsek, U.S. Patent 4,831,086, (May 1989).
(21) J. C. Abed and J. E. McGrath, ACS Polymer Materials Science and Engineering, 69, (1993), p. 291.
(22) C. A. Fyyfe, J. Niu, S. J. Rettig, N. E. Burlinson, C. M. Reidsema, D. W. Wang and M. Poliks, Macromolecules, 25, (1992), p. 6289.
(23) A. Osei-Owusu, G. C. Martin, and J. T. Gotro, Polymer Engineering and Science, 31, (22), (1991), p. 1604.
(24) Rhone-Poulenc Technical Document, Specialty Resins-Formulating AroCy Cyanate Esters for Resin Transfer Molding Applications, (May 1992), p. 3.

(25) A. M. Gupta, Macromolecules, 24, (1991), p. 3459.
(26) M. Bauer, J. Bauer, G. Kuhn, Acta Polymerica, 37, (1986), p. 715.
(27) J. M. Barton, D. C. L. Greenfield, I. Hamerton and J. R. Jones, Polymer Bulletin, 25, (1991), p. 475.
(28) A. M. Gupta and C. W. Macosko, Makromol. Chem., Macromol. Cymp., 45, (1991), p. 105.
(29) S. L. Simon, J. K. Gillham, and D. A. Shimp, ACS Polymeric Materials Science and Engineering, 62, (1990), p. 96.
(30) D. A. Shimp, J. R. Christenson, S. J. Ising, 3rd Intl. SAMPE Electronic Materials and Processing Conference, 3, (1989), p. 360.
(31) A. M. Gupta and C. W. Macosko, Macromol. Chem., Makromol. Symp., 45, (1991), 105.
(32) R. J. J. Williams, A. Vasquez, and J. P. Pascault, Polymer Bulletin., 28, (1992), p. 219.
(33) Rhone-Poulenc Technical Document, Specialty Resins-Formulating AroCy Cyanate Esters for Resin Transfer Molding Applications, (May 1992), p. 3.
(34) M. Bauer, J. Bauer, R. Ruhmann and G. Kuhn, Acta Polymerica, 40 (6), (1989), p. 397.
(35) A. J. Kinloch, S. J. Shaw, D.A. Tod, D. L. Hunston, Polymer, 24, (1983), p. 1341.
(36) G. R. Irwin, Appl. Mats. Res., 3, (1964), p. 65.
(37) H. M. Westergaard, J. Appl. Mech., 61, (1939), p. 49.
(38) G. R. Irwin, Appl. Mats. Res., 3, (1964), p. 65.
(39) See, for example, D5045-96, Annual Book of ASTM Procedures, 1996.
(40) G. C. Sih, "Handbook of Stress Intensity Factors for Researchers and Engineers", Lehigh Univ., Bethlehem, USA, 1973.
(41) H. Tada, P. Paris, G. R. Irwin, "The Stress Analysis of Cracks Handbook", Del Research Corp., Hellertown, USA, 1973.
(42) D. P. Rook, D. J. Cartwright, "Compendium of Stress-Intensity Factors", HMSO, London, 1976.
(44) A. J. Kinloch, R. J. Young, "Fracture Behavior of Polymers", Applied Science Publishers Ltd. 1983, p. 74.
(45) C. K. Riew, E. H. Rowe and A. R. Seibert in Toughness and Brittleness of Plastics, R. D. Deanin and A. M. Crugnola, Eds., ACS Advances in Chemistry Series 154, Washington, D.C., (1976), p. 326.
(46) E. M. Yorkgitis, C. Tran, N. S. Eiss Jr., T. H. Yu, I. Yilgor, G. L. Wilkes and J. E. McGrath, ACS Advances in Chemistry Series 208, Rubber Modified Thermoset Resins, C. K. Riew and J. K. Gillham, Eds., pg. 137.
(47) A. C. Maloney, H. H. Kausch and H. R. Steiger, Journal of Materials Science, 18, (1983) p. 208.
(48) C. B. Bucknall and I. K. Partridge, Polymer, 24, (1983), p. 639.
(49) G. D. Lyle, J. S. Senger, D. H. Chen, S., Kilic, S. D. Wu, D. K. Mohanty, and J. E. McGrath, Polymer, 30, (1989), p. 978.
(50) S. J. Pak, G. D. Lyle, R. Mercier, and J. E. McGrath, Polymer, 34(4), (1993), p. 885.
(51) S. P. Wilkinson, T. C. Ward, and J. E. McGrath, Polymer 34(4), (1993), p. 870.
(52) S. A. Srinivasan, Ph. D. Dissertation, VPI&SU, (1994).
(53) A. C. Garg, Y. W. Mai, Composite Science and Technology 31, (1988), p. 179.
(54) J. N. Sultan and F. J. McGarry, Journal of Applied Polymer Science, 13, (1973), p. 29.
(55) A. F. Yee and R. A. Pearson, Journal of Materials Science, 21, (1986), p. 2462.

(56) R. A. Pearson and A. F. Yee, Journal of Materials Science, 21, (1986), p. 2475.
(57) C. B. Bucknall, Toughened Plastics, Elsevier Applied Science Publications, London (1977).
(58) S. Kunz-Douglass, P. W. R. Beaumont, M. F. Ashby, Journal of Materials Science, 15, (1980), p. 1109.
(59) A. F. Yee and R. A. Pearson, Journal of Materials Science, 21, (1986), p. 2462.
(60) R. A. Pearson and A. F. Yee, Journal of Materials Science, 21, (1986), p. 2475.
(61) A. J. Kinloch, S. J. Shaw, D. A. Tod, and D. L. Hunston, Polymer, 24, (1983), p. 1341.
(62) A. C. Garg and Y. W. Mai, Composites Science and Technology, 31, (1988), p. 179.
(63) A. C. Maloney, H. H. Kausch, and H. R. Steiger, Journal of Materials Science, 18, (1983), p. 208.
(64) A. F. Yee and R. A. Pearson, Journal of Materials Science, 21, (1986), p. 2462.
(65) R. A. Pearson and A. F. Yee, Journal of Materials Science, 21, (1986), p. 2475.
(66) J. L. Hedrick, I. Yilgor, M. Jurek, J. C. Hedrick, G. L. Wilkes, and J. E. McGrath, Polymer, 32(11), (1991), p. 2020.
(67) S. C. Kim and H. R. Brown, Journal of Materials Science, 22, (1987), p. 2589.
(68) C. B. Bucknall and A. H. Gilbert, Polymer, 30, (1989), p. 213.
(69) F. Zengli and S. Yishi, Chinese Journal of Polymer Science, 7(4), (1989), p. 367.
(70) A. F. Yee and R. A. Pearson, Journal of Materials Science, 21, (1986), p. 2462.
(71) R. A. Pearson and A. F. Yee, Journal of Materials Science, 21, (1986), p. 2475.
(72) S. Zeng, M. Horsington, J. Seferis and D. A. Shimp, 37th Annual SAMPE Symposium, (March 7-10, 1988), p. 422.
(73) P. C. Yang, E. P. Woo, S. A. Laman, J. J. Jakubowski, D. M. Pickelman and H. S. Sue, 36th Annual SAMPE Symposium, (April 15-18, 1991), p. 431.
(74) C. Arnold, P. Mackenzie, V. Malhotra and E. Maskell, 35th International SAMPE Symposium, (March 9-12, 1992), p. 128.
(75) J. C. Hedrick, A. Viehbeck, J. T. Gotro, ACS Polymer Preprints, Polymer Chemistry, 35(1), (March 1994), p. 537.
(76) D. A. Shimp, F. A. Hudock, W. S. Bobo, 18th International SAMPE Technical Conference, (Oct. 7-9, 1986), p. 851.
(77) Z. W. Coa, F. Mechin, J. P. Pascault, Polymer Materials Engineering Science Preprint, 70, (1994), p. 91.
(78) S. A. Srinivasan, Ph. D. dissertation, Virginia Polytechnic Institute and State University, (1994).
(79) S. A. Srinivasan, SAMPE Quarterly, 24, No. 3, (1993), p. 25.
(80) Ibid.
(81) D. A. Shimp, F. A. Hudock and W. S. Bobo, 18th International SAMPE Technical Conference, (October 7-9, 1986), p. 851.
(82) J. N. Hay. Processing and Cure Schedules for Cyanate Ester Resins, in Chemistry and Technology of Cyanate Ester Resins, Ian Hamerton, Ed., Blackie Academic and Professional, London, (1994), p. 168.
(83) J. M. Barton, D. C. L. Greenfield, I. Hamerton and J. R. Jones, Polymer Bulletin, 25, (1991), p. 475.
(84) A. M. Gupta and C. W. Macosko, Makromol. Chem., Macromol. Cymp., 45, (1991), p. 105.
(85) S. L. Simon, J. K. Gillham, and D. A. Shimp, ACS Polymeric Materials Science

and Engineering, 62, (1990), p. 96.
(86) D. A. Shimp, J. R. Christenson, S. J. Ising, 3rd Intl. SAMPE Electronic Materials and Processing Conference, 3, (1989), p. 360.
(87) D. S. Porter and T. C. Ward, Unpublished results.
(88) D. A. Shimp, 32nd Int. SAMPE Symposium, 32, (1987), p. 1063.
(89) R. E. Uschold and J. B. Findlay, Applied Polymer Symposia, 25, (1974), p. 205.
(90) J. P. Pascault, J. Galy and F. Méchin, Additives and Modifiers for Cyanate Ester Resins, in Chemistry and Technology of Cyanate Ester Resins, Ian Hamerton, Ed., Blackie Academic and Professional, London, 1994, p. 133.
(91) W. D. Bascom, R. Y. Ting, R. J. Moulton, C. K. Riew and A. R. Seibert, Journal of Materials Science, 16, (1981), p. 2657.
(92) K. Yamanaka and T. Inoue, Polymer, 30, (1989), p. 662.
(93) D5045-96, Annual Book of ASTM Procedures, 1996.
(94) C. B. Bucknall, and T. Yoshii, British Polymer Journal, 10, (1978), p. 3.
(95) A. R. Seibert, In Rubber Modified Thermoset Resins, C. K. Riew and J. K. Gillham, eds., Advances in Chemistry 208, American Chemical Society: Washington, D. C., 1984, p. 261.
(96) J. N. Sultan and F. J. McGarry, Polymer Engineering and Science, 13, (1973), p. 29.
(97) W. D. Bascom, R. Y. Ting, R. J. Moulton, C. K. Riew and A. R. Seibert, Journal of Materials Science, 16, (1981), p. 2657.
(98) A. C. Garg, Y. W. Mai, Composites Science. and Technology., 31, 179, (1988).
(99) J. N. Sultan and F. J. McGarry, Journal of Applied Polymer Science, 13, (1973), p. 29.
(100) A. F. Yee and R. A. Pearson, Journal of Materials Science, 21, (1986), p. 2462.
(101) R. A. Pearson and A. F. Yee, Journal of Materials Science, 21, (1986), p. 2475.
(102) C. B. Bucknall, Toughened Plastics, Elsevier Applied Science Publications, London (1977).
(103) S. Kunz-Douglass, P. W. R. Beaumont, M. F. Ashby, Journal of Materials Science, 15, (1980), p. 1109.
(104) A. J. Kinloch, S. J. Shaw, D. A. Tod, and D. L. Hunston, Polymer, 24, (1983), p. 1341.
(105) A. C. Garg and Y. W. Mai, Composites Science and Technology, 31, (1988), p. 179.
(106) S. Kunz-Douglas, P. Beaumont, and M. Ashby, J. Mater. Sci., (1980), 15, p. 1109.
(107) A. J. Kinloch, S. J. Shaw and D. L. Hunston. Deformation, Yield, and Fracture of Polymers, Churchill College, Cambridge, Plastics and Rubber Institute, London, (1982), p. 29.
(108) S. Montarnal, J. P. Pascault, and H. Sautereau. In Rubber-Toughened Plastics, C. Keith Riew, Editor, Advances in Chemistry Series 222, ACS, Washington, D. C., 1989, p. 204.
(109) D. A. Shimp, J. R. Christenson, and S. J. Ising, Cyanate Ester Resins-Chemistry, Properties and Applications, Technical Bulletin, Ciba, Ardsley, NY.
(110) J. P. Pascault, J. Galy and F. Méchin, Additives and Modifiers for Cyanate Ester Resins, in Chemistry and Technology of Cyanate Ester Resins, Ian Hamerton, Ed., Blackie Academic and Professional, London, 1994, p. 137.

(111) R. J. J. Williams, J. Borrajo, H. E. Adabbo, A. J. Rojas, In Rubber-Modified Thermoset Resins; Riew, C. K.; Gillham, J. K., Eds.; Advances in Chemistry 208; American Chemical Society: Washington D.C., 1984; pp 195-213.
(112) L. C. Chan, J. K. Gillham, A. J. Kinloch, and S. J. Shaw, In Rubber Modified Thermoset Resins, C. K. Riew and J. K. Gillham, eds., Advances in Chemistry 208, American Chemical Society: Washington, D. C., 1984, p. 261.
(113) J. P. Pascault, J. Galy, and F. Mechin, Additives and Modifiers for Cyanate Ester Resins, in Chemistry and Technology of Cyanate Ester Resins, Ian Hamerton, Ed., Blackie Academic and Professional, London, 1994, p. 125.
(114) A. W. Snow, The Synthesis, Manufacture and Characterization of Cyanate Ester Monomers, in Chemistry and Technology of Cyanate Ester Resins, Ian Hamerton, Ed., Blackie Academic and Professional, London, 1994, p. 137.

Chapter 4: Modeling of the Phase Separation Process in Rubber-toughened Bisphenol-A Dicyanate

4.1 Introduction

The previously discussed systems of BADCy with HTBN and polyester additives provide improvement of fracture toughness through phase separation and formation of a second, toughener-rich phase. In this section, a single system will be examined in much greater detail – BADCy containing 10 weight percent of HTBN. This formulation is more typical of commercial toughened thermosetting systems; it is this system that was shown in Chapter 3 to have properties that were most affected by variations in cure temperature. This combination is therefore a good model to use for examination of the influence of a thermal gradient cure on properties. The analysis of phase separation behavior will be accomplished using a model developed for such a system. To parameterize the model requires consideration and determination of various physical and chemical properties of the monomer, toughener and their combination.

4.2 Literature Review

4.2.1 Flory-Huggins Theory

The thermodynamics of polymer solutions differs from solutions of low molecular weight materials. The best known treatment of the unique characteristics of polymer solutions was developed independently by Flory (1, 2) and Huggins (3, 4, 5) and is known generally as the Flory-Huggins theory. The basic outline of the conditions necessary for phase separation to occur in a binary system were outlined in Chapter 3 where a toughener-rich second phase developed during the polymerization of a thermoset. Change in the configurational entropy of the system drives the dissolved

polymer out of solution, and the thermodynamics of this demixing process may be described by the Flory-Huggins theory. Here, the development of this theory will be presented in greater detail to facilitate its application to the system of interest.

4.2.1.1 Entropy of Mixing

The physical placement of solute molecules in a solvent may be visualized in a number of ways. We will consider this placement on a lattice with sites of identical size that may be occupied by either a volume unit of solvent or an identical volume unit of solute. For low molecular weight materials, we can consider the number of arrangements of units on the lattice compared to arrangements on lattices where the unmixed units initially resided (Figure 4-1).

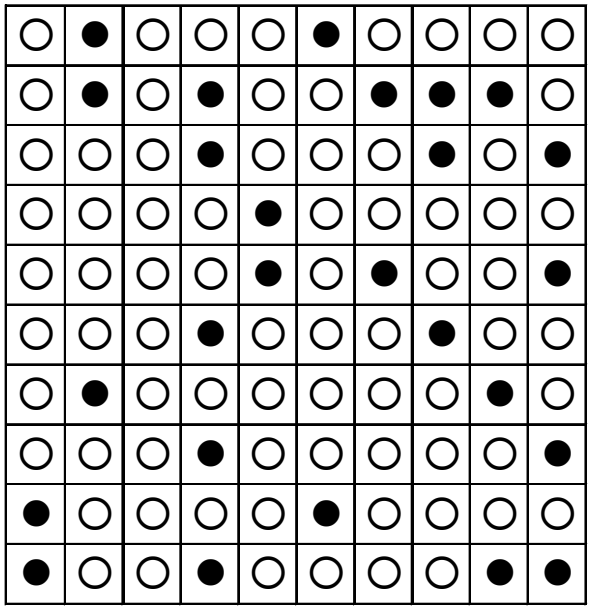

Figure 4-1. Random arrangement of solvent and solute molecules on a lattice.

For an ideal solution (random mixing) with athermal mixing, the free energy change consists only of an entropic contribution. Using Boltzmann's equation, the

expression for the free energy of mixing was determined from simple combinatorial formulas to be

$$\Delta G_M = -T\Delta S_M = kT(n_1 \ln N_1 + n_2 \ln N_2) \qquad \textbf{(4-1)}$$

where n_1 is the number of solvent molecules, n_2 is the number of solute molecules, N_1 is the mole fraction of solvent and N_2 is the mole fraction of solute. Note that this expression always predicts miscibility of the components at thermodynamic equilibrium.

The critical deduction of Flory and Huggins in treating the solution behavior of polymers began with changes in combinatorial entropy of these solutions. Polymeric molecules have large molecular weights and corresponding molar volumes that are multiples of the constituent repeat unit as given by the degree of polymerization of that molecule. It is this long-chain structure due to the connectivity of the repeating volume units that fundamentally changes the mixing behavior relative to a low molecular weight solution.

Returning to the lattice considered previously, it is clear (initially assuming equivalent molar volume of lattice sites for solvent and solute repeat units) that there is a restriction of the number of possible ways that the polymer molecule may be placed on this lattice with the solvent due to the interconnectivity of the repeat units. In Figure 4-2, we see a lattice on which polymer molecules have been placed. The significant point to note is that the initial placement of the first polymer segment is possible anywhere on the lattice, for a total number of choices of lattice sites n_0. However, the next polymer segment must occupy a contiguous site, so the number of choices z for this placement is restricted to the number of neighboring sites. Now the fraction of cells previously

occupied by other segmental units (i) in the n_0 total cells is defined as f using a mean field approximation:

$$f_i = \frac{xi}{n_0} \qquad \textbf{(4-2)}$$

where x is the number of contiguous lattice sites. This makes the fraction of unoccupied, available sites $1\text{-}f_i$. So the number of available sites for the next segment is $z(1\text{-}f_i)$. Addition of the third segment (and all subsequent segments) finds one less site available due to the addition of the second segment. Now the number of available sites for placement of this next segment is $(z\text{-}1)(1\text{-}f_i)$.

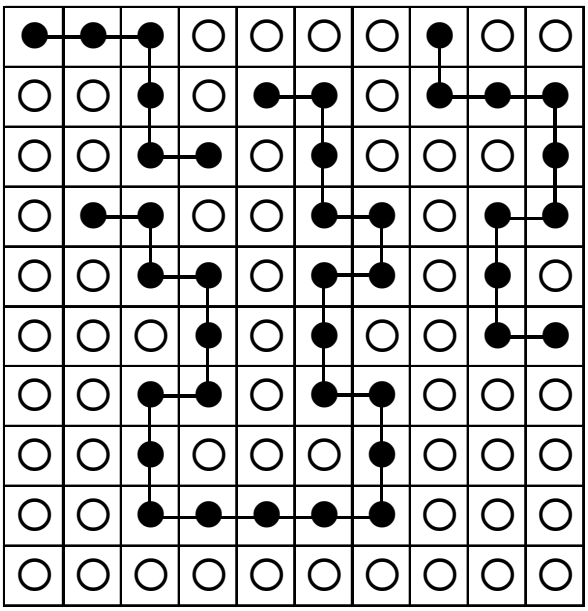

Figure 4-2. Arrangement of polymer solute molecules on a lattice.

We can now write an expression for the number of ways ω_i to place a polymer chain in a lattice:

$$\varpi_{i+1} = (n_0 - xi)z(1 - f_i)\left[(z-1)(1-f_i)^{x-2}\right] \qquad \textbf{(4-3)}$$

If we replace the expression for z in the above equation with the approximation z-1 and also substitute the fraction of available lattice sites with the expression $\frac{n_0 - xi}{n_0}$, we arrive at an approximation of the number of ways to place a polymer chain on the lattice:

$$\omega_{i+1} = (n_0 - xi)^x \left(\frac{z-1}{n_0} \right)^{x-1} \qquad \textbf{(4-4)}$$

Assuming independent placement of the identical units on the lattice, the total number of combinatorial configurations will be

$$\Omega(n_1, n_2) = \frac{1}{n_2!} \prod_{i=1}^{n_2} \omega_i = \frac{1}{n_2!} \prod_{i=0}^{n_2 - 1} \omega_{i+1} \qquad \textbf{(4-5)}$$

Equation 4-4 may then be substitued to write a useful expression for the number of ways that a polymer chain may be placed in the lattice:

$$\ln \Omega = \sum_{i=0}^{n_2 - 1} x \ln(n_0 - xi) + n_2 (x-1) \ln \left(\frac{z-1}{n_0} \right) - \ln n_2! \qquad \textbf{(4-6)}$$

The first (summation) part of the above equation may be substituted with an approximate integral form

$$\begin{aligned} \ln \Omega &= \int_0^{n_2 x} \ln(n_0 - xi) d(xi) + n_2 (x-1) \ln \left(\frac{z-1}{n_0} \right) - \ln n_2! \\ &= n_1 \ln \frac{n_0}{n_1} + x n_2 \ln n_0 - x n_2 + n_2 (x-1) \ln \left(\frac{z-1}{n_0} \right) - \ln n_2! \end{aligned} \qquad \textbf{(4-7)}$$

Stirling's approximation is applied to obtain

$$\ln \Omega = n_1 \ln \frac{n_0}{n_1} + n_2 \ln \frac{n_0}{n_2} + n_2 (x-1) \ln \left(\frac{z-1}{e} \right) \qquad \textbf{(4-8)}$$

whereby we arrive at the expression for configurational entropy change for placement of the polymer and solvent on the lattice, which is given by the Boltzman relationship

$$S_0 = k \ln \Omega = k \left[n_1 \ln \frac{n_0}{n_1} + n_2 \ln \frac{n_0}{n_2} + n_2 (x-1) \ln \left(\frac{z-1}{e} \right) \right] \qquad \textbf{(4-9)}$$

This is the change in entropy for mixing a zero-entropy polymer (full lattice) and zero-

entropy solvent. To complete our expression, we must determine the entropy change for mixing of an amorphous polymer. To do this, we temporarily ignore the solvent component and focus on the placement of the polymer alone on the lattice

$$S_a = k\left[n_2 \ln x + n_2 (x-1) \ln\left(\frac{z-1}{e} \right) \right] \qquad \textbf{(4-10)}$$

where the total number of lattice sites n_0 is now the total number of sites occupied by one polymer chain multiplied by the number of solute molecules and we have zero solvent lattice sites. Together, the expression for the entropy of mixing is

$$\Delta S_m = S_0 - S_a - S_1 \qquad \textbf{(4-11)}$$

which is written as

$$\Delta S_m = k\left[n_1 \ln \frac{n_0}{n_1} + n_2 \ln \frac{n_0}{x n_2} \right] \qquad \textbf{(4-12)}$$

A final and customary simplification may be made by substituting into the expression the volume fraction of the polymer components. The volume fraction of the solvent component ϕ_1 may be represented by n_1/n_0 and the volume fraction of the polymer component ϕ_2 can be represented by xn_2/n_0 to yield

$$\Delta S_m = -k\left[n_1 \ln \phi_1 + n_2 \ln \phi_2 \right] \quad \textbf{(4-13)}$$

4.2.1.2 Enthalpy of Mixing

Consideration of the other component of the free energy of mixing also requires consideration of the long-chain nature of the polymer solute. To treat the enthalpy of mixing, we will only consider interaction occurring between adjacent lattice sites due to the strong decrease of the interactions with distance and ignoring any interactions that might change the placement of the solute polymer on the lattice (structuring). Begin by considering three different interactions between segmental units: solvent-solvent, solvent-

polymer, and polymer-polymer. The energy change for the formation for these contacts starting with unmixed segments is

$$\Delta w_{12} = w_{12} - \frac{1}{2}[w_{11} + w_{22}] \qquad \textbf{(4-14)}$$

The enthalpy of mixing can be calculated from this by multiplying this heat of individual interaction by the number of total 1-2 contacts (p_{12}):

$$\Delta H_m = p_{12}\Delta w_{12} \qquad \textbf{(4-15)}$$

To calculate the enthalpy of mixing, we must consider the calculation of the average value of p_{12}. Returning to our lattice treatment, we consider a lattice site occupied by a polymer chain segment which has attached additional chain segments, surrounded by z other sites, two of which must be occupied by other segments. This gives z-2 available sites. There are x chain segments, and we will consider all but the endgroups, leaving x-2 segments, which gives (x-2)(z-2) adjacent sites. For the two endgroup segments, there are 2(z-1) adjacent sites. The total number of adjacent sites for a polymer chain is then (x+2)(z-2). The total number of 1-2 contacts can be calculated as

$$p_{12} = n_2((z-2)x+2)\phi \qquad \textbf{(4-16)}$$

by equating the probability that an adjacent site is solvent or solute to the volume fraction ϕ_1 of solvent in solution. This can be further simplified to

$$p_{12} \cong n_2 zx\phi_1 = n_1 z\phi_2 \qquad \textbf{(4-17)}$$

Using this number of contacts, the enthalpy of mixing is

$$\Delta H_m = z\Delta w_{12} n_1 \phi_2 \qquad \textbf{(4-18)}$$

We further take into account the enthalpy of mixing long-chain materials, where the solvent may occupy a plurality of adjacent lattice sites x_1 by

$$\Delta H_m = z\Delta w_{12} x_1 n_1 \phi_2 \qquad \textbf{(4-19)}$$

Now it is possible to define the Flory-Huggins interaction parameter by the expression

$$\chi_1 = \frac{z\Delta w_{12} x_1}{kT} \qquad \textbf{(4-20)}$$

Finally, the complete expression for free energy of mixing may be written:

$$\Delta G_M = kT(n_1 \ln \phi_1 + n_2 \ln \phi_2 + \chi_1 n_1 \phi_2) \qquad \textbf{(4-21)}$$

A molar free energy of mixing may be written by substituting in volume fractions for number of solvent and solute molecules to yield the final expression:

$$\Delta \overline{G}_M = RT\left[\phi_1 \ln \phi_1 + \frac{\phi_2}{x} \ln \phi_2 + \chi_1 \phi_1 \phi_2\right] \qquad \textbf{(4-22)}$$

4.2.1.3 Limitations of Flory-Huggins Theory

There are several assumptions in the Flory- Huggins theory of polymer solution thermodynamics, some of which are apparent from the above derivation. These assumptions often arise in discussions of shortcomings. Flory-Huggins assumes that lattice sites are uniformly occupied; however, as the solution becomes more dilute, areas of lower density must occur between solute chains. Also, the filling of the lattice does not consider any changes of flexibility as the transition from solid state to solution occurs. In this case, the combinatorial entropy would be the only component of the entropy of mixing, and would ignore any contribution from chain movement in solution. The theory also does not consider orientation of the component solvent molecules due to specific interactions with the polymer. A basic assumption made is that the placement of segments upon the lattice is perfectly random – this is true only in the case of zero specific interactions between polymer and solvent molecules. Among the most often-cited deficiencies of the Flory-Huggins approach is that the theory does not assign a concentration dependency to the interaction parameter. This concentration dependency is now often considered to better describe mixing behavior in certain systems. Finally,

Flory-Huggins theory assumes that the interaction parameter is a purely enthalpic contribution, while it has been subsequently shown that there is a signficant entropic component. This entropic component could arise from such sources as the establishment of solvent-solute interactions which change the frequency and direction of the motions of the molecules. As such, the interaction parameter may be better viewed as a free energy parameter, containing both entropic and enthalpic contributions. The interaction parameter is often written to reflect this as

$$\chi_1 = \chi_H + \chi_s \qquad \textbf{(4-23)}$$

where

$$\chi_H = -T\left(\frac{d\chi_1}{dT}\right) \qquad \textbf{(4-24)}$$

and

$$\chi_s = \frac{d(T\chi_1)}{dT} = -\frac{\Delta S}{k} \qquad \textbf{(4-25)}$$

Some evidence suggests that the largest contribution to the interaction parameter is actually the entropic component. However, even with justifiable criticism, and many applied corrections, the Flory-Huggins approach maintains a prominent place in polymer solution thermodynamics schemes today.

4.2.2 Phase Equilibria

Phase diagrams may be obtained from Flory-Huggins theory by searching the ΔG_M curves for common tangents as shown in Figure 2-7. This may be achieved through the use of mathematical software packages, or even in spreadsheets where numerical solvers are included. Once the critical point is calculated from knowledge of the ratio of molar volume of the components, common tangents to the free energy curve may be

found by identifying pairs of points in the two phase regions corresponding with the composition of each phase. Both a common slope (found from the derivative of the free energy curve) and a common intercept characterize these tangents which locate the mutual chemical potentials of the components by the intercept.

In fact, one method of calculating the phase diagram from the Flory-Huggins equation depends on calculation of the chemical potential μ of the components. For a binary system, thermodynamic equilibrium depends on the chemical potentials of any selected component being the same in both phases. This condition is achieved as represented by the following for a binary system:

$$\begin{aligned} \Delta\mu_1' &= \Delta\mu_1'' \\ \Delta\mu_2' &= \Delta\mu_2'' \end{aligned} \quad \textbf{(4-26)}$$

where 1 and 2 denote the mixture components and prime and double prime indicate the individual phases.

The chemical potential of component 1 may be calculated by differentiating the free energy of mixing:

$$\begin{aligned} \Delta\mu_1 = \mu_1 - \mu_1^{\,0} &= \frac{\partial G_m}{\partial m_1} \\ &= N_A \frac{\partial}{\partial n_1}\left[kT(n_1 \ln\phi_1 + n_2 \ln\phi_2 + n_1\chi_1\phi_2\right] \\ &= RT\left[\ln\phi_1 + n_1\frac{\partial \ln\phi_1}{\partial n_1} + n_2\frac{\partial \ln\phi_2}{\partial n_1} + \chi_1\phi_2 + n_1\chi_1\frac{\partial\phi_2}{\partial n_1}\right] \quad \textbf{(4-27)} \\ &= RT\left[\ln\phi_1 + \phi_2 - n_2\frac{\phi_1}{n_1} + \chi_1\phi_2 - \chi_1\phi_1\phi_2\right] \\ &= RT\left[\ln(1-\phi_2) + \left(1-\frac{1}{x}\right)\phi_2 + \chi_1{\phi_2}^2\right] \end{aligned}$$

and similarly we arrive at

$$\Delta\mu_2 = RT(\ln\phi_2 + (1-x)(1-\phi_2) + x\chi_1(1-\phi_2)^2) \qquad \textbf{(4-28)}$$

A phase diagram showing variation of χ with composition for various ratios of solute to solvent size (Z) is shown in Figure 4-3. From this phase diagram and a temperature dependent χ relationship such as one of the form χ=a+b/T, one may generate a T-ϕ phase diagram.

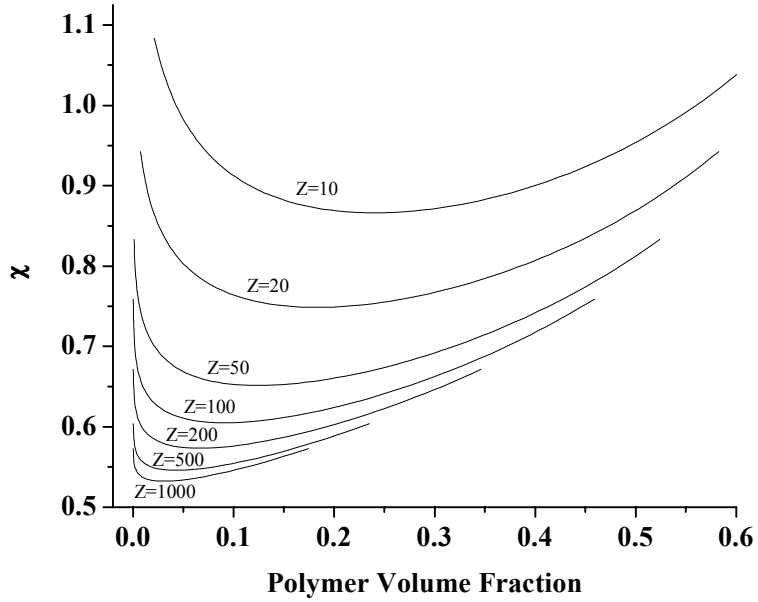

Figure 4-3. χ–ϕ phase diagram showing the coexistence curves as degree of polymerization Z is increased. (After P. A. Small, Journal of Applied Chemistry, 3, (1953), p. 71.)

Alternatively, construction of phase diagrams may be achieved using the method of Horst. (6, 7, 8) This approach relies on a geometric construction, where a common tangent is found on either side of the critical point. The advantage of using this technique is that no derivatives are required; when multicomponent systems are considered, derivative expressions can often get excessively complex. This method is also easily adapted to systems where modifications to Flory-Huggins theory require the inclusion of additional terms.

The above approaches describe the method used to determine the phase diagram from a complete set of Flory-Huggins parameters. Thus, since Flory-Huggins is used in this thesis to describe and model the phase diagram, a discussion of the selection of such parameters is appropriate. In its derivation, the Flory-Huggins equation utilizes a lattice model; and, in application, a reference size for each lattice element must be known. Practically, a reference volume for the lattice element must be chosen and is assumed in the Flory-Huggins theory to be the ratio of this reference volume to the polymer's volume. There is some conflicting information in the literature regarding how the relative molar volumes should be selected. Williams et al. (9, 10) employ the number average molecular weight when considering solutions of rubber tougheners in epoxies. However, in the various analyses of the effect of polydispersity on the polymer solutions, consideration must be given to the higher molecular weight chains. In discussions of polymer fractionation, the propensity of higher molecular weight chains to precipitate first illustrates that the higher molecular weight chains in solution need to be emphasized in successful models. Stockmayer (11) showed that the spinodal curve and critical point depend on the weight average molecular weight which more heavily emphasizes the higher molecular weight tail of the distribution in calculations of the molecular weight average.

In an early paper, Shultz and Flory (12) used cloud point curves to determine a temperature-dependent χ. Later, Koningsveld et al. (13) observed that the shape of the binodal line could be significantly affected depending upon the molecular weight distribution of the polymer in solution. This has subsequently been re-examined by several other authors, and treatments of the effect of polydisperse polymer solutions on

cloud point have been developed. Rehage (14) and Solc (15) developed methods of calculating cloud point curves taking into account the polydispersity of the constituent polymer component. Kamide et al. (16, 17, 18) also presented theories for treating a solution of a polydisperse polymer in a monodisperse solvent using an interaction parameter consisting of a summation of interaction parameters for the different molecular weights of polymer in solution. Kamide later (19) compared this method with Solc's approach. One advantage of the Kamide scheme is its computer-friendly nature due to the value range of necessary the parameters. In addition, the Solc method underestimates χ at low volume fractions of dissolved polymer, though the difference is small. However, the Solc method may be solved more readily. With more modern computers, it is likely that any computationally-driven disadvantages will not pose a problem for any theory, and the more accurate method (Kamide) would be a more attractive choice.

Reflecting the many limitations discovered for the Flory-Huggins expression, the interaction parameter may be necessary in describing the thermodynamics of polymer solutions but has shortcomings that must be considered carefully. The estimation of χ can often be complex and contains contributions from multiple factors. χ is temperature-dependent; and, as noted previously, has been recognized to be dependent on concentration and molecular weight of the solute, as well as hydrogen bonding. Finally, because χ reflects pairwise interactions, the treatment of solutions of multiple components (different species) is complicated by the choice of a single χ value. (20)

4.2.3 Determination of the interaction parameter

Several methods of determining the Flory-Huggins interaction parameter have been developed. Some examples of this include inverse gas chromatography (21),

osmotic pressure, light scattering and sedimentation equilibrium (22), freezing point depression, swelling equilibrium, intrinsic viscosity (23), temperature dependence of precipitation (24), and critical solution temperature (25). In addition, Riedl and Prud'homme have reviewed various methods for determination of χ. (26) Mumby et al. (27) have proposed a method of calculating the phase diagram, taking into account variations of χ with temperature and concentration, and treating these as empirical functions. Later, the calculation of χ from cloud point data (28) using this same approach was described. Both of these investigations take into account the polydispersity of the polymer component.

In examining the thermodynamics of demixing of toughened thermosets, determination of χ has been achieved by measuring cloud point curves as temperature was varied. This is the approach of Williams et al. (29) for the evaluation of χ for use in the same model of phase separation adopted in the present thesis. For epoxy-CTBN systems using the diglycidyl ether of bisphenol-A and carboxyl-terminated butadiene acrylonitrile toughener, a temperature dependent interaction parameter was evaluated as (0.35+90/T). (30) For the case of a different cyanate ester monomer (AroCy L10, or 4,4'-dicyanate-1,1'-diphenylethane) and a nonfunctional butadiene acrylonitrile toughener ($<M_n>$=2800 g mol^{-1} and $<M_w>$=5300 g mol^{-1}, 18 mole% acrylonitrile) the chi parameter was found to be equal to –0.0372 + 68.7/T. (31) This system was compared to a solution of the same rubber toughener in DGEBA epoxy. In this case, chi could be represented by the equation χ=-0.0254+56.089/T. For this latter toughener, the cyanate ester is actually a better solvent for the toughener than the epoxy (critical temperature T_c is lower), in contrast to what is suggested by the values for χ. This may be understood by

comparing the molar volume of the two solvents. Because the cyanate ester has a smaller molar volume, there is a larger entropic contribution to the free energy of mixing.

In another relevant paper, the thermodynamics of mixing of a system of a polyetherimide (GE Ultem) in a DGEBA-based epoxy was investigated by measuring cloud point temperature dependency with volume fraction of polyetherimide. (32) The equation describing the best fit interaction parameter from the cloud point data was χ=-0.1872+246.86/T. In this paper, the authors also compare the interaction parameter of the DGEBA/Ultem system to a system containing DGEBA as well as a diamine curing agent. One curing agent examined (4,4'-methylenebis[3-chloro-2,6-diethylaniline]) increased miscibility of the toughener in the matrix, while diaminodiphenyl sulfone decrease miscibility. This highlights one of the major difficulties encountered with previous measurements of miscibility of tougheners in thermosetting systems - the assumption of a binary mixture. Clearly, while polydispersity of one or both solution components makes this assumption questionable, the addition of a third component (curing agent), such as a diamine, further complicates the analysis and conclusions drawn therefrom. A single component system, such as a cyanate ester as used in our work, eliminates this complication.

The Flory-Huggins interaction parameter can also be determined by a method which incorporates the difference in solubility of the components. This use of solubility parameter for estimating the phase behavior of toughened thermosets was discussed by Chen et al. (33) who conclude that this approach is not adequate to describe miscibility of toughened thermosetting systems. These workers cite the error of solubility parameter estimates (34) as being excessive, and refer to the entropic contributions to the demixing

of toughened thermosets noting that the solubility parameter method considers the excess free energy. Experiments showed the miscibility of a polyetherimide with DGEBA epoxy and diaminodiphenyl sulfone was poorer than for DGEBA/4,4'-methylenebis[3-chloro-2,6-diethylaniline], which is contrary to miscibility predicted by comparison of solubility parameters (where the former system was more miscible than the latter).

In the case of BADCy, solubility parameters have been used to design high-performance toughenners with specific goals in mind. (35) Srinivasan et al. calculated the solubility parameter of BADCy to be 9.7 $(cals/cc)^{1/2}$ (20 $MPa^{1/2}$), and measured a value of 9.3-9.5 $(cals/cc)^{1/2}$. While no quantitative thermodynamic information was developed, the difference in solubility parameters was "tuned" to provide a material that would phase separate into a toughener-rich second phase with a controlled, small particle size. Materials displaying total miscibility of the toughener at high conversions are generally found to display little, if any, enhancement of toughness; those that exhibit gross macrophase separation occuring at low degrees of conversion show poor mechanical properties. In this manner, Srinivasan et al. developed polysulfone-based toughenners which had improved toughness without significant reduction of the good high temperature properties of the polycyanurate.

Determination of χ can be complicated by changes in the chemistry as well as changes in the physical properties of the monomer as it polymerizes. This criticism is not limited only to the estimation of χ from solubility parameter but extends to the utilization of values of χ at zero conversion for prediction of mixing thermodynamics at a higher degree of conversion. It is well known that the polymerization of a thermosetting system results in a decrease in volume of the system (shrinkage), and a decrease in the volume

per repeat unit of the polymer will result in an increase in the solubility parameter. However, in opposition to this effect, it is argued that for the case of cyanate ester materials that the polycondensation of the cyanate ester decreases the overall solubility parameter due to corresponding chemical changes. In one example using cyanate esters (36), the solubility parameter was found to change from 20.1 $MPa^{1/2}$ $(9.8\ cal/cc)^{1/2}$ to 18.4 $MPa^{1/2}$ $(9.0\ cal/cc)^{1/2}$ during the polymerization. This could help explain the origin of the difference between Srinivasan's calculated and measured solubility parameter values.

4.2.4 Cyanate Ester Reaction Kinetics and Network Development

Several authors have worked to model the growth of molecular weight during trimerization of cyanate esters. Description of the increase of molecular weight during cure for cyanate esters was made by Gupta (37) who detailed a kinetic solution for the trimerization reaction. His approach begins by considering that the polymerizing molecule will always have an odd number of connected repeat units. An equation describing the degree of polymerization is then generated from a triply summed contribution from the number of polymer species that would yield a molecule of size 2n+1, where n is the number of interconnected monomer units. This equation also considers the simultaneous disappearance of molecules remaining in the system that could react with any given polymer molecule. The formula is converted to a moment equation which subsequently yields the number average degree of polymerization $<X_n>$ for the cyanate ester system as:

$$< X_n >= \frac{1}{1-\frac{4}{3}p} \qquad \textbf{(4-29)}$$

where p is the fractional cure conversion. From the second moment of this equation, the weight average degree of polymerization $<X_w>$ may be written

$$< X_w >= \frac{1+2p}{1-2p} \qquad \textbf{(4-30)}$$

These equations predict a gel point of p=0.5, as can be seen in Figure 4-4. This has been verified by experiment. (38, 39).

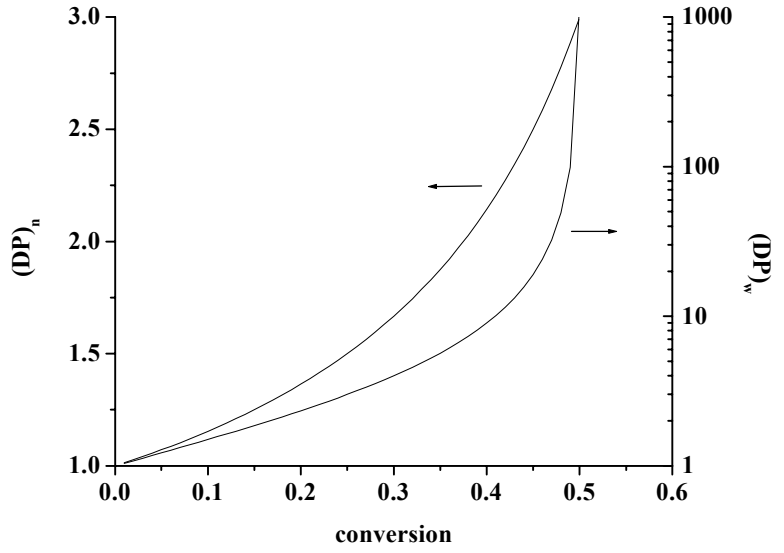

Figure 4-4. Average degrees of polymerization versus cure conversion for cyanate ester monomer. (After A. M. Gupta, Macromolecules, 24, (1991), p. 3459.)

Despite many studies of the reaction kinetics, a completely accurate picture of the cyanate ester reaction mechanism has yet to appear. Because the reaction proceeds slowly for the case of the pure monomer, and catalysis occurs due to a species formed during cure, an autocatalytic mechanism has been suggested. (40) The presence of small amounts of impurities originating during synthesis were found to allow uncatalyzed samples of cyanate esters to react. One proposed mechanism includes a second step in

which an iminocarbonate with two cyanate ester groups forms the triazine ring structure. (41)

To account for the case of both catalyzed and uncatalyzed cyanate ester polymerization, a second order autocatalytic expression has been proposed (42):

$$\frac{dp}{dt} = k_1(1-p)^2 + k_2 p(1-p)^2 \qquad \textbf{(4-31)}$$

which allows good description of the kinetics at very early stages. However, where the concentration and/or type of catalyst is sufficient, and the temperatures are high, the polymerization of cyanate esters is well represented by a simple n^{th} order kinetic equation:

$$\frac{dp}{dt} = k(1-p)^n \qquad \textbf{(4-32)}$$

where n is usually one. These kinetic expressions all describe the polymerization where diffusion control is not a limiting factor. Description of the polymerization of such metwork systems are limited to predicting polymerization rates prior to the approaching of the glass transition where vitrification will interfere. A description of the kinetics of the cyanate reaction in regions where diffusion control is a limitation has also appeared. (43) Values of activation energy for the cyanate ester reaction have been found to be about 80 kJ mol^{-1}. (44, 45)

A variety of methods exist to determine the speed at which a thermosetting material polymerizes. Common methods involve a quantitation of the appearance or disappearance of different chemical species via spectroscopy (such as NMR or FTIR), by extraction of the sol portion, from GPC characterization of sol portion, and by calorimetric techniques.

Calorimetric methods for kinetics depend on the formation of chemical bonds to produce a heat of reaction during the cure of the thermosetting material. This technique has been used often to determine reaction kinetics for curing cyanate esters. (46, 47, 48, 49) From these experiments, it has been found that the heat of the cyanate ester reaction is about 105 kJ mol^{-1} of cyanate groups. DSC is a convenient calorimetric method and has been used to determine the kinetics of reactions of thermosetting resins in several different ways, all depending on the total heat produced during cure. In the first of these methods, the sample is reacted for a given amount of time at a given temperature, then is scanned up in temperature in the DSC to reach its ultimate conversion. The fractional heat released relative to the total possible exotherm reveals the amount of material reacted for that reaction time. In a second method, the rate of heat released with time during an isothermal hold is compared to the total amount of heat given off for full conversion. In a third procedure, "dynamic" scans are made, which involve raising the temperature of the sample at a given rate in a DSC. Then the accumulated areas under the exothermic curve can be taken to determine the fraction of total heat given off at a selected instantaneous temperature. A final dynamic technique (50) involves the use of various temperature scan rates, and kinetics are determined from the shift in the maximum of the DSC exotherm peak with the various heating rates.

FTIR techniques have often been used to determine the reaction kinetics of cyanate esters. (51, 52) The characteristic CN bond absorbance is monitored and its disappearance corresponds to the increase in triazine formation. This spectroscopic technique works well on samples which are partly cured (to a conversion less than the gel point) and can be dissolved; or, for insoluble samples, the material may be placed in KBr

pellets. A unique application of this method involves the in-situ cure monitoring of curing cyanate esters via remote FTIR. (53) This technique provides the possibility of monitoring of composite assemblies as they cure in order to assure final properties for quality control purposes.

4.2.5 Interfacial Free Energy

One of the basic relationships used for prediction of interfacial free energy γ between two phases is the relationship of Antonoff (54):

$$\gamma_{12} = \gamma_2 - \gamma_1 \quad \textbf{(4-33)}$$

where the surface free energy of component 2 is larger than that of component 1. This relationship may be obtained directly from the Young equation, which introduces the contact angle θ and solid liquid and vapor subscripts are indicated.

$$\gamma_{LV} \cos\theta = \gamma_{SV} - \gamma_{SL} \quad \textbf{(4-34)}$$

Here, the liquid is in equilibrium with its vapor. Because high polymers have infinitely low vapor pressure, this equilibrium can never be obtained; and, as a result, the actual interfacial free energy is overpredicted by equation **(4-33**. Girifalco and Good (55) proposed the following relationship

$$\gamma_{12} = \gamma_1 + \gamma_2 - 2\phi(\gamma_1\gamma_2)^{\frac{1}{2}} \qquad \textbf{(4-35)}$$

where ϕ is an interaction parameter that includes the work (energy) of adhesion. This factor is unity when both components are of the same polarity, and ϕ is related to the energy of adhesion (W_a) and the energy of cohesion (W_c) of each phase through

$$\phi = \frac{W_a}{(W_{c1}W_{c2})^{1/2}} \qquad \textbf{(4-36)}$$

Surface and interfacial thermodynamics of epoxy systems have been investigated previously. Chen et al. (56) measured the surface free energy of several epoxies as a function of temperature using the Wilhelmy plate method. Surface energies for DGEBA epoxy was found to be in a range of about 42 to 45 mN m^{-1}, agreeing well with previous values found in the literature. The temperature dependence of this surface energy was found to be between -0.06 and -0.13 mN m^{-1} K^{-1}, also in agreement with the literature. One additional experiment described in this study examined the influence of curing agents (four amines and one anhydride). The variation of surface energy of the amines was higher than the anhydride, with values for all curing agents ranging from about 30 mN m^{-1} to about 45 mN m^{-1}. Increase of molecular weight of the epoxy monomer was found to have only a small effect on surface energy, while a larger change was found for the case of functional polyoxyethylene/oxypropylene curing agents. Blends of DGEBA with CTBN showed a marked increase in surface free energy below two (weight) percent CTBN. Blends of curing agents and DGEBA were not examined, presumably because of the reaction between these amines and the epoxy at the temperatures of interest.

Of interest to the present thesis, interfacial tension between rubber tougheners and epoxies was studied by Sohn and coworkers (57) using pendant drop techniques. The was done with the goal of verifying assumptions made by Williams in the derivation of his phase separation model, which required the use of Antonoff's rule to estimate interfacial thermodynamics. Their results indicate that this assumption does quantitatively predict the interfacial tension. In addition, another method (discussed below) of estimating the interfacial tension produces poor results through an overestimation of the interfacial

tension and predicting a reverse temperature dependence. This second method employed a value of the Flory-Huggins interaction parameter χ, either measured or estimated, to calculate the interfacial tension through the relationship

$$\gamma = \left(\frac{\chi}{6}\right)^{1/2} \rho_0 bkT \qquad \textbf{(4-37)}$$

where ρ_0 is the monomer density and b is the polymer statistical segment length. (58) Estimates of interfacial free energy for this toughened thermosetting system using simple approximations thus produce reasonable agreement with experiment; however, these methods predict increasing interfacial tension with temperature, the opposite of what is actually measured. Taken together with the finding that a significant change in interfacial free energy produces little change in the Williams model prediction, the use such of estimates to obtain the interfacial parameters provides a convenient method of addressing this facet of the model and will be utilized in the following research.

4.2.6 Particle Size Transformation

Upon initial examination, the idea of measurement of the morphological features in toughened thermosetting resins (or any multiphase system) appears straightforward. However, direct measurement of particle size can only be accomplished in specific cases; e.g., such as where the medium is transparent, and has been most commonly employed in biological systems. However, these techniques (such as the use of confocal microscopy) are either complicated or impossible to employ for opaque specimens. More experimentally accessible techniques examine features on a planar sample surface, and result in a two-dimensional representation of the actual three-dimensional distribution occupied by that phase.

With closer examination, it becomes apparent that a two-dimensional representation will not, in the majority of cases, accurately represent the true three dimensional distribution of particle sizes. This has been identified by many previous workers (for example, 59, 60, 61) and the conclusion becomes obvious when the methods of measuring particle size are considered. The morphological features of interest are generated by sample sectioning to produce a surface (typically with a microtome) or by fracture. In the case of slicing, it is clear that features such as particle size may be obscured since cross-sections occur randomly through the size distribution, not always at each particle's equator. To overcome this difficulty, the fracture technique has often been employed – this technique examines a fracture surface and assumes that the fracture has separated the particle at its equator. A difficulty arising from this procedure is the calculation of the total area examined (which is likely to be nonplanar), and so quantitative characterization of morphological features such as number density is difficult or impossible.

To better characterize the true three dimensional particle size distribution from the measured two dimensional characteristics, several researchers have developed mathematical transformations between the two representations. (62, 63, 64) This task is simplified by the assumption that the particles are spherical, which fortunately is often the case.

Kwon at Virginia Tech has extensively examined the application of these techniques to toughened thermosetting systems. (65, 66) In these publications, various schemes are compared using a virtual system of predefined particle size. This method allowed a determination of the number of particles that must be sampled to develop an

accurate metric of the actual particle size distribution. Up to 600 particles must be examined to gain the most accurate representation, though the numerical refinement is quite small after 300 particles have been measured. In addition, various technique for performing a transformation between a two dimensional circle distribution and three dimensional sphere distribution were compared, and certain methods were found to be superior to others in various cases. In general, no method was generally classified as superior to another except in the case of a small-particle enriched particle size distribution. In this case, the Cruz-Orive method showed a discrepancy from the other techniques, either over- or underestimating the average particle size. However, the Saltykov method was shown to produce a universally acceptable transformation to a truly representative particle size distribution, and the refinements of the other techniques are generally not necessary or even desirable. It is suggested that the most reliable procedure is the averaging of the results of several methods. In the development of the Williams model for phase separation, there was no effort to account for the difference between two-dimensional particle size and the actual three dimensional distribution. This is unfortunately also the case for many descriptions of toughened thermoset morphology.

4.2.6.1 Saltykov 3D Transformation Method

When considering the transformation from 2-D circle radius distribution to 3-D sphere radius distribution, the radii must be sorted into groups, in steps of increasing radius. These groups are incremented by step size $\Delta=R_{max}/m$, where m is the number of groups into which the entire distribution is to be separated. It is significant that in considering the inputs and outputs of the Saltykov transformation, the circle radius values

utilized are a continuous distribution while the resultant sphere radius distribution is discrete.

$$k_{ij} = \begin{cases} 2\Delta\left[\sqrt{j^2-(i-1)^2} - \sqrt{j^2-i^2}\right] & \text{for } j \geq 1 \\ 0 & \text{for } j < i \end{cases} \qquad \textbf{(4-38)}$$

From the estimated three dimensional particle size distribution, various parameters may be extracted that characterize that distribution. For example, the number average radius $\overline{R}_N$ may be calculated:

$$\overline{R}_N = \frac{\sum_{i=1}^{m} N_V(i) R_i}{\sum_{i=1}^{m} N_V(i)} \qquad \textbf{(4-39)}$$

The volume average radius $\overline{R}_A$ is obtained as shown in the following equation

$$\overline{R}_A = \left[\frac{\sum_{i=1}^{m} N_V(i) R_i^{\,2}}{\sum_{i=1}^{m} N_V(i)}\right]^{1/2} \qquad \textbf{(4-40)}$$

and the volume average radius is calculated by

$$\overline{R}_V = \left[\frac{\sum_{i=1}^{m} N_V(i) R_i^{\,3}}{\sum_{i=1}^{m} N_V(i)}\right]^{1/3} \qquad \textbf{(4-41)}$$

Parameters necessary to define the morphology include the volume fraction of the second phase, the mean free distance between particles and surface density. The volume fraction V_f of the second phase is simply the total volume of the second phase included in the total volume, which is calculated from the following relationship:

$$V_f = \frac{4\pi}{3}\sum_{i=1}^{m} N_V(i) R_i^3 \quad \textbf{(4-42)}$$

The mean free distance is the average surface-to-surface distance between particles in the system. This parameter carries information of use especially for consideration of toughness, where stresses predicted by a particular toughening mechanism will depend on interparticle distance. To arrive at a mean free distance, the surface density S_V must first be found, which is the ratio of total particle surface area in the system to the total system volume:

$$S_V = 4\pi\sum_{i=1}^{m} N_V(i) R_i^2 \quad \textbf{(4-43)}$$

From the volume fraction and surface density, the mean free distance may then be calculated:

$$\lambda = 4\frac{1-V_f}{S_V} \quad \textbf{(4-44)}$$

4.2.7 Derivation of Williams Model

Williams et al. (67) made a comprehensive survey of the phase separation of toughened thermosets. This fundamental examination of the underlying thermodynamics and kinetics of the process resulted in the reasonably successful development of a model for the phase separation in this type of system. The Williams model begins with consideration of the basic thermodynamics of demixing of the components, and considers phase separation kinetics specifically for the case of a nucleation and growth mechanism (indicative of phase separation occurring in the metastable state). The development of the theory will be outlined, while adaptation of the model for phase separation of a cyanate ester-based toughened thermoset system will be treated in the experimental section of this chapter.

4.2.7.1 Flory Huggins Equation as a Function of Conversion

The free energy of mixing for the unreacted monomer/polymer toughener solution is a useful basis for examining the evolution of the phase diagram as a function of the increase of molecular weight as the system undergoes curing. The model begins by treating the thermodynamics of component mixing with the Flory-Huggins equation in the form

$$\Delta G^{M}{}_{V} = \frac{RT}{\overline{V}_1}\left[(1-\phi_2)\ln(1-\phi_2) + \frac{\phi_2}{Z}\ln\phi_2 + \chi\phi_2(1-\phi_2)\right] \qquad \textbf{(4-45)}$$

where $\Delta G^{M}{}_{V}$ is the free energy change of mixing per unit volume, $\overline{V}_1$ is the molar volume of the cyanate monomer, ϕ_2 is the volume fraction of the preformed polymer, Z is the ratio of preformed polymer molar volume to epoxy monomer molar volume, and χ is the interaction parameter per mole of solvent. Equation (4-45 is applicable to the system in the unreacted state; however, the increase of molecular weight due to curing clearly affects the free energy of the system.

Using the ideas of Flory (68) and Stockmayer (69) or Macosko (70), various expressions for the molecular weight averages as a function of the degree of conversion may be employed in the model. These expressions treat the statistics of polymerization depending on the nature of the system; i.e. the functionality of the reactants. Using the Stockmayer approach (71), the average degrees of polymerization for the epoxy system considered by Williams in developing the model are

$$\overline{X}_n = \frac{\overline{M}_{np}}{\overline{M}_{n0}} = \frac{1}{1-2p} \qquad \textbf{(4-46)}$$

and

$$\overline{X}_w = \frac{\overline{M}_{Wp}}{\overline{M}_{W0}} = \frac{1+p}{1-3p} \quad \textbf{(4-47)}$$

where p is the degree of conversion and $\overline{X}_n$ and $\overline{X}_w$ are the weight and number average degrees of polymerization, respectively, and M_0 is the molecular weight of the monomer.

The following equations relate the evolution of molar volume, molar volume ratio and interaction parameter at any conversion to their value at zero conversion

$$\overline{V}_1 = \overline{V}_{10}\frac{\overline{M}_{np}}{\overline{M}_{n0}} = \frac{\overline{V}_{10}}{1-2p} \quad \textbf{(4-48)}$$

$$Z = \frac{\overline{V}_2}{\overline{V}_1} = \frac{\overline{V}_2}{\overline{V}_{10}}(1-2p) = Z_0(1-2p) \quad \textbf{(4-49)}$$

$$\chi = \chi_0\frac{\overline{V}_1}{\overline{V}_{10}} = \frac{\chi_0}{1-2p} \quad \textbf{(4-50)}$$

where the 0 subscript indicates the initial value of these quantities at zero conversion. The molar volumes of each preformed polymer component may be calculated using the number average molecular weights as determined by using experimental techniques and the density. Using the above equations, the Flory-Huggins equation may be rewritten in terms of the volume fraction of the second component (preformed polymer in this case) as well as conversion. This expression is:

$$\Delta G^{M_V} = \frac{RT}{\overline{V}_{10}}\left[(1-2p)(1-\phi_2)\ln(1-\phi_2) + \frac{\phi_2}{Z_0} + \chi\phi_2(1-\phi_2)\right] \quad \textbf{(4-51)}$$

Using equation (4-51, the evolution of free energy of mixing of the solution as a function of cure may be described, providing information about the regions where either one or two phase behavior may be expected. For the case of spinodally decomposing samples, the phase diagram described by this equation is sufficient to predict phase composition. In the case of nucleation and growth, a more detailed description is necessary to describe this process.

4.2.7.2 Nucleation

Formation of the second phase requires the formation of an initial nucleus, or site, where the second phase particle may begin growth through fluctuations. To form a stable nucleus, the positive free energy required for the formation of a new surface area should be more than balanced by the negative free energy change produced by the formation of a new phase, predicted as described above by the Flory-Huggins equation. Assuming a spherical geometry, the free energy required for formation of a new phase goes through a maximum with radius of the forming particle. This maximum of free energy is at the critical radius, which is the point where the nucleus will survive and grow in size. If the nucleus does not attain this critical size, it will be reabsorbed into the parent medium. The formation of these sites is caused by local fluctuations in composition. The rate of formation of nuclei can be expressed as follows

$$\frac{dN}{dt} = F_0 D \exp\left(\frac{-G_c - E_F}{RT}\right) \quad \textbf{(4-52)}$$

where ΔG_c is the free energy at the critical radius size, F_0 is a proportionality constant, D is the diffusion coefficient of the preformed polymer in the polymerizing resin, and E_F is the energy barrier for composition fluctuation. The rate of composition fluctuation per unit volume is

$$\frac{dF}{dt} = F_0 D \exp\left(-\frac{E_F}{RT}\right) \quad \textbf{(4-53)}$$

4.2.7.3 Interfacial Free Energy

Because the formation of a nucleus is dependent on the associated interfacial energy, the interfacial surface free energy must be known in order to produce an accurate prediction. The free energy expression for the formation of a new spherical phase is

$$\Delta G(r) = \frac{4\pi}{3} r^3 \Delta G_N + 4\pi r^2 \sigma \qquad \textbf{(4-54)}$$

where σ is the interfacial free energy and ΔG_N is the free energy change of new phase formation per unit volume. This equation is used to calculate r_c, the critical radius and ΔG_c, the critical free energy of formation of a new phase

$$r_c = -\frac{2\sigma}{\Delta G_N} \qquad \textbf{(4-55)}$$

and

$$\Delta G_c = \frac{16\pi\sigma^3}{3\Delta G_N^2} \quad \textbf{(4-56)}$$

Particles larger than r_c are assumed to survive and grow, while those smaller than this value dissolve into the matrix. The nucleation rate may be expressed as the rate of composition fluctuations equation (4-53) multiplied by a Boltzmann exponential containing an energy barrier of ΔG:

$$\frac{dN}{dt} = \frac{dF}{dt} \exp\left(-\frac{\Delta G_c}{kT} \right) = \frac{dF}{dt} \exp\left(-\frac{N_A \Delta G_c}{RT} \right) \qquad \textbf{(4-57)}$$

with N_A being Avogadro's number.

The interfacial energy σ must be known to apply these ideas to model nucleation density. In derivation of this model, the assumption was made that the separating phases are pure in each component. While this is certainly not the case, the particle size and size distribution is a much stronger function of the growth rate (72) than the surface energy, so this complication need not be further considered.

4.2.7.4 Epoxy Reaction Kinetics

The epoxy system considered by Williams was assumed to follow a second order reaction rate equation

$$\frac{dp}{dt} = A(1-p)^2 \exp\left(-\frac{E_a}{RT}\right) \quad \textbf{(4-58)}$$

In his development, the parameters for the reaction constant k and activation energy E_a were chosen as 83 kJ mol^{-1} and 5 x 10^7 sec^{-1}, respectively. Kwon further refined this model through the use of a second order autocatalytic description of the reaction kinetics. (73)

4.2.7.5 Viscosity and Rheology Relation to Growth Rate

The growth of the particles generated via fluctuations as described above is a function of the viscosity of the matrix together with the number of growth sites per unit volume and the driving force for growth. This driving force is proportional to the amount of deviation of the volume fraction of preformed polymer in the thermoset rich phase from the equilibrium value, (ϕ_{2c}-ϕ_2^T). The growth rate may then be described as the increase in volume of second phase per time unit:

$$\frac{dV}{dt} = 4\pi r^2 k_\phi N_V (\phi_{2c} - \phi_2^{\,T}) = 4\pi r_2 N_V \frac{dr}{dt} \qquad \textbf{(4-59)}$$

where k_ϕ is the mass transfer coefficient and N_V is the number of particles per unit volume. The mass transfer coefficient may be evaluated using the assumption of a growing sphere in a stationary medium which is expressed as:

$$k_\phi = \frac{D}{r} \qquad \textbf{(4-60)}$$

where D is the diffusion constant. Using equation (4-60) together with the growth rate expression above, we obtain a new expression for growth rate of the radius per unit time:

$$\frac{dr}{dt} = \frac{D}{r}\left(\phi_{2c} - \phi_2^{\,T}\right) \qquad \textbf{(4-61)}$$

To obtain the diffusion coefficient, the Stokes-Einstein diffusion relationship is employed:

$$D = \frac{D_0 T}{\eta} \qquad \textbf{(4-62)}$$

which relates diffusion to the viscosity, a function of molecular weight increase as cure proceeds, as well as temperature. Finally, combining equations, the relation for temperature and molecular weight effects on viscosity (considering change in molecular weight as a function of conversion) are included to yield:

$$\eta(T,p) = \eta_0 \left(\frac{\overline{M_w}(p)}{\overline{M_w}(0)} \right)^{3.4} \exp\left[\frac{E_\eta}{RT} \right] = \eta\big|_{\alpha \to 0, T \to \infty} \left(\frac{1+p}{1-3p} \right)^{3.4} \exp\left[\frac{E_\eta}{RT} \right] \qquad \textbf{(4-63)}$$

where E_η is the activation energy for the viscosity. Here, the viscosity may also be expressed as a function of conversion using the quantity shown earlier for weight average molecular weight as a function of conversion for the dicyanate. The parameters necessary to evaluate equation (4-63) may be obtained with simple experiments.

4.2.7.6 Modeling Particle Size Distribution During Cure

The process of generating predictions from the Williams model may be approached by solving these equations by rewriting the nucleation rate expression in terms of the degree of cure, p, the number of fluctuations with time expression, and the kinetic expression using the Stokes-Einstein diffusion relationship, equation (4-63).

$$\frac{dN}{dp} = \frac{F'_0 T}{A\eta\big|_{p \to 0, T \to \infty}} \left(\frac{1-3p}{1+p} \right)^{3.4} \exp\left[\frac{E_a - E_\eta - E_F - \Delta G_c}{RT} \right] \qquad \textbf{(4-64)}$$

where $F'_0 = D_0 F_0$ is a quantity that is adjustable to fit the generated particle size distribution to the real distribution; this can include a scaling factor, as well. Using the previously developed relationships with the Stokes-Einstein relationship, the growth rate may be expressed as

$$r\frac{dr}{dt} = D(\phi_{2c} - \phi_2{}^T) = D_0\frac{T}{\eta}(\phi_{2c} - \phi_2{}^T)$$

$$= D_0\frac{T}{\eta|p\to 0, T\to\infty}\left(\frac{1-3\alpha}{1+\alpha}\right)^{3.4}\exp\left[-\frac{E_\eta}{RT}\right](\phi_{2c} - \phi_2{}^T) \qquad \textbf{(4-65)}$$

$$= B\left(\frac{1-3\alpha}{1+\alpha}\right)^{3.4}(\phi_{2c} - \phi_2{}^T)$$

where $B = \frac{D_0 T}{A\eta|_{\alpha\to 0, T\to\infty}}\exp\left[\frac{E_a - E_\eta}{RT}\right]$. This equation may also be rewritten as a function of conversion using the kinetic expression for polymerization

$$r\frac{dr}{dp} = \frac{B}{1-p}\left(\frac{1-3p}{1+p}\right)^{3.4}(\phi_{2c} - \phi_2{}^T)\exp\left[\frac{E_a}{RT}\right] \qquad \textbf{(4-66)}$$

$$= B'\left(\frac{1-3p}{1+p}\right)^{3.4}(\phi_{2c} - \phi_2{}^T)$$

where

$$B' = \frac{D_0 T}{A\eta|_{\alpha\to 0, T\to\infty}}\exp\left[\frac{E_a - E_\eta}{RT}\right]$$

The previous equations regarding kinetics may be combined with the equations describing nucleation and growth rate as well as viscosity and diffusion expressions to obtain differential equations describing the number density and radius of the particles of the second phase that are formed. Considering an isothermal cure, the quantities F_0, D_0, η_0, A, E_a, E_η and T are independent of the conversion.

Solution of the differential equations described above for an isothermal cure condition may be considered after the conversion reaches a point at which the free energy curve predicted by the Flory-Huggins equation indicates that phase separation will occur. Practically, mathematical solutions are obtained by incrementing the a small amount which allows numerical solution of the above equations to give the number density and the radius of dispersed particles.

4.2.7.7 Phase Composition from the Williams Model

The Williams model allows calculation of the number of particles and their radii at a certain degree of cure completion. From this data, the volume fraction of particles may be obtained. This is represented by

$$V_t(p) = \frac{4}{3}\pi r(p)^3 N_V(p) \qquad \textbf{(4-67)}$$

and

$$\phi_{20} = \phi_{2N}(p)V_d(p) + \phi_{2c}{}^{cured}(p)(1-V_d)(p) \qquad \textbf{(4-68)}$$

where $V_t(p)$ is the volume fraction of toughener rich phase at a conversion p and $N_V(p)$ is the number of particles at that conversion. ϕ_{20} is the original toughener composition and $\phi_{2c}{}^{cured}$ is the composition of toughener in the continuous phase that results. By simple mass balance, knowing the amount of the rubber rich phase, together with the final composition of the rubber rich phase and the initial amount of rubber included in the mixture, we can find the amount of toughener remaining in the continuous phase. This remaining amount of rubber mixed into this phase will depress its glass transition temperature. The glass transition temperature of the thermoset rich phase may now be predicted and compared to the measured glass transition temperature. Using this mass balance idea, expressions may be developed to treat the thermoset-rich phase's toughener composition starting with descriptions of particle formation described above. With each increment of conversion, the particles grow. Assuming the composition of any particle is homogeneous, the composition of a particle originating at conversion p_i and growing until conversion p_j is

$$\phi_{2N}(i,j) = \frac{1}{r_{i,j}{}^3} \sum_{k=1}^{j} \phi_{2N}(k,k)(r_{i,k}{}^3 - r_{i,k-1}{}^3) \qquad \textbf{(4-69)}$$

A particle can have one of a number of compositions of the toughener component since concentration varies with the increment of conversion. In this case, the average composition is of interest. This is

$$<\phi_{2d}(j)> = \frac{\sum_{i=1}^{j} \phi_{2N}(i,j) r_{i,j}{}^3 n_i}{\sum_{i=1}^{j} r_{i,j}{}^3 n_i} = \frac{\sum_{i=1}^{j} \sum_{i=1}^{j} \phi_{2N}(k,k)(r_{i,k}{}^3 - r_{i,k-1}{}^3) n_i}{\sum_{i=1}^{j} r_{i,j}{}^3 n_i} \qquad \textbf{(4-70)}$$

$$= \frac{\sum_{i=1}^{j} \phi_{2N}(i,j) V_d(i,j)}{\sum_{i=1}^{j} V_d(i,j)} \qquad \textbf{(4-71)}$$

where $<\phi_{2d}(j)>$ is the average toughener composition, n_i is the number of nuclei formed at conversion p_i and $V_d(i,j)$ is volume fraction of particles formed at p_i and grown to conversion p_j. The total volume fraction of phase rich in component 2 is the sum over all particles. This is

$$V_d(j) = \sum_{i=1}^{j} V_d(i,j) \qquad \textbf{(4-72)}$$

The composition of toughener in the thermoset rich phase is now

$$\phi_{2c,j} = \frac{\phi_{20} - \frac{4\pi}{3} \sum_{i=1}^{j} \phi_{2N}(i,j) r_{i,j}{}^3 n_i}{1 - \frac{4\pi}{3} \sum_{i=1}^{j} r_{i,j}{}^3 n_i} = \frac{\phi_{20} - <\phi_{2d}(j)> V_{D,j}}{1 - V_{D,j}} \qquad \textbf{(4-73)}$$

4.3 Experimental

4.3.1 Derivation of Williams Model for a Cyanate Ester System

The derivation of the Williams model for prediction of toughened thermoset characteristics will be presented in this section. While quite similar to the case of a rubber-toughened epoxy presented previously, differences in molecular weight buildup

with conversion change the relevant equations. This current derivation is necessary for application in a subsequent section of this chapter.

4.3.1.1 Thermodynamics of Mixing

In description of the phase separation behavior of polymer systems, including toughened thermosets having phases separating as a result of increase of cure conversion, it is necessary to employ thermodynamic descriptions to describe the phase formation. The Flory-Huggins treatment has been modified by Williams et al. to illustrate and model the thermodynamics of mixing of a polymeric component and a polymerizing component whose increase in molecular weight is responsible for demixing of the solution.

The Flory-Huggins expression again may be written as

$$\Delta G^{M}{}_{V} = \frac{RT}{\overline{V}_1}\left[(1-\phi_2)\ln(1-\phi_2) + \frac{\phi_2}{Z}\ln\phi_2 + \chi\phi_2(1-\phi_2)\right] \quad \textbf{(4-74)}$$

in terms of the volume fraction of the second component, ϕ_2. Here, $\Delta G^{M}{}_{V}$ is the free energy of mixing per unit volume, R is the gas constant, T is the absolute temperature, Z is the ratio of the molar volume of the second component to that of the first component, and χ is the Flory-Huggins interaction parameter.

As discussed above, the ideas of Flory (17), and Stockmayer (18), or Macosko (19), can be utilized to generate various expressions for the molecular weight averages as a function of the degree of conversion. These equations treat the statistics of polymer polymerization depending on the type of system; i.e. the functionality of the reactants. The polymerization of dicyanate monomers has been studied in depth. (74) It has been found that the average degrees of polymerization for the dicyanate system are

$$\overline{P}_n = \frac{1}{1-\frac{4}{3}p} \quad \textbf{(4-75)}$$

and

$$\overline{P}_w = \frac{1+2p}{1-2p} \quad \textbf{(4-76)}$$

where p is the degree of conversion and P_w and P_n are the weight and number average degrees of polymerization, respectively. The average degree of polymerization is

$$\overline{P}_n = \frac{\overline{M}_n}{\overline{M}_0} \quad \textbf{(4-77)}$$

and

$$\overline{P}_w = \frac{\overline{M}_w}{\overline{M}_0} \quad \textbf{(4-78)}$$

where M_0 is the molecular weight of the monomer. Therefore, the number and weight average molecular weights have the following form

$$\overline{M}_n = \frac{\overline{M}_0}{1-\frac{4}{3}p} \quad \textbf{(4-79)}$$

$$\overline{M}_w = \overline{M}_0 \frac{1+2p}{1-2p} \quad \textbf{(4-80)}$$

The following equations relate the evolution of molar volume, molar volume ratio and interaction parameter at any conversion to their value at zero conversion:

$$\overline{V}_1 = \overline{V}_{10} \frac{\overline{M}_n(p)}{\overline{M}_n(0)} = \frac{\overline{V}_{10}}{1-\frac{4}{3}p} \quad \textbf{(4-81)}$$

$$Z = \frac{\overline{V}_2}{\overline{V}_1} = \frac{\overline{V}_2}{\overline{V}_{10}}\left(1-\frac{4}{3}p\right) = Z_0\left(1-\frac{4}{3}p\right) \quad \textbf{(4-82)}$$

where the 0 subscript indicates the quantity taken at zero conversion.

Using the above equations, the Flory-Huggins equation may be rewritten in terms of the volume fraction of the second component (preformed polymer in this case) as well as conversion. This expression is

$$\Delta G_V{}^M = \frac{RT}{\overline{V}_{10}}\left[\left(1-\frac{4}{3}p\right)(1-\phi_2)\ln(1-\phi_2)+\frac{\phi_2}{Z}\ln\phi_2+\chi_0\phi_2(1-\phi_2)\right] \quad \textbf{(4-83)}$$

which is the dicyanate analog of equation (4-51).

4.3.1.2 Nucleation and Growth

The equations describing the derivation of the Williams model for the cyanate ester system are in many cases identical to the epoxy example originally used by Williams. Many of these have been presented in the above literature review; however, because they are required at this point, for completeness they will be repeated here with only brief comment.

The rate of formation of nuclei can be expressed as follows

$$\frac{dN}{dt} = F_0 D \exp\left(\frac{-G_c - E_F}{RT}\right) \quad \textbf{(4-84)}$$

where ΔG_c is the free energy at the critical radius size, F_0 is a proportionality constant, D is the diffusion coefficient of the preformed polymer in the thermoset resin, and E_F is the energy barrier for composition fluctuation. The rate of composition fluctuation per unit volume is

$$\frac{dF}{dt} = F_0 D \exp\left(-\frac{E_F}{RT}\right) \quad \textbf{(4-85)}$$

4.3.1.3 Interfacial Free Energy

The free energy expression for the formation of a new spherical phase is

$$\Delta G(r) = \frac{4\pi}{3} r^3 \Delta G_N + 4\pi r^2 \sigma \quad \textbf{(4-86)}$$

where σ is the surface free energy and ΔG_N is the free energy change of new phase formation per unit volume. This equation is used to calculate the critical values r_c, the critical radius and ΔG_c, the critical free energy of formation of a new phase as follows:

$$r_c = -\frac{2\sigma}{\Delta G_N} \quad \textbf{(4-87)}$$

and

$$\Delta G_c = \frac{16\pi\sigma^3}{3\Delta G_N{}^2} \qquad \textbf{(4-88)}$$

The nucleation rate may be expressed using an energy barrier of ΔG:

$$\frac{dN}{dt} = \frac{dF}{dt}\exp\left(-\frac{\Delta G_c}{kT}\right) = \frac{dF}{dt}\exp\left(-\frac{N_A \Delta G_c}{RT}\right) \qquad \textbf{(4-89)}$$

with N_A being Avogadro's number.

Measurement of σ, the interfacial energy, must be known to make this calculation, and this quantity will be estimated for this purpose in a subsequent section.

4.3.1.4 Viscosity and Rheology Relation to Growth Rate

The growth rate may be described as the increase in volume fraction of second phase per time unit

$$\frac{dV}{dt} = 4\pi r^2 k_\phi N_V (\phi_{2c} - \phi_2{}^T) = 4\pi r_2 N_V \frac{dr}{dt} \qquad \textbf{(4-90)}$$

where k_ϕ is the mass transfer coefficient and N_V is the number of particles per unit volume. Here, the quantity $(\phi_{2c}-\phi_2{}^T)$ is the driving force for growth, the difference between the equilibrium and actual composition of second component in the thermoset-rich phase. The mass transfer coefficient may be evaluated using the assumption that the particle is a sphere in a stationary medium, and results in:

$$k_\phi = \frac{D}{r} \qquad \textbf{(4-91)}$$

Using this together with the growth rate expression above, a new expression for growth rate of the radius per unit time is obtained:

$$\frac{dr}{dt} = \frac{D}{r}\left(\phi_{2c} - \phi_2{}^T\right) \qquad \textbf{(4-92)}$$

To arrive at the diffusion coefficient, use is made of the Stokes-Einstein diffusion relationship

$$D = \frac{D_0 T}{\eta} \qquad \textbf{(4-93)}$$

which connects diffusion to the viscosity, which is a function of molecular weight increase as cure proceeds, as well as temperature. Together, the relation for temperature and molecular weight effect on viscosity is given by

$$\eta(T,p) = \eta_0 \left(\frac{\overline{M_w}(p)}{\overline{M_w}(0)} \right)^{3.4} \exp\left[\frac{E_\eta}{RT} \right] = \eta\big|_{p\to 0, T\to\infty} \left(\frac{1+2p}{1-2p} \right)^{3.4} \exp\left[\frac{E_\eta}{RT} \right] \qquad \textbf{(4-94)}$$

where E_η is the activation energy for the viscosity. The viscosity parameters necessary will be determined in a subsequent section.

4.3.1.5 Modeling Particle Size Distribution

Intial steps for solving the equations of the model require rewriting the nucleation rate expression in terms of the degree of cure, p, the number of fluctuations with time expression, and the kinetic expression using the Stokes-Einstein diffusion relationship

$$\frac{dN}{dp} = \frac{F'_0 T}{(1-p) A\eta\big|_{p\to 0, T\to\infty}} \left(\frac{1-2p}{1+2p} \right)^{3.4} \exp\left[\frac{E_a - E_\eta - E_F - \Delta G_c}{RT} \right] \qquad \textbf{(4-95)}$$

where $F'_0 = D_0 F_0$ is a quantity that is adjustable to fit the generated particle size distribution to the real distribution. Using the previously developed relationships along with the Stokes-Einstein relationship, the growth rate may be expressed as

$$r\frac{dr}{dt} = D(\phi_{2c} - \phi_2^{\,T}) = D_0 \frac{T}{\eta}(\phi_{2c} - \phi_2^{\,T}) \qquad \textbf{(4-96)}$$

$$= D_0 \frac{T}{\eta|p\to 0, T\to\infty} \left(\frac{1-2p}{1+2p} \right)^{3.4} \exp\left[-\frac{E_\eta}{RT} \right] (\phi_{2c} - \phi_2^{\,T})$$

$$= B \left(\frac{1-2p}{1+2p} \right)^{3.4} (\phi_{2c} - \phi_2^{\,T})$$

where $B = \frac{D_0 T}{A\eta\big|_{p\to 0, T\to\infty}} \exp\left[\frac{E_a - E_\eta}{RT} \right]$. This equation may also be expressed as a function of conversion using the kinetic expression for dicyanate conversion

$$r\frac{dr}{dp} = \frac{B}{1-p}\left(\frac{1-2p}{1+2p}\right)^{3.4}(\phi_{2c} - \phi_2{}^T)\exp\left[\frac{E_a}{RT}\right] \qquad \textbf{(4-97)}$$

$$= B'\left(\frac{1-2p}{1+2p}\right)^{3.4}(\phi_{2c} - \phi_2{}^T) \qquad \textbf{(4-98)}$$

where

$$B' = \frac{D_0 T}{(1-p)A\eta\big|_{p\to 0, T\to\infty}}\exp\left[\frac{E_a - E_\eta}{RT}\right] \qquad \textbf{(4-99)}$$

The previous equations regarding kinetics may be combined with the equations describing nucleation and growth rate as well as viscosity and diffusion expressions to obtain differential equations describing the number density and radius of particles of the second phase that are formed. The solution to this set of equations is similar to the original model for toughened epoxy systems as presented by the original author Williams. Practically, this is accomplished using a computer.

4.3.2 Determination of Physical Parameters

4.3.2.1 Cure Kinetics

Kinetics experiments were performed to generate a description of the molecular weight evolution of the growing polymer with increasing degree of cure. This is necessary for the modeling process. In addition, because phase composition is a function of the degree of phase separation, the speed at which the matrix reaches the gel point is important in determining the diffusion rate and, therefore, the rate of growth of the disperse toughener-rich phase. In this segment of the experimental section, the speed of the cyanate trimerization polymerization which connects both the just presented processes will be determined. This provides a basis upon which comparisons may be made of the rate of phase separation with the rate of reaction. As the gel point is reached and diffusivity and molecular mobility are restricted, the disperse phase no longer grows,

and the composition of each phase is fixed in a state of thermodynamic nonequilibrium as sufficient time for phase separation does not exist. Though a number of techniques are available to determine degree of reaction, for this thesis investigation the differential scanning calorimeter, or DSC, was used to evaluate the thermally activated polymerization of the cyanate material.

The kinetic description of the BADCy polymerization was simplified through the assumption of first order kinetics. The exact mechanism of polymerization is still unknown. Thus, a suitable description of the conversion as a function of time at an isothermal cure temperature was made without choosing a specific mechanism; rather, by empirical best fit criteria. Because the cure proceeds relatively rapidly with respect to uncatalyzed BADCy, this kinetics simplification is justified. Additionally, other kinetic descriptors, such as the autocatalytic kinetic equations, might better describe the cure at short times and degrees of conversion. However, at the degrees of conversion necessary for phase separation to occur, a first order expression was found to be completely sufficient.

In summary, where temperature or catalyst concentration drive the reaction rapidly, as in this example, the polymerization rate may be very well described using a simple $n^{\underline{th}}$ order kinetic expression:

$$\frac{dp}{dt} = k(1-p)^n \qquad \textbf{(4-100)}$$

where k is the reaction constant and n has been shown to be one. (75, 76) The temperature dependence of k is assumed to be of the form

$$A = \exp\left(-\frac{E_a}{RT}\right) \qquad \textbf{(4-101)}$$

which, combined with the above expression, yields

$$\frac{dp}{dt} = A\exp\left(-\frac{E_a}{RT}\right)(1-p)^n \qquad \textbf{(4-102)}$$

Samples were prepared by putting controlled masses (10 mg +/- 1 mg) of catalyzed, unreacted monomer into Seiko sealed DSC sample pans, placing these in a preheated oven and holding isothermally for known times. This was followed by a quench in liquid nitrogen. These samples were examined in a TA Instruments 2920 DSC which was ramped up in temperature at 10 °C min^{-1} to 325 °C to complete the cure and measure the residual reaction exotherm. Several specimens were kept uncured to determine the heat of reaction for the totally unreacted monomer. The heat of reaction was found to be 703.2 J g^{-1} (± 7.8 J g^{-1}), or 195.7 kJ mol^{-1} (97.9 kJ mol^{-1} per cyanate group), which agrees reasonably well with the literature value of approximately 105 kJ mol^{-1} per cyanate group. (77) The fractional conversion p was calculated as

$$p = \frac{\Delta H(T,t)}{\Delta H_0} \qquad \textbf{(4-103)}$$

where ΔH_0 is the integrated enthalpy of reaction per mole for a totally unreacted monomer sample and $\Delta H(T,t)$ is the enthalpy of reaction after a well define cure cycle of cure temperature T and time t. Plots of conversion versus time for four different temperatures (150 °C, 170 °C, 190 °C and 210 °C) are shown in Figure 4-5.

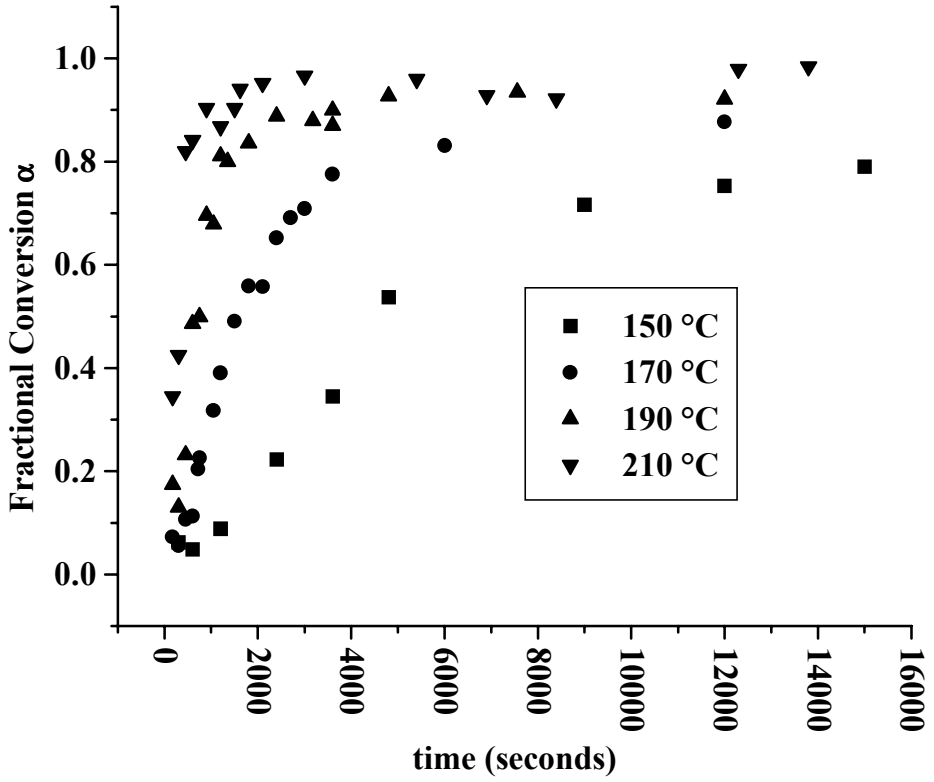

Figure 4-5. Fractional conversion versus time data determined via DSC for the BADCy system.

A graph of the raw data together with the first-order best-fit curves is shown in Figure 4-6. The data show a reasonably good fit to the first order expression. At the lower temperature, 150 °C, a small discrepancy is apparent. This type of slower, low temperature kinetic behavior would probably best be described using autocatalytic expressions, which account for the low initial rate of the reaction in some situations. Slower rate phenomena have been investigated for the cyanate resins and explained using some of the proposed mechanisms for the cyanate polymerization. The reaction has been postulated to develop an iminocarbonate from the reaction of the cyanate ester with a phenolic hydroxyl functionality. (78) If extremely pure monomers are heated, no

reaction takes place. However, the reaction mechanism is poorly understood, and is known to vary with the added catalyst or monomer impurities. Figure 4-6 shows the kinetic data together with the first order fits. The quality of agreement is sufficient for the purposes of this thesis.

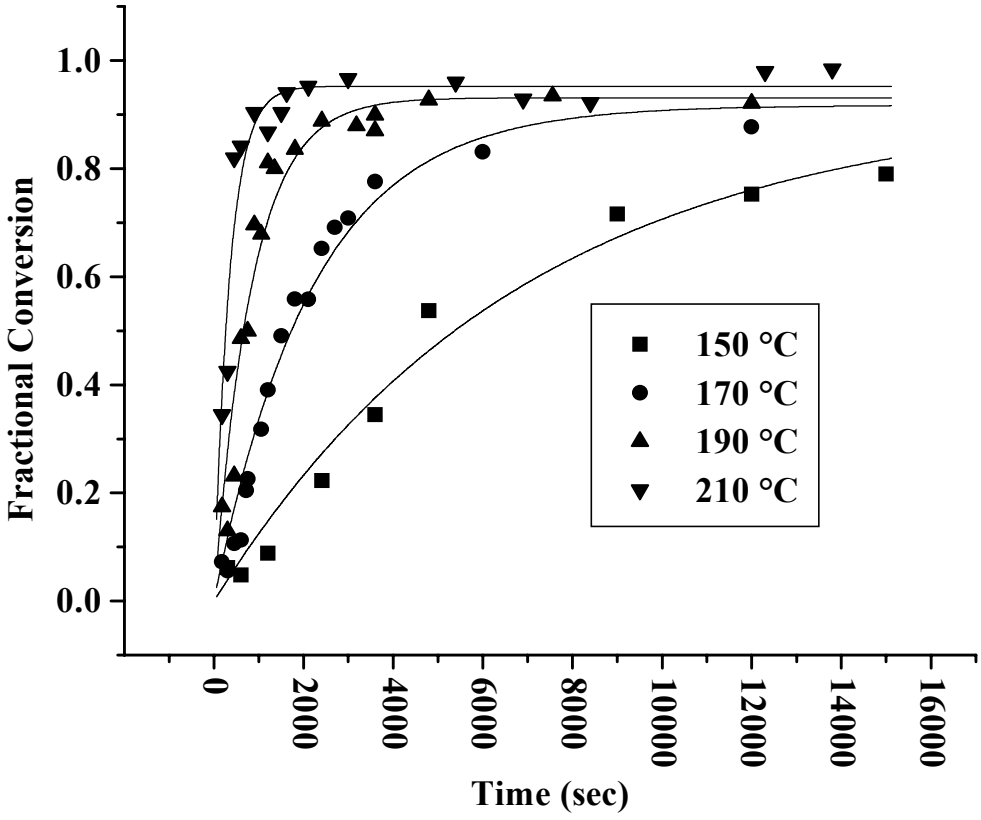

Figure 4-6. Fits of experimental data to first order kinetic expression.

An Arrhenius plot has been constructed from this kinetic data by plotting the log of the reaction constant versus the inverse absolute temperature. A straight line was fitted to these four temperature points, with a statistical r^2 value of 0.9996, indicating an excellent fit. Using the slope of this line, the activation energy of the reaction has been determined to be 84.2 kJ mol^{-1}, which is in excellent agreement with reported literature

values of about 80 kJ mol^{-1}. (79, 80) The y-intercept of this plot also provides the frequency factor for the reaction, which was found to be 3.66 X 10^6 s^{-1}. The Arrhenius plot is shown in Figure 4-7.

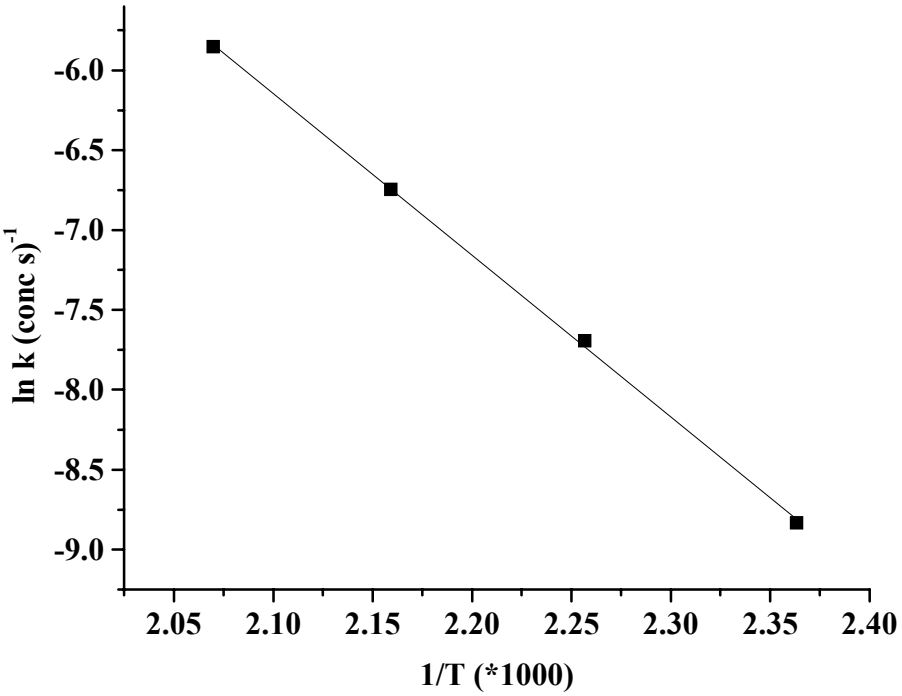

Figure 4-7. Arrhenius plot of BADCy reaction constant for calculation of activation energy.

4.3.2.2 Determination of Rheological Parameters

The Williams model for phase separation in thermosetting resins containing a polymer additive depends fundamentally upon the competition between conversion (polymerization of the thermoset) versus the rate of diffusion of the toughener out of the thermoset-rich phase during phase separation. This diffusion rate may be estimated as explained in the literature review through the use of the Stokes-Einstein relationship.

Such an approach will be developed in this chapter. Some of the information required for fitting the Williams theory to the present experimental system is now discussed.

To treat the diffusion rate, rheological data must be collected for the cyanate ester resin. This is based on viscosity data as well as the dependency of viscosity on temperature. The measurement of viscosity with varying temperature was accomplished using a Brookfield digital viscometer with cone-and-plate measuring fixture. Temperature was maintained with a circulated mineral oil bath around the measuring fixture. One milliliter of molten, uncatalyzed BADCy was placed between the cone and plate and was preheated to approximately 82 °C to keep the material from crystallizing. The viscometer was started and operated at 12 rpm. Temperature was increased in randomly-sized steps to approximately 130 °C and was recorded from a thermocouple immersed in the oil bath after equilibration at that temperature for exactly one minute. Typical data is shown in Figure 4-8.

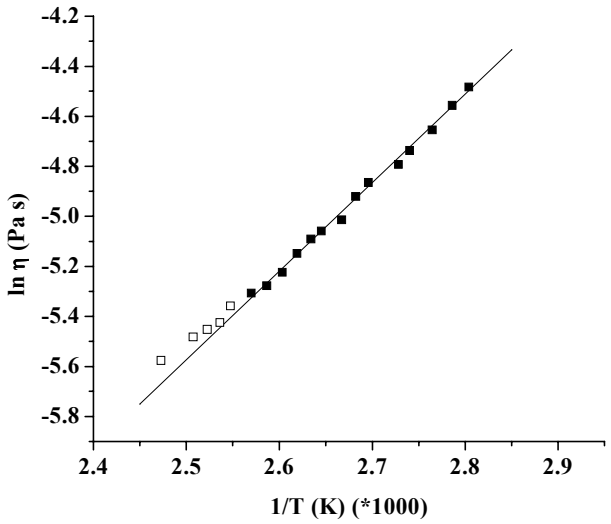

Figure 4-8. Change in viscosity of BADCy monomer with temperature. Solid symbols are data used for calculation, hollow symbols are higher temperature data showing effect of molecular weight increase due to reaction.

The resultant rheological data were analyzed using the Arrhenius relationship, and a representative graph is shown in Figure 4-8. Here, the viscosity is seen to increase linearly with inverse temperature over a large portion of the lower temperature range. At higher temperatures, the relationship becomes nonlinear, with higher viscosities than predicted being observed. This is likely due to the reaction of the monomer and the increase in molecular weight at these higher temperatures. This strongly increases the measured viscosity in the expected fashion. Accordingly, only data in the linear region are used in the calculation of activation energy since the required E_a is for unreacted monomer. The slope and intercept in the linear region were taken as the average values from three iterations of the experiment. One of the most obvious initial observations that may be made notes the extremely low viscosity of the cyanate ester monomer. This illustrates a feature that has been pointed out previously about possible uses of this material, namely, that such a very low viscosity makes it suitable for easy impregnation of fibers or other materials in composite structures. From the average slope of the three experiments, an activation energy of 29.3 kJ mol^{-1} was determined and an extrapolated viscosity at infinite temperature of 5.14 x 10^{-7} Pa s. Unfortunately, no data exist in the literature to compare with these values; however, this number reflects a lower limiting viscosity than that of the epoxy used for the derivation of the Williams model, which was about 2 x 10^{-6} Pa s. (81) It is noteworthy that the activation energy of cyanate ester viscosity is not significantly different than that of the DGEBA epoxy monomer, which has been found to have an activation energy of 33.3 kJ mol^{-1} (82). The consequences of this will be more fully explored in subsequent sections of this chapter.

4.3.2.3 Determination of Flory-Huggins Interaction Parameter

As was discussed above, the model currently employed to predict particle size distributions relies heavily on the Flory-Huggins approach to predict phase separation. Various quantities must be evaluated in order to use Flory-Huggins (or indeed any) more detailed thermodynamic treatment of phase behavior. For example, for the model, we must know the molar volume of both components, and in the case of the treatment of Flory and Huggins, the χ interaction parameter. While the particulars of this quantity and its physical meaning have been discussed at great length for many different systems and summarized in the review portion of this chapter, in this particular section we will only consider the empirical determination of χ. In this present study, the cloud point curve for the system of interest, BADCy and HTBN, was determined in an apparatus designed and built specifically for this measurement.

To evaluate χ, both density and molecular weight data for the resin and polymer toughener were obtained. Molecular weights were measured using a Waters 150C Gel Permeation Chromatograph with Viscotek online viscometer for absolute molecular weight characterization. The molecular weight averages obtained for the HTBN toughener were $<M_n>$=3880 g mol^{-1} and $<M_w>$=6560 g mol^{-1}. Because the difference in number and weight average molecular weight for the toughener is relatively small (consistent with previous findings for functional butadiene-acrylonitrile tougheners, as shown previously (83)), the assumption of a true binary mixture for our model is better than it would be in the case of a more polydisperse system. Note that this assumption is better than the case for an epoxy system due to the high purity (pure monomer) of the cyanate ester monomer. Density was measured using a Micromeritics AccuPyc 1330 gas

pycnometer. The pycnometer was calibrated and 0.6465 grams of HTBN were placed in the measurement cup with careful prior removal of any trapped air bubbles using a vacuum oven. This mass of material filled the cup approximately 2/3 full. The density of this toughener was found to be 0.9407 g cm^{-3}, ±0.0001 g cm^{-3} at 25 °C.

The molar volume for BADCy was estimated from the density data of Armistead and Snow. (84) These workers employed dilatometry to determine a density of 1.1667 g cm^{-3} at 25 °C (Figure 4-9). For the case of BADCy monomer, the molecular weight may be taken to be the formula weight due to the high purity of the monomer. For BADCy, this is 278.31 g mol^{-1} and from this a molar volume of 238.5 cm^3 mol^{-1} was calculated.

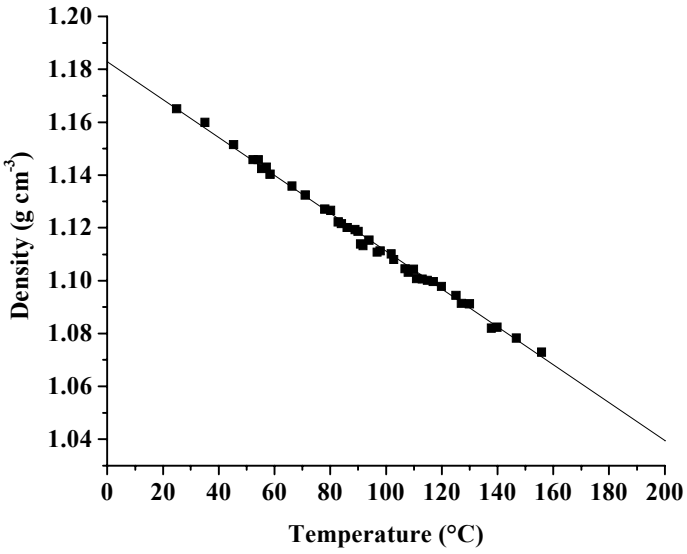

Figure 4-9. Density of BADCy monomer in liquid state (adapted from A. W. Snow and J. P. Armisted, Dilatometry on Thermoset Resins, NRL Memorandum Report 6848, NTIS ADA239276, (1991).).

To experimentally determine the χ interaction parameter for the HTBN-BADCy mixture, the cloud points of various concentrations of HTBN in BADCy were measured. This method detects scattering via a decrease in the transmitted intensity through the

sample. Experimentally, the cloud point is indicated by the magnitude of the sample scattering light, or clouding, which occurs due to the formation of a second phase of sufficient size to scatter light, providing that this second phase has a refractive index sufficiently different from the initial phase. Because some light is scattered, the transmitted intensity drops, and the cloud point is taken to be the onset point of this transmission decrease.

To assure accurate cloud point determinations, a new measurement device was designed and constructed. The heart of this apparatus is an Olympus BX50 optical microscope, which provided optics and a mechanical foundation for the apparatus. Temperature of the sample was controlled via a Linkham THMS600 heated microscope stage and controller. The internal light source of the microscope was used to provide illumination through the sample. Light intensity was measured using a Graesby Optronics UDTS370 digital optometer (light intensity meter), which was fitted to the camera port of the microscope with a custom adapter. This optometer is sensitive to extremely small changes in light intensity. Data were acquired from both the hot stage and optometer using an IBM-compatible personal computer. Serial port data from the hot stage was acquired simultaneously with IEEE-bus data from the optometer. The temperature data from the hot stage and light intensity from the optometer were stored to a text file using a custom program written using Microsoft QuickBASIC. A schematic diagram of this apparatus is shown in Figure 4-10.

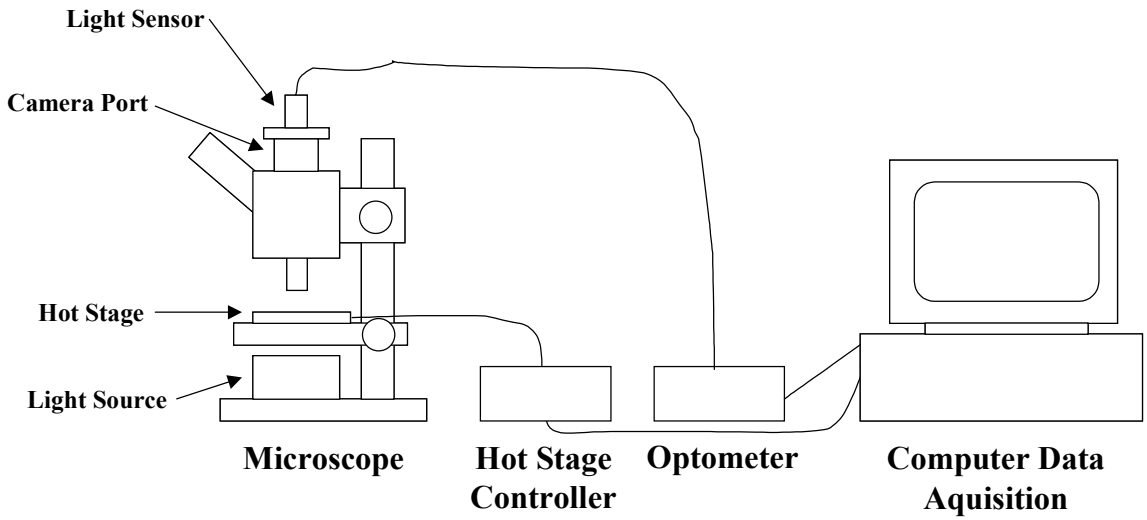

Figure 4-10. Cloud point determination apparatus.

The operating technique for the cloud point apparatus involved the use of custom-made "wells" or sample cells which were put together using sheet gasketing which was cut to provide washers. These washers were subsequently attached to round glass coverslips using silicone sealant. Several wells were constructed at a time, these and were cured overnight at 100 °C to finalize the degree of cure of the silicone. Solutions of each concentration were prepared as detailed in Chapter 3. This required using direct dissolution of HBTN in molten, uncatalyzed BADCy at approximately 90 °C with vigorous stirring. These solutions were used immediately after preparation when several drops were transferred to the preheated sample cell placed on the hotstage. The samples were then cooled at several different cooling rates using gas cooling of the hotstage cell.

The formation and growth of a second phase is a kinetically controlled process, particularly where the process proceeds via a nucleation and growth mechanism. The formation of nuclei, together with the growth of these particles to a size sufficient to scatter visible light (approximately 100 nm) (85), takes time. Because the second phase

development is a time consuming process, the effect of cooling rate on the cloud point may not be dismissed.

Raw data from the computer file collecting the acquired data was analyzed for the cloud point onset using TA Instruments Universal Analysis software version 2.4. In this case, the raw data were inserted into the software as a text file using the TA Instruments file header. The software provides for easy and accurate calculation of onset point, the temperature where the light intensity began to rapidly decrease as the sample was cooled. The onset points of the different rates of cooling were extrapolated to an infinitely slow cooling rate, to provide a cloud point result as near to thermodynamic equilibrium as possible.

Samples were prepared by introducing HTBN into BADCy at 5, 7.5, 10, 12.5, 15, 17.5, 20, 22.5, and 25 weight percent HTBN levels. Samples were cooled from 105 °C to about 40 °C at 20, 10, 5, 2, and 1 °C per minute. A representative construction of a cloud point onset using the TA software is shown in Figure 4-11, which also illustrates a typical temperature/transmitted intensity result. The calculated cloud points were compiled for the case of 10% HTBN for the various cooling rates. These data are shown in Figure 4-12. Figure 4-13 illustrates the extrapolation of cooling rate to an infinitely slow rate, and Figure 4-14 is the completed cloud point curve.

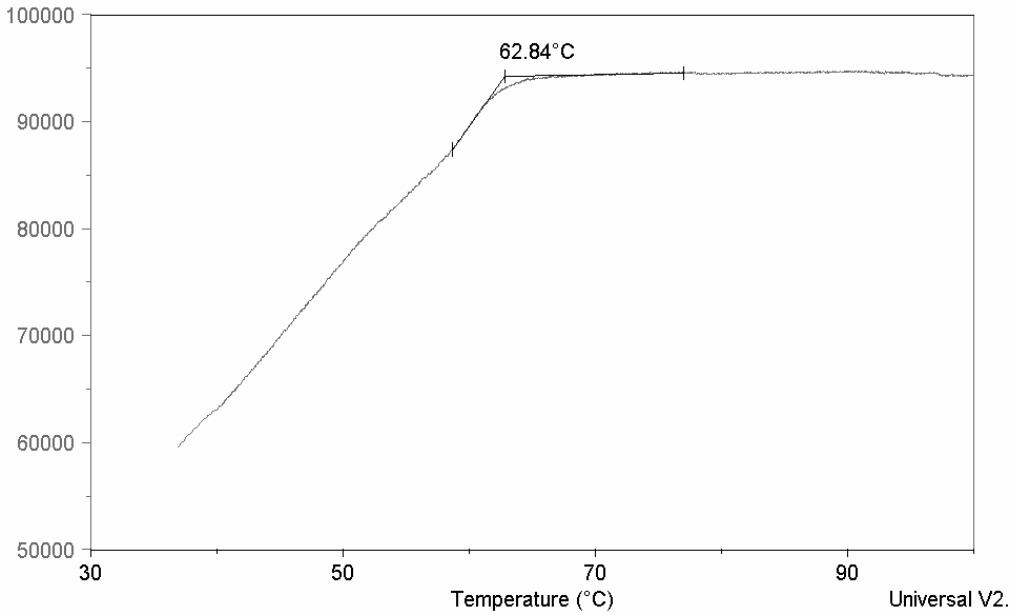

Figure 4-11. Construction of cloud point onset measurement.

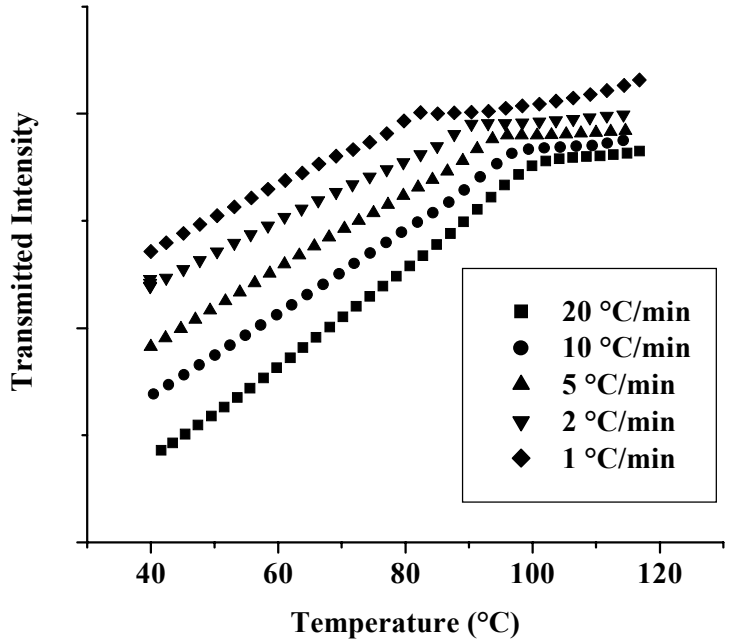

Figure 4-12. Typical cloud point results as a function of cooling rate.

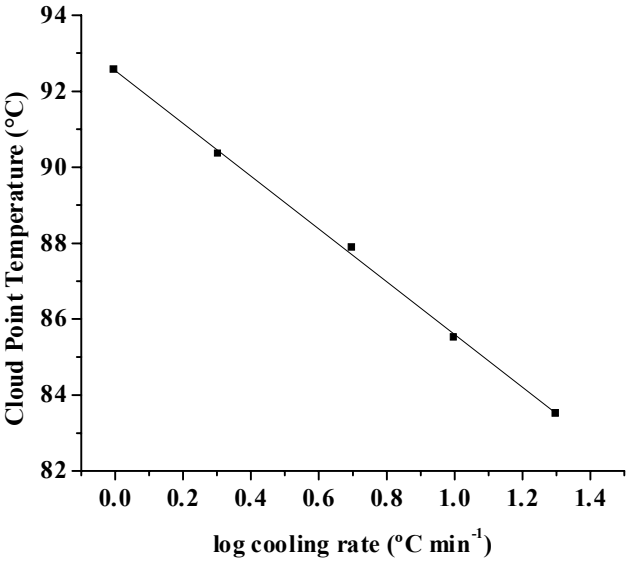

Figure 4-13. Extrapolation of cloud point to zero cooling rate for a representative sample.

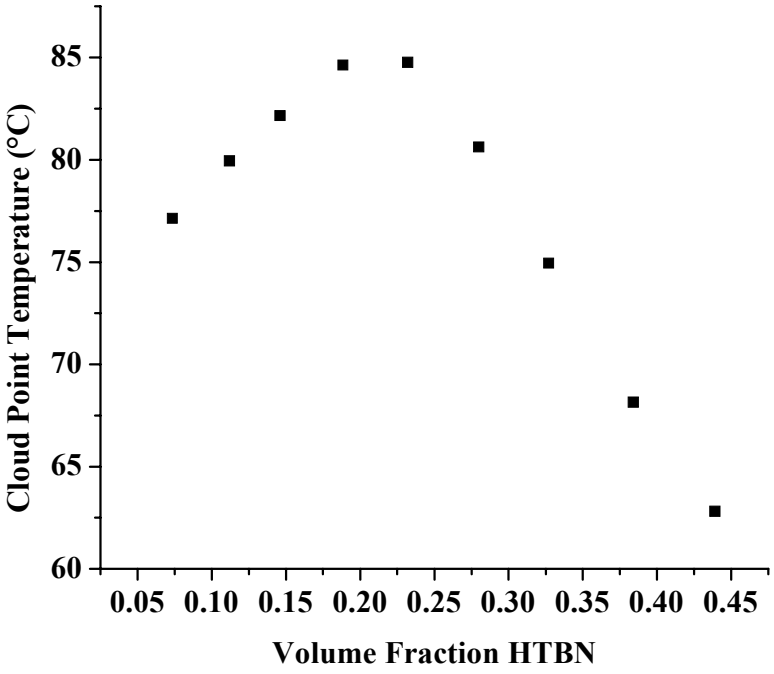

Figure 4-14. Cloud point curve for BADCy/HTBN system.

Two methods were initially used to numerically determine χ by fitting the cloud point curve to obtain a value of χ for this system – a numerical search of the free energy curves for common tangents and a method based on the technique of Schultz and Flory (86) for the calculation of phase diagrams. After several initial investigations and iterations with various example data, the latter method was chosen as the most suitable method for the determination.

The technique is described as follows: the ratio of molar volume (Z) of solvent to solute for the BADCy/HTBN system was calculated to be 17.27. Once Z is known, χ_{cr} and ϕ_{cr} were calculated; these were found to be 0.7993 and 0.2091, respectively. A computer program was written which equated the value of χ in both phases (self-consistency requirement), while an iterative process was performed to find and test values for temperature and ϕ_2.

Cloud point data were fitted to the a+b/T form of χ. This yielded an expression for χ of 0.3819 + 411.6/T. The resultant phase diagram showing the binodal and spinodal lines obtained as described previously is shown in Figure 4-15 together with the cloud point data. This fitting procedure was found to provide good agreement with the cloud point data relative to similar toughened thermosetting systems detailed previously. (87)

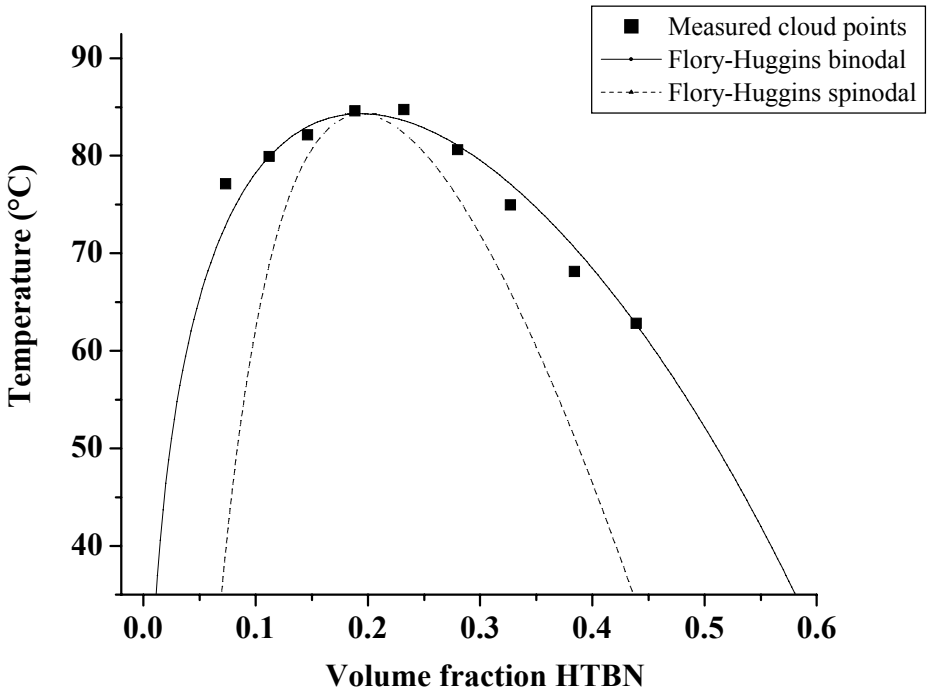

Figure 4-15. Cloud points fitted to Flory-Huggins binodal curve.

The value of the interaction parameter was determined using several assumptions that have a bearing on the accuracy of the measurement. The first assumption is that the cloud point determined represents the actual thermodynamic equilibrium point for formation of the two phases from a single initial phase. The extrapolation of the cloud point to infinitely slow cooling rate assists in reducing kinetic effects on phase separation. Additionally, cloud points were collected based on transmission of light rather than scattering. Due to the wavelength of light, light scattering techniques are limited to detecting separated particles of the second phase that are on the order of microns. While much previous work has been done in the area of polymer solution thermodynamics with only visual determination of the cloud point (see for example (88)), it has been recognized that the use of alternative analytical techniques such as small angle X-ray scattering provide improved information, allowing resolution

of areas of increased concentration or electron density down to sizes much smaller than detectable with visible light. Lastly, the polydispersity of the HTBN toughener polymer component (as well as any polydispersity in the monomer) can significantly alter the shape of the binodal line. (89) For measurements of coexistence curves with fewer complications, idealized systems may be chosen which optimize the attainment of equilibrium. An example of this would be the use of monodisperse molecular weight solutes. Our chosen system does, however, have the advantage of a very low viscosity, which allows fast phase separation kinetics. With the care taken in extrapolating to infinitely slow cooling rate and the obviously reasonable fit of the data to our model, the adequacy of the generated results for its intended purpose is judged to be sufficient. In addition, the fit of this cloud point data compares quite favorably to that obtained on reasonably similar systems (epoxy/butadiene-acrylonitrile) used for a similar purpose. (90)

4.3.2.4 Surface and Interfacial Parameters

Estimation of the interfacial energy has been made to enable accurate calculation of the nucleation parameters necessary for application of the Williams phase separation model. Measurements of interfacial parameters are not straightforward - a number of methods have been developed to allow an accurate assessment to be made. The approach initially adopted was to determine the surface energy of the HTBN toughener as well as the surface energy of the cured polycyanurate. Here, the assumption was made that the surface energy of the fully cured polycyanurate would approximate the surface energy of the polymerizing cyanate resin at a conversion equivalent to the point of phase separation. While this assumption may be an oversimplification, it is quite difficult to measure the dependence of surface energy on conversion over the entire region of phase

separation and to include this dependence in the model calculations. Moreover, the experimental difficulties of measuring interfacial energy at the point of immisciblity (and at slightly higher conversions) are obviously great.

A plaque of unmodified polycyanurate was cast in a steel mold at 150 °C and cured for 4 hours, followed by cooling at ambient conditions to room temperature were achieved, and then postcured at 250 °C for two hours. During the cure cycle, the mold was covered with aluminum foil to prevent contamination of the surface. Following cure, the sample plaque was stored (covered) in a dessicator at room temperature.

The harmonic mean method (91) was used to determine the surface energy of the air side of the cured polycyanurate plaque. This method involves the use of two probe liquids, methylene iodide and water, to determine the various contributions to surface free energy of the solid. Two simultaneous equations are then solved to provide the dispersive as well as the polar components of the surface energy. These equations are

$$(1+\cos\theta_1)\gamma_1 = 4\left(\frac{\gamma_1^{\,d}\gamma_s^{\,d}}{\gamma_1^{\,d}+\gamma_s^{\,d}} + \frac{\gamma_1^{\,p}\gamma_s^{\,p}}{\gamma_1^{\,p}+\gamma_s^{\,p}}\right) \quad \textbf{(4-104)}$$

$$(1+\cos\theta_2)\gamma_2 = 4\left(\frac{\gamma_2^{\,d}\gamma_s^{\,d}}{\gamma_2^{\,d}+\gamma_s^{\,d}} + \frac{\gamma_2^{\,p}\gamma_s^{\,p}}{\gamma_2^{\,p}+\gamma_s^{\,p}}\right) \quad \textbf{(4-105)}$$

where γ_1^p and γ_1^d are the polar and dispersive components of the first liquid and γ_2^p and γ_2^d are the polar and dispersive components of the second liquid. Probe liquids one (water) and two (methylene iodide) were used with values of γ_1^p=50.7 mN $m^{-1}$and γ_1^d=22.1 mN m^{-1} and γ_2^p=6.7 mN m^{-1} and γ_2^d=50.8 mN m^{-1}, respectively. Contact angle measurements of both liquids on the surface were made. These experiements yielded contact angles of 67.8 ±4.2 degrees for water and 37.7 ± 3.0 degrees for methylene iodide

on the cured cyanate ester sample. The equations were solved to yield a surface energy for the polycyanurate of 46.6 mJ m^{-2}, with a dispersive component of 30.4 mJ m^{-2} and a polar component of 16.2 mJ m^{-2}. This value is somewhat high for polymers, and is close to the reported surface free energy of nylon 6,6. However, our number is in reasonable agreement with the magnitude of surface energy that may be calculated using correlations with solubility parameter values. From the solubility parameter calculations made by Srinivasan (92) on the BADCy monomer, a prediction of the surface free energy of the polycyanurate was made using the technique of Hildebrand and Scott (93). The predicted surface free energy calculated in this way was found to be about 43 mJ m^{-2}.

To determine the surface energy of HTBN and therefore the interfacial free energy between the cyanate ester material and HTBN, a contact angle method was attempted. This was subsequently abandoned due to lack of confidence in the results of the measurement. A difficulty was that the HTBN has a very high viscosity; because of this, the system takes a relatively long time to reach equilibrium. Combined with the difficulty of handling this material and the difficulty of producing droplets of accurate and consistent volume, further work on this type of experiment was not attempted.

Due to the experimental difficulties of measuring surface properties of HTBN, an estimate of its interfacial energy with the cyanate ester material was made. In the previous application of the Williams model for phase separation, interfacial energy was approximated using the difference in the surface tensions of liquid diglycidyl ether of bisphenol-A (DGEBA) and a butadiene-acrylonitrile copolymer, with measurement of the surface energies performed using the capillary rise technique. This approach assumes that the phases are pure in each component, which is certainly not representative of the

actual situation. In testing of the model, the particle size and size distribution was found to be a much stronger function of the growth rate than of the surface energy (94). The consequence of this insensitivity to the interfacial energy number is that a rough evaluation of this quantity will be satisfactory. Therefore, the value of the surface free energy of HTBN was obtained from various rubber tougheners previously examined by Chen and coworkers (95), resulting in a value of approximately 40 mN m^{-1}. Using Antonoff's rule, the combined surface energies predict an interfacial tension of approximately 6.6 mJ m^{-2} at 25 °C (using the experimental value for polycyanurate). However, as shown by Sohn et al. (96), the interfacial tension decreases as temperature is increased. The decrease in interfacial free energy of the butadiene-acrylonitrile tougher/epoxy system was estimated to be 0.01 mN m^{-1} $°C^{-1}$. This temperature dependence is included in the approximation of interfacial tension used in the model.

4.3.2.5 Determination of Particle Size Distribution

Measurement of the generated particle size distribution on curing must be made to finally apply the model described above to the actual polymerizing system. Samples cured at one of the chosen isothermal cure temperatures were sectioned using a microtome to obtain a thin section that was subsequently examined using transmission electron microscopy (TEM). A sufficient number of particles were examined to yield acceptable statistics as defined in the previous review discussion; for all cases, more than 300 particles were measured.

Determination of particle sizes was made beginning with micrographs generated by TEM. Samples were prepared for this use starting with the standard freshly prepared 10% HTBN in BADCy formulation, and carefully cured in aluminum molds. These

molds were thermostatted in a well-controlled oven at the cure temperature for a time sufficient to bring the samples to gelation to "fix" the morphology, then postcured at 250 °C in the oven for two hours to maximize the degree of conversion. These samples were removed, sectioned using a microtome, then mounted and examined in a Philips 420T electron microscope. Typical images are shown for three cure temperatures in Figure 4-16.

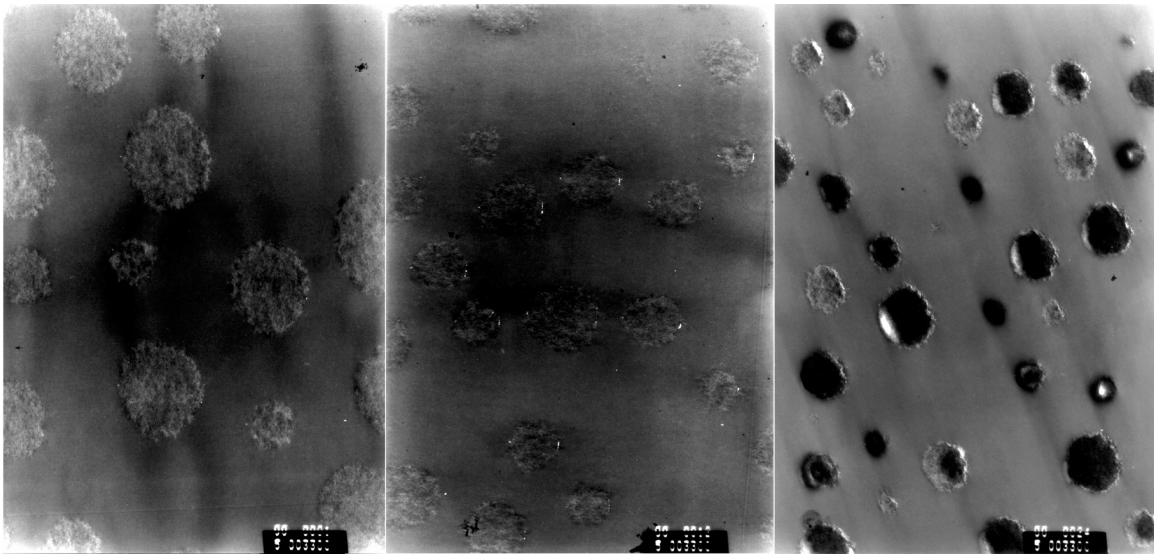

Figure 4-16. Representative TEM images used for particle size determination. From left to right: 150 °C cure, 180 °C cure, and 210 °C cure.

The resultant microscope images were printed, and the particle diameters on the prints were manually measured using digital calipers. Together with a magnification factor for the microscope thisallowed the collection of two dimensional particle size diameters. Histograms of resulting two dimensional morphology data for the three isothermal cures are shown in Figure 4-17. This resultant two dimensional data is of limited utility. As has been discussed in the literature review, the actual three dimensional distribution of sphere sizes may or may not include features seen in the two dimensional distribution of particle diameters. In this case, no bimodal distribution of

particle diameters was seen, as has been reported for the rubber toughened epoxy system referenced earlier in this section. However, for the purposes of relating and analyzing improvements in mechanical properties as well as modeling formation of the phase separated morphology, it has been emphasized above that an examination of the three dimensional distribution of sphere sizes is necessary. Unfortunately, direct measurement of this is not easily accomplished, and we must rely on an approach based on those covered above in the literature review to transform this two dimensional distribution of particle areas to a more representative three dimensional distribution of sphere sizes.

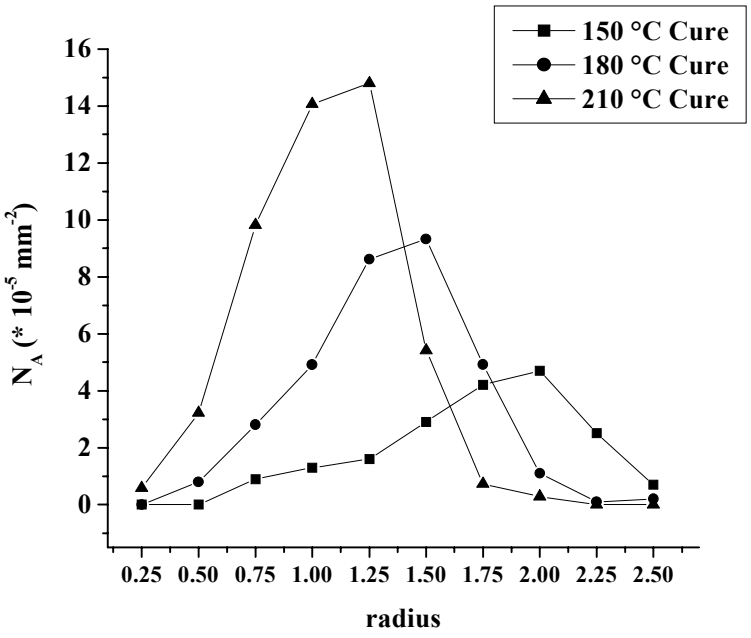

Figure 4-17. Two dimensional distribution of particle size for three different cure temperatures.

To generate a three dimensional representation of the particle size distribution, the method of Saltykov was employed. (97) This operation has been implemented using a computer mathematics package (Mathematica 3.0, Wolfram Research) to execute this

operation. A resulting histogram of three dimensional particle size distribution data is shown in Figure 4-18.

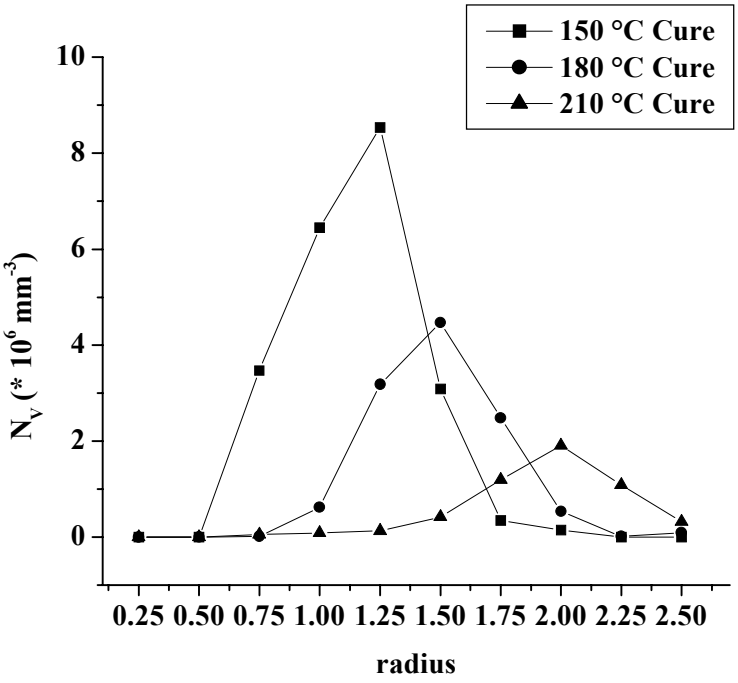

Figure 4-18. Histogram of transformed three dimensional particle size distribution data.

From Figure 4-18, it is clear that there is a significant difference in particle size between cure temperatures. This is in contrast to a relatively small difference in particle size produced in a representative rubber-toughened epoxy system. This difference arises, as discussed by Kwon (98) and by Williams (99), due to the similar activation energy of reaction and viscosity for the epoxy system, in contrast to the different activation energies for the cyanate system discussed here. Additionally, the shoulder on the two dimensional particle size distribution data disappears when transformed into a three dimensional distribution. This emphasizes one of the advantages of making interpretations using the

transformation, that a more representative distribution of 3-D particle sizes may be obtained. In this case, sections of particles not occurring at the equator which formed the small diameter shoulder are more properly depicted as a monomodal distribution of particle sizes. Further morphological characteristics of this system are shown in Table 4-1, including the average radius, the volume average radius, the volume fraction, surface density and mean free distance as well as number density of particles.

	150 °C	180 °C	210 °C
average radius	2.24	1.67	1.23
$<R_V>$	2.12	1.61	1.24
V_f	0.172	0.169	0.159
S_V	0.25	0.32	0.38
mean free distance	13.57	10.22	8.92
total N_V (mm^{-3})	4.19×10^6	9.79×10^6	1.99×10^7

Table 4-1. Morphological characteristics of the system considered as a function of cure temperature.

4.3.3 Williams Model Results

4.3.3.1 Phase Diagram as a function of conversion

Using the equations developed for mixing thermodynamics as a function of conversion (such as equation (4-83), and the system parameters obtained as just described, phase diagrams were calculated for the BADCy/HTBN system using the Flory-Huggins interaction parameter determined previously. This was accomplished using a computer program (Mathematica, Wolfram Research) and the resultant phase diagrams are shown in Figure 4-19.

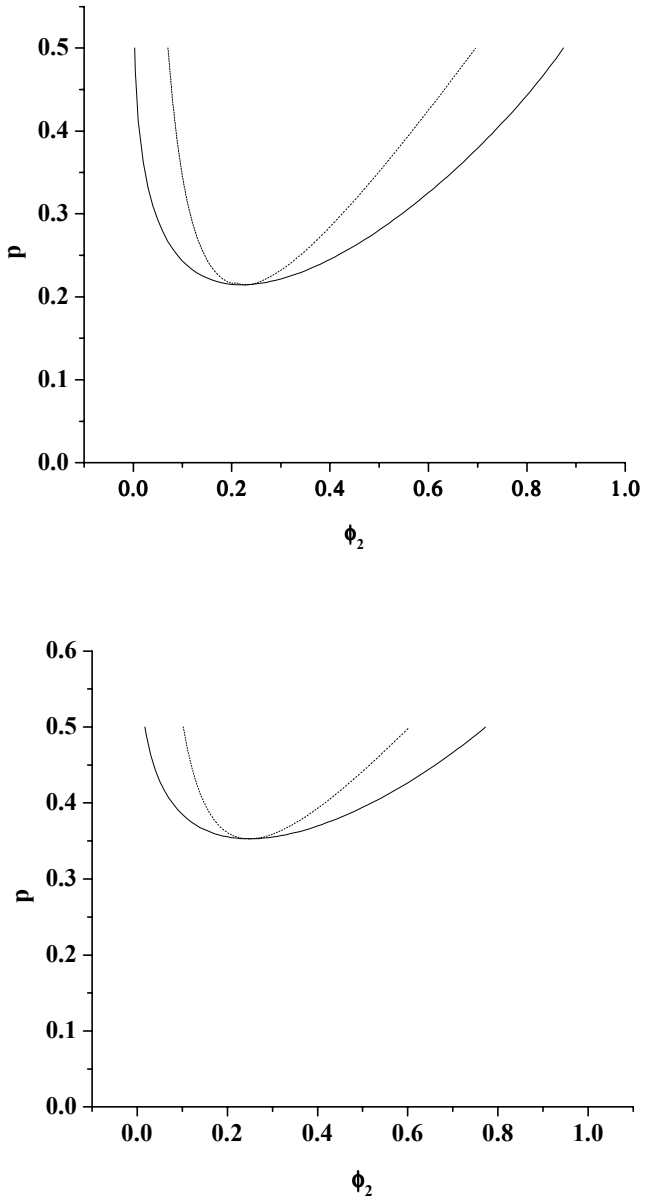

Figure 4-19. Phase diagrams as a function of degree of conversion (p) for the BADCy/HTBN system. The cure temperatures are 150 °C (top) and 210 °C (bottom). The continuous line is the binodal line, and the dashed line is the spinodal line.

Several features of the phase diagrams in Figure 4-19 are significant. Practically, this indicates that at higher cure temperature, there exists the potential for a higher concentration of the rubber toughener to remain dissolved in the continuous phase. There are two different shifts that are important in producing this result. The first is the shifting

of the critical point (and the entire phase diagram as well) to a higher ϕ_2 value at higher temperatures. The critical point is at a ϕ_2 of 0.222 at 150 °C, and at 0.249 at 210 °C. This means that the equilibrium line that determines the composition of the phases will indicate a cyanate-rich phase that contains more HTBN. In addition, the critical point and phase diagram are shifted to higher conversions at higher temperatures. This also suggests higher concentrations of toughener dissolved in the cyanate-rich phase, because at the gel point, the phase separation process is effectively halted. Because of the curvature of the phase diagram, this shift upwards in conversion means that the gel point intersects the equilibrium line closer to the critical point, where the composition of the continuous phase is richer in the HTBN component. At 150 °C, the critical conversion p is 0.214, and at 210 °C is 0.353. Taken together, at the gel point, these effects produce a binodal line that defines the composition of the continuous phase (left branch of the curve) to be 0.259 percent HTBN for a 150 °C isothermal cure, and 1.71 percent HTBN for a 210 °C isothermal cure, assuming the phases are at thermodynamic equilibrium. We note that given these compositions and this system, a difference in T_g for the continuous phase of approximately 13 °C would exist (using the Fox equation (100)) for the different cure temperatures.

A set of experiments was conducted to compare the experimental cloud point as a function of conversion to the predicted cloud point. These measured cloud points superimposed upon the calculated phase diagram is shown in Figure 4-20. A reasonable agreement is seen to be obtained.

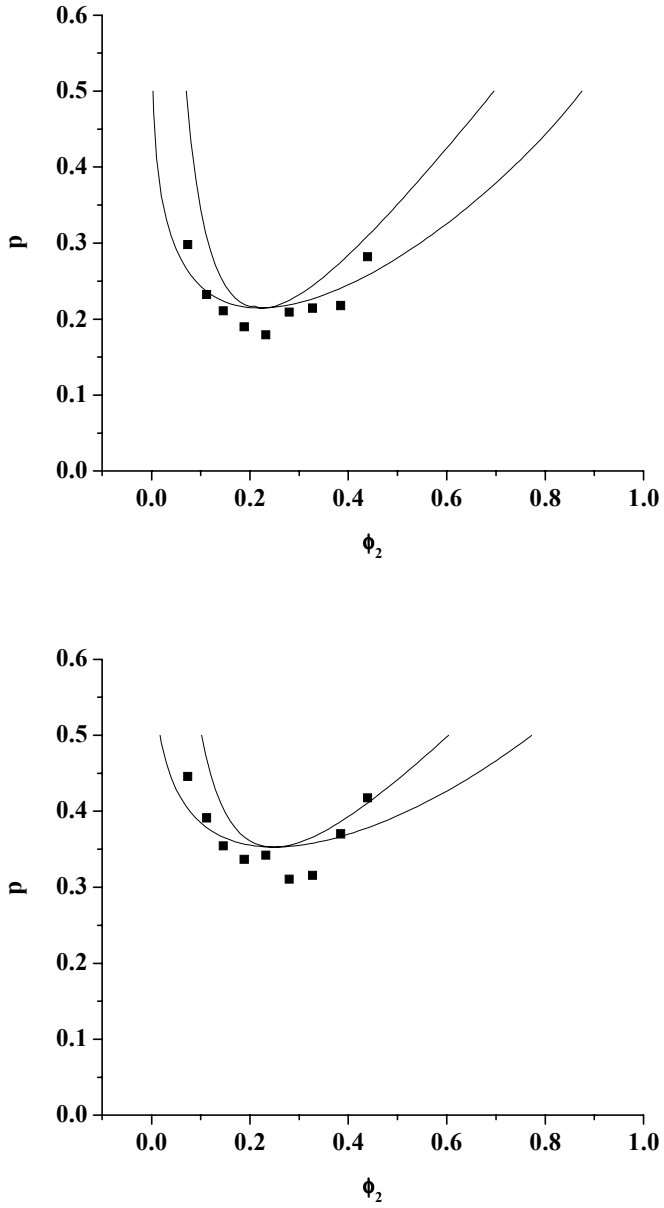

Figure 4-20. Experimental cloud point curves during cure versus thermodynamic prediction for 150 °C cure (top) and 210 °C cure (bottom).

4.3.3.2 Particle Size Distribution Prediction

The Williams model must be adapted to the experimentally determined particle size distribution through adjustment of the parameter F_0' in equation 4-95. For this purpose, three cure temperatures were explored in this section, and these were the

outermost cure temperatures (150 °C and 210 °C) together with an intermediate temperature (180 °C). The F_0' value was adjusted to generate the best fit of the particle size distribution at the intermediate temperature. This value of the adjustable parameter was then held constant as the temperature was varied to the cure temperature extremes. Comparison of predicted versus experimentally determined particle size distributions is shown in Figure 4-21. Here, reasonable agreement between experiment and theory is shown, suggesting that the proper factors are included in the model for this system and that the magnitude of the various parameters determined for the BADCy/HTBN system is correct. With the use of the 180 °C data to 'calibrate' the model, the predictions for the 150 °C and 210 °C cures were very reasonable, confirming the validity of the overall approach.

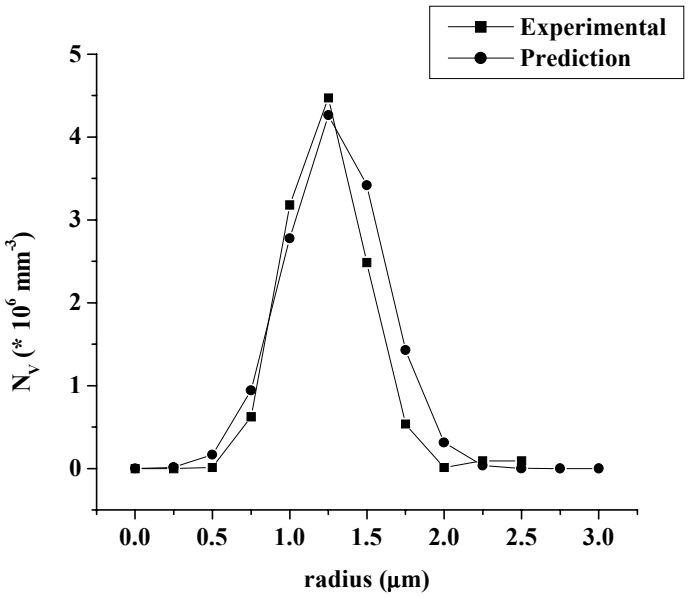

Figure 4-21. Experimentally determined and model predicted particle size distribution for 180 °C cure.

With F_0' determined for the intermediate cure temperature of 180 °C, the cure temperature of the model was changed, and the particle size distribution predicted for the

two extremes of cure temperature, 150 °C and 210 °C. These modeled particle size distributions are shown in Figure 4-22. A significant variation of average particle size is shown as cure temperature is varied between the extremes.

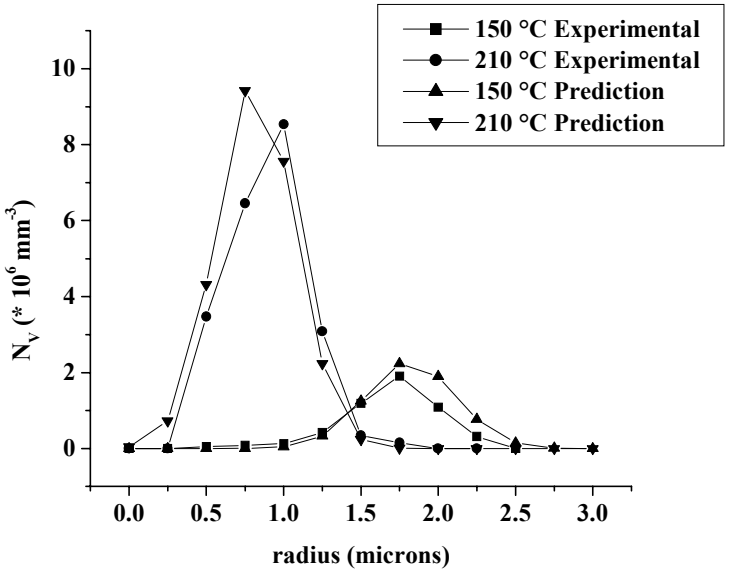

Figure 4-22. Experimental particle size distributions compared to model predictions for samples cured at 150 °C and 210 °C.

The phase separation model presented in this thesis successfully predicts the particle size distribution during cure with the only variation of input parameters being the temperature of the cure. Because (as extensively discussed in the prior text) fracture properties of many systems depend on the specific morphology that is developed, this present modeling of particle size distribution is important for an understanding of the final properties of a given thermosetting system. Moreover, through the use of particle size distributions and the measurement of model parameters for prediction of these distributions, other useful conclusions about system properties may be made as are now presented.

4.3.3.3 Phase Composition Predictions

While much of the focus for toughened thermosetting polymers has been directed at making improvements in fracture properties through the addition of a toughener-rich phase, there are other performance features which can also vary as cure temperature is changed. Interestingly, as discussed in Chapter 3, no significant variation in toughness of the cyanate ester/HTBN system has been found as the cure temperature was varied over the range of interest in spite of the marked effect on particle size distribution.

One additional effect of the change in cure temperature is modification of the glass transition temperature of the continuous phase. The T_g was shown in the previous chapter to vary with cure temperature. To explain this, examine the evolution of phase composition as predicted with the Williams model, shown in Figure 4-23 superimposed upon the phase diagram.

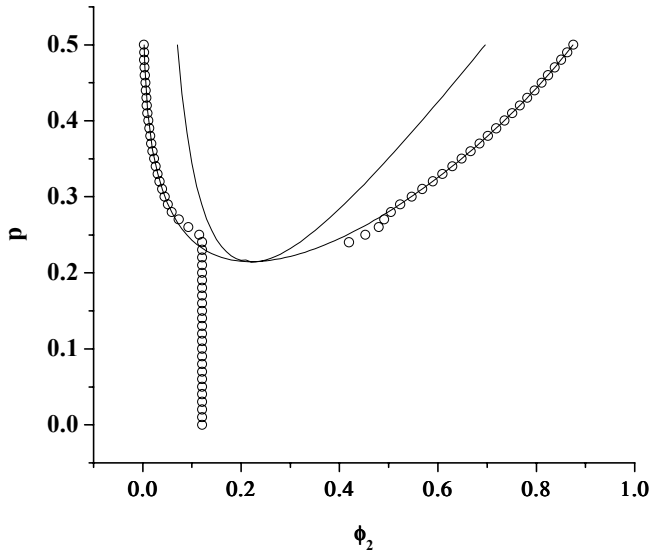

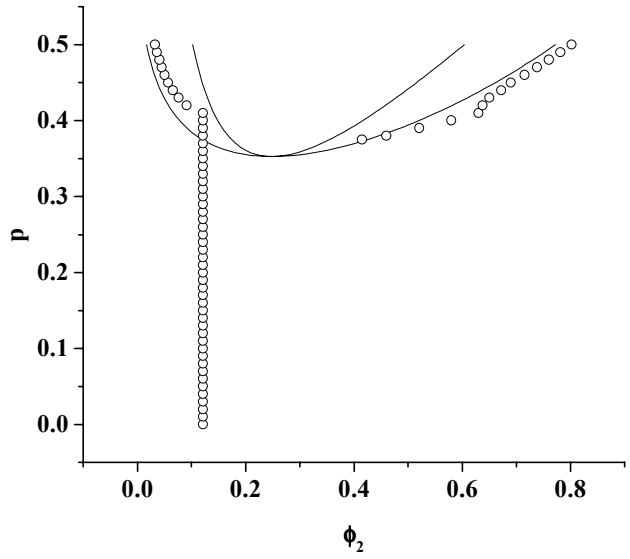

Figure 4-23. Evolution of phase composition for the BADCy/HTBN system as a function of degree of cure. Top, 150 °C cure, bottom, 210 °C cure.

To interpret Figure 4-23, note that each system starts as a single phase with a rubber composition ϕ_2=0.12 and as cure progresses (the vertical circles), eventually encounters the equilibrium line and passes into the metastable region between the spinodal and bimodal (solid) lines, where phase separation may take place. As the mixture begins to phase separate, the composition of the individual phases begins to approach the equilibrium prediction given by an appropriate horizontal tie line. However, as cure continues, the extent to which the curing sample follows the equilibrium prediction is dependent upon the rate of phase separation relative to the rate of cure as well as specific characteristics of the system like the viscosity. At low temperatures, there is adequate time for phase separation to occur, so that the phase compositions in this case are very close to those predicted for equilibrium. However, at high rates of phase separation, such as for the cure at 210 °C, the rate of phase separation cannot keep up with the rate of cure, and the actual phase composition deviates from the

equilibrium limit. For some curing systems, e.g. bisphenol-A epoxy and BN rubber toughener (101), at high cure rates little or no phase separation may occur. However, in the case of the BADCy system considered here, for practical cure temperatures, the second phase will appear. The difference in these two example systems resides in the initial viscosity, which affects the diffusion rate, which in turn controls the phase separation rate. Because the cyanate ester is of such low initial viscosity, diffusion occurs relatively quickly, allowing some phase separation to occur and produce phase compositions close to equilibrium regardless of cure temperature. This phenomenon is also responsible for the continual increase in number of particles per unit volume with cure temperature increases for the BADCy system. In contrast, with epoxies at high cure temperatures where there is incomplete phase separation, the number density of particles can go through a maximum with cure temperature since some of the toughener can remain in the continuous phase.

Miscibility of the toughener in the monomer also plays a key role in the phase morphology. When phase separation occurs relatively early in the cure process, it matures rather completely, even allowing coalescence to occur. A manifestation of these circumstances is observable in some results shown in Chapter 3 where at high volume fractions of rubber toughener and certain cure conditions, gross macrophase separation was observed. In that case, phase separation occurs at lower cure conversions, and sufficient time (plus rapid diffusion) elapses between the start of phase separation for coalescence to take place producing the gross macrophase separation seen in the micrographs.

The volume fraction concentrations of toughener at the gel point predicted by the modified Williams model for the 150 °C cure condition are 0.0026 for the continuous phase, and 0.876 for the disperse phase. For the 210 °C cure temperature, the corresponding predicted phase compositions are 0.033 for the continuous phase and 0.802 for the disperse phase. In Chapter 5, measurements of the glass transition temperature at these different cure temperatures will be described and compared with numbers that are calculated using these compositions. Then the implications for mechanical properties will be examined based on the T_g effects.

4.4 Conclusions

In this chapter, a thermodynamic plus kinetic model for predicting the effects of various cure temperatures on a thermosetting HTBN/cyanate ester resin was developed from Williams' initial treatment. Experiments to determine the various parameters necessary for the model were performed. The necessary data included the kinetics of the reaction, various rheological parameters, estimation of surface free energy, measurement and calculation of the χ interaction parameter, and particle size distribution determinations.

Though many assumptions and simplifications were made in this and the original derivation of the model, a major refinement coming from the present thesis was use of the three dimensional particle size distributions for comparison and fitting the output of the model. The quite reasonable agreement of the generated model with the actual particle size distribution also indirectly justifies the required assumptions and the overall choice of this model as well as the choice of data from an intermediate cure temperature to fix one required parameter. Then, with changes of only the cure temperature, good

prediction of the particle size distributions were obtained. This strongly suggest that this model can indeed more generally succeed for systems other than epoxy-rubber, as in our application to cyanate ester/HTBN. One reason for the successful adaptation of the Williams model was that the cyanate ester-based system also more closely represents the binary mixture assumption used in the model derivation due to the single-component nature of the cyanate ester and the monodispersity of the uncured monomer.

Summarizing the best features of the model, while predicting the particle size distribution, phase composition information was simultaneously produced as a function of conversion. The lower cure temperature phase compositions at and beyond the gel point were accurately predicted to be very close to those expected for thermodynamic equilibrium. The higher cure temperature concentrations were found to vary somewhat from equilibrium values, though the low viscosity of the cyanate (relative to epoxy systems) allows sufficient diffusion to stay close to equilibrium, and the use of equilibrium calculations for phase composition is likely to provide relatively good predictions of phase composition in this case. From all of these considerations, a higher concentration of low T_g toughener remains mixed in the continuous phase after cure at high cure temperatures. The consequences on mechanical response of this higher concentration, which lower the continuous phase T_g, will be more thoroughly examined in Chapter 5.

4.5 References

(1) P. J. Flory, Journal of Chemical Physics, 9, (1941), p. 660.
(2) P. J. Flory, Journal of Chemical Physics, 10, (1942), p. 51.
(3) M. L. Huggins, Journal of Physical Chemistry, 46, (1942), p. 151.
(4) M. L. Huggins, Journal of the American Chemical Society, 64, (1942), p. 1712.
(5) M. L. Huggins, Journal of the American Chemical Society, 64, (1942), p. 2716.

(6) R. Horst, Macromol. Theory Simul., 5, (1996), p. 789.
(7) R. Horst and B. A. Wolf, Macromol. Theory Simul., 5, (1996), p. 81.
(8) R. Horst and B. A. Wolf, Macromolecular Symposia, 112, (1996), p. 39.
(9) R. J. J. Williams, J. Borrajo, H. Adabbo, and A. J. Rojas. A Model for Phase Separation During a Thermoset Polymerization, in Rubber-Modified Thermoset Resins, C. K. Riew and J. K. Gillham, Eds., American Chemical Society Advances in Chemistry Series 208, Washington, D.C., (1984), p. 195.
(10) D. Verchere, H. Sautereau, J. P. Pascault, S. M. Moschiar, C. C. Riccard, and R. J. J. Williams, Rubber Modified Epoxies: Analysis of the Phase-Separation Process, in Toughened Plastics I: Science and Engineering, C. K. Riew and A. J. Kinloch, eds., ACS Advances in Chemistry Series 233, Washington, D. C., (1993), p. 335.
(11) W. H. Stockmayer, Journal of Chemical Physics, 17, (1949), p. 588.
(12) A. R. Shultz and P. J. Flory, Journal of the American Chemical Society, 74, (1952), p. 4760.
(13) R. Koningsveld, L. A. Kleintgens and A. R. Shultz. Journal of Polymer Science, Part A-2, 8, (1970), p. 1261.
(14) G. Rehage, D. Moller, and O. Ernst. Makromolecular Chemie, 38, (1965), p. 232.
(15) K. Solc, Macromolecules, 3, (1970), p. 665.
(16) K. Kamide and Y. Miyazaki, Polymer Journal, 13, (1981), p. 13.
(17) K. Kamide, T. Abe and Y. Miyazaki. Polymer Journal, 14, (1982), p. 355.
(18) K. Kamide, S. Matsuda, T. Dobashi and M. Kaneko. Polymer Journal, 16, (1984), p. 839.
(19) K. Kamide, S. Matsuda, and H. Shirataki, European Polymer Journal, 26, (1990), p. 379.
(20) N. Schuld and B. A. Wolf, Polymer-Solvent Interaction Parameters, in CRC Handbook of Solubility Parameters and Other Cohesion Parameters, CRC Press, A. F. M. Barton, Ed., (1991).
(21) D.R. Lloyd, H.P. Schreiber and T.C. Ward (Ed.), Inverse Gas Chromatography, ACS Symposium Series No. 391, American Chemical Society, Washington, D.C. (1989).
(22) K. S. Siow, G. Delmas, and D. Patterson. Macromolecules, 5, (1972), p. 29.
(23) S. J. Mumby, C. Qian, and B. E. Eichinger. Polymer, 33, (1992), p. 5105.
(24) J. Bergman, H. Kehlen, M. T. Ratzsch. Journal of Physical Chemistry, 91, (1987), p. 6567.
(25) K. Solc and R. Koningsveld, Journal of Physical Chemistry, 89, (1985), p. 2237.
(26) B. Riedl, and R. E. Prud'homme. Polymer Engineering and Science, 24, (1984), p. 1291.
(27) C. Qian, S. J. Mumby and B. E. Eichinger, Macrmolecules, 24, (1991), p. 1655.
(28) S. J. Mumby and P. Sher, Macromolecules, 27, (1994), p. 689.
(29) R. J. J. Williams, J. Borrajo, H. Adabbo, and A. J. Rojas. A Model for Phase Separation During a Thermoset Polymerization, in Rubber-Modified Thermoset Resins, C. K. Riew and J. K. Gillham, Eds., American Chemical Society Advances in Chemistry Series 208, Washington, D.C., (1984), p. 195.
(30) L. T. Manzione, J. K. Gillham and C. K. McPherson. Journal of Applied Polymer Science, 26, (1981), p. 889.
(31) J. Borrajo, C. C. Riccardi, R. J. J. Williams, Z. Q. Cao and J. P. Pascault.

Polymer, 36, (1995), p. 3541.
(32) C. C. Riccard, J. Borrajo, R. J. J. Williams, E. Girard-Reydet, and H. Sautereau. Journal of Polymer Science: Part B: Polymer Physics, 34, (1996), p. 349.
(33) D. Chen, J. P. Pascault, R. J. Bertsch, R. S. Drake, and A. R. Siebert. Journal of Applied Polymer Science, 51, (1994), p. 1959.
(34) A. F. M. Barton, in CRC Handbook of Solubility Parameters and Other Cohesion Parameters, CRC Press, A. F. M. Barton, Ed., (1991).
(35) S. A. Srinivasan, Ph. D. dissertation, Virginia Tech, 1993.
(36) J. Borrajo, C. C. Riccardi, R. J. J. Williams, Z. Q. Cao and J. P. Pascault. Polymer, 36, (1995), p. 3541.
(37) A. M. Gupta, Macromolecules, 24, (1991), p. 3459.
(38) L. J. Kasehagen and C. W. Macosko, Polymer International**,** 44, (1997), p. 237.
(39) M. Bauer, J. Bauer, and G. Kuhn. Acta Polymerica, 37, (1986), p. 218.
(40) S. L. Simon and J. K. Gillham. Proceedings of the American Chemical Society, Polymer Materials Science and Engineering, 32, (1991), p. 182.
(41) M. Bauer, J. Bauer, and G. Kuhn. Acta Polymerica, 37, (1986), p. 218.
(42) S. L. Simon and J. K. Gillham. Proceedings of the American Chemical Society, Polymer Materials Science and Engineering, 32, (1991), p. 182.
(43) S. L. Simon and J. K. Gillham. Proceedings of the American Chemical Society, Polymer Materials Science and Engineering, 66, (1992), p. 453.
(44) M. Bauer, J. Bauer, and G. Kuhn. Acta Polymerica, 37, (1986), p. 218.
(45) M. Bauer, J. Bauer, and B. Garske. Acta Polymerica, 37, (1986), p. 604.
(46) M. Bauer, J. Bauer, and B. Garske. Acta Polymerica, 37, (1986), p. 604.
(47) Y. P. Kanna R. Kumar and S. Das, Polymer Engineering and Science, 30, (1990), p. 1171.
(48) A. Osei-Owusu, G. Martin, and J. T. Gotro, Polymer Engineering and Science, 31, (1991), p. 1604.
(49) O. Georjon, J. Galy, and J. P. Pascault. Journal of Applied Polymer Science, 49, (1993), p. 1441.
(50) ASTM method E698.
(51) M. Bauer, J. Bauer, and G. Kuhn. Acta Polymerica, 37, (1986), p. 218.
(52) A. M. Gupta and C. W. Macosko, Macromolecules, 26, (1993), p. 2455.
(53) J. M. Brown, S. Srinivasan, A. Rau, T. C. Ward, J. E. McGrath, A. C. Loos, D. Hood, and D. E. Kranbeuhl. Polymer, 37, (1996), p. 1691.
(54) G. Antonoff, Journal of Physical Chemistry, 46, (1942), p. 497.
(55) L. A. Girifalco and R. J. Good, Journal of Physical Chemistry, 61, (1957), p. 904.
(56) D. Chen and J. P. Pascault, Makromolecular Chemie, 192, (1991), p. 867.
(57) J. E. Sohn, J. A. Emerson, A. Thompson, and J. T. Koberstein, Journal of Applied Polymer Science, 37, (1989), p. 2627.
(58) E. Helfhand and Y. Tagami, Journal of Chemical Physics, 56, (1972), p. 3592.
(59) E. Scheil, Z. Metallk., 27, (1935), p. 199.
(60) S. A. Saltykov, Stereometric Metallography, 2nd Ed., Moscow, 1958.
(61) L. M. Cruz-Orive, Journal of Microscopy, 112, (1978), p. 153.
(62) E. Scheil, Z. Metallk., 27, (1935), p. 199.
(63) S. A. Saltykov, Stereometric Metallography, 2nd edition, Metallurgizdat: Moscow, 1958.

(64) L. M. Cruz-Orive, Journal of Microscopy, 112, (1978), p. 153.
(65) Ojin Kwon, Ph. D. Dissertation, Virginia Tech, 1998.
(66) O. Kwon and T. C. Ward. Computational and Theoretical Polymer Science, 8, (1998), p. 297.
(67) R. J. J. Williams, J. Borrajo, H. Adabbo, and A. J. Rojas. A Model for Phase Separation During a Thermoset Polymerization, in Rubber-Modified Thermoset Resins, C. K. Riew and J. K. Gillham, Eds., American Chemical Society Advances in Chemistry Series 208, Washington, D.C., (1984), p. 195.
(68) P. J. Flory, Journal of the American Chemical Society, 63, (1941), p. 3083.
(69) W. H. Stockmayer, J. Chem. Phys. 11, (1943), p. 45.
(70) C. W. Macosko and D. R. Miller, Macromolecules, 9, No. 2, (1976) p. 199.
(71) W. H. Stockmayer, Journal of Chemical Physics, 11, (1943), p. 45.
(72) A. Vasquez, A. J. Rojas, H. E. Adabbo, J. Borrajo, and R. J. J. Williams, Polymer, 28 (1987), p. 1161.
(73) Ojin Kwon, Ph. D. Dissertation, Virginia Tech, 1998.
(74) A. M. Gupta, Macromolecules, 24, (1991), p. 3459.
(75) M. Bauer, J. Bauer, and B. Garske, Acta Polymerica, 37, (1986), p. 604.
(76) M. Bauer, J. Bauer and G. Kuhn, Acta Polymerica, 37, (1986), p. 715.
(77) M. Bauer and J. Bauer, Aspects of the kinetics, modelling and simulation of network build-up during cyanate ester cure, in Chemistry and Technology of Cyanate Ester Resins, Ian Hamerton, Ed., Blackie Academic and Professional, London, (1994), p. 67.
(78) M. Bauer, J. Bauer and G. Kuhn. Acta Polymerica, 37, (1986), p. 715.
(79) M. Bauer, J. Bauer and B. Garske. Acta Polymerica, 37, (1986), p. 604.
(80) M. Bauer, J. Bauer and G. Kuhn. Acta Polymerica, 37, (1986), p. 715.
(81) L. T. Manzione, J. K. Gillham, and C. A. McPherson. Journal of Applied Polymer Science, 26, (1981), p. 889
(82) R. J. J. Williams, J. Borrajo, H. Adabbo, and A. J. Rojas. A Model for Phase Separation During a Thermoset Polymerization, in Rubber-Modified Thermoset Resins, C. K. Riew and J. K. Gillham, Eds., American Chemical Society Advances in Chemistry Series 208, Washington, D.C., (1984), p. 195.
(83) J. Borrajo, C. C. Riccard, R. J. J. Williams, Z. Q. Cao, and J. P. Pascault, Polymer, 36, (1995), p. 3541.
(84) A. W. Snow and J. P. Armistead, Journal of Applied Polymer Science, 52, (1994), p. 401.
(85) D. Verchere, H. Sautereau, J. P. Pascault, S. M. Moschiar, C. C. Riccardi, and R. J. J. Williams, Polymer, 30 (1989), p. 107.
(86) A. R. Schultz and P. J. Flory, Journal of the American Chemical Society, 74, (1952), p. 4760.
(87) D. Verchere, H. Sautereau, J. P. Pascault, S. M. Moschiar, C. C. Riccard, and R. J. J. Williams, Rubber Modified Epoxies: Analysis of the Phase-Separation Process, in Toughened Plastics I: Science and Engineering, C. K. Riew and A. J. Kinloch, eds., ACS Advances in Chemistry Series 233, Washington, D. C., (1993), p. 335.
(88) A. R. Shultz and P. J. Flory, Journal of the American Chemical Society, 74, (1952), p. 4760.
(89) H. M. Schoffeleers, L. A. Kleintjens, and R. Koningsveld, Pure and Applied

Chemistry, 39, (1974), p. 1.
(90) D. Verchere, H. Sautereau, J. P. Pascault, S. M. Moschiar, C. C. Riccardi, and R. J. J. Williams, Polymer, 30 (1989), p. 107.
(91) S. Wu. Journal of Polymer Science C, 34, (1971), p. 19.
(92) S. A. Srinivasan, Ph. D. dissertation, Virginia Tech, 1993.
(93) J. H. Hildebrand and R. L. Scott. The Solubility of Non-Electrolytes. Van Nostrand, Princeton, N. J., (1950).
(94) R. J. J. Williams, J. Borrajo, H. Adabbo, and A. J. Rojas. A Model for Phase Separation During a Thermoset Polymerization, in Rubber-Modified Thermoset Resins, C. K. Riew and J. K. Gillham, Eds., American Chemical Society Advances in Chemistry Series 208, Washington, D.C., (1984), p. 195.
(95) D. Chen, J. P. Pascault, and D. Sage, Makromolecular Chemie, 192, (1991), p. 867.
(96) J. E. Sohn, J. A. Emerson, and J. T. Koberstein. Journal of Applied Polymer Science, 37, (1989), p. 2627.
(97) S. A. Saltykov, Stereometric Metallography, 2nd edition, Matallurgizdat: Moscow, 1958.
(98) Ojin Kwon, Ph. D. Dissertation, Virginia Tech, 1998.
(99) R. J. J. Williams, J. Borrajo, H. Adabbo, and A. J. Rojas. A Model for Phase Sparation During a Thermoset Polymerization, in Rubber-Modified Thermoset Resins, C. K. Riew and J. K. Gillham, Eds., American Chemical Society Advances in Chemistry Series 208, Washington, D.C., (1984), p. 195.
(100) T. G. Fox, Bulletin of the American Physical Society, 1, (1956), p. 123.
(101) Ojin Kwon, Ph. D. Dissertation, Virginia Tech, 1998.

Chapter 5: Viscoelastic Characteristics of Neat and Toughened Cyanate Ester Networks using Single-Temperature and Gradient Cure Profiles

5.1 Introduction

Many techniques have been applied to the study of relaxation phenomena in polymer blends. Among the most common and notable are dynamic mechanical analysis (DMA), dielectric spectroscopy (DES), and nuclear magnetic resonance, although there are other techniques of merit. DMA and DES have been used to measure the glass transition temperatures of blends as well as examine the distribution of relaxation times. Both of these methods have been used to characterize the degree of concentration fluctuations in polymer blends and the intermolecular interaction and coupling. (1) DES has often been employed for to its ability to conveniently measure the relaxations (dispersions) over a very large range of frequencies, typically from 10^{-5} to 10^{5} Hz or more, depending on the type of equipment. DMA is usually limited to about decades of frequency sweep, from about 10^{-2} to 10^{2} Hz, though some ultrasonic equipment has been employed at higher frequencies. (2, 3) The use of NMR to monitor relaxation phenomena in blends has also been extensively applied. Where isotopically labelled polymers are available, two-dimensional solid state NMR can yield information on one component. (4,5) Monitoring of both components independently and simultaneously has been accomplished through the use of magic angle spinning techniques as well as measurement of NMR line broadening.

There are important differences between the various approaches to characterization of the relaxation properties of polymer blends. DMA probes cooperative motions that

involve a relatively large number of bonds. DES is more sensitive to local segmental motions that may involve only a few bonds, i.e., a smaller relxation volume is examined compared to DMA. (6) The use of DMA and DES together can often provide valuable complementary information not available by either method alone.

5.2 Literature Review

5.2.1 Dynamic Mechanical Analysis

A common technique for characterizing the time and temperature dependent mechanical properties of materials is dynamic mechanical analysis. In an instrument's oven a specimen is subjected to a continually varying periodically modulated force. The outputs of this type of experiment are typically dynamic storage modulus, dynamic loss modulus, and mechanical damping, or tan delta.

In a typical experimental setup, the applied stress has a sinusoidal periodicity over time. The response of polymers depends upon the specific polymer as well as the frequency of the stress field as well as the test temperature. This viscoelastic behavior results in a measured strain response following the applied periodic stress. A consequence of the viscoelastic nature of these materials is that the resultant strain is out of phase with the applied stress by some phase angle δ. Using these ideas, methods for probing the molecular motion that underlies the bulk mechanical response have been developed. These will be considered later in this section.

Dyamic stress and strain (σ and ε, respectively) can be described as follows:

$$\sigma = \sigma_0 \sin(\omega t + \delta) \qquad \textbf{(5-1)}$$

and

$$\varepsilon = \varepsilon_0 \sin(\omega t) \qquad \textbf{(5-2)}$$

where ω is the frequency in radians per second. In this case, we can combine the in-phase ($\sigma_0 \cos\delta$) and out of phase ($\sigma_0 \sin\delta$) stress components together to form the total stress:

$$\sigma = \sigma_0 \sin(\omega t)\cos\delta + \sigma_0 \cos(\omega t)\sin\delta \qquad \textbf{(5-3)}$$

To obtain the modulus, the stress divided by the strain, we can define a storage modulus (E') and a loss modulus (E") which are the in-phase, or real, and 90° out of phase, or imaginary, components of the modulus, respectively.

$$\sigma = \varepsilon_0 E' \sin(\omega t) + \varepsilon_0 E'' \cos(\omega t) \qquad \textbf{(5-4)}$$

$$E' = \frac{\sigma_0}{\varepsilon_0}\cos\delta \qquad \textbf{(5-5)}$$

$$E'' = \frac{\sigma_0}{\varepsilon_0}\sin\delta \qquad \textbf{(5-6)}$$

$$\varepsilon = \varepsilon_0 \exp(i\omega t) \qquad \textbf{(5-7)}$$

$$\sigma = \sigma_0 \exp(\omega t + \delta)i \qquad \textbf{(5-8)}$$

The constituent parts of storage and loss modulus together form the complex modulus. The real component (E') can be considered to reflect the relative stiffness of the sample as it stores and release potential energy of deformation, while the imaginary component (E") is representative of stiffness associated with nonrecoverable strain energy. This loss modulus is sometimes considered to arise from "internal friction" of the material that dissipates energy, and together with the storage modulus reflect the various molecular motion processes (relaxations, transitions and dispersions) as well as any global or system changes on a larger scale, such as those associated with morphology or compositional variations.

5.2.2 Time-Temperature Superpositioning

It is often desirable to obtain information about the long-term behavior of polymeric materials, in many cases over time periods much longer than that available for testing. For viscoelastic materials, properties such as modulus are dependent on time at isothermal conditions. At isochronal conditions, the variation of temperature also affects the viscoelastic functions. The principle of time-temperature superpositioning (tTSP) combines the two independent variables, time and temperature, to describe properties over extended scales of time and temperature, including times and temperatures unavailable or untested. Using superposition ideas, the data desired (such as modulus at very long times) which normally might have to be measured directly are collected over a more experimentally practical time period, by varying temperatures. According to the principles of time-temperature superpositioning, the relationship between time and temperature allows extrapolation between the two.

The principles of time-temperature superpositioning have been well established for some time. (7) An example of this procedure on some typical test data, together with the final information generated, is shown in Figure 5-1. Using an unshifted isotherm at a reference temperature of 25 °C, other isotherms of modulus are shifted horizontally on the log time axis until they are smoothly intersected with the reference curve to form an exact superposition. This resultant curve, covering a much larger period of time, is called a master curve. While this construction clearly shows moduli over longer (and shorter) time periods than the original experimental data, the corresponding manipulation of the data to obtain information at other temperatures may not be immediately obvious. To obtain this further prediction, the number of log time units each isotherm is shifted to

match its neighbor is collected and place in a "shift factor plot", shown in the inset of Figure 5-1. Using this shift factor graph, the entire master curve may now be shifted to obtain the modulus at another temperature. The ordinate of the shift factor plot reveals the amount of shift required to reposition the master curve on the log time axis for a given new temperature chosen on the abscissa.

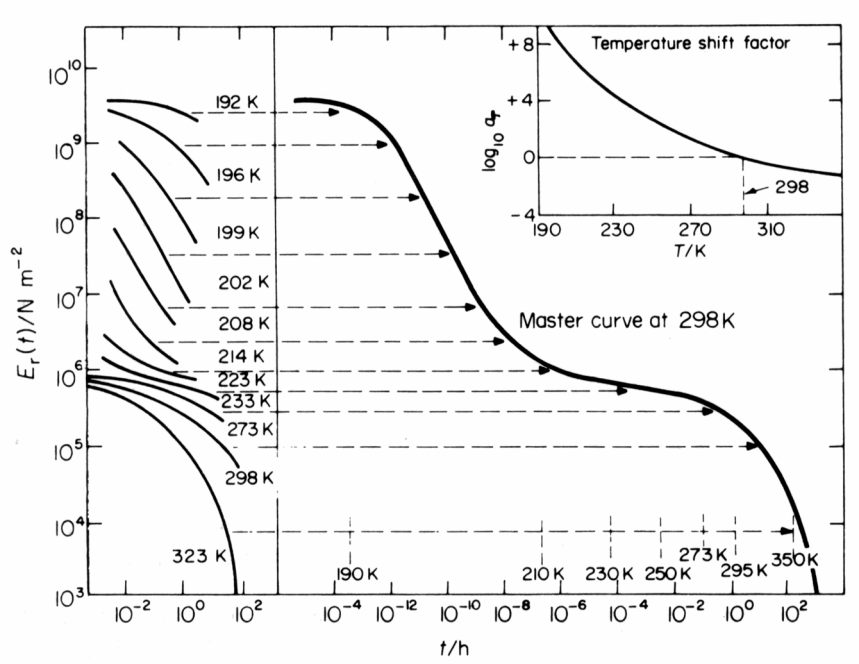

Figure 5-1. Time temperature superpositioning of modulus of polyisobutylene. (After J. M. G. Cowie, Polymers: Chemistry and Physics of Modern Materials, 2nd edition, 1993.)

Time temperature superpositioning of viscoelastic data is valid in many instances and its usefulness is obvious; however, it is important to consider where the application of this technique is not legitimate. Physical and chemical phenomena initiated by the temperature changes can change or even negate the time-temperature equivalency. Effects such as chemical degradation can in certain circumstances modify the measured properties in ways not predicted using time-temperature superpositioning. If successful, there should generally be a smooth, monotonic master curve and shift factor plot,

indicating that the mechanism of the relaxation is unchanged over this range of temperatures and times. The validity of time-temperature superpositioning has been addressed in detail (8), with the general guidelines that there be a reasonable amount of overlap between isotherms, and that the same shift factor should translate all of the viscoelastic functions (such as both storage and loss moduli). An even more thorough treatment of these guidelines, including a scaling method to predict applicability of time-temperature superpositioning, has been presented. (9)

The characteristic shape and form of the tTSP shift factor plot, as well as the comparisons between shift factor plots for different polymer systems, can be significant. For the case of polymers in the glass transition temperature range (specifically, between the reference temperature T_{ref} and T_{ref} + 100 °C), the amount of shift required to generate the master curve at a given displacement from T_{ref} may be described using the Williams-Landel-Ferry equation. (10) The WLF equation is

$$\log a_T = \frac{-C_1(T - T_g)}{C_2 + (T - T_g)} \qquad \textbf{(5-9)}$$

and describes the log a_T shift through the temperature range described previously, typically that of the transition region and beyond into the plateau and terminal regions. C_1 and C_2 are constants that were initially believed to be universal for all polymer systems, with values of C_1=17.44 and C_2=51.6, and these are still a good starting point for those systems although C_1 and C_2 are now known to vary. The origin of these constants is best explained by looking at the derivation of the WLF equation, which is based on the Doolittle relationship. (11) Beginning with definitions in liquids, the free

volume v_f is the difference between the occupied specific volume v_0 and the measured macroscopic or bulk specific volume v of the fluid:

$$v_f = v - v_0 \qquad \textbf{(5-10)}$$

In this approach, v_0 can be interpreted as the value of the measured specific volume extrapolated to absolute zero. This can be translated to the viscosity of liquids with the use of the following equation:

$$\eta = a \exp \frac{b}{f} \qquad \textbf{(5-11)}$$

where η is the viscosity, a and b are constants, and f is the fractional free volume, or v_f/v. If we now take the glass transition temperature as the reference temperature, the shift factor may be written as the ratio of the average relaxation times at the temperature of interest and at the glass transition temperature.

$$\log a_T = \log \frac{\tau(T)}{\tau(T_g)} \approx \log \frac{\eta(T)}{\eta(T_g)} = \frac{b}{2.303}\left(\frac{1}{f(T)} - \frac{1}{f(T_g)} \right) \qquad \textbf{(5-12)}$$

which, assuming the free volume increases linear with temperature yields:

$$f(T) = f(T_g) + \alpha_f (T - T_g) \qquad \textbf{(5-13)}$$

where α_f is the coefficient of thermal expansion. Then we obtain on substitution

$$\log a_T = -\frac{\left(\frac{b}{2.303 f(T_g)} \right)(T - T_g)}{\left(\frac{f(T_g)}{\alpha_f} \right) + (T - T_g)} \qquad \textbf{(5-14)}$$

which is equivalent to the WLF equation where the universal constants $C_1 = b/2.303f(T_g)$ and $C_2 = f(T_g)/\alpha_f$.

For relaxations other than that associated with the glass transition, or alpha dispersion, such as those at lower temperatures typical of the so-called beta relaxation, an Arrhenius relationship may better describe the time-temperature shift. This alternative equation is

$$\log a_T = \frac{-\Delta E}{2.303R}\left(\frac{1}{T} - \frac{1}{T_{ref}}\right) \quad \textbf{(5-15)}$$

where ΔE is an activation energy, R is the gas constant, T is the absolute temperature and T_{ref} is the reference temperature for the shifting process. The WLF equation is, in effect, able to describe an activation energy that varies through the transition region, where the Arrhenius equation describes an invariant activation energy. It is the varying activation energy characteristic of the glass transition that is of interest in describing relaxation phenomena in polymers.

Additional techniques have been developed using the concept of superpositioning, specifically the so-called "doubly reduced" master curves, which involve the shifting of property data with changes of multiple variables in addition to temperature. The same ideas apply as in time-temperature superpositioning, with the requirements that there be no change in the mechanism of the process over the raw data collection range. Applications of this type of methodology include investigations of the effect of temperature and humidity on the peel energy of silicone sealants. (12) Reduction of the curves by both temperature and humidity allowed the long-term behavior of the sealant to be predicted. In a comprehensive study of the diffusion of various penetrants on adhesive systems, Kwan (13) describes the use of a diffusion-time shift factor that may be used to predict the weight uptake and mechanical properties of that system. This is based upon

knowledge of the diffusion coefficient and the plasticizing effect of the introduced penetrant.

5.2.3 Distribution of Relaxation Times in Polymers

There have been many descriptions and models of the characteristically broad distribution of relaxation times found in polymeric materials. (See, for example, (14, 15)) For simple, low molecular weight liquids, a single relaxation time model adequately describes their behavior. For polymers, the very long-chain structure that gives them their unique and useful properties also results in a viscoelastic response that necessitates description by multiple overlapping relaxations, or a broad distribution of relaxation times. The development of this characterization has been summarized and will be briefly presented here as a review. (16)

An early mathematical treatment of the relaxation characteristics of low molecular weight materials was presented by Debye. (17) This treatment introduces a time decay function $\phi(t)$, described by the following exponential form:

$$\phi(t) = \exp\left(\frac{-t}{\tau}\right) \qquad \textbf{(5-16)}$$

where τ is the (singular) relaxation time. Using this function as the basis, various other functions may be derived to describe the relaxation behavior. Here, we examine the relationship classically used to describe dynamic experimental data, often obtained using dielectric spectroscopy:

$$\frac{\varepsilon^* - \varepsilon_\infty}{\varepsilon_s - \varepsilon_\infty} = \frac{1}{1 + i\omega t} \qquad \textbf{(5-17)}$$

where ω is the frequency, ε^* is the complex dielectric constant, ε_s is the fully relaxed dielectric constant and ε_∞ is the fully unrelaxed dielectric constant. Experimentally, the

fully unrelaxed dielectric constant may be obtained by measurement at very high frequencies or very low temperatures and the fully relaxed dielectric constant conversely may be determined using measurement at very low frequencies or very high temperatures. The denominator quantity (ε_s-ε_∞) on the left hand side of Equation 5-17 is the so-called "oscillator strength".

The use of mechanical relaxation spectroscopy techniques, often called dynamic mechanical analysis, is often experimentally convenient. In some cases, such as highly non-polar polymers, polymers with significant electrical conductivity, or awkward sample geometries, dielectric analysis is difficult or impossible. The previously presented Debye relationship for dynamic experiments may be rewritten with the mechanical terms substituted for their dielectric equivalents:

$$\frac{E^* - E_\infty}{E_s - E_\infty} = \frac{1}{1 + i\omega\tau} \qquad \textbf{(5-18)}$$

where E* is the complex Young's modulus and E_∞ is the Young's modulus at very high frequencies or low temperatures.

This model cannot accurately describe behavior typical of real polymers because the breadth of their relaxation time distribution requires more than a single relaxation time for adequate description. A modification to the having a single relaxation time offered above considers now a distribution which is to be a linear summation of single relaxation time decay functions as (18)

$$\phi(t) = \sum_i A(\tau_i) \exp^{\left(\frac{-t}{\tau_i}\right)} \qquad \textbf{(5-19)}$$

In this case, a term $A(\tau_i)$, which is a weighting factor, appears to quantify the importance of an individual relaxing element having a relaxation time τ_i. This expansion of the models can also be written in a form suitable for describing mechanical relaxations as

$$\frac{E^* - E_\infty}{E_s - E_\infty} = \frac{1}{1 + (i\omega\tau_0)^{1-\alpha}} \qquad \textbf{(5-20)}$$

with τ_0 being the central, or mean, relaxation time of the distribution. α is a parameter varying between 0 and 1, controlling the breadth of the distribution. When α=0, Equation 5-20 is equivalent to the Debye relationship given earlier. A key limitation of this approach is that though this relationship allows accommodation of a broadening of relaxation times about the central value, any asymmetry in the distribution cannot be described.

A common graphical representation of the relaxation process is called the Argand diagram, also referred to as the Cole-Cole diagram, which plots the imaginary component of the dielectric or dynamic mechanical test against the real component. This description presents a semicircular representation of the relaxation in the particular case of a single relaxation time.

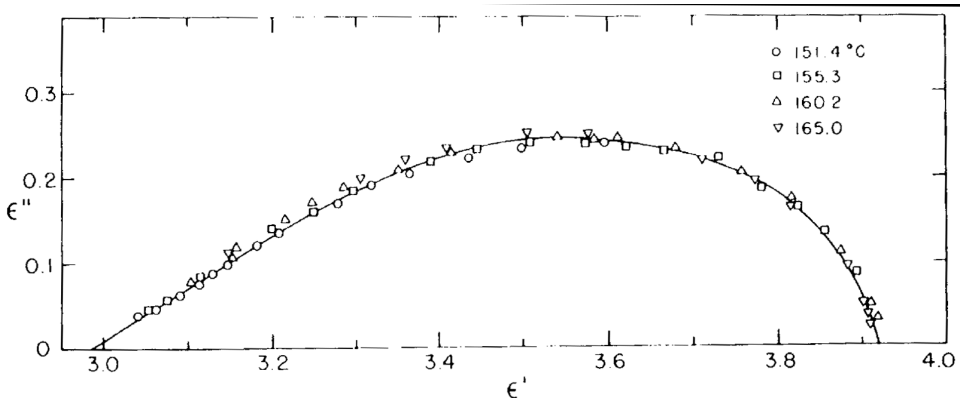

Figure 5-2. Argand (Cole-Cole) diagram for the relaxation of measured with dielectric spectroscopy. (after Aklonis and Macknight, Introduction to Polymer Viscoelasticity, Wiley and Sons, 1983.)

As the breadth of the distribution of relaxation times increases, the semicircle becomes increasingly flattened, as shown in Figure 5-2. An expression derived by Cole and Cole describes this case. In terms of mechanical parameters, this is given by:

$$\left[E' - \frac{E_s + E_\infty}{2}\right]^2 + \left[E'' + \frac{(E_s - E_\infty)}{2}\cot an\frac{(1-\alpha)\pi}{2}\right]^2 = \left[\frac{(E_s - E_\infty)}{2}\operatorname{cosec}\frac{(1-\alpha)\pi}{2}\right]^2$$

(5-21)

Using this expression as a basis, the following expressions may be derived and used to find experimental values for τ_0 and α:

$$\frac{E'(\omega) - E_\infty}{E_s - E_\infty} = \frac{1 + (\omega\tau_0)^{1-\alpha}\sin\left(\frac{\alpha\pi}{2}\right)}{1 + 2(\varpi\tau_0)^{1-\alpha}\sin\left(\frac{\alpha\pi}{2}\right) + (\omega\tau_0)^{2(1-\alpha)}} \quad \textbf{(5-22)}$$

and

$$\frac{E''(\omega)}{E_s - E_\infty} = \frac{(\omega\tau_0)^{1-\alpha}\cos\left(\frac{\alpha\pi}{2}\right)}{1 + 2(\omega\tau_0)^{1-\alpha}\sin\left(\frac{\alpha\pi}{2}\right) + (\omega\tau_0)^{2(1-\alpha)}} \quad \textbf{(5-23)}$$

While this approach represents an improvement upon the single relaxation time model, the behavior of polymers is better represented by models that can also take into account the broadening of loss curves with increasing frequency.

Such a model was proposed by Davidson and Cole to describe skew in the semicircular Argand diagram. The following equations result from these authors' work:

$$\frac{E^* - E_\infty}{E_s - E_\infty} = \frac{1}{(1 + i\omega\tau_0)^\gamma} \quad \textbf{(5-24)}$$

$$\frac{E'(\omega) - E_\infty}{E_s - E_\infty} = (\cos\phi)^\gamma \cos(\phi\gamma) \quad \textbf{(5-25)}$$

$$\frac{E''(\omega)}{E_s - E_\infty} = \cos(\phi)^\gamma \sin(\phi\gamma) \quad \textbf{(5-26)}$$

In these relationships, $\phi=\arctan(\omega\tau_0)$ and γ varies between 0 and 1 as a fitting parameter. In the limit of 1, this description is equivalent to the Debye description where there is a single relaxation time. This is equivalent to a regain of symmetry in the Argand diagram.

The next step towards a better description of the relaxation behavior of polymers is a merging of the Cole-Cole and Cole-Davidson approaches in which both the flattening and asymmetry of the Argand diagram may be accommodated. This treatment was developed by Havriliak and Negami (19) by combining both parameters α and γ while retaining their original meanings from the Cole-Cole and Cole-Davidson models.

$$\frac{E^* - E_\infty}{E_s - E_\infty} = \frac{1}{(1 + (i\omega\tau_0)^{1-\alpha})^\gamma} \quad \textbf{(5-27)}$$

The same relationships between the real and imaginary components of the modulus have been developed (20) for the Havriliak Negami (H-N) relationship as for the previous cases:

$$E'(\omega) - E_\infty = r^{-\frac{\gamma}{2}}(E_s - E_\infty)\cos(\theta\gamma) \quad \textbf{(5-28)}$$

and

$$E''(\omega) = r^{-\frac{\gamma}{2}}(E_s - E_\infty)\sin(\theta\gamma) \quad \textbf{(5-29)}$$

where $r = \left((1 + (\omega\tau_0)^{1-\alpha})\sin\left(\frac{\alpha\pi}{2}\right)\right)^2 + \left((\omega\tau_0)^{1-\alpha}\cos\left(\frac{\alpha\pi}{2}\right)\right)^2$ and

$$\theta = \arctan\left(\frac{(\omega\tau_0)^{1-\alpha}\cos\left(\frac{\alpha\pi}{2}\right)}{1 + (\omega\tau_0)^{1-\alpha}\sin\left(\frac{\alpha\pi}{2}\right)}\right)$$

The effect of variations of alpha and gamma on loss modulus can be seen in Figure 5-3 and Figure 5-4, respectively.

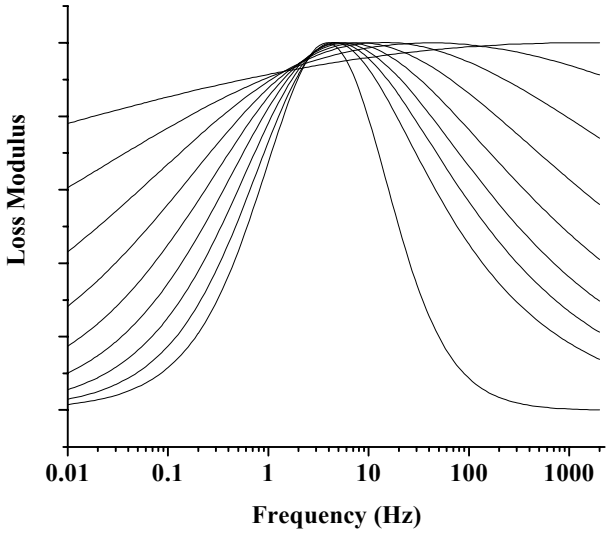

Figure 5-3. Variation of loss response as a function of varying H-N alpha parameter. Breadth of distribution increases with increasing value of α.

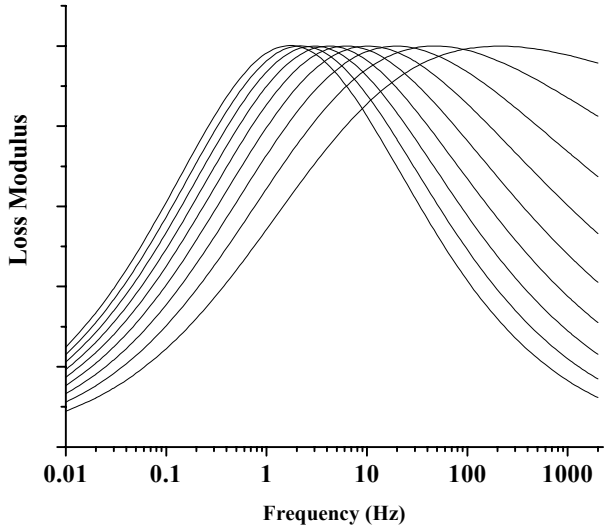

Figure 5-4. Variation of loss response as a function of varying H-N gamma parameter. Peak shift toward higher frequencies increases with increasing values of γ.

These relationships may be used to obtain values for the various parameters necessary to fit the observed relaxation behavior of polymers. It is also useful to return to

the time decay function to represent the relaxation distribution of the polymer system. This type of expression is difficult to derive from the Havriliak-Negami representation (21, 22), although through the use of a Fourier transform the following basic relationship may be presented (23):

$$\frac{E^* - E_\infty}{E_s - E_\infty} = \int_0^\infty \exp(-i\omega t)\left[\frac{d\Phi(t)}{dt}\right]dt \qquad \textbf{(5-30)}$$

The time and frequency domain portions of the above equation are then, respectively,

$$f(t) = -\frac{d\Phi(t)}{dt} \qquad \textbf{(5-31)}$$

and

$$g(\omega) = \frac{E'(\omega) - E_\infty}{E_s - E_\infty} \qquad \textbf{(5-32)}$$

The Fourier transformations of these functions are then

$$-\frac{d\Phi(t)}{dt} = \frac{2}{\pi}\int_0^\infty \left(\frac{E'(\omega) - E_\infty}{E_s - E_\infty}\right)\cos(\omega t)d\omega \qquad \textbf{(5-33)}$$

and

$$-\frac{d\Phi(t)}{dt} = \frac{2}{\pi}\int_0^\infty \left(\frac{E''(\omega)}{E_s - E_\infty}\right)\sin(\omega t)d\omega \qquad \textbf{(5-34)}$$

Integrating, we arrive at descriptions for the time decay function that may be obtained by inserting the frequency domain data as fitted by the Havriliak-Negami expression. These final equations are

$$\Phi(t) = \frac{2}{\pi}\int_0^\infty \left(\frac{E'(\omega) - E_\infty}{E_s - E_\infty}\right)\frac{\sin(\omega t)}{\omega}d\omega \qquad \textbf{(5-35)}$$

and

$$\Phi(t) = \frac{2}{\pi}\int_0^\infty \left(\frac{E''(\omega)}{E_s - E_\infty}\right)\frac{\sin(\omega t)}{\omega}d\omega \qquad \textbf{(5-36)}$$

The application of the Havriliak-Negami analysis (or one of several alternative descriptions of molecular relaxations, such as Cole-Cole, Cole-Davidson, or Kohlrausch-Williams-Watts) to experimental data has been well documented. (24) Recently, Snyder

and Mopsik (25) explored the fitting of restricted ranges of experimental data with these expressions. Their conclusions indicate that when using narrow ranges of frequency, it is difficult to obtain meaningful descriptions of a relaxation. Their observations become obvious when one of the purposes of the H-N description is considered: the description of the high frequency asymmetry of the glass transition process in polymeric materials. Typically, for mechanical or dielectric relaxation, data are collected over a restricted range of frequencies, due to limitations of the experimental apparatus. Because this relaxation usually is not centered in this frequency range at ambient temperature, the temperature is varied to locate the loss maximum within the frequencies measured. Especially in the case of mechanical measurements, the available frequencies are limited to about four decades of coverage. This does not allow the direct measurement of the relaxation from below the peak into the high frequency asymmetry domain. If this region is not sampled, there is obviously no way to reliably fit the data. One case specifically cited by these authors is that of a very broad relaxation, where the results are characterized as having "unrealistic parameters". In this case, for the segment of frequencies chosen, a good agreement was achieved even using a linear fit. Clearly, fitting of this type of relaxation data over small ranges of frequencies is ill-advised. In this case, little difference can be accurately discerned regardless of the fitting function chosen. Additional focus on this issue has been presented by Havriliak and Havriliak. (26)

5.2.4 Relaxation Phenomena in Multi-component Polymer Systems

The use of blends or solutions of polymeric materials to obtain adventitious combinations of properties has received much attention. Polymer blends are made to

combine some of the useful properties of the components for various improvements, such as cost or performance issues. While a large amount of work has been expended in understanding the thermodynamics of mixing of blends, less attention has been placed on the molecular relaxations of the resultant materials. It is these relaxation characteristics that determine useful properties such temperature resistance, ductility and impact resistance.

Studies of the relaxation characteristics of blends often are focused on the effects on the glass transition as a consequence of the constituent's miscibility. This is a result of the well-known change of the (single) glass transition temperature to a new point somewhere between the glass transition temperatures of the pure components if miscibility results. Immiscible systems show two distinct glass transitions, reflecting two phases. The glass transition temperatures of any distinct phase is a function of its composition. The appearance of a single glass transition in a polymer blend signifies that there is intimate mixing of the chains on a molecular level.

Much of the previous focus on the dynamics of polymer blends has centered on the apparent broadening of the glass transition resulting from miscibility. (27,28,29) These effects were first discussed in detail using an examination of blends of poly(2,6-dimethyl-1,4-phenylene oxide) and copolymers of sytrene and 4-chlorostyrene. Below 67 mole percent 4-chlorostyrene the blends were miscible. The glass transition as measured with DSC was shown to broaden with higher chlorostyrene content. In a miscible blend, there exist local concentration fluctuations, meaning that a polymer chain segment undergoing relaxation sees a different environment and will therefore relax at different rates. The broadening of the relaxation is the result of these structural

inhomogeneities. Further evidence of the differing environment experienced by polymer chains in blends is that the density of polymer blends can be different from that predicted by simple additivity rules. (30) This obviously suggests a difference in packing of the chains versus the pure polymer components. Another significant characteristic of polymer blend relaxations is the additional asymmetry that arises in the alpha relaxation versus that in the pure polymers. This asymmetry appears at the low frequency end of the relaxation; this is in direct contrast to pure polymers where a significant characteristic of the relaxation is an asymmetry at the high frequency end. (31,32)

In the PPO/styrene-chlorostyrene blended systems, and typical of polymer blends in general, the alpha relaxation broadens on blending, with the amount of broadening corresponding to the difference between the glass transition temperature of the components. Alexandrovich et al. (33) compared poly(vinyl methylether) and poly(styrene) to the polystyrene/poly(2-chlorostyrene) blends. The relaxation of the PS/PVME blend is broader than the polystyrene/polychlorostyrene blends due to the larger difference in glass transition temperature of the components (125 °C versus 30 °C, respectively).

A strong temperature dependency and a pronounced asymmetry of dispersions of blends at lower frequencies has been noted for the blended PS/PVME system by Roland and Ngai (34) and Zetsche et al. (35) This has been explained using a coupling model. The temperature dependency of this system suggests that in this case the use of time-temperature superpositioning cannot be applied. Another system, tetramethyl-bisphenol-A polycarbonate and polystyrene, has displayed the same result. (36) In this case, the polar nature of the polycarbonate component allows it to be monitored alone using DES.

Interestingly, the broadness of the relaxation of this blend goes through a maximum at polycarbonate compositions between 60 and 80%. This results most probably from the reduction of free volume upon mixing. Other authors have reported a similar result as well. (37)

Many instances of compositional dependence of the broadening of the glass transition have been reported for miscible blends. While initially it might be assumed that this is due to contributions due to the differing mobility of the blended chains, depending on their glass transition temperatures, Katana et al. (38) found that for polycarbonate (PC)/tetramethyl polycarbonate (PTMPC) blends that this is not the case. In this work, the PC/PTMPC system did not show a broadening of the relaxation as measured with either DSC or DES. This was reasoned to be due to a lack of change in the local environment for the chains.

In addition to the effects of blending on the alpha relaxation, sub-T_g relaxations are also affected by blending. A large variety of effects are observable depending on the particular system evaluated. In some cases, supression of the beta relaxation has been seen (39, 40), similar to that noted by incorporation of certain additives, such as relatively low molecular weight materials that plasticize the sample. (41) These effects are significant because sub-T_g relaxations are often correlated to important polymer properties such as toughness.

The addition of a second component to a polymer system can affect the sub-T_g relaxations. Many mixtures of low-molecular-weight additives, such as plasticizers, tend to reduce the magnitude of these relaxations and lead to a condition known as antiplasticiation. However, this is not usually the case for higher molecular weight

additives, presumably because of their immiscibility. Studies by some workers have indicated that the local free volume fluctuations that suppress the beta relaxation in mixtures with low molecular weight components are not encountered in higher molecular weight mixtures. This was associated with the much smaller volume fluctuations for the systems examined. (42, 43) For the case of PC/PTMPC, the beta processes of each component are sufficiently separated (with the PTMPC/PC system having a beta relaxation occuring at a signficantly higher temperature) that they may be independently examined and considered, as may be seen in Figure 5-5. The change in relaxation magnitude with composition scales with volume fraction alone, which was not found to be the case in another study employing the same system. (44) Interestingly, although the beta relaxation of the PTMPC/PC does not shift significantly in position, the PC's beta relaxation shifts toward lower temperatures with increasing PTMPC content. This is suspected to be due to inhibition of localized motions of the PC, resulting in the reduction of magnitude of the high-temperature portion of that relaxation. This also results in a decrease of the associated activation energy with increasing PTMPC content. In noting the absence of changes in the relaxation processes for this system, it has been suggested that there is no change in the local environments of these systems upon blending. (45, 46) This was theorized to be due to the absence of true mixing at a very localized level. Alternatively, the observed data have been attributed to the small magnitude of free volume fluctuations in blends of high molecular weight materials (47), or to specific interactions between the component materials which can affect molecular motions responsible for these relaxations.

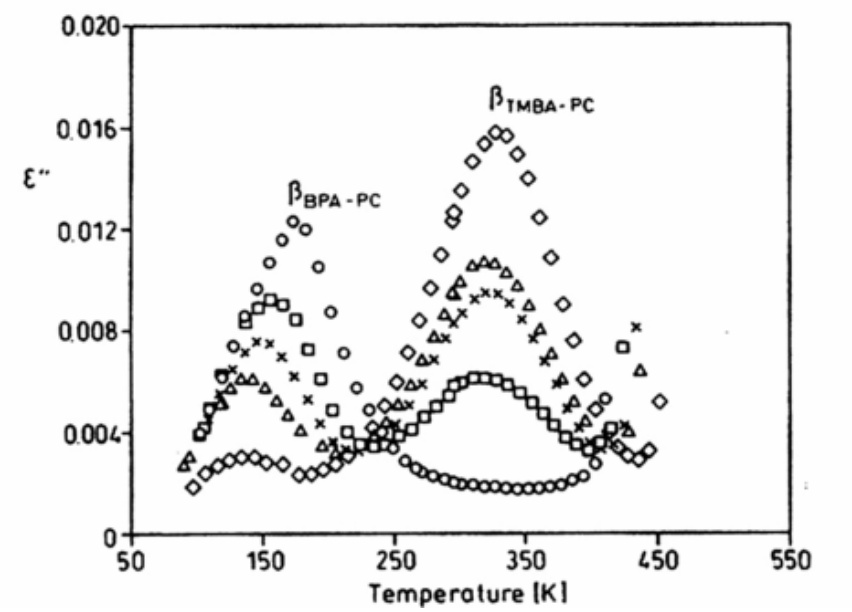

Figure 5-5. Change in magnitude of beta relaxations with composition in a PTMPC-PC blended system. After Katana et al., Macromolecules, 26, (1993), p. 3075.

Other systems which have been considered include mixtures of polyphenylene oxide (PPO) and polystyrene (PS). The microstructure of this system has been probed using WAXS, which suggests that the introduction of the PPO disrupts a "stacking" effect of the phenyl rings of the PS. (48) This argument is also used to at least partially explain the increase in density of the mixture, which is associated with specific interactions. Using NMR, the relaxation motions of the phenyl rings have been studied and found to be equivalent in the blend, whereas in the pure polymer, PPO's phenyl relaxation occurs about five times faster than that of PS. This has been used to explain the difference in properties of the blends such as the impact strength. The similarity of the blend and component's relaxation times has been attributed to the pi-pi interaction between rings. (49) However, this work is in contrast to that of other authors (50), who show a slight decrease in the overall number of quickly-relaxing phenyl rings in PS as a result of blending with PPO. In this case, a more pronounced beta relaxation process

seems to be not a result of the apparently small change in the phenyl motion, but rather is due to better resolution which separates the beta from the (now higher temperature) alpha relaxation experimentally.

For multiphasic blends, relaxation effects of the second (added) component may be seen as well as the relaxation behavior of the first component. As an example, the reponse of bisphenol-A polycarbonate/polymethylmethacrylate (PMMA) blends was studied in the two-phase composition region, where the dispersions detected initially appeared to be simply a superposition of the two components characteristic features. However, in the PC-rich phase, DMA showed no evidence of the well-known beta process associated with the polycarbonate. NMR revealed that the motion of the phenyl rings in the polycarbonate was hindered by blending with PMMA, leading to a broader proton resonance. Interestingly, there has been little effect noted on the PMMA beta relaxation as a result of blending. (51) In a blend of Chloral (bisphenol-C) PC and PMMA, the ring flipping process in the polycarbonate was inhibited due to the presence of PMMA. A coupling of the methyl ester group rotation and the beta relaxation was noted at high concentrations of PMMA.

Now considering the topic of non-uniform, or gradient, polymeric materials, discussion of some of the observed relevant relaxation properties was presented in Chapter 3. Relaxation properties of these anisotropic materials showed very different behavior when compared to samples with homogeneous compositions. A complete survey of the relaxation behavior of polymer materials swollen with low molecular weight penetrants was accomplished using mechanical relaxation techniques. (52) In this work, comparison was made between both samples that were exposed and unexposed to

the fluids. One effect of the plasticization was a shifting the isothermal alpha relaxation to higher frequencies. Additionally, it was hypothesized that samples that were partially swollen to a non-equilibrium condition would show a broadened distribution of relaxation times as compared to materials with a homogeneous distribution of components. This expansion of the relaxation time distribution was attributable to the difference in mean relaxation times of portions of the sample having different penetrant compositions. Therefore it was speculated that these materials could possess a gradient of glass transition temperatures which reflected the measured broadened relaxation time distribution. This was not observed, however, possibly because the diffusion rates for the particular experiments reported were sufficient (given the allowed swelling times) to erase any formation of gradient structure.

5.3 Experimental

The origins of the chemicals described below have been presented in Chapter 2. Samples of toughened thermoset were produced from bisphenol-A dicyanate (BADCy) (Figure 5-6). This material was used as received, and was mixed with one of two different toughenners: a hydroxyl-terminated butadiene acrylonitrile copolymer (HTBN) and Vitel 3200, an amorphous, low T_g copolyester, both used as received. These two toughener polymers differ both in chemical composition and molecular weight. The HTBN has a number average molecular weight of approximately 4500 g mol^{-1} while the Vitel 3200 has a number average molecular weight of about 20000 g mol^{-1}.

The HTBN was dissolved directly in the BADCy at 90 °C. Because of the relatively high molecular weight of the Vitel material, it was necessary to add this toughener to the BADCy as a solution in methylene chloride. The BADCy monomer was

melted at 90 °C, and the Vitel 3200/methylene chloride solution was then added slowly with stirring. The majority of the solvent flashed off in this step. The mixture was stirred briefly after the addition in order to allow further solvent evaporation, and was subsequently stirred under vacuum. The mixture was cooled under vacuum and allowed to crystallize. Next, the solution was melted under vacuum to remove any final traces of solvent that remained. Both types of resin mixtures were catalyzed with 2 phr of nonylphenol and 250 ppm of aluminum acetylacetonate and used immediately.

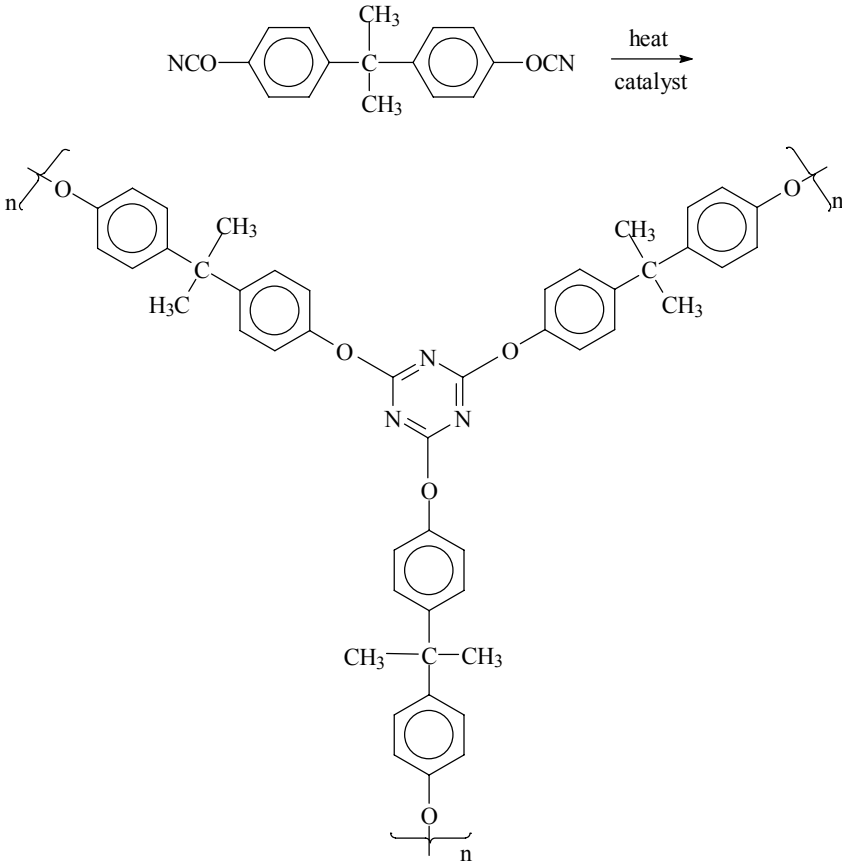

Figure 5-6. Cyanate ester monomer and network structure.

The material was isothermally cured into samples at various selected. Accurate cure temperatures were assured through the use of thermally massive aluminum molds capable of dissipating the cure exotherm from the curing sample. Also important in this

regard was a preheating of the mold and curing of the resin in a forced-air oven. Samples were cured via a controlled temperature gradient through the use of a specially-designed thermal gradient molding device. (53) This apparatus consists of a thermally massive aluminum block sectioned to contain the sample that was placed between two heated steel platens maintained at different temperatures. After thermal equilibrium was reached, the mixture of resin and toughener was pumped into the mold and proceeded to cure at a variety of temperatures depending on their mold location. Temperatures typically fluctuated less than 2 °C at any given point along the length of the mold during the cure cycle. Each specimen was cured for a length of time sufficient to react the sample at the lowest temperature sufficiently that it exceeded its gel point, then cooled to room temperature. The sample was then uniformly postcured at 250 °C for two hours to allow for maximum cure, then cooled again and removed from the mold.

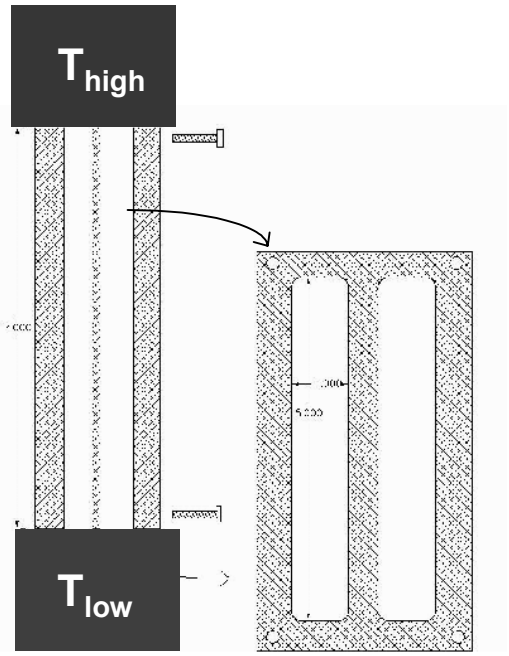

Figure 5-7. Diagram of mold apparatus used for gradient cure temperatures.

Dynamic mechanical analysis was used to determine relaxation properties and glass transition temperatures. Samples were analyzed using a TA Instruments 2980 DMA with liquid nitrogen cooling used for subambient operation. Temperature scans to determine glass transition temperatures were carried out at a heating rate of 1 °C min^{-1} and 1 Hz. Mechanical relaxation measurements were completed in step isothermal experiments with temperature steps of 3 °C at frequencies of 0.01, 0.02, 0.05, 0.1, 0.2, 0.5, 1, 2, 5, 10, 20, 50 and 100 Hz.

5.4 Results

5.4.1 Isothermally (Non-Gradient) Cured Samples

The glass transition temperature of polymers, and blends specifically, have been measured in a variety of ways. (54) In this work, DMA was chosen for determining glass transition temperature because of good reproducibility and ease of sampling. Representative results are shown in Figure 5-8 for the HTBN based cyanate ester polymer and in Figure 5-9 for the copolyester-toughened material. From this data, it was determined that samples containing 10% HTBN would be the optimum subject of further study of the gradient cure temperature effect and therefore this system was chosen for further characterization. Other samples with differing compositions of the toughener may show even greater dependence of cure temperature on resultant glass transition temperature than our example. However, specimens of this concentration of the toughener do show a glass transition temperature difference consistently, at higher amounts of HTBN, gross macrophase separtation can take place, complicating results.

From the mechanical data (Figure 5-8 and Figure 5-9) it is clear that large differences exist between the two tougheners for the cyanate ester system. All of the

polyester materials show miscibility (single-phase behavior) at the concentrations studied except Vitel 3200. Because a superior additive would improve toughness while producing no other effects on the cured resin, the miscible polyesters were not further explored. The depression of glass transition temperature was too extreme for practical uses.

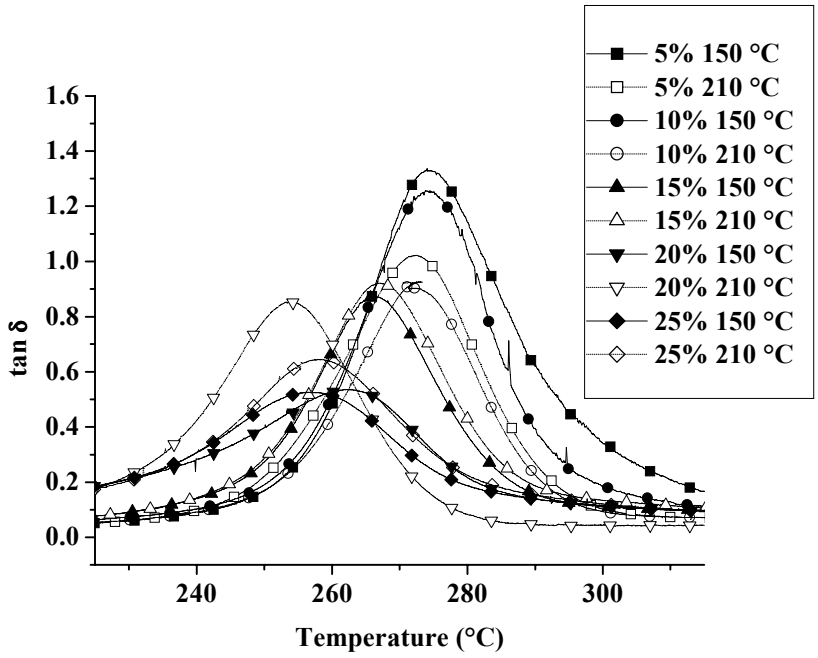

Figure 5-8. DMA showing alpha relaxation behavior of various HTBN compositions and cure conditions of cyanate esters.

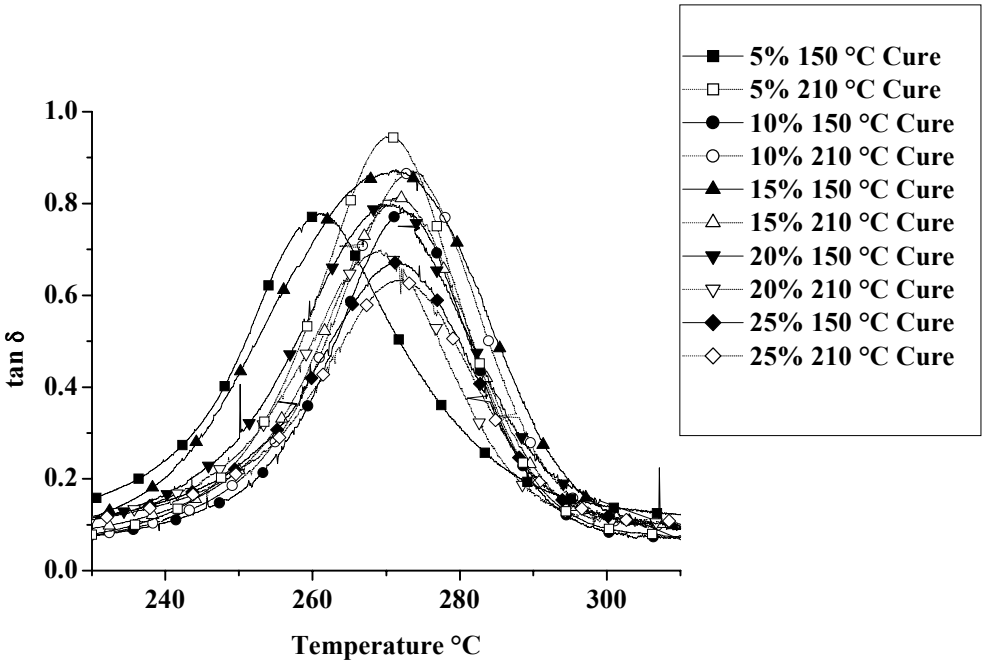

Figure 5-9. DMA showing alpha relaxation behavior of various Vitel 3200 compositions and cure conditions for cyanate esters.

Returning to Figure 5-8 and Figure 5-9, one notes that there are significant differences in DMA response that arise from changing cure profiles of these toughened thermosets. Because of the large variation of cure temperature and subsequent rate of the trimerization reaction, the extent of phase separation is not seen to be as great in the lower cure temperature examples. This effect depends upon the specific solubility characteristics of the toughener in the polymerizing cyanate ester as well as other factors discussed in Chapter 4. The predominant cure temperature influence is not a difference in equilibrium phase composition, but the variation in non-equilibrium phase composition that arises as a result of impending gelation of the cyanate ester-rich phase. This gelation slows the diffusion rate to the point where the phase separation can be considered to stop completely. The departure from equilibrium conditions is mainly a reflection of the difference in reaction rate and diffusion rate, and its temperature dependence as reflected

in the corresponding activation energies. These details are considered expansively in the preceding chapter. Considering the just-presented preliminary observations, the 10% HTBN modified polycyanurate system was chosen for further study. The relaxation characteristics of that system will be further investigated in this chapter.

Additional DMA temperature scans at 1 Hz were performed to better quantify the cure temperature effects on the relaxation behavior of the 10% HTBN-modified cyanate ester. Typical data for each of four cure conditions are shown in Figure 5-10 for the case of 150 °C, 180 °C, 210 °C isothermal cures as well as a gradient cure condition. The gradient cure temperature varied linearly with position along the sample length from 166 °C to 206 °C as noted above. In addition, DMA experiments were run to determine the glass transition temperature of the toughenes as well as the untoughened polycyanurate. In the case of untoughened polycyanurate, the effect of cure temperature on the resulting glass transition temperature was investigated with samples cured at temperatures that matched those for the toughened samples. Five samples were run for each case in determining the T_g. The results of these experiments were used with the Fox equation (55) to show that the composition of the polycyanurate-rich phase cured at 150 °C contains 2.97% HTBN, while the sample cured at 210 °C contains 4.33% HTBN.

$$\frac{1}{T_g(ab)} = \frac{w(a)}{T_g(a)} + \frac{w(b)}{T_g(b)} \qquad \textbf{(5-37)}$$

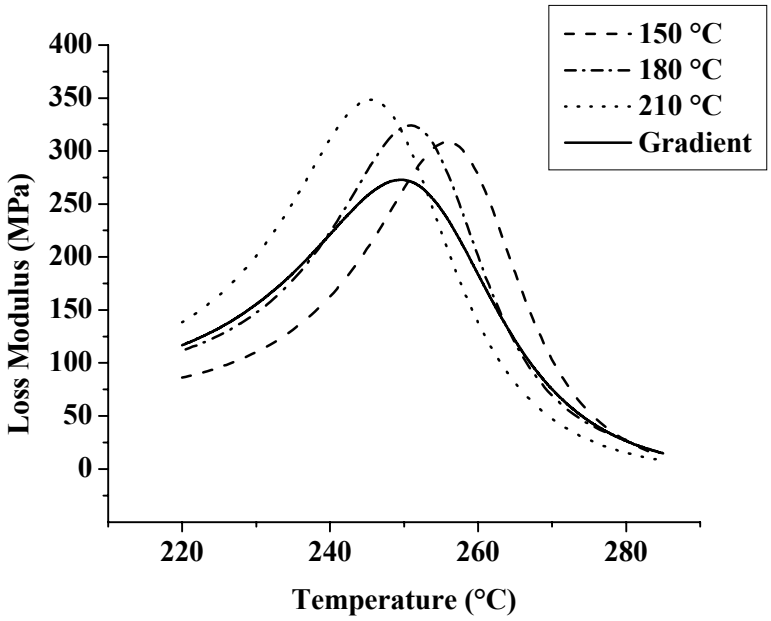

Figure 5-10. Dynamic mechanical analysis of 10% HTBN in BADCy at various cure temperatures.

Considering the Fox calculation, the depression of glass transition temperature due to toughener miscibility in the thermoset-rich phase was revealed using this well-known relationship. This equation is a very simplified approach to the prediction of the glass transition temperature in a miscible blend from the fractional composition and the glass transition temperature of the initial components. There are many other theories for estimating the glass transition temperature of miscible blends (see, for example, reference 56). Because in this thesis the depression of glass transition temperature is used to calculate the composition of the continuous phase for each different specimen, an accurate equation is very important for making conclusions about phase composition. At first glance, an attractive option might be the method of predicting phase composition using a comprehensive model of phase separation of a curing toughened thermoset

system that was presented in the previous chapter. However, because the glass transition is only depressed a small amount with respect to the untoughened material, the cyanate ester-rich phase contains only a small amount of the toughener, and the comprehensive theory is not useful.

A major argument against the use of the simple Fox relationship is that it cannot adequately describe deviations from additivity of the components. There is no information available about the positive or negative deviation from additivity in the miscible cyanate ester/HTBN system. Further, because of increasing immiscibility during the building of molecular weight during cure, the determination of such a relationship cannot be approached directly. However, the deviations from additivity are described by various other authors' attempts to account for this phenomena. Particularly in regions of intermediate composition, where each component occupies a significant fraction of the blend, alternate calculations are more successful. In the case considered in this work, at compositions near those of the pure components, the difference between the blend behavior described by these various other relationships and the values obtained by the Fox approach is quite small. For the systems examined, the difference in glass transition temperature of the two initial components is quite large, greater than 300 °C, while the depression of glass transition temperature resulting from cure conditions is relatively small by comparison. It is therefore reasonable to expect that at these small glass transition depressions the composition of the cyanate-rich phase varies only slightly from that of the pure polycyanurate. This justification is presented for use, therefore, of the Fox relationship in this thesis.

Another measure of the differences in glass transition temperature resulting from two chosen cure temperatures is the relative position of the mechanical loss maximum measured isothermally while varying the DMA frequency. The various loss isotherms may be shifted into a mastercurve using the time-temperature-superpositioning technique. Because this technique depends on the relationship between the time (or frequency) dependent behavior of the material and its corresponding temperature dependence, the difference in glass transition temperature of samples resulting from differing cure temperature may be examined in this way. Figure 5-11 shows the two mastercurves generated using tTSP. The sample cured at 150 °C shows a peak

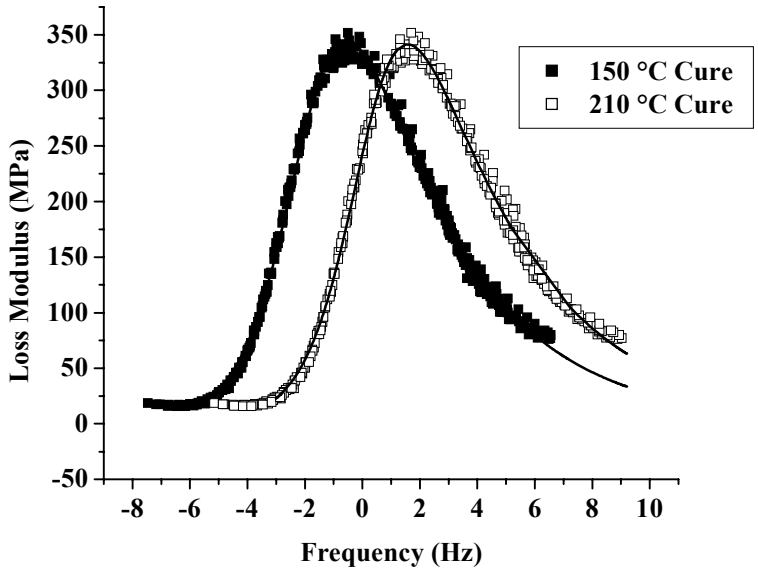

Figure 5-11. Variation of peak position with cure temperature at same T_{ref} (254 °C).

at a lower frequency than that of the sample cured at 210 °C, indicating a higher glass transition temperature. Because time and temperature for these particular samples are related through the shift factor relationship, the difference in glass transition temperature of these specimens may be estimated. However, as described by the WLF equation (57), and evidenced by the shift factor plot, the temperature dependence of the glass transition

process is a non-linear function. The shift of frequency between peaks of the two different cure temperature samples is seen in Figure 5-11 to be relatively small (about 72.4 Hz). To estimate a change in glass transition temperature from this data requires determination of the shift factors, and to do this we begin by considering that the reference temperature chosen is approximately the glass transition temperature (a reasonably good assumption, as T_{ref}=254 °C, which may be compared to the glass transition temperature determined from the plot shown in Figure 5-10). In the small region about the glass transition peak frequency, the shift factor was taken referenced to T_{ref} by taking the difference in peak frequency and centering that difference at T_{ref}, and using the WLF equation to determine the $T-T_{ref}$ values. In other words, this is an average of the shift factors both at half the frequency difference greater and less than $T-T_{ref}=0$ (the glass transition temperature taken as the loss peak maximum). From this procedure, and using the WLF equation with universal constants C_1=17.44 and C_2=51.6, the corresponding temperature difference between the peaks may be obtained. While this is obviously an estimate, the calculated value of 7.9 °C agrees reasonably well with that measured from the temperature sweeps (10.4 °C).

It has been demonstrated that variations in the cure temperature of the HTBN/cyanate ester system produce variations in the glass transition temperature. Thus, the possibility of building materials with continually varying gradients of properties by applying gradient cure temperature techniques was suggested. The variation of glass transition temperature within a single sample by cure temperature variation within that sample has many practical implications. It is important to understand that these effects might occur, whether planned or accidental, and to characterize the resultant materials.

5.4.2 Gradient Temperature Cured Samples

5.4.2.1 Thermomechanical and Relaxation Measurements

The characterization of the unique mechanical behavior of gradient cured network systems was approached by considering the viscoelastic properties. Because the glass transition of the samples varied as a function of position within the sample, any measurement of the thermomechanical properties of the overall (global) sample will necessarily include what can be considered as many distinct composite sections of slightly, yet continuously, varying glass transition temperatures. When considered along with the principles of time-temperature equivalence, this one would predict a broadening of the effective global system relaxation time distribution. Those portions of the sample relaxing at higher temperatures would contribute to the lower frequency response, and the lower T_g sections contributing in the higher frequency range.

Characterization of the relaxation dispersion associated with the glass transition has been the subject of a great deal of interest for obvious reasons in many polymers. Of all the mathematical forms that might be chosen to describe and analyze this dispersion, the Havriliak-Negami (H-N) relationship (58) was chosen. One advantage to H-N for our purposes is that it is not derived from a molecular mechanism or basis, being strictly phenomenological. This mathematical relationship was also applied to the description of the glass transition process because it includes convenient parameters that describe the breadth of the relaxation. Having two adjustable parameters as H-N does allows more versatility in the description of different relaxation characteristics. Using this H-N description, the relaxations of samples cured at a single temperature (and with a resultant "single" glass transition temperature) are compared below to samples cured in a

temperature gradient. As will be shown, indeed, the expected broadened relaxation was the consequence of gradient processing.

This characterization begins with obtaining information about the relaxation that is suitable for choosing parameters in the Havriliak-Negami relationship. Most often, H-N has been is associated with dielectric spectroscopy rather than DMA. This is due to the larger range of frequencies that may be practically obtained with the use of an electric field as a probe rather than a mechanical deformation. In spite of this, many applications of the Havriliak-Negami relationship to mechanical data appear in the literature (59, 60, 61, 62, 63, 64, 65, 66, 67, 68). However, questions about the applicability of this description to data recorded over the typically small range of frequencies available with dynamic mechanical analysis rightfully have been raised. (69) This limitation may be addressed by consideration of the previously presented time-temperature superpositioning principle which also deals with extrapolating otherwise inaccessible data from actual experiments.

In order to make comparisons between the DMA results over a narrow range of frequencies to the much larger frequency range available through the use of tTSP, individual isotherms were first fitted to the H-N model. This was only possible for a small number of the isotherms which demonstrated a maximum of loss modulus associated with the glass transition, as consequence of the numerical fitting technique used. Five sets of isotherms were successfully fitted with the Havriliak-Negami equation. Typical results for a single isotherm for each cure condition are shown in Figure 5-13, Figure 5-14 and Figure 5-15 for cure temperatures of 150 °C, 210 °C and gradient cure temperature conditions, respectively. Due to the limited frequency range, meaningful

data regarding the temperature dependence of the resultant H-N parameters is not available – a larger temperature range produces mechanical responses that do not show maxima, and are not able to be reliably fitted. However, examination of the dynamic mechanical results over a larger range of frequencies made available via tTSP reveals the absence of any other transitions or processes that would violate the necessary condition of thermorheological simplicity in the region of the relaxation. This absence is also essential for the successful application of time-temperature superpositioning. (70)

The numerical fitting procedure represented by the curves in Figure 5-13 through Figure 5-13 was carried out using Microsoft Excel, minimizing the sum of the squares of the residuals. This procedure yielded excellent fits, as shown in the accompanying plots. However, in detailed comparison of the various isotherms shown in the figures, it may be seen that the shapes of fitted curves are not necessarily equivalent outside of the range of data collected. In these cases, the value of having additional frequency data is clearly evident, which validates some of the criticism associated with fitting mechanical data to H-N due to its relatively small range of available frequencies. An additional feature of the plots is that the range of temperatures required to capture the peak changes with the difference in glass transition temperature of the samples, with the gradient sample being intermediate between the two cure temperature extremes. This observation simply reflects the difference in glass transition temperatures. Comparison of these DMA results with those obtained through fitting a wider range of extrapolated frequencies will be discussed below.

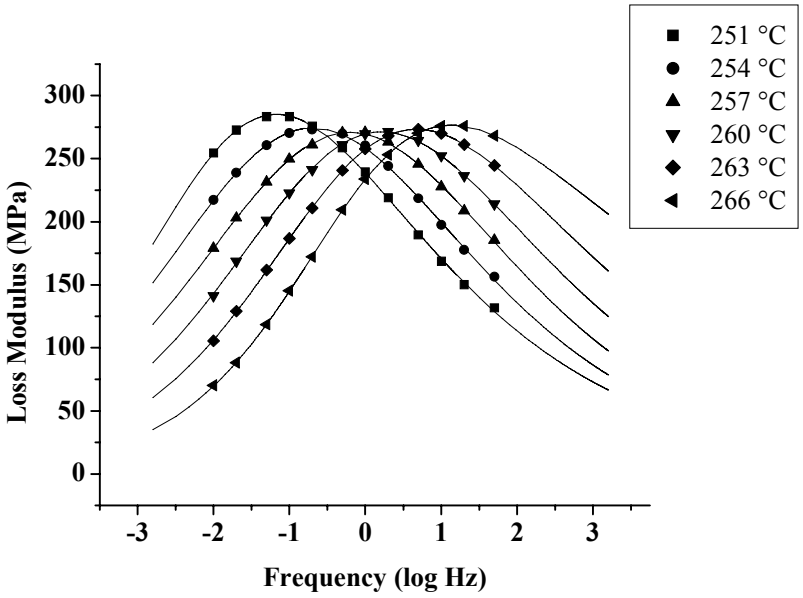

Figure 5-12. Typical isothermal H-N fits of dynamic mechanical analysis data, untoughened polycyanurate.

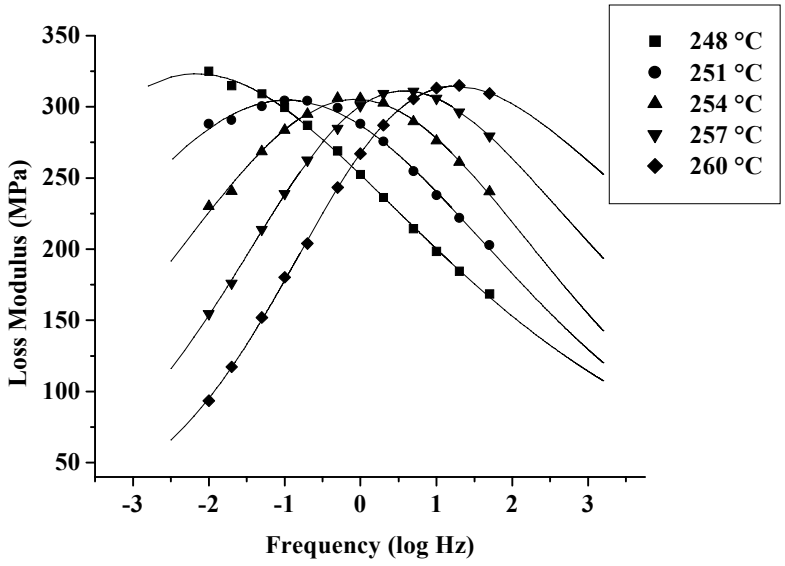

Figure 5-13. Typical isothermal H-N fits of dynamic mechanical analysis data, 10% HTBN, 150 °C cure.

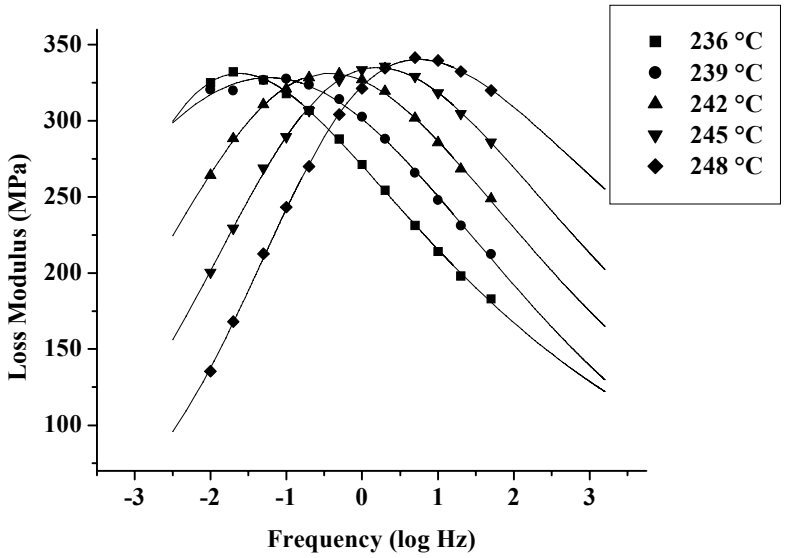

Figure 5-14. Typical isothermal H-N fits of dynamic mechanical analysis data, 210 °C cure.

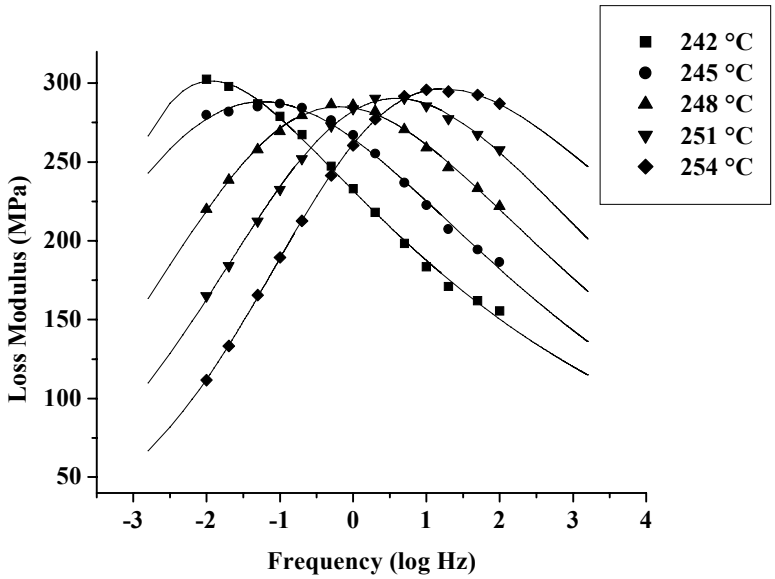

Figure 5-15. Isothermal H-N fits of dynamic mechanical analysis data, gradient cure.

5.4.2.2 Time-temperature superpositioning

Expansion of the experimental frequency axis of the DMA data was accomplished by horizontal shifting of isothermal data to create the mastercurves to be used in the

Havriliak-Negami description. Isotherms of loss modulus were collected using DMA. The temperature range was chosen so as to collect sufficient data on both sides of the peak, depending on the test frequency. Five data sets at each cure condition (150 °C, 210 °C and gradient temperature cure) plus the data for the untoughened cyanate ester cured at 210 °C were shifted and shift factor relationships were generated. The resultant shift factor plot contained results that were averaged within sample types. These averaged shift factor plots, together with the WLF shift factors predicted using the universal constant values in the WLF equation showed good agreement at $T-T_g>0$. This information is summarized in Figure 5-16 along with a best fit WLF line as well. Values of the fitted WLF parameters are $C_1=14.76$ and $C_2=61.38$. This plot shows how similar each of the shift factor graphs is between cure conditions, and the agreement with WLF prediction using the universal constants. This similarity is to be expected due to the compositional similarity of the different samples. Using this idea, it was decided that an averaged shift factor plot could be extracted from the different cure conditions which would allow for identical shifting of all data. This unique method eliminates some of the subjectivity inherent in the shifting process. While every effort was made to shift accurately and objectively, the possibility that the shifting process could be made more uniform between sample types was considered carefully. The isothermal data was again shifted using the averaged shift factors. The resultant five sets of reshifted data were then fitted to the Havriliak-Negami equation. The Havriliak-Negami parameters were then compiled and averaged and are presented in Table 5-1.

Untoughened Sample			150 °C Cure		
Loss Curve Origin	α	γ	Loss Curve Origin	α	γ
251 °C Isotherm	0.3482	0.6343	248 °C Isotherm	0.2572	0.5422
254 °C Isotherm	0.3358	0.6748	251 °C Isotherm	0.2223	0.9255
257 °C Isotherm	0.3505	0.5788	254 °C Isotherm	0.2530	0.9111
260 °C Isotherm	0.3710	0.4591	257 °C Isotherm	0.3314	0.4678
263 °C Isotherm	0.4209	0.2750	260 °C Isotherm	0.3810	0.2653
average	0.3653	0.5244	average	0.2890	0.6224
std. dev.	0.0336	0.1613	std. dev.	0.0652	0.2886
Mastercurve 1	0.4331	0.3736	Mastercurve 1	0.4250	0.2889
Mastercurve 2	0.4388	0.3765	Mastercurve 2	0.4027	0.2761
Mastercurve 3	0.4408	0.3681	Mastercurve 3	0.4247	0.2611
Mastercurve 4	0.4322	0.3441	Mastercurve 4	0.4112	0.2381
Mastercurve 5	0.4275	0.3602	Mastercurve 5	0.4024	0.2564
average	0.4345	0.3645	average	0.4132	0.2641
std. dev.	0.0053	0.0130	std. dev.	0.0112	0.0194

210 °C Cure			Gradient Temperature Cure		
Loss Curve Origin	α	γ	Loss Curve Origin	α	γ
236 °C Isotherm	0.4269	0.2723	242 °C Isotherm	0.5360	0.1822
239 °C Isotherm	0.2160	0.8635	245 °C Isotherm	0.2764	0.4317
242 °C Isotherm	0.3074	0.4629	248 °C Isotherm	0.3025	0.3940
245 °C Isotherm	0.3436	0.3717	251 °C Isotherm	0.3070	0.4077
248 °C Isotherm	0.4093	0.2125	254 °C Isotherm	0.3499	0.2510
average	0.3406	0.4366	average	0.3544	0.3333
std. dev.	0.0849	0.2571	std. dev.	0.1049	0.1101
Mastercurve 1	0.3991	0.3210	Mastercurve 1	0.3946	0.3134
Mastercurve 2	0.4129	0.2767	Mastercurve 2	0.3720	0.2779
Mastercurve 3	0.4111	0.2716	Mastercurve 3	0.3577	0.2657
Mastercurve 4	0.4166	0.2695	Mastercurve 4	0.3627	0.2952
Mastercurve 5	0.4028	0.3007	Mastercurve 5	0.3660	0.3053
average	0.4085	0.2879	average	0.3706	0.2915
std. dev.	0.0073	0.0223	std. dev.	0.0144	0.0196

Table 5-1. Havriliak-Negami fitting parameters α and γ for isotherms and for mastercurve data.

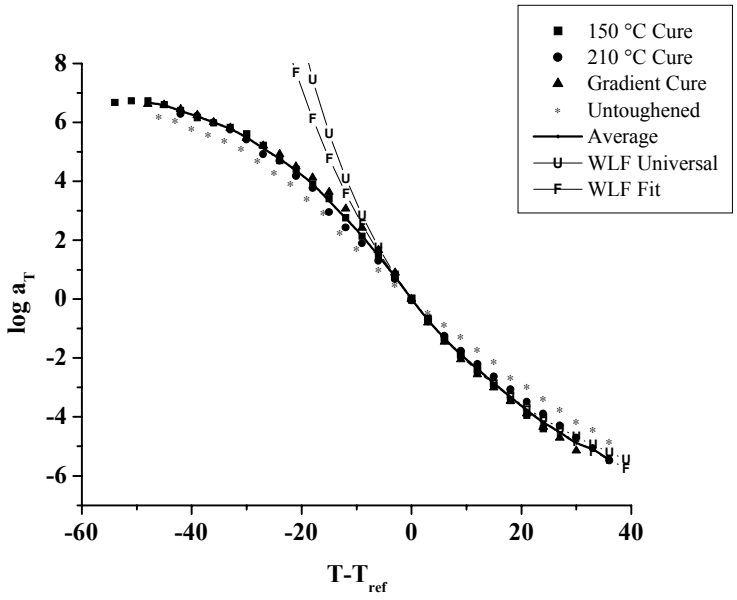

Figure 5-16. Shift factor plot for various mastercurves together with WLF shift factor predictions using either universal constants or fitted constants.

Representative loss modulus mastercurves are shown in Figure 5-18, Figure 5-19, Figure 5-20 and Figure 5-20, together with their Havriliak-Negami fits. The H-N expression fits the relaxation behavior very well in each example now that the expanded frequency scale is available following tTSP.

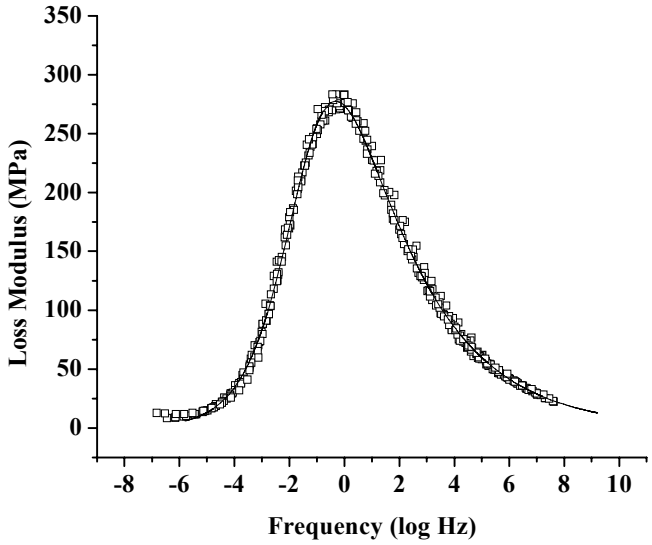

Figure 5-17. Untoughened polycyanurate mastercurve fitted to the Havriliak-Negami expression.

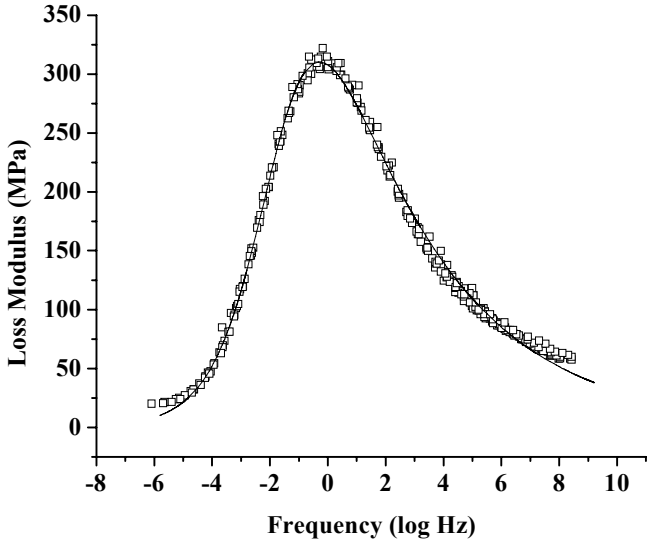

Figure 5-18. 150 °C cured polycyanurate toughened with 10% HTBN, mastercurve fitted to the Havriliak-Negami expression.

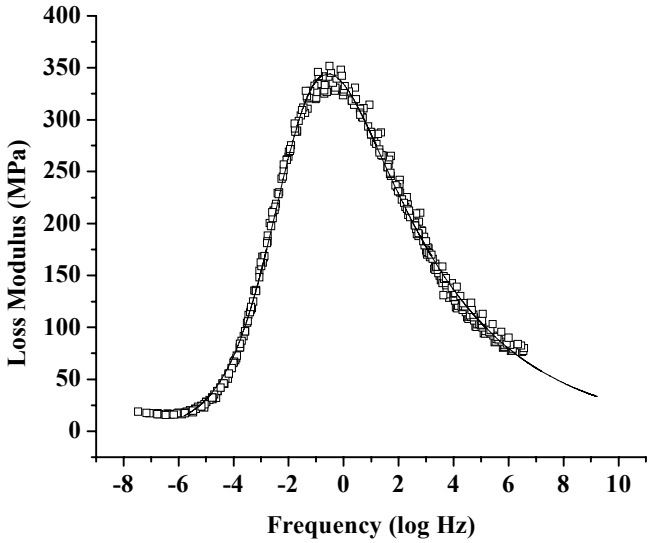

Figure 5-19. 210 °C cured polycyanurate toughened with 10% HTBN, mastercurve fitted to the Havriliak-Negami expression.

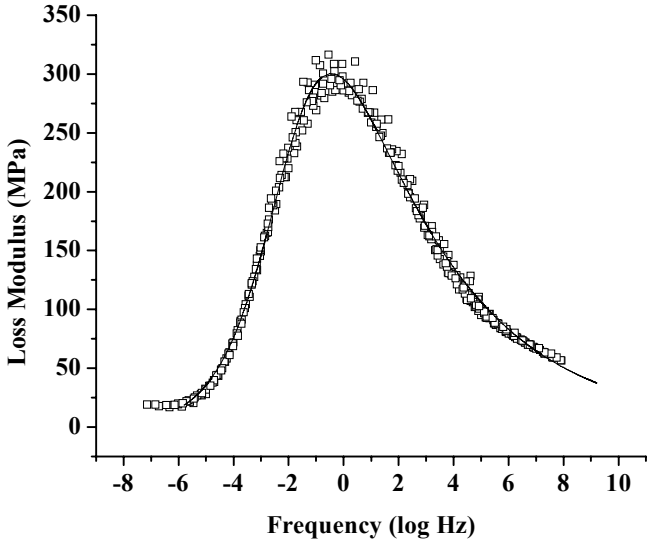

Figure 5-20. Gradient temperature cured polycyanurate toughened with 10% HTBN, mastercurve fitted to the Havriliak-Negami expression.

Comparison of the Havriliak-Negami parameters for the narrow frequency range isotherms and the data generated using time-temperature superpositioning shows the reproducibility available through the use of tTSP. While the process of creating the mastercurve is subjective, the excellent reproducibility of the data demonstrates that real

and relatively small differences in viscoelastic behavior can be described using this method. Differences between values of the Havriliak-Negami parameters for the master curve and unshifted isotherm data also partially confirms the criticisms of Snyder et al. (71) against the use of data of a very small range of frequencies with the Havriliak-Negami description. The Havriliak-Negami parameters generated using the very small range of frequencies obtainable using conventional DMA equipment can yield very different results, especially when examining relatively small differences in behavior. This is only reasonable when it is considered that this expression was employed for the purpose of better representing the high-frequency asymmetry of this relaxation; where there is no high frequency data to consider, the inclusion of such a term becomes meaningless. However, this same technique can produce data suitable for use with the Havriliak-Negami relationship if used in conjunction with time-temperature superpositioning, and using this time-temperature equivalence to yield test results at frequencies beyond the limits of practicality or equipment.

The values of the Havriliak-Negami parameters show the effect of the variation of glass transition temperature within the same. The gradient temperature cured samples display a lower numerical value of alpha, the parameter representing the broadness of the distribution. This is a direct result of the increased range of glass transition temperatures within the sample, and therefore an increased breadth of the relaxation time distribution. This is shown in a composites chart in Figure 5-21. Here, we see the narrower curve described by the untoughened cyanate ester system. The addition of any toughener increases the breadth of the distribution, consistent with the findings of other authors as discussed previously in this chapter. As has been discussed previously, the higher cure

temperature prevents phase separation from occurring as completely as it might at lower cure temperatures. Because the gradient sample contains a range of glass transition temperatures, this sample has the largest apparent distribution of relaxation times.

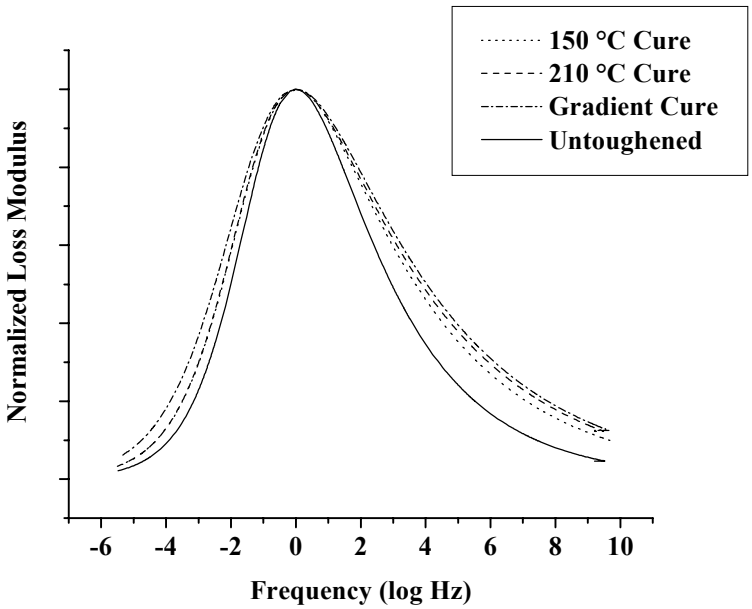

Figure 5-21. Havriliak-Negami fits of mastercurves, comparing the two isothermally cured materials with the gradient temperature cured sample.

5.4.2.3 Time Decay Function

An appropriate depiction of the apparent increase in relaxation time distribution due to cure temperature gradients is an illustration of the time dependence of the sample changing from a fully unrelaxed state to a fully relaxed one. This can be used as a different description of the relaxation process as a function of time. In this type of plot, the slope of the function is indicative of the relaxation rate. The difficulty in converting dynamic measurements to this type of representation has been overcome through the use of a Fourier transform. (72, 73) Parameters from the Havriliak-Negami fitting procedure were used to generate the time decay function as discussed in the literature review portion

of this chapter. This procedure was discussed in the literature review, and the mathematical procedure was performed using Mathematica (Wolfram Research). Here, the same mean relaxation time was used for each different sample, together with the average HN parameters from the mastercurves to generate the time decay curves.

From these curves, it is again clear that the change in cure temperature affects the relaxation time distribution. The effect of differing cure temperature on the isothermal curves can be seen, though this difference is, as has been discussed previously, small. The greater slope of the gradient curve indicates the speed of transition from a totally relaxed to a totally unrelaxed condition in this sample reflects the gradient of glass transition temperatures within the gradient sample, relative to the isothermally cured samples. At the midpoint of the relaxation, the curves meet, describing (approximately) the same mean relaxation time (because this parameter made equivalent for each system in this representation). The gradient sample shows a longer time for the relaxation of the entire system consisting of an exaggerated range of glass transition temperatures, through a smaller slope. Though the differences between samples are relatively small, the different cure temperature conditions produce significant differences, the most important of these being the increase in apparent relaxation time distribution due to macroscopic-scale effects.

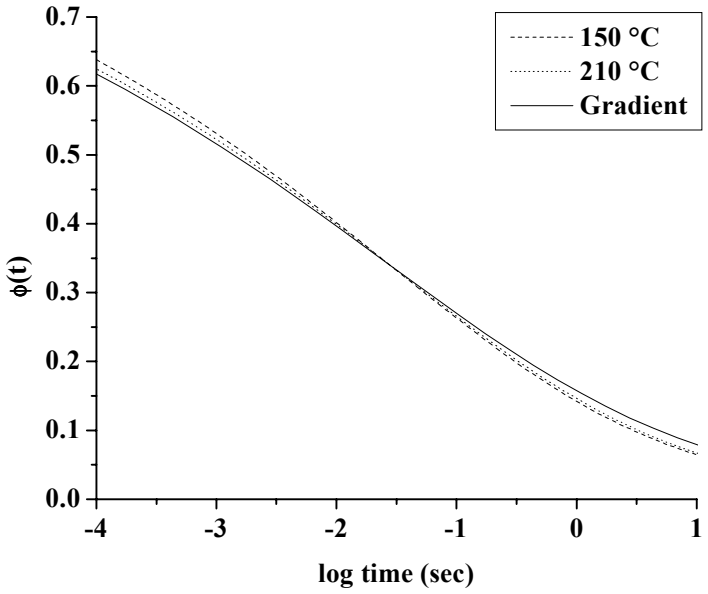

Figure 5-22. Time decay function of isothermally cured samples compared with gradient cured sample.

5.5 Conclusions

The relaxation properties of a set of toughened polycyanurate systems as a function of toughener type as well as cure temperature have been studied. Because the relaxation characteristics of the material determine important use properties, differences can have important practical implications. A common method of mathematically describing the alpha relaxation has been used to quantify difference between the various cases studied. This description, the Havriliak-Negami relationship, does not carry any molecular information, and was chosen due to its flexibility in describing the glass transition phenomena. The addition of HTBN toughener to the cyanate material broadens this relaxation. For the concentration studied, the amount of broadening varies with the cure temperature, as this determines the amount of toughener that phase separates and the amount that remains mixed into the continuous cyanate-rich phase. Curing at a higher temperature causes more low glass transition temperature toughener to remain mixed,

which by itself appears to slightly broaden the relaxation time distribution. However, this also causes a lowering of the glass transition temperature of the polycyanurate phase. Cure temperature, therefore, has a direct effect on the phase composition and resultant glass transition temperature. Real thermosetting materials often do not cure at a uniform temperature. Because of the thermal lag in heating a specimen and carrying away heat from the curing reaction, real samples inevitably cure at a range of temperatures. To understand the effects of this condition on relaxation properties, gradient cure temperature samples were fabricated and cured at practical extremes. The glass transition temperature of these samples was found to vary with cure temperature. When these samples were cured at a gradient cure temperature condition, the change in glass transition temperature along the sample gave rise to an apparent broadened distribution of relaxation times versus isothermally cured samples at either cure temperature extreme.

The characterization techniques used here have in the past typically been used to differentiate between local, molecular-level phenomena; this is true for homopolymers as well as both miscible and immiscible systems. For the system examined in this study, it is clear that the bulk of the effects seen arise from system differences on a macroscopic scale. The applicability of discriptions such as Havriliak-Negami is due to their general nature; they are not derived or tied to any particular molecular-level phenomena. This has not prevented the various parameters being assigned to molecular phenomena; in this work there is clearly demonstrated the case of macroscopic phenomena affecting these parameters. In addition to this, though, the versatility of these expressions has been employed to characterize this system of gradient properties of glass transition

temperature, reflected in a broadening of the system, if not molecular level, relaxation of a specimen.

5.6 References

(1) A. Zetsche, F. Kremer, W. Jung, and H. Schulze. Polymer, 31, (1990), p. 1183.
(2) I. Alig, D. Lellinger, J. Sulimma, and S. Tadjbakhsch. Rev. Sci. Instrum., 68, (1997), p. 1536.
(3) I. Alig, D. J. Lellinger. Journal of Applied Physics, 72, (1992), p. 5565.
(4) Y. H. Chin, P. T. Inglefield and A. A. Jones. Macromolecules 26, (1993), p. 5372.
(5) Y. H. Chin, C. Zhang, P. Wang, P. T. Inglefield, A. A. Jones, R. P. Kambour, J. T. Bendler, and D. M. White. Macromolecules, 25, (1992), p. 3031.
(6) S. Spall, A. A. Goodwin, M. D. Zipper, and G. P. Simon. Journal of Polymer Science, Part B: Polymer Physics, 34, (1996), p. 2419.
(7) M. L. Williams, R. F. Landel and J. D. Ferry. Journal of the Amercian Chemical Society, 77, (1955), p. 3701.
(8) J. D. Ferry, Viscoelastic Properties of Polymers, 2nd edition, John Wiley Interscience, New York, (1970).
(9) F. Povolo and N. Fontelos, Res Mechanica, 22, (1987), p. 185.
(10) M. L. Williams, R. F. Landel and J. D. Ferry. Journal of the Amercian Chemical Society, 77, (1955), p. 3701.
(11) A. K. Doolittle, Journal of Applied Physics, 22, (1951), p. 471.
(12) N. E. Shepard, Ph. D. Dissertation, Virginia Tech, 1995.
(13) K. S. Kwan, Ph. D. Dissertation, Virginia Tech, 1998.
(14) N.G. McCrum, B.E. Read, and G. Williams, Anelastic and Dielectric Effects in Polymeric Solids, Dover Publications, New York, 1967.
(15) J.J. Aklonis and W.J. MacKnight, Introduction to Polymer Viscoelasticity, 2 nd ed., Wiley-Science Publication, New York. (1983).
(16) N.G. McCrum, B.E. Read, and G. Williams, Anelastic and Dielectric Effects in Polymeric Solids, Dover Publications, New York, 1967.
(17) P. Debye, *Polar Molecule*s, Dover, New York, 1929.
(18) K.S. Cole and R.S. Cole, Journal of Chemical Physics, 9, 341 (1941).
(19) S. Havriliak and S. Negami, Polymer, 8¸161 (1967).
(20) T. Park, Ph.D. Dissertation, Virginia Polytechnic and State University, 1994.
(21) S. Havriliak and S. J. Havriliak. Dielectric and Mechanical Relaxation in Materials. Hanser Publications, Cincinnati, (1997), p. 354.
(22) D. Boese and F. Kremer, Macromolecules, 23, 829-835 (1990).
(23) T. Park, Ph. D. Dissertation, Virginia Tech, (1994).
(24) S. Havriliak and S. J. Havriliak. Dielectric and Mechanical Relaxation in Materials. Hanser Publications, Cincinnati, (1997).
(25) C. R. Snyder and F. I. Mopsik, Journal of Applied Physics, 84, (1998), p. 4421.
(26) S. Havriliak and S. J. Havriliak. Dielectric and Mechanical Relaxation in Materials. Hanser Publications, Cincinnati, (1997), p. 53.
(27) J. R. Fried, F. E. Karasz, and W. J. MacKnight. Macromolecules, 11 (1978), p. 150.

(28) R. E. Wetton, W. J. MacKnight, J. R. Fried, and F. E. Karasz. Macromolecules, 11, (1978), p. 158.
(29) S. F. Lau, J. Pathak, B. Wunderlich. Macromolecules, 15, (1982), p. 1278.
(30) J. R. Fried, F. E. Karasz, and W. J. MacKnight. Macromolecules, 11, (1978), p. 150.
(31) C. M. Roland and K. L. Ngai. Macromolecules, 25, (1992), p. 363.
(32) K. J. McGrath and C. M. Roland. Journal of Non-Crystalline Solids, 172-174, (1994), p. 891.
(33) P. S. Alexandrovich, F. E. Karasz, and W. J. MacKnight, Journal of Macromolecular Science, Physics, B17, (1980), p. 501.
(34) C. M. Roland and K. L. Ngai, Macromolecules, 25, (1992), p. 363.
(35) A. Zetsche, F. Kremerm, W. Jung and H. Schulze, Polymer, 31, (1990), p. 1883.
(36) J. M. O'Reilly and J. S. Sedita, Journal of Non-Crystalline Solids, 131-133, (1991), p. 1140.
(37) A. A. Mansour and S. A. Malbouly. Polymer International, 37, (1995), p. 267.
(38) G. Katana, F. Kremer, E. W. Fischer, and R. Plaetschke. Macrmolecules, 26, (1993), p. 3075.
(39) H. de los Santos Jones, Y. Liu, P. T. Inglefield, A. A. Jones, C. K. Kin, and D. R. Paul. Polymer, 35, (1994), p. 57.
(40) C. J. T. Landry and P. M. Henrichs. Macromolecules, 22, (1989), p. 2157.
(41) E. W. Fischer, G. P. Hellmann, H. W. Spiess, F. J. Horth, U. Ecarius, and M. Wehrle. Makromolecular Chemistry-Makromolecular Chemistry and Physics, S12, (1985), p. 189.
(42) E. W. Fischer, G. P. Hellmann, H. W. Spiess, F. J. Horth, U. Ecarius, and M. Wehrle, Macromol. Chem.-Macromol. Chem. Phys., X12, (1985), p. 189.
(43) G. Katana, F. Kremer, E. W. Fischer, and R. Plaetschke, Macromolecules, 26, (1993), p. 3075.
(44) Y. J. Jho and A. F. Lee. Macromolecules, 24, (1991), p. 2261.
(45) A. A. Mansour and S. A. Madbouly, Polymer International, 36, (1995), p. 4486.
(46) A. A. Mansour and S. A. Malboudy, Polymer International, 37, (1995), p. 267.
(47) E. W. Fischer, G. P. Hellmann, H. W. Spiess, F. J. Horth, U. Ecarius, and M. Wehrle, Macromol. Chem.-Macromol. Chem. Phys., X12, (1985), p. 189.
(48) G. R. Mitchell and A. H. Windle. Journal of Polymer Science: Polymer Physics Edition, 23, (1985), p. 1967.
(49) H. Feng, Z. Feng, H. Ruan, and L. Shen. Macromolecules, 25, (1992), p. 5981.
(50) J. Zhao, Y. H. Chin, Y. Liu, A. A. Jones, P. T. Inglefield, R. P. Kambour, and D. M. White, Macromolecules, 28, (1995), p. 3881.
(51) C. J. T. Landry and P. M. Henrichs. Macromolecules, 22, (1989), p. 2157.
(52) Kermit Kwan, Ph. D. dissertation, Virginia Tech, (1998).
(53) D. S. Porter, *Proceedings of the Adhesion Society Annual Meeting*, Hilton Head, South Carolina. February, 1997.
(54) O. Olabisi, L. M. Robeson, and M. T. Shaw. *Polymer-Polymer Miscibilit*y, Academic Press, New York, 1979.
(55) T. G. Fox, Bulletin of the American Physical Society, 1, (1956), p. 123.
(56) P. R. Couchman and F. E. Karasz, Macromolecules, 11, (1978), p. 117.
(57) M. L. Williams, R. F. Landel, and J. D. Ferry, Journal of the American Chemical

Society, 77, (1955), p. 3701.
(58) S. Havriliak and S. Negami, Polymer, 8¸161 (1967).
(59) D. A. Ivanov and A. M. Jonas. Polymer, 39(15), (1998), p. 3577.
(60) W. B. Liau, Polymer, 40(3), (1998), p. 599.
(61) J. Colmenero, A. Alegria, J. M. Alberdi, F. Alvarez, and B. Frick. Physical Review B, Condensed Matter, 44(14), (1991), p. 7321.
(62) F. Garwe, A. Schoenhals, M. Beiner, K. Schroeter, and E. Donth. Journal of Physics: Condensed Matter, 6(35), (1994), p. 6941.
(63) Jeffry J. Fedderly, Gilbert F. Lee, John D. Lee, Bruce Hartmann, Karel Dusek Jan Somvarsky, Miroslava Smrckova, Macromolecular Symposia, 148 (7th International Conference on Polymer Characterization (POLYCHAR-7)), (1999), p. 1.
(64) W. M. Davis, J. P. Szabo. Computational and Theoretical Polymer Science, 11(1), (2000), p. 9.
(65) F. Alvarez, A. Alegria and J. Colmenero, Physical Review B: Condensed Matter, 47(1), (1993), p. 125.
(66) R. Knudsen, Ph. D. Dissertation, Virginia Tech, (1999).
(67) K. Kwan, Ph. D. Dissertation, Virginia Tech, (1998).
(68) M. Muggli, Ph. D. Dissertation, Virginia Tech, (1998).
(69) C. R. Snyder and F. I. Mopsik, Journal of Applied Physics, 84(8), (1998), p. 4421.
(70) J. D. Ferry, Viscoelastic Properties of Polymers, John Wiley Interscience, New York (1970).
(71) C. R. Snyder and F. I. Mopsik, Journal of Applied Physics, 84(8), (1998), p. 4421.
(72) K. Kwan, Ph. D. Dissertation, Virginia Tech, (1998).
(73) T. Park, Ph. D. Dissertation, Virginia Tech, (1994).

Chapter 6: Conclusions

Thermosetting polymers offer many advantageous properties, which arise in part from the presence of a crosslinked topology. These desirable properties do not come without disadvantages, however. Often, thermosetting polymers can have an unacceptably high brittleness, which necessitates the use of toughening additives. The mechanism of action of these toughening additives is the formation of a separate, toughener-rich phase which can significantly improve the toughness of the thermosetting matrix through a variety of mechanisms.

Details of the formation of this second phase, as well as other cured thermoset properties, are often highly dependent on the cure schedule. Cure conversion, morphology, glass transition temperature, toughness, and tensile strength, among other important properties, depend on not only the extent of cure but on the particular processing pathway taken to obtain a given degree of cure. The composition of both thermoset-rich phase and toughener-rich phase specifically are affected by the cure cycle.

Cure conditions within a sample may vary considerably due to both variations in ambient cure conditions and heat generated internally from the crosslinking reaction. These effects can produce gradients of cure temperature within the resin/thermosetting system, owing to poor thermal conductivity of the curing material. This low thermal conductivity also causes a significant lag in the heating of the core of the thermoset system compared to the outer regions, which can also induce cure temperature gradients.

The effect of continual variation of properties across the dimensions of a sample may be desirable in some applications. In addition, where gradients of properties are present, characterization of the effects on global behavior of the material must be considered. This thesis has considered the effect of specific isothermal cure conditions as well as gradient cure profiles on the mechanical behavior of novel toughened thermosetting systems.

In this study, gradient temperature cure samples have been prepared using a thermal gradient mold to produce a gradient cure temperature along a single specimen of toughened thermoset. This mold has been developed specifically for this work using heat transfer theory. The mold was placed between the platens of a molding press which has independent controls for each platen. The thermal gradient mold produces linear, stable thermal gradients, and combined with an injection technique, provides excellent control of cure conditions within the sample. This stable gradient cure manifests itself as a continuous and substantial change in microstructure of the cured toughened thermosets examined in the first part of this study.

Particle size in both the polysulfone and HTBN-toughened samples shows influence of cure temperature. While this has been theorized to produce significant changes in fracture toughness, no statistically significant difference in this property was evident. Because many properties of toughened thermosets are affected by cure temperature; however, additional work was necessary to characterize these changes.

An investigation of alternative polymers for toughening the BADCy system was made, and results compared to previously known tougheners. These alternative materials were a series of commercial, low T_g thermoplastic copolyester materials marketed under

the Vitel trademark. The thermo-oxidative stability of the copolyester Vitel materials was shown to be greater than the butadiene-acrylonitrile copolymer. Comparison of the phase separation behavior of the Vitel materials versus the HTBN materials in BADCy showed significant differences. While particle size varied with cure temperature in both systems, samples including Vitel 3200 showed a smaller variation, irregular particle shape and a much smaller size overall as examined using AFM. Little evidence of a phase separated morphology was apparent for the other Vitel copolyesters. The extent of phase separation in all samples was investigated using DMA, which showed clear evidence of phase separation with the Vitel 3200 and HTBN copolymers. The other Vitel materials remained mixed in the BADCy matrix, shifting its glass transition to lower temperatures.

Only Vitel 3200 and HTBN produced statistically significant improvements in fracture toughness when added to the BADCy resin. Examination of the fracture surface of cured samples of these materials using SEM revealed good particle-matrix adhesion for the HTBN-containing samples and a highly roughened surface for the Vitel 3200-containing samples with no obvious particle debonding. Increases in the concentration of both effective modifiers produced good toughness improvements up to 15% inclusion in the case of HTBN and continued improvement up to 25% addition of Vitel 3200. Only small differences in fracture toughness resulted from a 60 °C variation of the cure temperature with either toughener even though the HTBN-containing samples showed large variations in particle size. This suggests that for the samples studied here, toughening mechanisms dependent upon a correlation of toughness with particle size are less significant. Because of significant differences in surface roughness and particle size,

it is probable that contributions from several different toughening mechanisms are important in these experiments.

To more completely understand the effects of temperature on phase separation, the Williams model for toughened thermoset phase separation was applied to the HTBN-BADCy system. This model predicts the effect of temperature on microstructure and phase composition. This model was rewritten to describe the cure of the BADCy/HTBN mixture as it was originally developed for a toughened epoxy thermoset. Various parameters necessary to apply the model were determined. The Flory-Huggins interaction parameter (χ) was determined through determination of cloud points for the unreacted system. This necessitated the construction of an instrument suitable for accurate determination of the cloud point. This instrument was built using an optical microscope as the foundation, controlling the sample temperature with a microscope hotstage, and collecting transmitted light using a precision optometer. A computer was used for control and data acquisition. Cloud points were extrapolated to zero cooling rate and a cloud point temperature-composition curve was constructed from this data. With molar volume ratio data, this data was fitted to determine a temperature dependent Flory-Huggins interaction parameter.

Other data necessary to apply the model were also determined. Cure kinetics were measured using a calorimetric residual heat method. Data were fitted to a first order kinetic equation, which described the cure data well. Activation energy of the cure reaction was then calculated and applied to the model together with activation energy of viscosity from rheology experiments. To calibrate the Williams model to experimental observations, accurate characterization of the phase separated microstructure was

necessary. This was achieved by measuring significant numbers of toughener-rich particle areas using TEM. This two dimensional representation was transformed to a three dimensional representation using the Saltykov method. This improved representation of the true particle size distribution was used to set an adjustable parameter in the Williams model using data taken at an intermediate cure temperature (180 °C). The Williams model was then used to predict the particle size distributions at the two extremes of cure temperature, and resulting model predictions were found to fit the experimental data quite well. Finally, the Williams model was used to calculate the evolution of phase composition during cure. It was found that there is sufficient variation of phase composition to cause a moderate depression of the glass transition temperature in the continuous, cyanate-rich phase at higher cure temperatures relative to samples cured at the lowest cure temperature.

This portion of the study demonstrated that the Williams model for phase separation may be successfully applied to systems other than the epoxy system for which it was originally developed. The cyanate ester/HTBN mixture is a comparatively simple system, closer to the truly binary system assumed in thermodynamic treatments of other toughened thermosets. Though many other assumptions and simplifications were necessarily made, a major refinement employed here was use of the three dimensional particle size distributions for comparison and fitting of the output of the model.

The consequences of variation of phase composition with cure temperature on mechanical behavior were also explored. The relaxation properties of a series of toughened polycyanurate systems have been studied as a function of toughener type as

well as cure temperature. Because the relaxation characteristics of a material determine important use properties, variations can have important practical implications.

The representation of relaxation behavior employed here (Havriliak-Negami or H-N) has in the past typically been used to differentiate between local, molecular-level phenomena; however, the applicability of the H-N description is due to its general nature – it is not derived or tied to any specific molecular-level phenomena. It is because of this versatility that H-N has been employed to characterize this system of gradient properties of glass transition temperature, reflected in a potential broadening of the relaxation of a specimen by macroscopic system features.

The relaxation properties of single temperature (isothermally) cured BADCy is broadened by the addition of HTBN toughener, regardless of the cure temperature examined. The amount of broadening varies with the cure temperature through the composition of the phases in the sample, with higher cure temperatures producing small increases in broadness of the relaxation time distribution relative to the lowest cure temperature. Higher cure temperatures not only produce broader relaxations, but they are centered at lower temperatures. Gradient temperature cured samples were subsequently characterized. The change in glass transition temperature along the sample's length produced by the gradient cure gave rise to an increased broadness of relaxation time distribution versus isothermally cured samples at either cure temperature extreme. This broadened relaxation was transformed from a frequency domain function to a time decay function in the time domain to further illustrate the effect of gradient cure temperature on behavior.

Vita

David Scott Porter was born the second son of Doris and Andrew B. Porter, Jr. on April 30th, 1971. He grew up in rural Dinwiddie County, Virginia, attending high school at Saint Vincent de Paul in the nearby city of Petersburg, and graduating there in 1989. From high school, he attended Virginia Tech, studying chemistry and participating in the cooperative education program at Allied Signal corporation (now Honeywell). During his senior year of undergraduate work, he was fortunate to have the opportunity to pursue research under Dr. Thomas C. Ward, who inspired his current interest in polymers. David graduated with his bachelor's degree in Chemistry in May, 1994, to continue his studies of polymer science with Professor Ward in the Doctoral program in Chemistry at Virginia Tech. In 1997, his greatest blessing was realized when he wed the former Shelley Risch beneath the War Memorial pylons on the campus of Virginia Tech. Shelley and David currently reside in Kingsport, Tennessee, employed at Eastman Chemical Company.